BEHAVIOUR AND ANALYSIS OF A REINFORCED CONCRETE BOX GIRDER BRIDGE

by

Mohamed I. Soliman

A Thesis submitted to the Faculty of Graduate Studies and Research in partial fulfilment of the requirements for the degree of Doctor of Philosophy

Department of Civil Engineering
and Applied Mechanics
McGill University
Montreal, Quebec,
Canada

March 1979

TO MY BELOVED PARENTS

and

TO MY WIFE, MONA

BEHAVIOUR AND ANALYSIS OF A REINFORCED CONCRETE BOX GIRDER BRIDGE

by

Mohamed I. Soliman

Department of Civil Engineering
and Applied Mechanics
McGill University
Montreal, Quebec, Canada

Ph.D. Thesis
March 1979

ABSTRACT

This study was aimed at investigating the strength and deformational behaviour of a reinforced concrete box girder bridge under symmetrical and unsymmetrical loading conditions. The experimental phase consisted of tests on a 1/2.82 scale, direct model of the intermediate span of a continuous box girder bridge.

The flexural and torsional stiffnesses of the box girder decreased with an increase in the applied load due to the formation and propagation of cracks and inelasticity of concrete. The loaded web showed a deflection of about twice that for the unloaded web; also, the lateral and longitudinal displacements of both webs varied from about 5 per cent to 8 per cent of the respective midspan vertical deflections.

For the symmetrical loading case, higher stresses were observed at the web-flange junction compared with other regions of the cross-section on account of the shear lag phenomenon. The warping restraint can have a significant influence on some behavioural aspects of the box

structures especially for the unsymmetrical loading cases which are more frequent in practice. Therefore any restraint of warping must be carefully considered in the design of a box section structure. Significant transverse stresses result from any unsymmetrical loading and these can be of the same order as the longitudinal stresses at the same location.

The conventional simple beam theory seriously underestimated all types of stresses in the box section. Inclusion of torsional and distortional warping effects improved the predicted stresses slightly; however, even these were only about 60 per cent of the experimental values. Therefore, there is a need for a suitable non-linear analysis technique to account for the cracking of concrete and its inelasticity and other deformations which occur in a box section structure.

An inexpensive, quasi-nonlinear analysis was used to study the nonlinear behaviour of the bridge after cracking. The stiffness of the girder was varied in stages by incorporating information about cracking patterns and crack widths from the experimental data. This relatively inexpensive technique was used successfully to study the influence of two parameters - the element stiffness perpendicular to the cracks and the shearing force transferred across the cracks.

COMPORTEMENT ET ANALYSE D'UN PONT A POUTRES-CAISSON

EN BETON ARME

par
Mohamed I. Soliman

Département de génie civil
et de mécanique appliquée
Université McGill
Montréal, Québec, Canada

Thèse de doctorat
Mars 1979

Résumé

Le but de cette étude fut d'examiner la résistance et le comportement d'un pont à poutres-caisson en béton armé soumis à des charges symétriques et asymétriques.

La phase expérimentale consistait en des tests sur un modèle réduit à l'échelle 1/2.82 d'une travée intermédiaire d'un pont à poutres-caisson continu. Les rigidités un flexion et en torsion de la poutre-caisson ont diminué avec une augmentation de la charge appliquée à cause de la formation et de la propagation des fissures et de l'inélasticité du béton. Le fléchissement de l'âme chargée a été deux fois supérieur à celui de l'âme non-chargée; de plus dans les deux cas de chargement, les déplacements latéraux et expérimentaux ont varié d'environ 5 à 8 pour cent des déplacements verticaux de la section médiane de la portée. Dans le cas du chargement symétrique, de plus larges contraintes one été observées à la jonction âme-semelle par rapport aux autres régions de la section transversale à cause de la déformation dûe au cisaillement.

La restriction imposée au gauchissement peut avoir une influence significative sur certains aspects du comportement des structures à

section creuse spécialement pour les cas de chargement asymétrique qui sont les plus fréquents en pratique. Donc, toute restriction du gauchissement doit être considérée très soigneusement dans le dimensionnement d'une structure à section creuse.

Des contraintes transversales significatives résultent de n'importe quel chargement asymétrique et elles peuvent être du même ordre de grandeur que les contraintes longitudinales produites au même endroit. La théorié conventionnelle de la poutre simple sous-estime sérieusement tous les types de contraintes dans la section creuse. La considération des effets de torsion et de gauchissement a amélioré légèrement les contraintes prédites; cependant même ces contraintes représentaient seulement 60% des valeurs expérimentales. Il est donc nécessaire d'utiliser une technique appropriée d'analyse non-linéaire qui tient compte de la fissuration du béton et de son inélasticité ainsi que des autres déformations qui se produisent dans les structures à section creuse.

Une analyse quasi non-linéaire, peu coûteuse, a été utilisée pour étudier le comportement non-linéaire du pont fissuré. La rigidité de la poutre fut variée par échelons en introduisant les données expérimentales obtenues sur le mode de fissuration et l'épaisseur des fissures.

Cette technique relativement peu coûteuse a été utilisée avec succès pour étudier l'effet des deux paramètres: la rigidité d'un élément perpendiculaire aux fissures et l'effort tranchant transmis à travers les fissures.

ACKNOWLEDGEMENTS

The author wishes to express his deepest gratitude to his research director, Professor M. S. Mirza, for his guidance, valuable suggestions, constant encouragement and precious advice during the course of this study and the writing of the thesis.

Thanks are also due to Professor G. R. Thomas for his help and guidance with the finite element program.

The author also wishes to express his appreciation and gratitude to Professors P. J. Harris and D. Mitchell for their suggestions and encouragement during the experimental phase of this study.

The helpful suggestions of fellow graduate students and the valuable discussions with them have contributed significantly to this thesis.

Contributions from the staff of the Strength of Materials Laboratory, McGill University, are gratefully acknowledged.

Thanks are also due to Miss Joyce Richards for her typing of this thesis, to Mrs. Yvonne Thorpe for carefully proof-reading the thesis, and to Mr. Nisar Ahmed for the drafting work.

The financial assistance of the Department of Education of the Government of Quebec, and of the Natural Sciences and Engineering Research Council of Canada, to continuing research programs at McGill University, is gratefully acknowledged.

The support of the Ministry of Education of the Arab Republic of Egypt in granting the author a study leave for Ph.D. studies at McGill University is gratefully acknowledged.

Without the love, support and encouragement of family and friends, especially the author's parents and wife, Mona, this study would have been impossible.

TABLE OF CONTENTS

CHAPTER Page

APPENDICES

LIST OF FIGURES

Figure No. | Page

LIST OF NOTATIONS

A_m	Cross-sectional area of the model steel
A_p	Cross-sectional area of the prototype steel
Ag	Gross cross-sectional area
A_{enc}	Area enclosed by the centreline of the wall of the closed portion of the cross-section
A_v	Area of shear reinforcement within a distance S
b	Breadth between centreline of webs
b_{cant}	Breadth of the cantilever slab
b_w	Web width
d	Distance from extreme compressive fiber to centroid of tension reinforcement
$\underset{\sim}{D}$	Elasticity matrix for the orthotropic case
E_c	Modulus of elasticity of the concrete
E_p	Modulus of elasticity of concrete perpendicular to the crack direction
E_s	Modulus of elasticity of the steel
EI	Flexural rigidity of the reinforced concrete section
EI_g	Gross flexural rigidity of concrete = $E_c \times I_g$
f'_c	Compressive strength of concrete
f_c	Design compressive strength of concrete
f_s	Stress in tension steel
f_t	Tensile strength of concrete
f_y	Yield strength of reinforcement
G	Shear modulus of elasticity

h	Overall thickness of member
h_{top}	Thickness of top slab
h_{bot}	Thickness of bottom slab
h_{web}	Thickness of web
I_g	Moment of inertia of the gross cross-section
I_{cr}	Moment of inertia of the cracked cross-section
J_{eq}	Equivalent polar moment of inertia of the cross-section for the circular section, and torsional constant for non-circular section
ℓ	Bridge span
M	Bending moment at any section
M_{cr}	Bending moment at cracking
M_T	Torsional moment
S	Shear or torsion reinforcement spacing
v_c	Permissible shear stress carried by concrete
v_u	Total applied design shear stress at the section
V_u	Total applied design shear force at the section
w	Unit weight of concrete, lb. per cu. ft.
x,y,z	Global coordinates
u,v	Local coordinates
ε_c	Concrete compressive strain
ε_t	Concrete tensile strain
ε_s	Steel tensile strain
θ	Angle of twist

Additional symbols used are explained in the text.

LIST OF TABLES

CONVERSION FACTORS

The following is a list of the conversion factors for all imperial units (English system) used throughout this thesis to the "S.I. system".

Length	1 ft	=	0.3048 m
"	1 in	=	25.4 mm
Area	1 ft^2	=	.09290304 m^2
"	1 in^2	=	645.2 mm^2
Volume	1 in^3	=	16387.1 mm^3
Moment of Inertia	1 in^4	=	416231.4 mm^4
Force	1 pound	=	4.4482 Newtons
"	1 kip	=	4448.2 Newtons
Mass, Density	1 pound/ft	=	1.488 kg/m
Bending Moment or Torque	1 pound-ft	=	1.355818 Newton-meter
Rate of Loading	1 pound/ft^2	=	4.88242 kg/m^2
Force per Unit Area	1 pound/in^2 (psi)	=	6.895 Kilo-Pascals (kPa)
Stress,Modulus of Elasticity	1 kip/in^2 (ksi)	=	6.895 Mega-Pascals (MPa)

CHAPTER 1

INTRODUCTION

1.1 General

Reinforced and prestressed concrete bridges are an important part of the modern transportation system, and constitute a major proportion of the bridges used in North America. Post-war attempts to develop new economical bridge forms and construction techniques have led to the development of the box section. Compared with other types of concrete bridges, the box girder section is more economical and aesthetically attractive.

1.2 Objectives and Scope of the Present Study

The aims of this research program are as follows:

1. To study the general behaviour of a box girder bridge structure through tests on a large-scale direct model of a medium span bridge. (The model was 19 ft. long, 5 ft. wide and 14 in. deep, consisting of a single rectangular cell with 14 in. slab overhangs on either side). The specimen represents the intermediate panel of a continuous box girder bridge with the two ends simulating the warping restraint condition created by the heavy end blocks at the specimen ends. Provision of high tension bolts in the end blocks prevented longitudinal and transverse translation

and rotation and thus created a fixed ended condition. The specimen was suitably instrumented to obtain a complete picture of steel and concrete stresses in both longitudinal and transverse directions.

2. To study the effects of concrete cracking on the flexural and torsional behaviour of this type of box girder bridge.

3. To study the effect of warping restraint on the stress configuration along the length of the box girder and to assess the accuracy and validity of some presently available analytical tools.

4. To study the effects of crack formation and propagation on the shear transfer across the crack and on the element stiffness perpendicular to the crack direction. This information is necessary in formulating the necessary non-linear constitutive relationships to be used in the finite element analysis of the structure.

1.3 Previous Work

Over the past six decades, several investigators have attempted to analyse the box girder as a slab system, or as a slab on a network of beams [1]. For these cases, the slab and beam system is converted basically to an equivalent gridwork of beams or to an equivalent anisotropic slab, and its analysis has depended on the well-known distribution and relaxation techniques, plate theory and harmonic analysis.

Bretthauer and Kappei [2] analysed interconnected multicell girders by considering them to consist of interconnected, torsionally stiff T-beams. Ghali considered the bridge deck to be equivalent to two main girders, connected transversely by the slab and by cross girders [3]. He presented tables for the calculation of flexural and torsional stiffnesses which can be used in the analysis of simply supported straight and skew bridges of uniform cross-section. Homberg and Trenks [4] also presented extensive tables for analysis of grids with hollow-box main beams supporting transverse beams. The 1965 AASHTO Specifications [5] proposed a design method wherein a box girder bridge was considered to be composed of a number of identical I-shaped interior girders along with two exterior girders each of which had half a bottom flange. According to these specifications, each girder was designed as a separate member subjected to a certain fraction of a single longitudinal line of wheel loads from a standard truck. This fraction, known as the distribution factor $N_{w\ell}$, was given by the following equations:

$$N_{w\ell} = \frac{S}{7} \quad \text{for interior girders} \tag{1.1}$$

and

$$N_{w\ell} = \frac{S_1}{7} \quad \text{for exterior girders} \tag{1.2}$$

where S and S_1 were the flange widths of the interior and exterior girders, respectively, in feet.

It should be mentioned herein that, up to 1959, the value of $N_{w\ell}$ for box girder bridges was $\frac{S}{5}$ which placed the concrete box girder bridge in the same structural class as a concrete T-beam bridge. After recognizing the structural efficiency of the box girder section, the California State Department of Highways (1967) used a single value for the distribution factors, $N_{w\ell}$, for the entire width as follows:

$$N_{w\ell} = \frac{\text{Deck width in feet}}{7} \tag{1.3}$$

for both interior and exterior girders. However, this recognition called into question the whole process of bridge design on the basis of distribution factors.

Massonnet and Gandolfi [6] presented an approximate method to determine values of flexural and torsional stiffness which were used in the existing Guyon-Massonnet method for the analysis of orthotropic plates to design bridge decks of cellular construction.

None of the above methods is directly applicable to the analysis of box girder bridges. Scordelis [7] commented that these analyses do not adequately simulate the interaction of the individual plates and, consequently, do not yield answers for the all important internal forces and moments in each plate element. He emphasized the need for further study into deformational behaviour of box girder bridges and also an examination of the distribution of applied loads between the webs in both longitudinal and transverse directions.

The effect of shear deformation on the total behaviour of box section structures has received considerable attention. Chu and Longinow [8] developed techniques to locate the shear centre of any 'open' or 'closed' cross-section. This enabled determination of the torsional moments due to external loads and the resulting primary shear stresses due to torsion without warping restraint. Kollbrunner and Basler [9] considered St. Venant torsion as distinct from warping torsion, and stated that the former dominated the behaviour of hollow closed sections. However, Heilig [10] showed that this depended on the structural properties. Blaise [11] used the Bredt-Batho method for analysis of multi-cell box sections subjected to torsion, while Benscoter [12] developed several methods for the calculation of primary shear flows in prismatic, multicellular members in torsion. These procedures included successive correction and iteration methods similar to the carry-over cycles of moment distribution. Only the relative values of the aspect ratios of the wall segments need to be known in the preliminary stage of design, when the cell areas are known but the thicknesses have yet to be determined. Dziewolski [13] used the theory of non-uniform torsion of long, thin-walled members to develop a method for computing the transverse load distribution factor for bridges of symmetric or unsymmetric, open, closed and compound sections. Valentin [14] suggested the use of shape factors to account for shear strain energy in evaluation of bridge deformation by the strain energy method. He noted that the values of these factors were higher for hollow sections than for solid sections.

Cziesielski [15] developed tables and graphs to enable evaluation of the shear resistance of box, I, and angle sections. Panc [16] developed a general theory for elastically-supported prismatic beams of open or closed cross-section symmetrical about the vertical axis. He noted that the shear strain in the middle surface of webs and flanges could not be neglected. Von Karman and Christensen [17] described a simple method for the analysis of axially constrained thin-walled structures having a constant cross-section (open, closed or a combination), and subjected to a varying twisting moment. Benscoter [18] pointed out that although the computed values of the basic transverse distribution of primary and secondary shear flows were relatively correct, the distribution of stresses and rotations calculated along the span was incorrect because of lack of sufficient accuracy in assessing the effect of shear strains on deflections. In analysing a single cell tube in warping torsion, Rudiger [19] neglected the influence of warping shear stresses on the deformation of a closed cross-section. However, Grasse [20] corrected this error and extended the work to include the warping torsion of a prismatic tube whose cross-section was open or closed and of an arbitrary shape. Dubrowski [21] investigated the influence of shear deformations on warping torsion of box beams with a deformable cross-section and diaphragms. He observed that the intermediate diaphragms and the support diaphragms caused the influence of shear to increase, while the warping moments due to profile deformation decreased.

In steel construction, for the commonly used proportions of wall thickness to breadth or depth of the box section and commonly used wall thicknesses, Heilig [22] observed that the simple Bredt-Batho theory gave results sufficiently accurate for practical purposes for breadth/depth ratios between $\frac{3}{5}$ and $\frac{5}{3}$. However, in concrete construction where the wall thickness is greater, tests by Leonhardt and Walther [23] showed significant warping stresses for similar breadth/depth ratios. Knittel [24] presented a simplified method to determine the stresses and displacements in single- and multi-cell structures with a constant, symmetrical cross-section. By suitable resolution of the loading into symmetric and antisymmetric components, it was possible to obtain mutually independent states of longitudinal bending, transverse bending and St. Venant torsion; torsional warping stresses, however, were neglected.

Gibson and Gardner [25] applied shell theory to the case of degenerate shells of very shallow curvature used to represent plates. Multi-shell structures of this kind can be considered as folded plates. Johanston and Mattock [26] tested a 1/4 -scale model of a composite box girder bridge without transverse diaphragms using a concentrated load applied eccentrically over one of the webs and noted a good agreement between the observed values and those calculated from the folded plate theory. This demonstrated the applicability of the folded plate theory to interconnected spine beams. Schardt [27] developed a folded plate analysis such that the elementary bending theory could be used with the introduction of new section properties which were tabulated. Meyer and Scordelis [28] presented a matrix formulation for the analysis of folded plate structures, where longitudinal and transverse stresses can be treated separately. Goldberg and Leve [29] considered both membrane and plate actions in the slabs, and expressed the analysis in a matrix formulation; displacements, rotations and stresses can be evaluated using this formulation.

Box section structures can also be analysed using the matrix progression method or transfer matrix method [30]. This technique is applicable to complex structures, in which the problem of analysis can be reduced to that of finding the variation of internal forces and displacements along one coordinate direction. In the case of multicell box girders, this coordinate can be the peripheral one, and the multicell section is treated as a branched configuration with a return branch [31]. Transverse bending action on the profile is included in the analysis, and prestress forces can be introduced as discontinuities. It is also possible to proceed longitudinally, analysing successive short lengths of the structure and incorporating at each stage such discontinuities of structural and/or loading configuration as may exist, including any prestressing forces. This avoids the difficulties encountered with sections varying along the span when the matrix progression is carried out along the peripheral coordinate.

These methods are not capable of determining the internal membrane and bending stresses within the structure. Maisel [32] conducted an elaborate review of 299 references on analysis and design of thin-walled beams to examine the effects of torsion, warping and distorsion on the cross-section. He developed the following recommendations for design of box beam sections along with some suggestions for future research programs.

1.3.1 Proportioning for Initial Design

The selection of the cross-section proportioning can be based either on the recommendation given by Wittfoht [33] and by Johanston and Mattock [26], or on the empirical rules given by the American Concrete Institute [34].

1.3.2 Analytical Tools

Maisel [32] examined all available analysis methods and concluded that the following analytical works were of particular merit:

(a) Dabrowski [21] presented the most comprehensive work on analysis of curved, thin-walled steel, composite or reinforced concrete beams. Design aids such as tables, influence lines and internal force diagrams are presented for straight and curved beams for up to a maximum of three spans.

(b) Heilig [35] assessed the significance of warping, geometry, loading and support conditions and presented a general method for analysis of straight, multi-cell box beams of arbitrary, undeformable cross-sectional shape. He developed extensive tables of formulas for the general loading conditions.

(c) Knittel [24] neglected warping but considered the cross-sectional deformations. He resolved the applied loading into symmetric and anti-symmetric components to obtain three mutually independent states: longitudinal bending, transverse bending and St. Venant torsion. He developed a simplified method of analysis for determining stresses and displacements in single- and multi-cell box beams of constant symmetrical cross-section. Maisel argued that because the warping stresses can be about 50 per cent of the primary bending stresses, a combination of Heilig's and Knittel's methods is a more useful analysis tool.

1.3.3 Limiting Thickness-depth or Width Ratio

Maisel [32] and Vlasov [36] pointed out the significance of the limiting thickness-depth ratio for webs and thickness-breadth ratios for the flanges in applying the various analytical methods to thin-walled beams. Maisel noted that in tests on models of the Mancunian Way [37] and the Western Avenue box girders [38], the thickness-depth ratios for the webs were 0.69 and 0.16 respectively. These proportions exceeded the range of applicability of the thin-walled beam theory. Therefore, Kollbrunner and Basler [9] pointed out that the thin-walled beam theory could still be applied to the concrete structures provided that the effective area of cross-section did not exceed the area enclosed by the wall centreline.

1.3.4 Limit States Design

Design by limit states requires consideration of the crack pattern and modes of failure. Maisel [39] summarized the experimental and analytical work required in this area as follows:

> "The majority of the experimental work reported concerned working load conditions in models made of materials other than concrete. Observations of deflexions, twists, reactions and strains have usually been made and, from these, stresses and load distribution coefficients have been evaluated, good correlation with theory usually being obtained. Tests on concrete models and prototypes have provided information on crack patterns and modes of failure, but the customary theories of failure do not give satisfactory results for all stress combinations, nor do they adequately explain observed failure conditions. Further information is required on the behaviour of cracked sections, the effect of cracking on bending and torsional stiffness, patterns of cracking corresponding to various load systems and structural configurations, ultimate loads, effective widths of flanges, diffusion of prestress, local effects near diaphragms and stresses in reinforcement.
>
> The main requirements for future research appear at present to be in the field of experimental work. The necessary theoretical development for limit state design is probably an extension of elasto-plastic finite element analysis, to predict cracking and ultimate load behaviour in combined bending, shear and torsion. "

Rowe and Best [40], Scordelis [41], Corboda [42], Tschanz [43], Soliman and Mirza [44] and Tabba [45] conducted tests on small and large-scale direct and indirect models to study the elastic and ultimate load behaviour of bridge structures which normally cannot be obtained by analytical procedures. Little and Rowe [46] tested a plexiglass model to determine the value of the torsional parameter α for the Guyon-Massonnet load distribution analysis for bridges, as applied to a structure which is neither a slab nor a simple grillage. They presented a method to evaluate α for a box section bridge, and compared the experimental values of the distribution factor with the theoretically derived values. They observed that the distribution properties of the deck were underestimated, though not seriously, by calculating α on the basis of one cell only and neglecting the interaction of cells. The theoretical results for load distribution did not show good agreement with the experimental results when the torsional stiffness of a multi-cell box was used to calculate α . It was observed that the local warping effects significantly influenced the effective torsional stiffness of the member. Nasser [47] developed a simple procedure for determining the lateral load distribution in bridge decks composed of precast hollow-core beam units linked by *in situ* shear keys and transverse prestressing. The method was based on orthotropic plate theory and experimental work on model and prototype bridge decks. For design purposes, the percentage of the axle load carried by a single beam for centre and edge loading conditions on the bridge can be determined from the graphs in Reference [48].

Cordoba [42] and Tschanz [43] tested a 1:3.76 scale model of a large-scale two-cell concrete box girder bridge with precast cells and cast-in-place deck. The objective of this investigation was to examine the behaviour of this type of bridge, with emphasis on load distribution. The experimental results were analysed by the Finite Element Method using a compatible rectangular shell element with four degrees of freedom at each node [49]. However, this analysis was limited to the elastic range of behaviour. Recent investigations have shown the potential of the Finite Element Method in studying the nonlinear behaviour of bridge and other concrete structures resulting from nonlinearities of materials and geometry. The bridge was tested for the H20-44 truck loading at the working load level. The ultimate load capacity was obtained using two point loads, placed over the outside webs at the midspan of the bridge, which were increased in stages until failure. They showed that this type of bridge provides a competitive alternative to other types of bridges in the 80 to 120 feet span range. They also observed that diaphragms did not have a significant effect on the behaviour of this type of bridge within the service load level. Leonhardt and Walther [23] tested two prestressed concrete, single cell, single span, box girders with side cantilevers, and transverse diaphragms at midspan and at each support. The first specimen was subjected to a concentric midspan loading until flexural failure was approached, and then the loading was made eccentric to induce torsion. The second girder was loaded with a more eccentric midspan load so that torsion dominated. In addition, a 1/10 -scale plastic model was tested under the same type of loading to ascertain the differences between the uncracked and cracked conditions. The design of the shear and torsional reinforcement was based on the simplifying assumptions of plane strain distribution and St. Venant's torsion theory. The experimental deformation values in the uncracked concrete girders agreed well with the values calculated using the elastic theory. It was noticed that the measured deflections and twists were slightly lower than the calculated values and they pointed out the need for further research in this area. As expected, they observed that cracking caused a decrease in the torsional rigidity. The diagonal compressive stresses in the side of the webs were noted to be a critical factor in the design of thin-walled structures, providing that the principal tensile stresses are adequately resisted by the reinforcement.

Fam [50] and Tabba [45] studied the behaviour of curved box girder bridges using the Finite Element Method for applied static and dynamic loads. A three-dimensional finite element program was developed for the analysis of curved cellular structures. Solutions of several problems involving static and dynamic responses were presented using the proposed and other sophisticated methods of analysis. An experimental study conducted on two curved box girder plexiglass models confirmed the reliability of the proposed method of analysis.

Swamy [51] reported tests on the behaviour of prestressed concrete single-cell box beams loaded in bending and torsion. The size and shape of the box section were varied and the effect of a nominal amount of torsional reinforcement was investigated. Bending moments were found to have a beneficial effect on the torsional behaviour. He observed that a box beam can be loaded up to 65 per cent of its ultimate bending capacity before its torsional strength decreases. Torsional stresses however reduce the bending strength slightly. Depending on the relative magnitude of bending and twisting moments, failure may occur either by crushing or by diagonal tension; interaction curves provide a useful tool as an empirical method of assessing failure loads under stress ratios ranging from pure bending to pure torsion.

Somerville, Roll and Caldwell [52] constructed and tested a 1/12 -scale micro-concrete model of a typical interior span of the Mancunian Way. The cross-section was a single-cell box with side cantilevers. Information was obtained on the diffusion of prestressing forces through the section and on the behaviour of the structure for three different loading conditions, under a concentrated loading on the cantilevers, and at ultimate load. The load factor for the ultimate condition was approximately 3 for the full live loading on the span.

A program of prototype tests on interconnected box section type bridges was undertaken at Lehigh University in order to develop a new design method [53]. The specimens tested were composed of prestressed concrete box units connected by an *in situ* reinforced concrete deck slab with curbs and parapets. Test results showed that, for interior girders, the observed distribution factors between webs were considerably less than those used in design, while for exterior girders the observed values were greater than the corresponding values used in design. Distribution factors based on the Guyon-Massonnet orthotropic plate theory were found to be 4-15 per cent higher than the observed values for interior girders, and 6-15 per cent lower than the observed values for exterior girders. Lin and Vanhorn [54] suggested that the curbs should be considered in assessing the strength of the exterior girders, although the distribution factors for interior girders should still be related to their spacing as at present.

Scordelis [55] tested a large 1/2.82 -scale direct model of a two-span box girder bridge with a diaphragm in the middle of one span. A slight improvement in load distribution characteristics was observed on the span with the diaphragm. He showed the need for revising the present AASHTO specifications to include important parameters in the design of bridges of this kind. Some of these parameters are: number of traffic lanes, total width, span and number of cells and continuity or fixity at the supports.

William and Scordelis [56] tested models of folded plates and compared the experimental results with the values calculated using the folded plate theory and the elementary beam theory. They concluded that the folded plate theory could be used to predict the behaviour of box section structures within the working load range and that, for the type of reinforced concrete model and loading used, either theory yielded satisfactory results for working load deflections. Scordelis [41] suggested that further experimental research on reinforced concrete models of various configurations and subjected to various types of loading was needed to determine the range of applicability of the elementary beam theory and the folded plate theory. Also, additional analytical and experimental studies were needed to document the behaviour of typical reinforced concrete folded plate structures over the entire load range.

Scordelis, Bouwkamp and Wasti [57,58] developed a general method of analysis for simply-supported box girder bridges. The study was concerned with the elastic analysis of these structures by methods suitable for electronic computers. A direct stiffness solution using the folded plate theory and a harmonic representation of the loading was used for analyses of these structures with and without diaphragms. They presented the details of the analysis and interpretation of the experimental and theoretical results obtained from tests on a large-sale, two-span, four-cell, reinforced concrete box girder bridge model. They used the Finite Element Method to analyse the bridge model and noted that the AASHTO empirical formula overestimated the girder moments for the two-lane HS-20-44 truck loading and underestimated it for the three-lane truck loading.

Godden and Aslam [59] conducted tests on a series of small-scale aluminum models of rectangular and skew box girders to check the accuracy of the available analytical solutions for the elastic behaviour of bridges of this type. All skew bridges were tested with and without transverse diaphragms at midspan, and were subjected to the action of a single vertical point load at various locations. Because of the scatter between the experimental and the calculated values, a need for further study of the behaviour of this type of bridges was stressed.

Comartin and Scordelis [60] investigated the behaviour of a simply-supported curved box girder bridge by the Finite Element Method, using quadrilateral elements having a total of 5 degrees of freedom per node. The theoretical results were compared with the experimental results from a previous study on aluminum model bridges of identical dimensions. They concluded that the present AASHTO specifications did not differentiate between straight and skew bridges and therefore it needed to be reviewed.

Scordelis, Bouwkamp and Larsen [61,62,63] investigated the structural behaviour of a large 1/2.82 -scale direct model of a curved two-span, four-cell, reinforced concrete box girder bridge. They presented the details of the design, construction, instrumentation and loading of this bridge model along with the experimental results. The responses of the bridge-to-point loads, conditioning loads and truck loadings all at working stress levels were determined. In addition, the bridge response was determined for conditioning loads at overstress levels and for point loads after conditioning overloads. Theoretical values were obtained from both the Finite Element Method using the three-dimensional beam element in the SAP IV Program [64], and the three-dimensional folded plate theory [65]. They concluded that based on the assumption that the bridge model was elastic, homogenous, isotropic and uncracked, the three-dimensional folded plate theory accurately predicted the behaviour of this type of bridge within the working load levels, while the finite element beam element could predict only the reactions and deflections for this type of bridge within the same load level. They showed the significance of diaphragms at midspan in improving the behaviour of the bridge at very high overload levels and during the final loading to failure. They also showed that the AASHTO Specifications [66] did not yield accurate girder moments, and accordingly it needed to be revised.

Swan [67] tested a 1/16 -scale continuous segmental microconcrete model of a typical span of a six-lane viaduct with three cells.

The precast cellular segments of the model were prestressed transversally and vertically in addition to the longitudinal prestressing. This research program was aimed at investigating the performance of post-tensioned segmental cellular structures subjected to the Ministry of Transport 'HA' and 'HB' loadings. They observed an increase in the stresses near the diaphragms above those predicted by the elementary beam theory. They related this phenomenon to the stiff diaphragms and the shear lag effects.

Swan [68] reported the characteristic features of 173 bridges built in the previous 15 years with a view to making recommendations for the initial proportioning of box girder bridges. Span lengths, total depths,methods of construction, longitudinal and cross-sectional configurations, web location and thicknesses, top and bottom flange thicknesses, transverse and longitudinal prestresses, were examined and discussed for both straight and skew box girder bridges. This information was presented as a guide to the available feasible economic options. More research and development work are needed in this area.

Redwood and Gurevich [69] used a membrane finite element in analysing single- and multi-cell skewed box girder bridges with variable sections and interior diaphragms. The longitudinal plate bending and twisting were ignored in the analysis and transverse bending was treated in an approximate manner as follows. A fictitious transverse diaphragm was used to carry membrane forces only. By this means and by ignoring other bending components, the analysis was treated as a membrane one involving only three translation degrees of freedom per node. Particular reference was made to multi-cell boxes with any plan form, and arbitrarily located diaphragms. Tinawi [49] analysed orthotropic bridge decks using the Finite Element Method; a compatible rectangular shell element which provided for in-plane rotation was developed to simulate the deck plate. For closed-type ribs, the same element was used, and for open-type ribs, a compatible eccentric beam element was used as an alternative. The analysis compared favourably with the available experimental data. Tinawi also studied the effect of varying the stiffener and cross-beam spacing and suggested an increase in the standard rib spacing in order to achieve greater economy in the fabrication process. Geometrical nonlinearities of the deck plate and the ribs were also studied, using the triangular shell element for the case of trapezoidal stiffeners with large openings.

Meyer and Scordelis [70] developed a general computer program to analyse any prismatic cellular or open folded plate structure with transverse diaphragms or frames and longitudinal beams. The solution is based on the Finite Element Method in conjunction with the Direct Stiffness Method. Kabir and Scordelis [71] developed a computer program for the analysis of continuous prismatic folded plate structures, which are circular in plan and have flexible interior diaphragms or supports. The Finite Strip Method was used to determine the strip stiffness. Interior diaphragms were defined by flexible beams, and interior supports were idealized as two-dimensional planar frame bents.

A direct stiffness harmonic analysis was used to analyze the assembled folded plate system. The program can be used to establish rational criteria for simplified methods for analysis and design of curved bridges, in which important design parameters such as cross-sectional dimensions, radius of curvature, span along the arc length, flexibility of the support and the skew angle can be varied to determine their effect on the bridge response.

In conclusion, all research programs on box section structures completed so far were aimed at studies of load distribution and behaviour and performance of such structures within the working load level. Once the section cracks under increasing load, the assumption of linearity is no longer valid and the departure becomes more pronounced under overload conditions. There is very little experimental or analytical research data available on the nonlinear deformational behaviour of the box section after the section has cracked and under overload conditions. Recently, there has been an increasing interest in the design of bridges based on limit load analysis; however, there are rather large differences in the ultimate load values calculated according to different limit load analyses [71]. This is due to the difficulty arising in including the influence of membrane forces in the presently available limit load theories and therefore the validity of these methods becomes limited.

In summary, there is a need for further studies of the behaviour and analysis of reinforced concrete box section structures which account for both membrane and bending actions, along with a consideration of non-linearities due to cracking and to the nonlinear response of concrete and steel [72].

1.4 Organization of the Thesis

This chapter is followed by a description of procedures used in the experimental phase (Chapter 2). This chapter includes the design, construction, instrumentation and loading of the box girder bridge. The results of the experimental work are detailed in Chapter 3 along with a discussion of the observed strengths and the deformational behaviour of the bridge. A summary of the experimental observation is presented at the end of Chapter 3.

The finite element analysis used in this investigation is described in Chapter 4. Results of a linear and a quasi-nonlinear finite element analysis of the bridge are presented. The linear analysis is conducted to study the effect of warping restraint on the total stress distribution and the results are compared for the two cases - one with warping restrained and the second with the warping not restrained. The quasi-nonlinear analysis is used to perform a parametric study to examine the influence of the element stiffness perpendicular to the crack and the shear transfer across the crack.

A summary of the findings and the conclusions are presented in Chapter 5. Some proposals for future study are also included in this chapter.

CHAPTER 2

EXPERIMENTAL PROGRAM

2.1 General

Models are being increasingly used for behaviour studies of simple and complex structural systems aimed at verifying the basic design assumptions and at modifying the existing design criteria [73]. Some of the empirical formulas in the current ACI Code [74] and the National Building Code of Canada [75], particularly the shear and torsion formulas, were derived from the results of tests on 1/2 - 1/3 scale direct models which were considered as small prototypes for all practical purposes. Besides, large-scale models have been successfully used in behaviour studies of bridges and building structures under applied static and dynamic loads [61,62,63]. Compared with the prototypes, these model structures are relatively simpler and less expensive to construct, instrument and test. Recent studies have also shown that 1/2 - 1/4 scale direct models of reinforced and prestressed concrete structures can predict the prototype behaviour and strength with an excellent degree of reliability within ± 15 per cent [76,77].

2.2 Details of the Tested Bridge

It was decided to test a large (1/2 - 1/3) scale model of a medium span box girder bridge. For all practical purposes, these small prototypes require construction techniques which are as close as possible to those used in the construction of the prototype. Also, the model materials used must simulate as closely as possible the basis characteristics of the prototype concrete and the reinforcing steel.

The main reinforcement in a typical box girder bridge normally consists of suitably spaced #11 deformed steel bars (nominal cross-sectional area = 1.56 sq. in.). Because of convenience, it was decided to simulate the #11 deformed steel bars by #4 deformed steel bars (cross-sectional area = 0.2 sq. in.). This resulted in a length scale factor given by

$$S_\ell = \frac{L_m}{L_p} = \sqrt{\frac{A_m}{A_p}} = \frac{1}{2.82} \qquad (2.1)$$

$$\left(S_\ell \text{ linear scale factor} = \frac{\text{Model quantity}}{\text{Prototype quantity}}\right)$$

which was adopted for the box girder model. This model was 19 ft. long 5 ft. wide and 14 in. deep and consisted of a single rectangular cell with 14 in. long cantilevered slabs overhanging on both sides. A typical cross-section of the box girder bridge is shown in Fig. 2.1 along with the details of the end blocks providing fixed-ended condition at the two ends.

Although it is relatively simple to satisfy the requirements for stress and strain similitude for model steel and concrete, it is

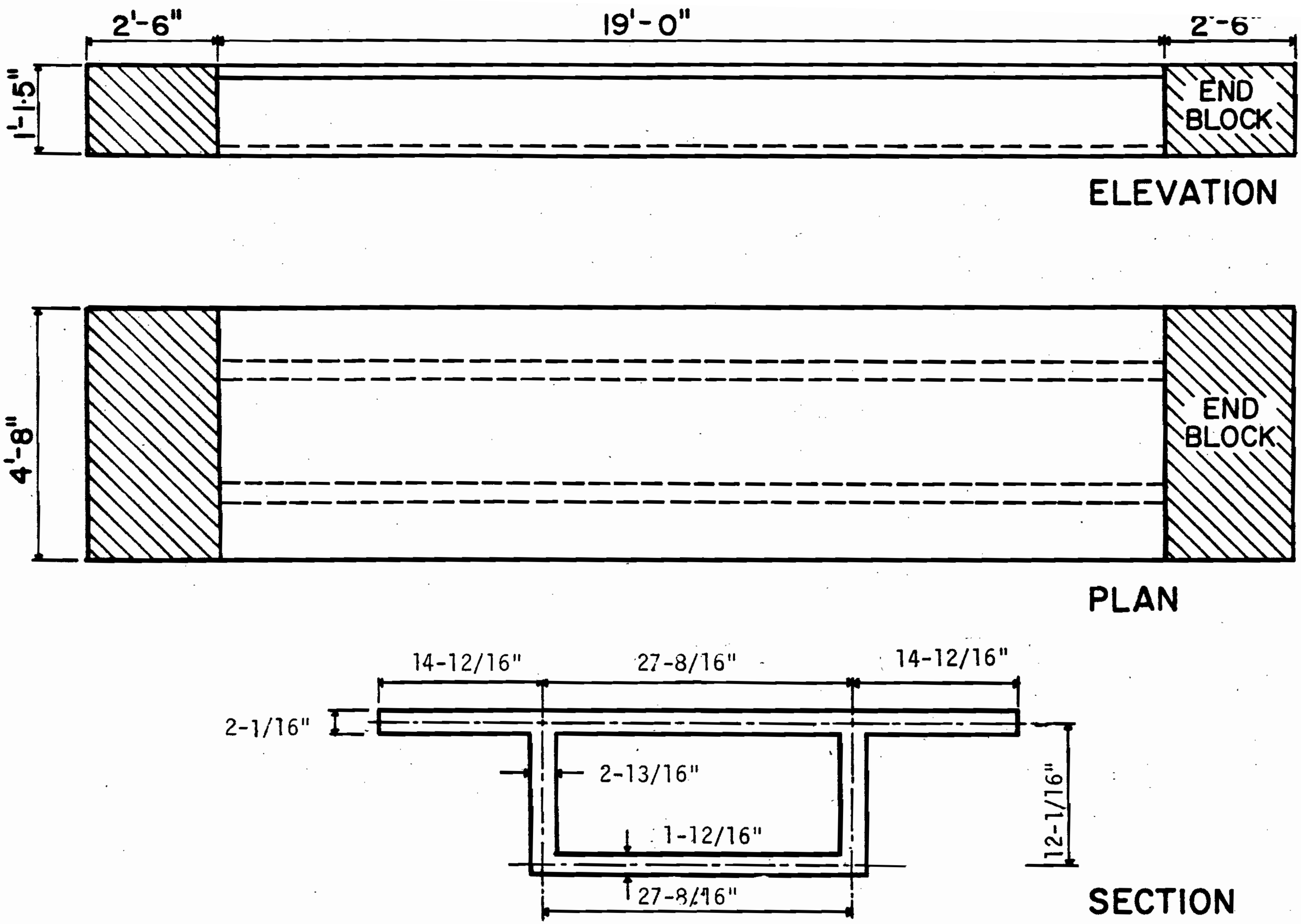

FIG. 2.1 BOX SECTION DETAILS

considerably more difficult to satisfy the bond requirements [76]. For structural concrete members or systems with predominance of flexural and/or shear, it is normally not necessary to satisfy all the requirements of bond similitude. It is enough to ensure that there is sufficient bond resistance so that bond failure does not occur. This can be achieved by providing sufficient embedment length to develop the yield strength of the bar.

The model concrete mix used consisted of a mixture of High Early Strength cement and a blended mixture of five grades of crushed quartz sand. The advantage of using such a mix compared with a mortar mix lies in its excellent simulation of the compressive and tensile (splitting and flexural) strengths, the modulus of elasticity and the ultimate compressive strain at failure.

For a true model, the density of the model material is given by

$$\rho_m = S_\ell \ \rho_p \tag{2.2}$$

where ρ_m density of the model material

ρ_p density of the prototype material

Therefore, in this case, the model concrete must be 2.82 times as heavy as the prototype concrete. This similitude condition can obviously not be achieved through the use of model concrete and extra dead load was used to properly simulate the dead weight of the prototype. The extra load required to be added to the model bridge structure was 450 lb/ft. Studies were made to determine the feasibility of renting steel billets and placing them suitably within the box girders of the bridge during its construction. This idea was abandoned because of the stress concentration caused by these steel billets in the lower slab. Instead, silica sand bags,concrete blocks measuring 15 in. x 15 in. x 15 in. and steel billets were distributed uniformly on the top and the bottom slabs throughout the span of the bridge. The sequence of placing these loads was as follows:

1. The box girder was filled with silica sand in addition to three steel billets uniformly distributed along the bridge span.

2. After casting the top slab, fourteen concrete blocks and four steel billets were distributed uniformly over the top slab along the bridge span.

This method eliminated any possible stress concentration from the extra dead loads used for dead load compensation.

The main reinforcing bars used for the bridge were #4 and #3 deformed steel bars, with nominal yield strengths of 60 ksi and 45 ksi, respectively. The main reinforcement in the maximum positive moment region consisted of 11 #4 bars, while that in the negative moment region consisted of 17 #4 bars. In addition, 6 #3 bars were provided in the top slab running through the span of the bridge, two over each web, and one at the end of the cantilever slab. The transverse reinforcement in the top and the bottom slabs and in both webs consisted of two layers of D_3 and D_4 deformed steel wires (cross-section areas 0.03 sq. in. and 0.04 sq. in., respectively) with a nominal yield strength of 38 ksi. The details of reinforcement for the top and bottom slabs and a typical cross-section are shown in Figs. 2.2, 2.3 and 2.4. The details of the end block reinforcing steel are shown in Fig. 2.5. This reinforcement consisted of closed #5 stirrups in the two orthogonal directions, in addition to 28-3/4 in. diameter high strength steel bolts at each end to prevent any end block translation and rotation, thus creating fixed-ended condition at the two ends.

Due to diagonal compression in the concrete at higher torsional loads, the concrete cover has a tendency to spall off, therefore it is important to detail the stirrups such that they will not loose their anchorage when spalling occurs. This is obtained by bending the free end anchorage length of the stirrups into the concrete [78]. In addition, it is necessary to provide proper end anchorage for the longitudinal reinforcement to enable this reinforcement to fully develop its yield strength. The reinforcement details adopted satisfy the fundamental requirements of strength, limited cracking, ductility and simplicity of construction.

2.3 Material Properties

2.3.1 Concrete

The selection of suitable materials to model concrete depends upon several requirements. The constituent materials must satisfy

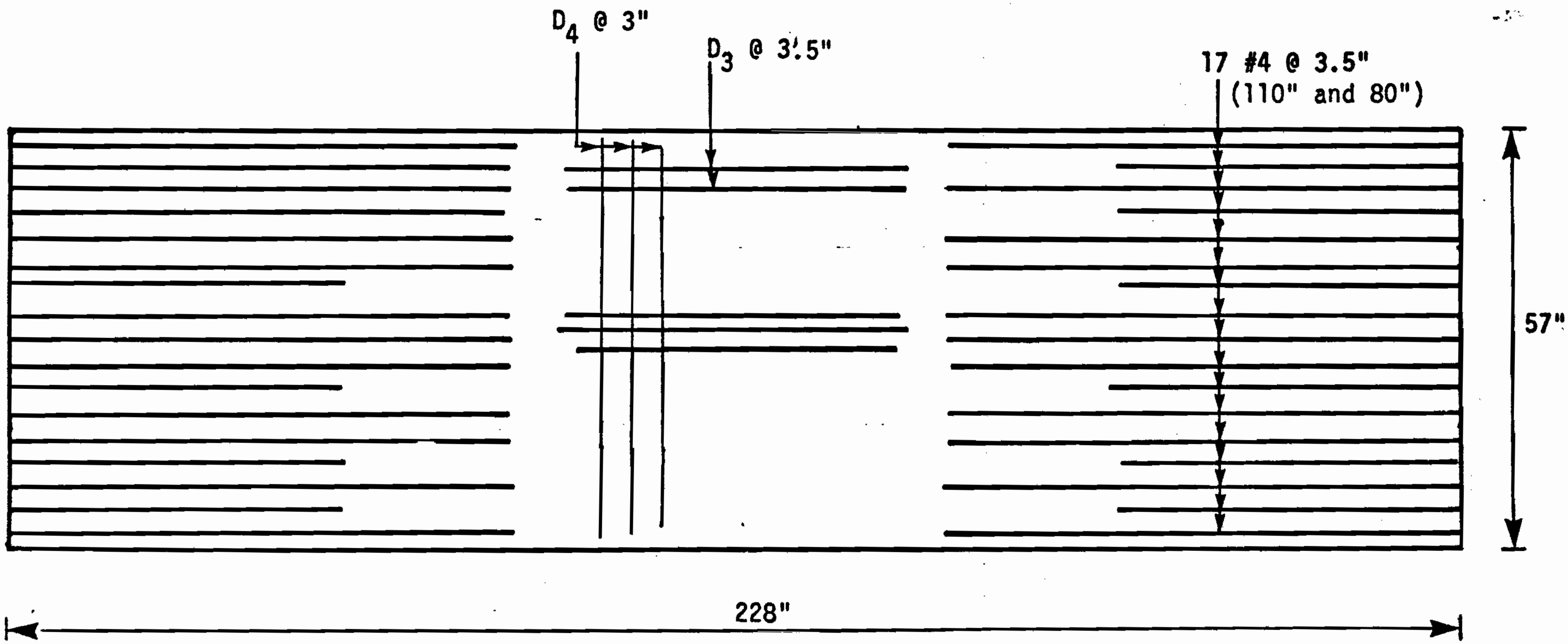

FIG. 2.2 DETAILS OF TOP SLAB REINFORCEMENT

(ALSO SEE TABLE 2.3)

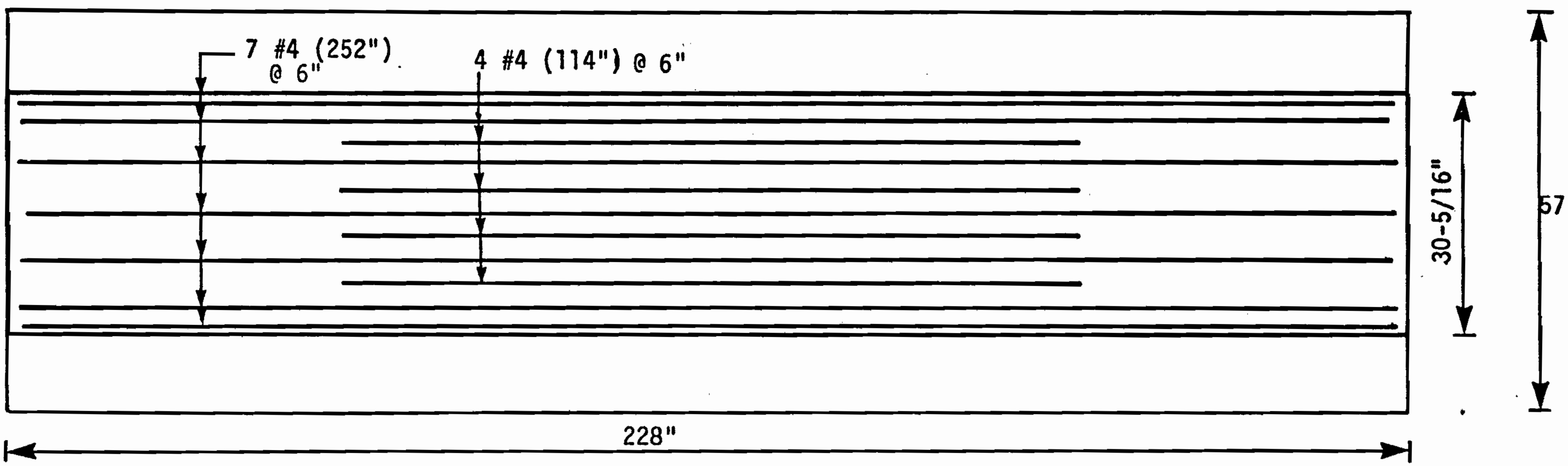

FIG. 2.3 DETAILS OF BOTTOM SLAB REINFORCEMENT

(ALSO SEE TABLE 2.3)

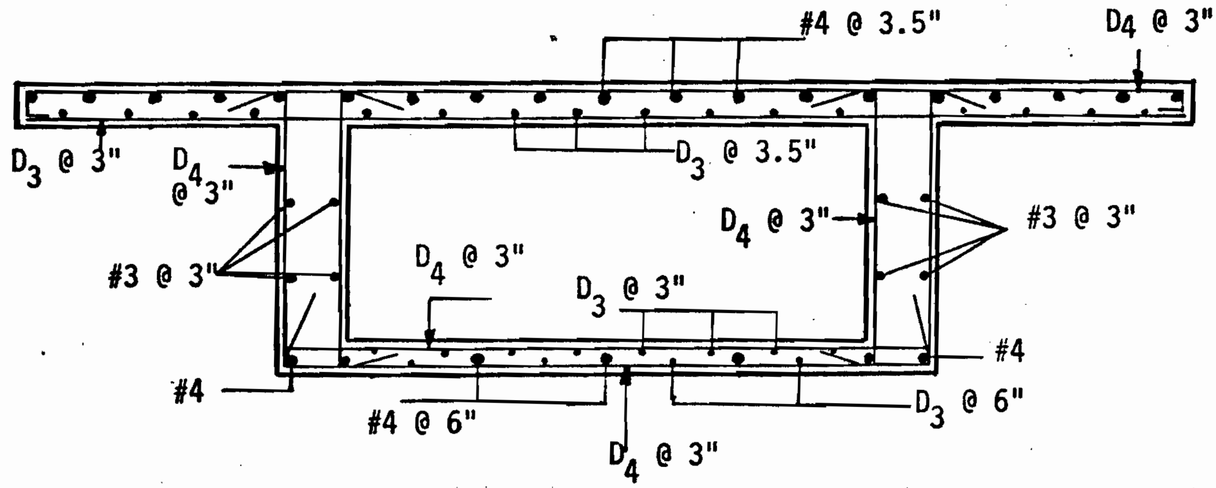

a. Support Section

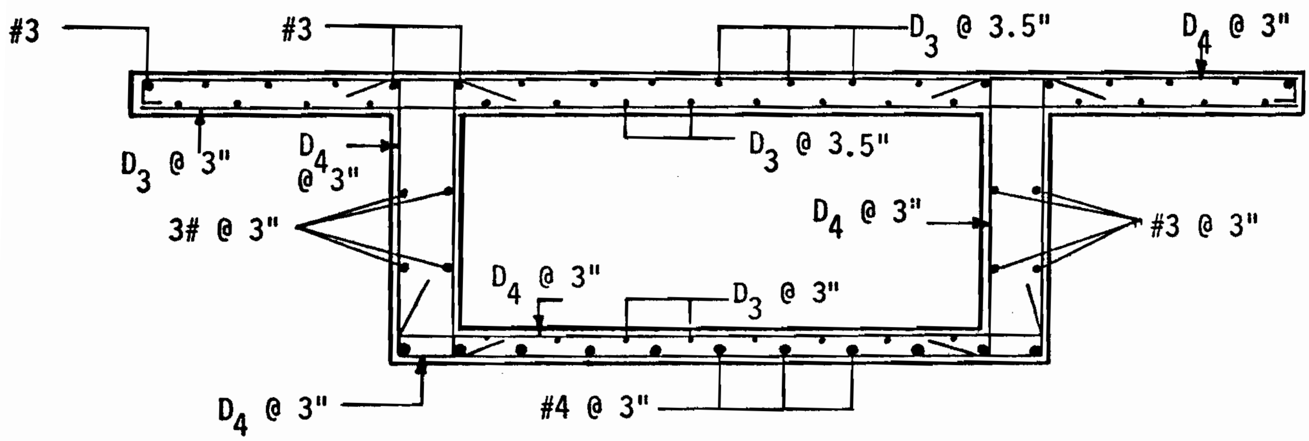

b. Midspan Section

FIG. 2.4 REINFORCEMENT DETAILS AT A TYPICAL CROSS-SECTION

(See Figs. 2.2 and 2.3, also Table 2.3)

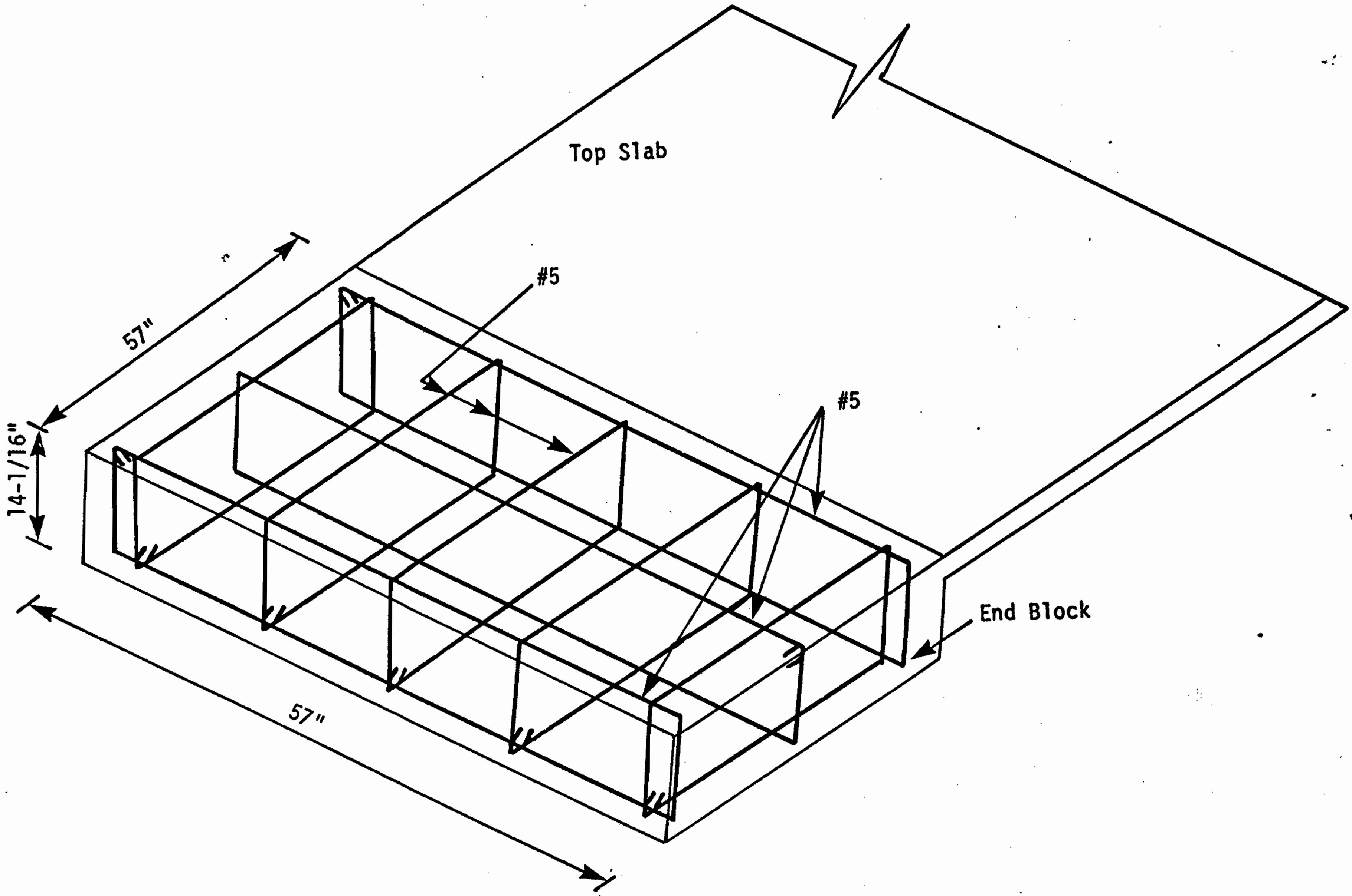

FIG. 2.5 REINFORCEMENT DETAILS FOR THE END BLOCK

(ALSO SEE TABLE 2.3)

the laws of similitude and must be readily available. While it is possible to use finer aggregates, it is not possible to use finer cements without appreciably increasing the water-cement ratio. Therefore, normal cements are used for model concrete mixes. As mentioned in the previous section, the stress-strain curve of the model concrete must be homologous to that of the prototype concrete. Besides the Poisson's ratio, the ratio of tensile strength to compressive strength and shrinkage of the model concrete must be equal to the corresponding prototype quantities [79].

Materials for structural models of reinforced concrete structures have been studied for several years at McGill University [80,81,82]. Mirza, Labonte and McCutcheon [83] investigated different model materials to simulate the prototype concrete. As a result of experiments on several mixes, they suggested preliminary designs for model concrete mixes for strengths ranging from 2500 psi to 6000 psi for use in reinforced and prestressed concrete model work. The concrete mix used in the present program was previously developed by Mirza [84] who experimented with several trial mixes using High Early Strength cement and local sands passing U.S. Sieve No. 4 and U.S. Sieve No. 8 respectively. A mixture of five grades of narrowly graded Crushed Silica Sands was blended for each batch of concrete as follows:

#10	Crushed Silica Sand	20 lbs.
#16	" " "	20 lbs.
#24	" " "	25 lbs.
#40	" " "	25 lbs.
#70	" " "	10 lbs.
	Sand	100 lbs.
	High Early Strength Cement	33.3 lbs.
	Water	13.3 lbs.

The resulting mix had water:cement:aggregate proportions of 0.55:1:3.0 by weight. These quantities provided a batch of approximately one cubic foot of model concrete mix.

2.3.2 Properties of Concrete Mix in Compression

Compression tests were performed in accordance with ASTM Standards (American Society for Testing and Materials) C 172 and C 31 (Compressive Strength of Concrete Cylinder). Eight cylinders of size 3 x 6 in. and eight cylinders of size 4 x 8 in. were cast for each stage of concrete. These cylinders were tested for compressive strength at ages of 7, 14 and 28 days and on the day of the test. Complete stress-strain curves were obtained from tests on cylinders instrumented with strain gauges. From the results obtained, evaluations were made of the compressive strength f'_c, and the modulus of elasticity of the concrete, E_c . The cylinders were moist-cured and dried a day prior to testing and were capped. The average values of the compressive strengths are given in Table 2.1; also, a typical stress-strain curve for the model concrete is shown in Fig. 2.6.

2.3.3 Properties of Concrete Mix in Flexure

The flexural tests for determining the modulus of rupture were performed in accordance with ASTM Standard C 78-59 (Flexural Strength of Concrete using Simple Beam with Third-Point Loading). Three specimens were tested during the period of the experimental program. Each beam was 6 x 6 in. in cross-section and 24 in. long, and the two loads were applied at the third points. In all cases, fracture occurred in the center section of the specimen. The results of the tensile strength tests after 28 days are given in Table 2.2 along with the values calculated using the ACI equation

$$f_t = 7.5 \sqrt{f_c'} \quad . \tag{2.3}$$

2.3.4 Steel Reinforcement

The principal characteristics of the prototype steel which should be simulated in reinforced concrete models are the following:

1 - yield and ultimate strength for tension and compression,

2 - shape of the stress-strain curve,

3 - ductility,

4 - bond characteristics at the steel-concrete interface.

TABLE 2.1

Compressive Strength of the Model Concrete Mix

Structural element	Age (days)	Compressive Strength 3 x 6" cylinder psi	Compressive Strength 4 x 8" cylinder psi	$E_c=57000\sqrt{f'_c}$ psi	$E_c=w^{1.5}33\sqrt{f'_c}$ psi
Lower slab	7	2886	2878	4.03×10^6	4.36×10^6
	14	3530	3300		
	28	4500	4600		
	day of testing	5230	5100		
Webs	7	3112	3010	4.03×10^6	4.36×10^6
	14	3680	3600		
	28	4600	4400		
	day of testing	5110	5020		
Upper slab	7	2830	2900	4.03×10^6	4.36×10^6
	14	3890	3750		
	28	4600	4780		
	day of testing	5075	5050		

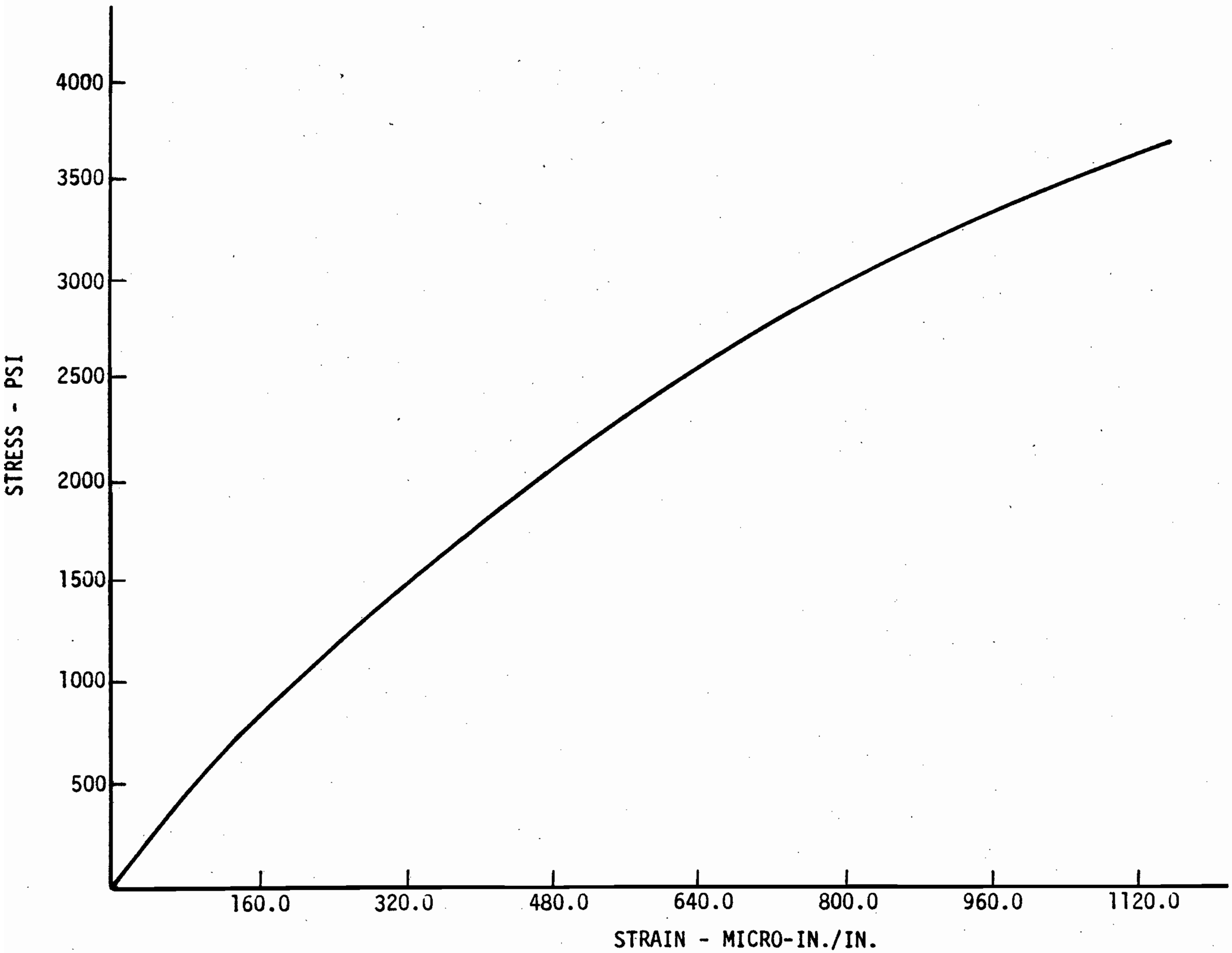

FIG. 2.6 TYPICAL STRESS-STRAIN CURVE FOR CONCRETE

TABLE 2.2

Tensile Strength of the Model Concrete Mix

Beam No.	Tensile strength f_z (psi)	f'_c (psi)	Tensile strength (ACI) $f_t = 7.5\sqrt{f_c}$
1	535	5100	535
2	400	5020	531
3	550	5050	534

It was decided to use #4 and #3 deformed steel bars as main reinforcement, and D_3 and D_4 deformed steel wires as secondary reinforcement. These deformed steel wires were initially cold drawn, and were annealed at a temperature of 1200°F for a period of one hour to reduce their yield strength from approximately 70 ksi to 38 ksi besides increasing their ductility, that is, increasing the percentage elongation available at failure.

The stress-strain curves of the deformed steel bars were determined by conducting tension tests on three randomly selected specimens for each bar type. Figures 2.7 and 2.8 show the stress-strain curves for #4 and #3 deformed steel bars and D_3 and D_4 deformed steel wires before and after annealing, respectively. Details of the reinforcing steel used in the construction of the box girder bridge are given in Table 2.3. The concrete cover was kept constant at 3/8 in. for all reinforcing steel. The spacing between the stirrups and the secondary steel was maintained constant at 3 in. centres over the entire bridge.

2.4 Description of the Testing Frame

The loading frame used in the present study was initially designed and constructed for a previous research program to study the behaviour of precast, prestressed open web bridge girders [42]. The frame was modified by adding an extra transverse beam at each end of

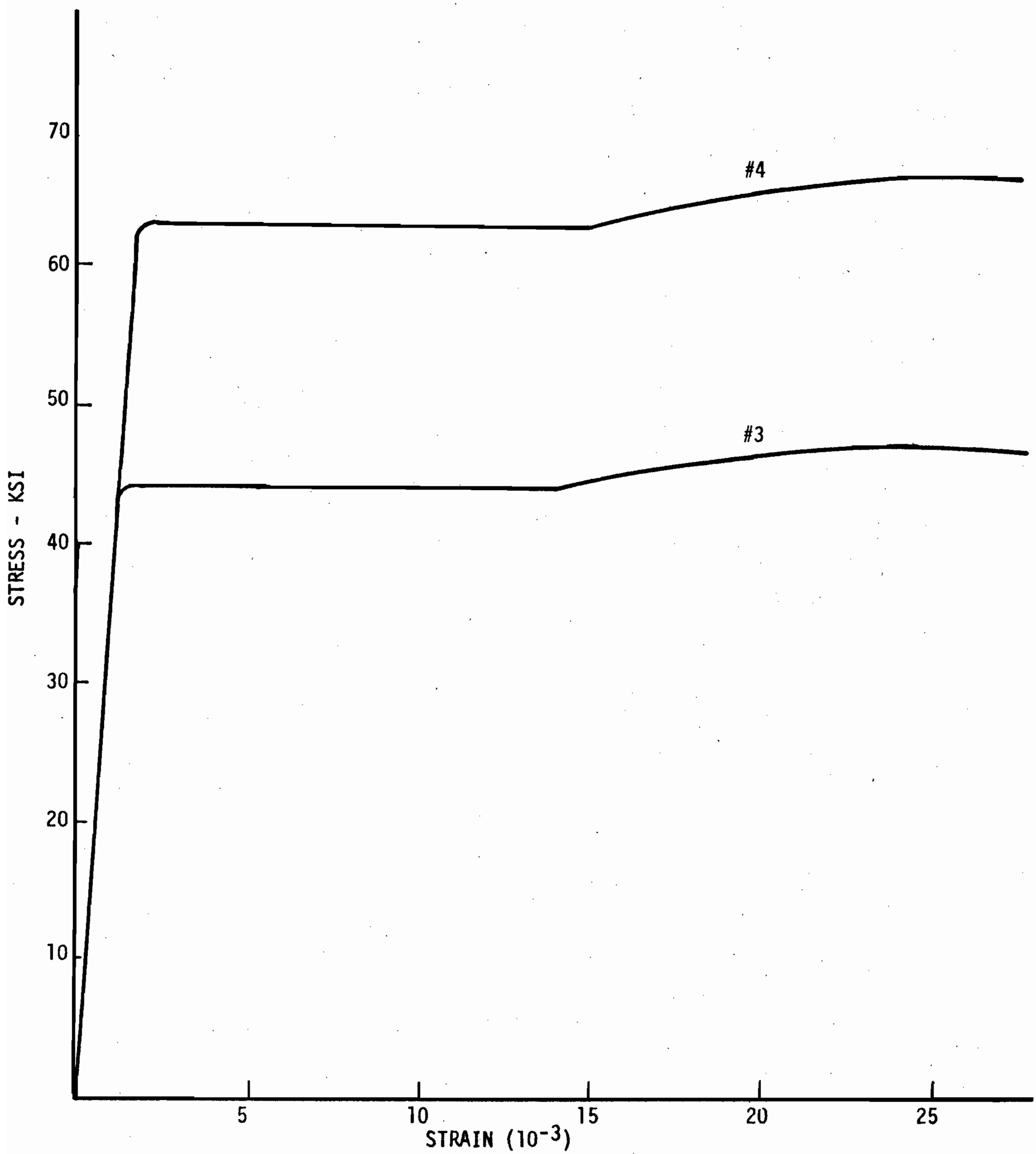

FIG. 2.7 TYPICAL STRESS-STRAIN CURVE FOR REINFORCING STEEL BARS

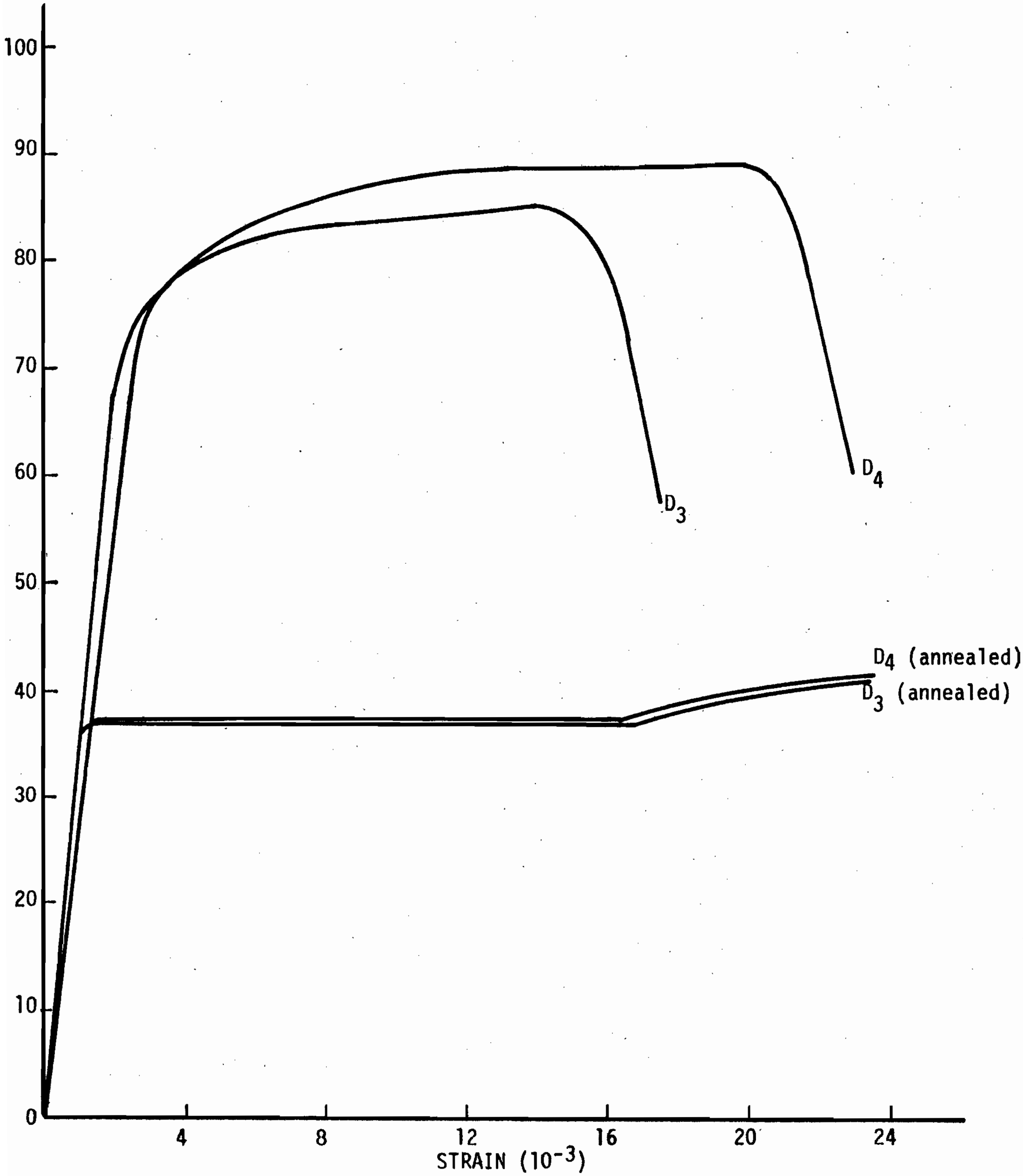

FIG. 2.8 TYPICAL STRESS-STRAIN CURVES FOR DEFORMED STEEL WIRES BEFORE AND AFTER ANNEALING

TABLE 2.3

Steel Reinforcement Details

	Shape and dimensions	No. of pieces	Kind	Purpose
1	56"; 2"; 2"; 1 5/8"	60	D_4	Transverse top reinforcement in top slab
2	56"	60	D_3	Transverse lower reinforcement, top slab
3	29 9/16"; 4"	60	D_4	Transverse top reinforcement, lower slab
4	160"	4	#4	Bottom longitudinal reinforcement
5	260"	6	#4	Bottom longitudinal reinforcement
6	140"	28	D_3	Secondary longitudinal steel, top slab
7	260"	6	#3	Longitudinal steel in top slab
8	110"; 6"	20	#4	Top longitudinal reinforcement
9	80"; 6"	16	#4	Top longitudinal reinforcement
10	4"; 29 9/16"; 13 5/16"	60	D_4	Stirrups
11	29"; 13 5/16"	10	#5	Stirrups for the end block
12	56"; 12"	6	#5	Stirrups for the end block
13	5"; 13 5/16"	120	D_4	Web reinforcement
14	56"; 12"	4	#5	Reinforcement of the end block

the frame to accommodate the end blocks designed to create a warping restraint condition. The testing frames assembled in the laboratory consisted of two identical 24 x 100 WF beams, 25 ft. long, placed horizontally parallel to each other. Two transverse 12 x 65 WF cross-beams, 6 ft. long, were placed at each end as supports for the end blocks. After casting the bridge and the end blocks, another two transverse 12 x 65 WF cross-beams were placed on top of the end blocks and connected to the transverse girders at the bottom by high strength bolts. The high strength bolts were designed to resist the longitudinal and transverse moments thus creating a fixed ended condition. They were embedded in the end block and connected the lower and the upper transverse beams. Fig. 2.9 shows this connection. The loading frame consisted of two identical, vertical frames attached to the horizontal 24 x 100 WF beams at its midspan. Each loading frame consisted of two vertical 12 x 65 WF beams, 6 ft. long, supporting two horizontal hollow sections, fabricated using two 15 x 40 channel sections welded together. Figure 2.10 shows the loading frame as connected to the tested frame. Four concrete blocks 18" x 18" x 24" were used to support the horizontal girders of the testing frame which were levelled properly.

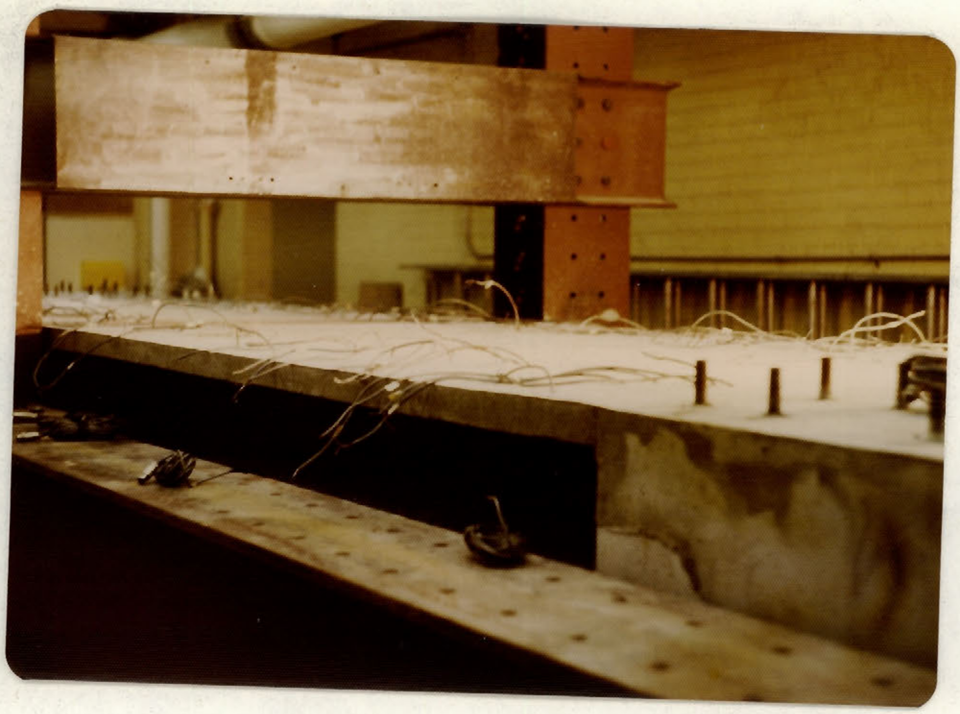

(a) Bridge model (construction just completed) and the loading frame

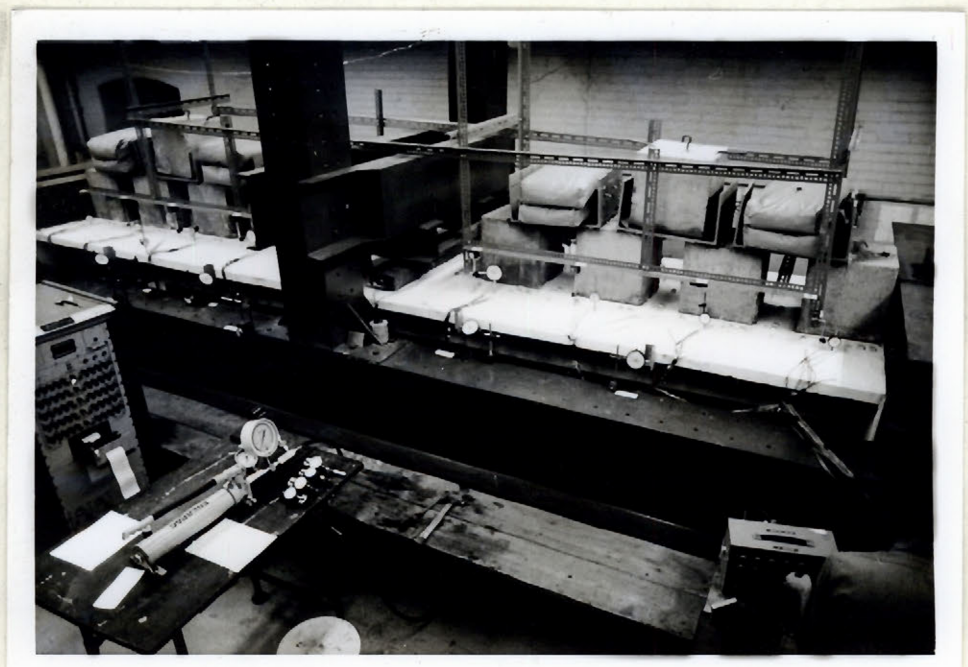

(b) Bridge model under test (concrete block and sand bags were used for prototype dead load simulation

FIG. 2.9 BRIDGE MODEL

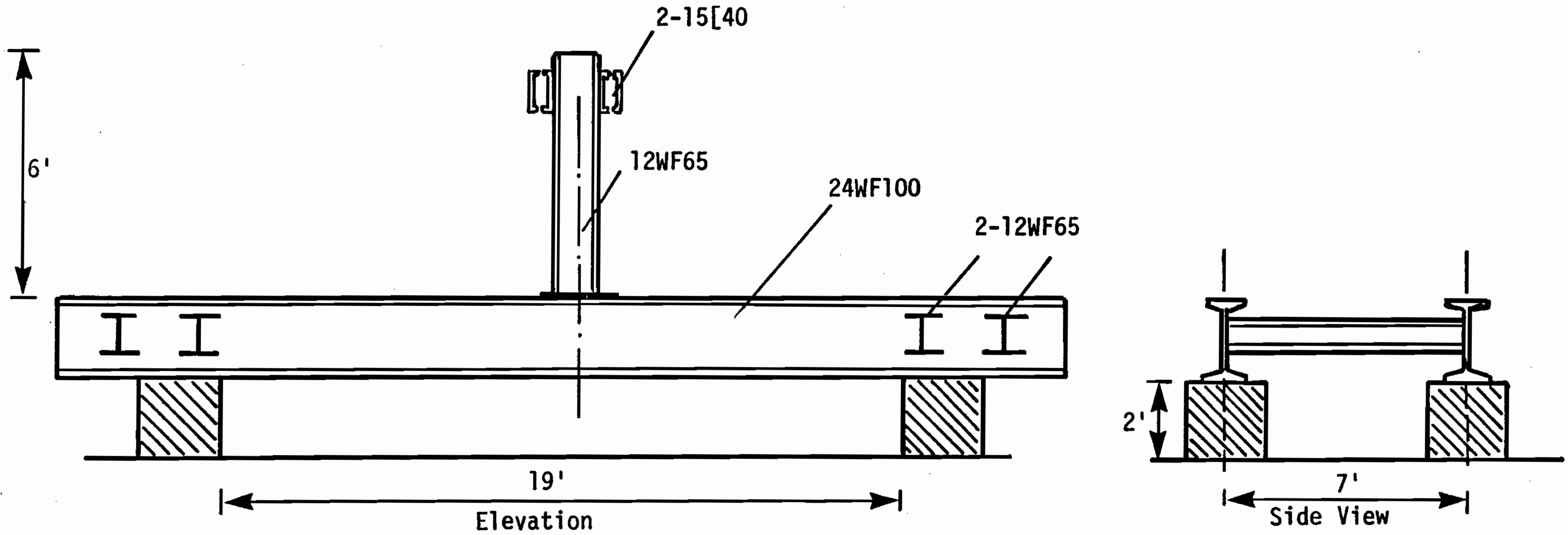

FIG. 2.10 TESTING FRAME DETAILS

2.5 Bridge Construction, Schedule and Casting of Concrete

The construction of the box girder bridge consisted of the following operations:

1. Construction of the formwork of the entire box girder bridge.
2. Preparation of the lower slab reinforcement and the web reinforcement, and installing and waterproofing the strain gauges on this reinforcement.
3. Casting and curing of the lower slab and one-third of the concrete end blocks.
4. Preparation of the formwork for the webs and longitudinal reinforcement in webs.
5. Casting and curing the webs in addition to the second third of the end blocks.
6. Filling the box section with silica sand and three steel billets.
7. Preparation of the formwork for the top slab, and finishing the longitudinal and transverse steel reinforcement for the top slab, and installing and waterproofing the strain gauges on this reinforcement.
8. Casting and curing of the top slab together with the last third of the end block and finishing the surface of concrete.
9. Placing the upper transverse beams (12 x 65 WF) on the top side of each end block and connecting them to the high strength steel bolts.

10. Placing the concrete blocks and the four steel billets on the top to compensate for the prototype dead load as shown in Fig. 2.11.

The concrete was conveyed from the mixer using a wheel barrow and was deposited, starting from one end of the box girder bridge working to the other end in short lengths to avoid any air pockets in the concrete. A special hopper was used to pour concrete uniformly into the webs to avoid any voids or honeycombing in the concrete. Before casting the webs and the top slab, the old concrete of the lower slab and the webs were cleaned by a steel brush and water to improve the bond between the old and new concrete. The concrete was compacted by using a needle vibrator. The concrete in each stage was cured for a period of one week by covering it with wet burlap and sprinkling it with water.

2.6 Removal of Formwork

Two weeks after the casting of the top slab, the formwork of the side cantilevers and the webs was removed and the five steel cross-beams which were acting as a temporary support for the formwork were removed. The bridge was painted with a white wash for observation of crack formation and propagation.

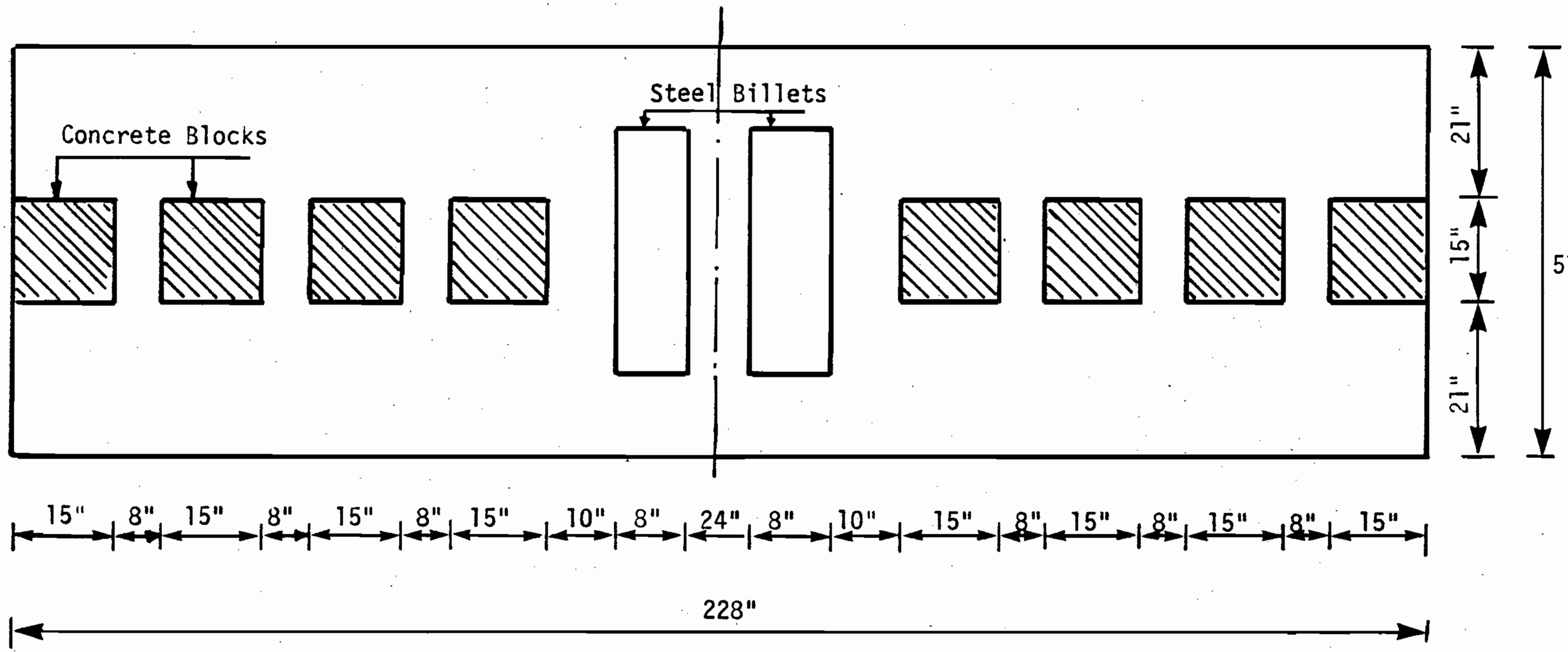

FIG. 2.11 LOCATIONS OF CONCRETE BLOCKS AND STEEL BILLETS ON THE TOP SLAB

2.7 Instrumentation

2.7.1 General

The experimental study of the bridge included the following measurements: steel and concrete strains on the top and bottom slabs and both webs, displacements of both webs and the tips of both cantilever slabs in the x, y and z directions, and rotations at different locations along the span of the bridge as well as across the box section.

2.7.2 Basic Measurements

The following measurements were made for each load stage:

2.7.2.1 Load

The load was applied using hydraulic jacks and measured directly from the dial gauges attached to them.

2.7.2.2 Deflections

The dial gauges used to measure the deformations were attached to an independent frame suspended from the ceiling of the laboratory. These gauges were placed at 23 inches on centre throughout the span of the tested bridge over both webs as well as at the ends of the cantilever slabs (Figs. 2.12, 2.13, 2.14). The dial gauges used had divisions of 10^{-3} in. and 10^{-5} in. for measurement of z and x and y displacements, respectively.

To check and measure the deformation within the box section at midspan and quarter span sections, a piano wire was attached to the

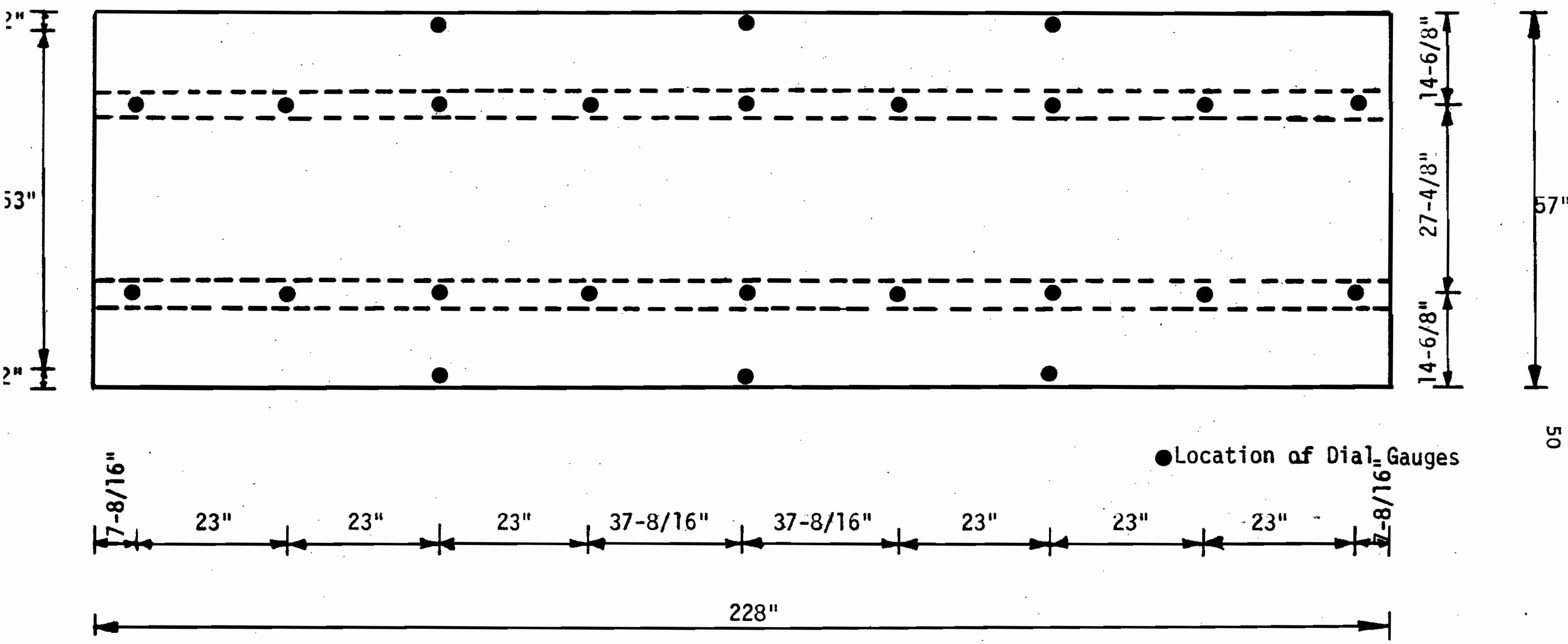

FIG. 2.12 DETAILS OF DIAL GAUGES FOR MEASURING VERTICAL DEFLECTIONS OF TOP SLAB

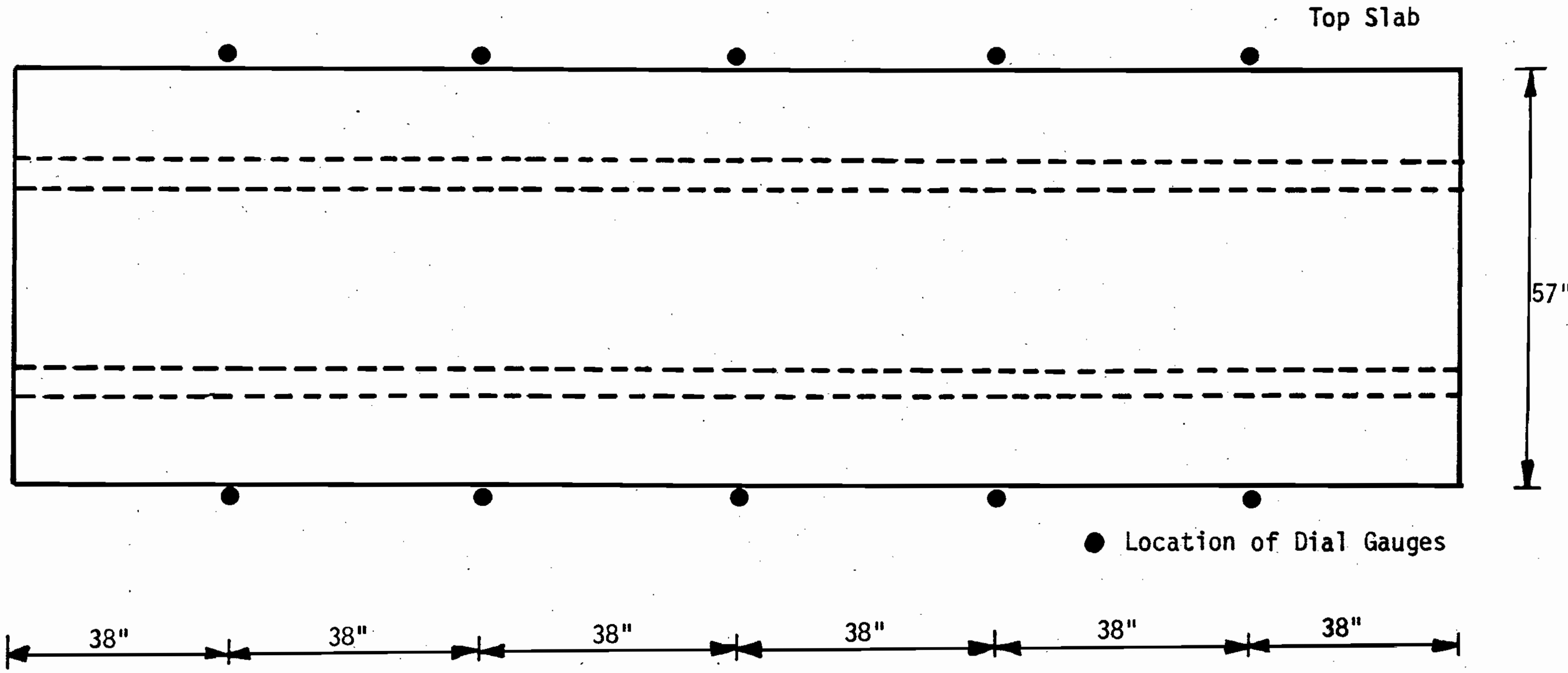

FIG. 2.13 DETAILS OF DIAL GAUGES FOR MEASURING LATERAL DISPLACEMENT OF TOP SLAB

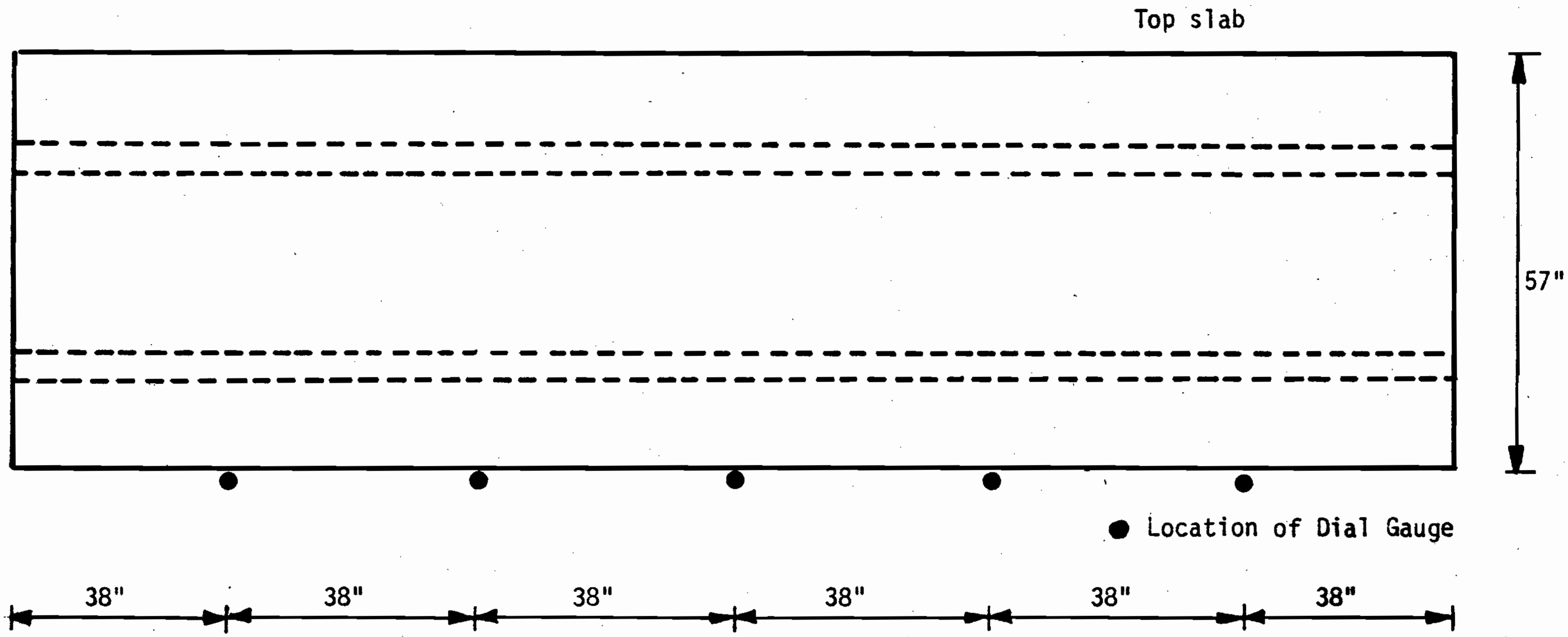

FIG. 2.14 DETAILS OF DIAL GAUGES FOR MEASURING LONGITUDINAL DISPLACEMENT OF TOP SLAB

lower corner of the box section at these locations and connected to a dial guage from the other end (least count = 10^{-5} in.). From the vertical and horizontal deflection readings at these positions, the distorsion within the box section was obtained. Figure 2.15 shows the details of the piano wire-dial guage arrangement.

2.7.2.3 Strains

Steel strains were measured using 155 PL-5-11 electrical strain gauges, and the concrete strains were measured by 100 mechanical strain gauges of 4 in. gauge length in addition to the 40 PL-5-11 electrical strain gauge.

The technique used for preparing the reinforcing bars for strain gauge application and for sealing the gauge assemblies followed, in general, the recommendations of the manufacturer. The reinforcing bars were ground and filed smooth in the regions where the gauges were to be located, cleaned with acetone, and dressed with a metal conditioner and neutralizer. The gauges were then applied by using an epoxy adhesive that cured at room temperature. Terminal tabs were applied at the same time, and the gauges were connected to these tabs.

After the lead cables were attached to the tabs, the gauge assemblies were waterproofed with M-Coat D which is a flexible epoxy that cures at room temperature. The assemblies were then covered with a thick layer of M-Coat G and after 24 hours were coated with a layer of M-Coat B for additional sealing and for physical protection from

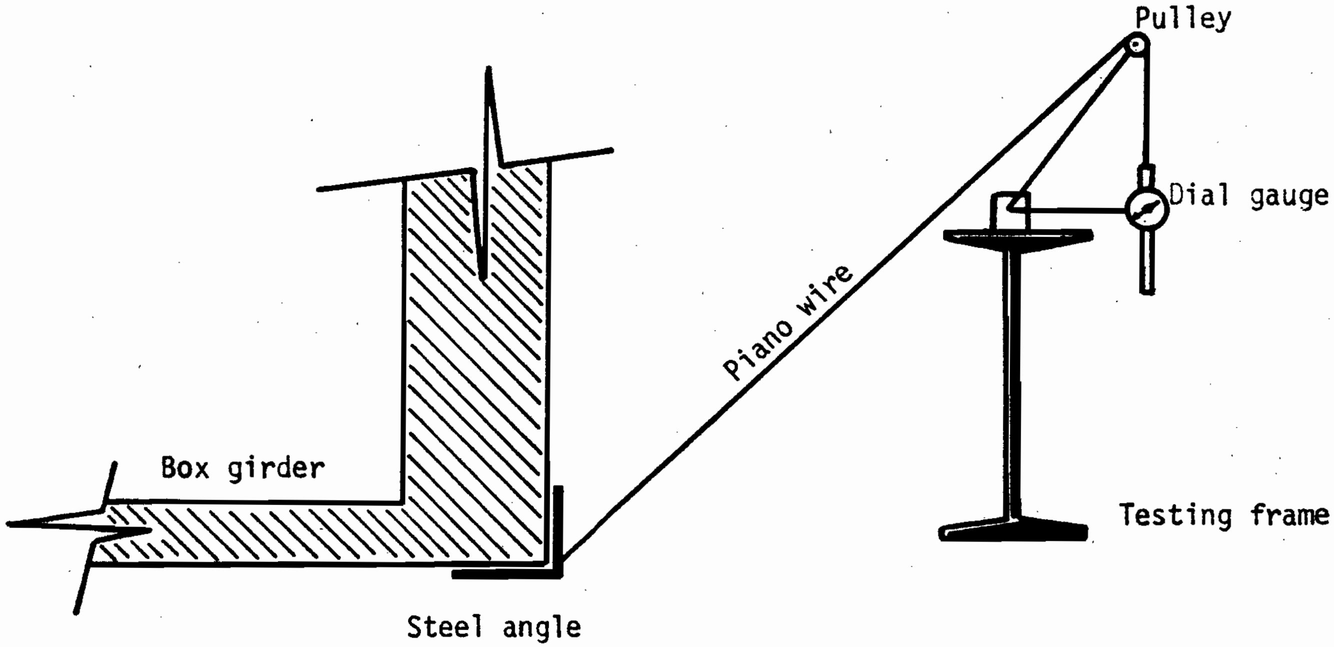

FIG. 2.15 DETAILS OF APPARATUS FOR MEASURING THE HORIZONTAL AND VERTICAL DISPLACEMENT OF LOWER SLAB

the wet concrete and the vibration equipment during casting. The preparation, the gauge application procedures, and the sealing techniques were the same for the concrete as for the reinforcing bars. Figures 2.16 to 2.20 show the location of the strain gauges on the reinforcing steel bars across the width of the box section and the length of the bridge. The mechanical strain gauges were used to measure the longidutinal and transverse concrete strain over the two webs and at the end of the cantilever slabs on the top slab at 23 in. intervals in the longitudinal direction of the bridge. The gauge length of the mechanical strain gauges was 4 in. Figures 2.21 and 2.22 show the location of the mechanical and electrical strain gauges on the bridge. All strain gauge readings were recorded and printed by means of two electronic multi-channel B & F digital strain indicators, model SY 161 Series, along with two units of switching boxes.

2.7.2.4 Angle of Twists and Slopes

The angle of twists of the box section and the web slopes relative to the horizontal were measured by means of inclinometers at 23 in. intervals along the span. These inclinometers were designed to measure these twists and slopes for gauge lengths ranging between 12 and 24 inches. It consisted of a dial gauge connected to an aluminum bar with a precision level bubble and a screw to adjust the level of the aluminum bar. The gauge length used in the present study was 12 in. The advantage of this device is that it can be used at different

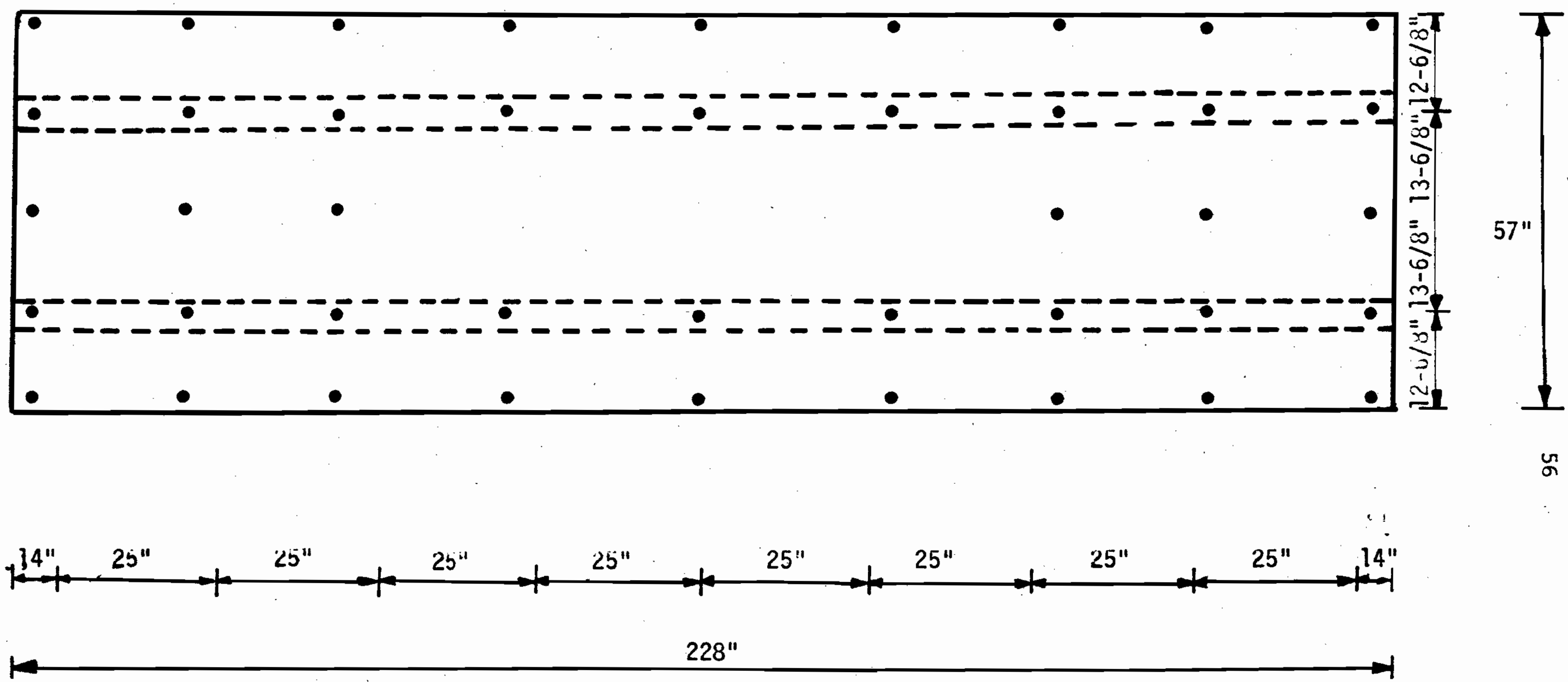

FIG. 2.16 DETAILS OF STRAIN GAUGES ON TOP SLAB LONGITUDINAL STEEL

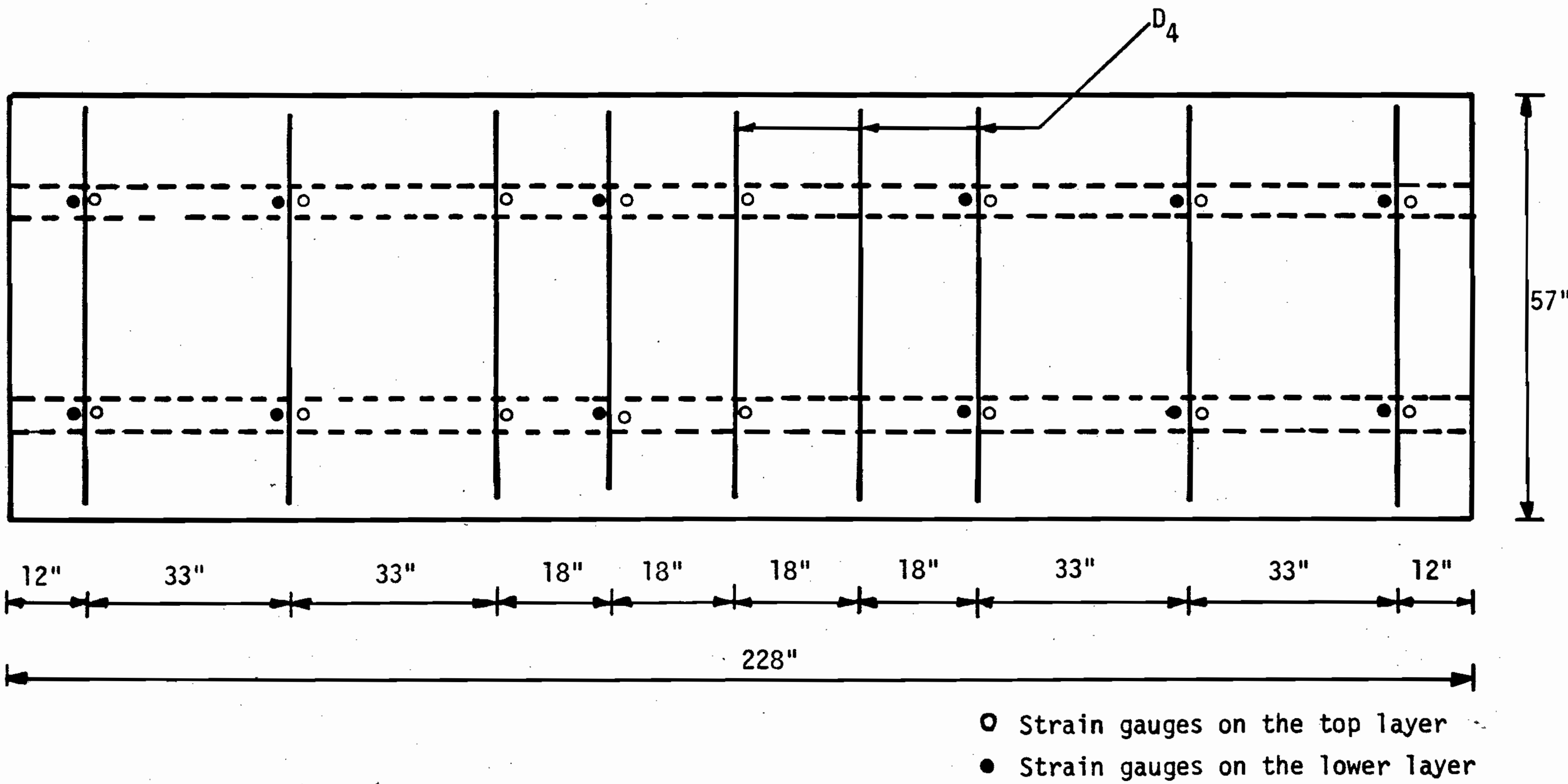

FIG. 2.17 DETAILS OF STRAIN GAUGES ON THE TOP SLAB TRANSVERSE REINFORCEMENT

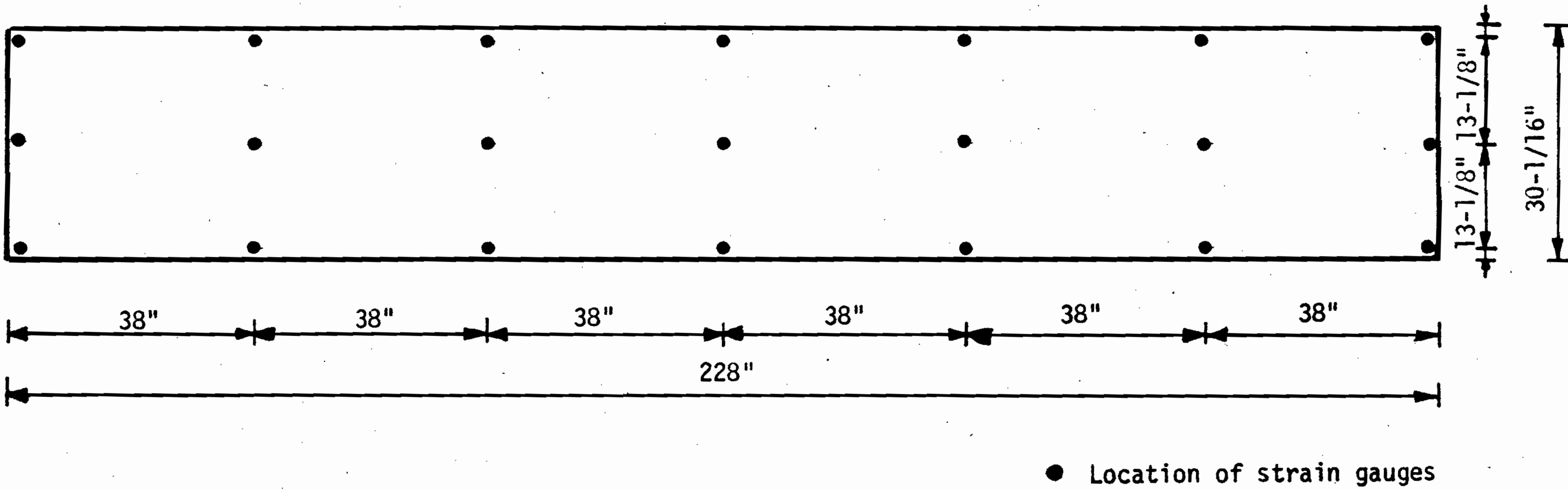

FIG. 2.18 DETAILS OF STRAIN GAUGES ON THE LOWER SLAB LONGITUDINAL STEEL

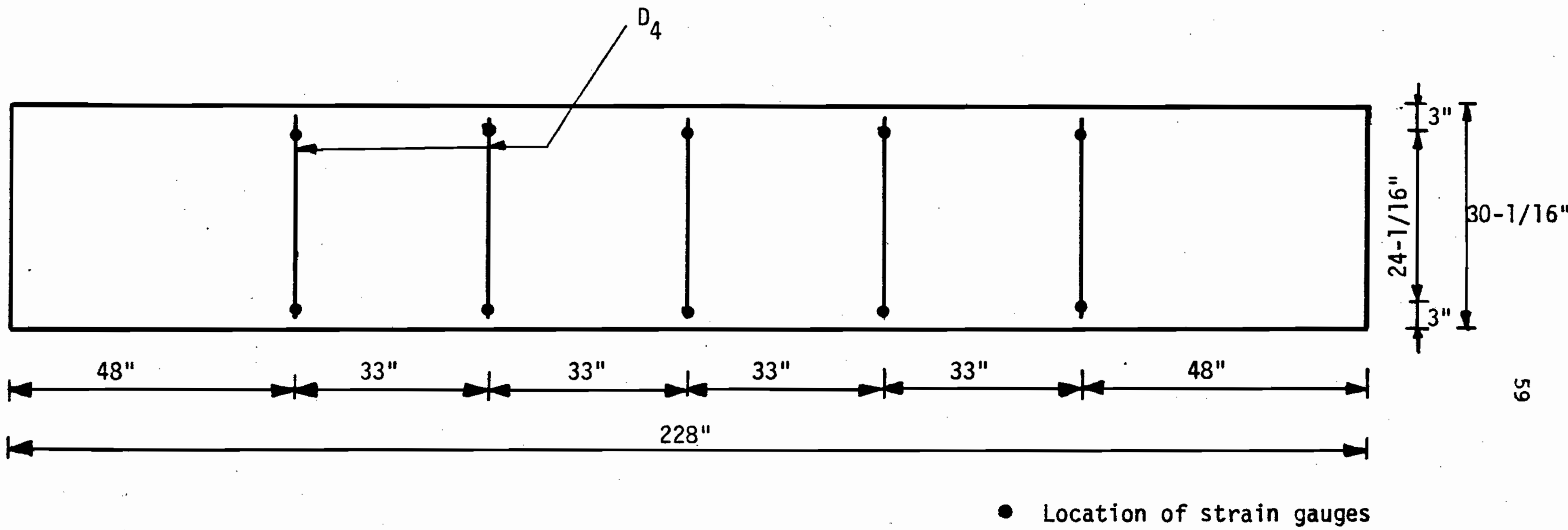

FIG. 2.19 DETAILS OF STRAIN GAUGES ON THE LOWER SLAB TRANSVERSE STEEL

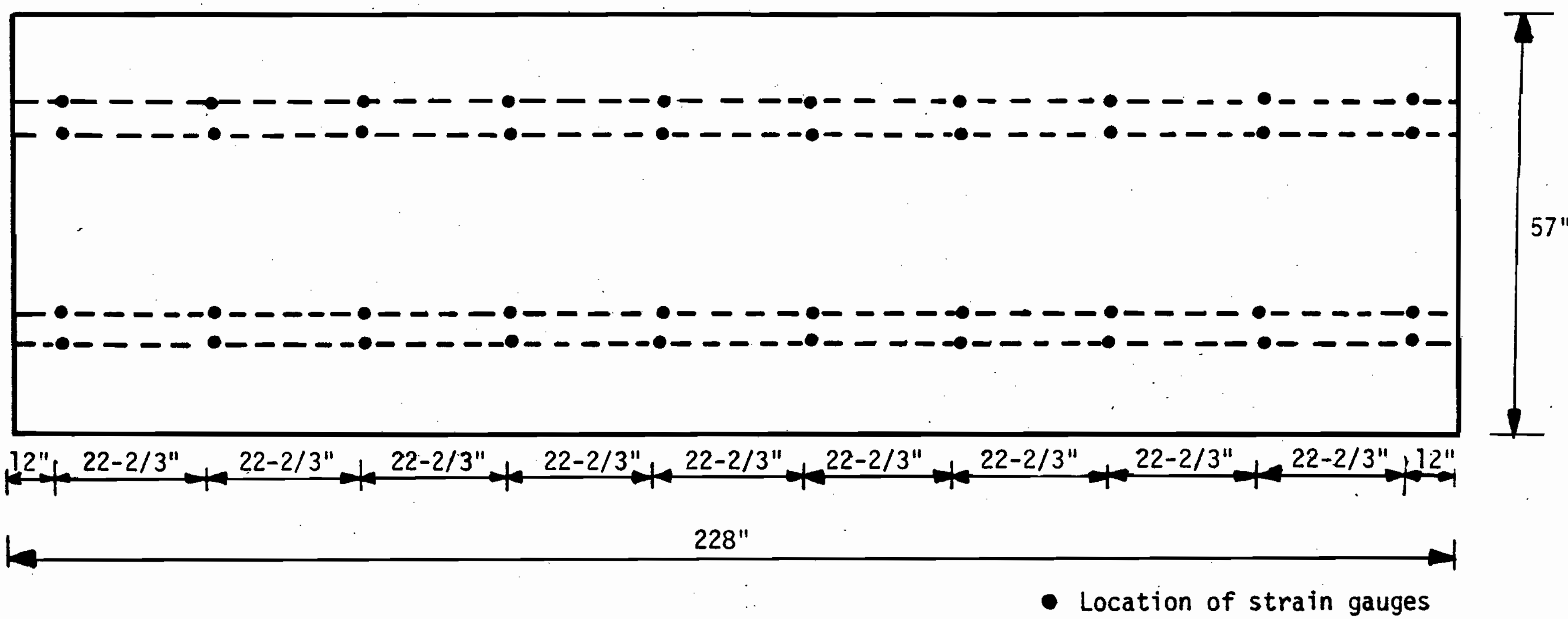

FIG. 2.20 DETAILS OF STRAIN GAUGES ON THE STIRRUPS (MID HEIGHT OF STIRRUP)

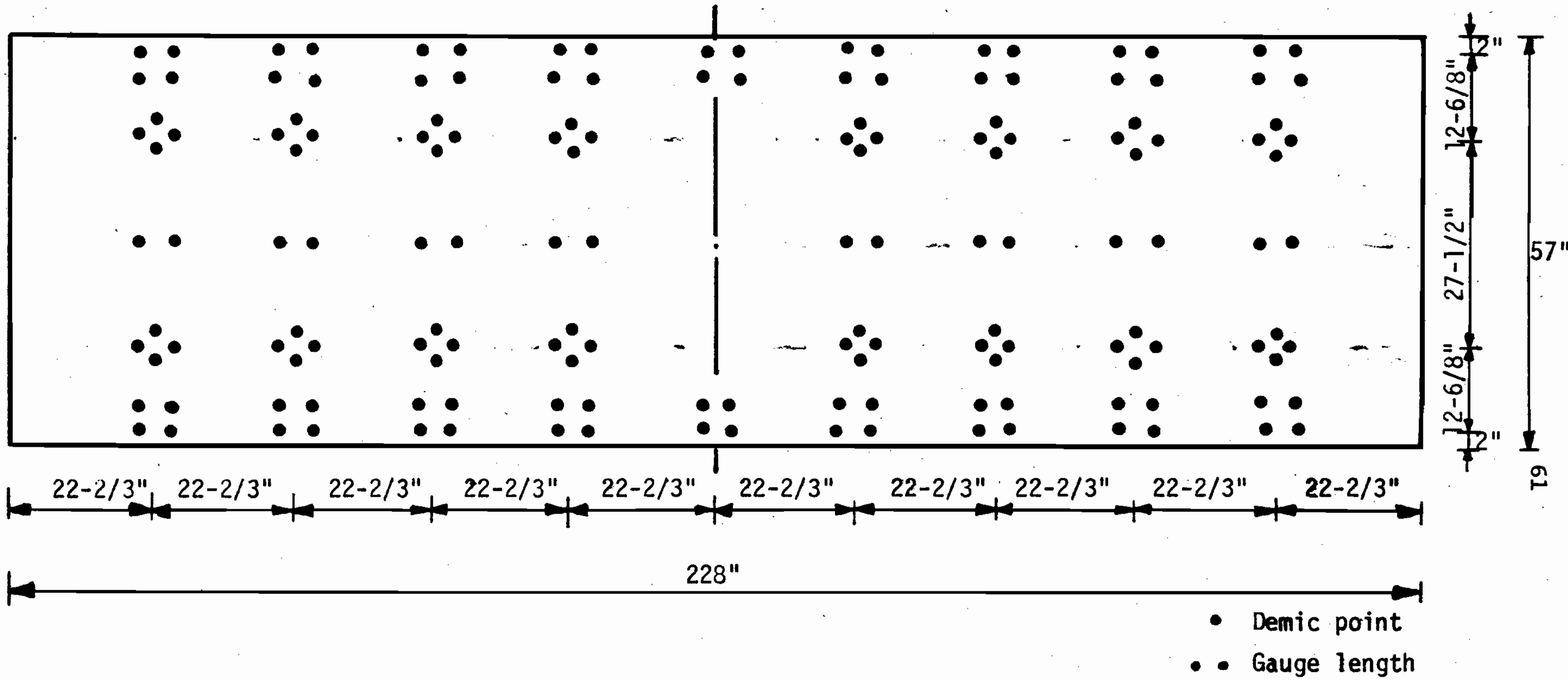

FIG. 2.21 DETAILS OF MECHANICAL STRAIN GAUGES ON THE TOP SLAB SURFACE

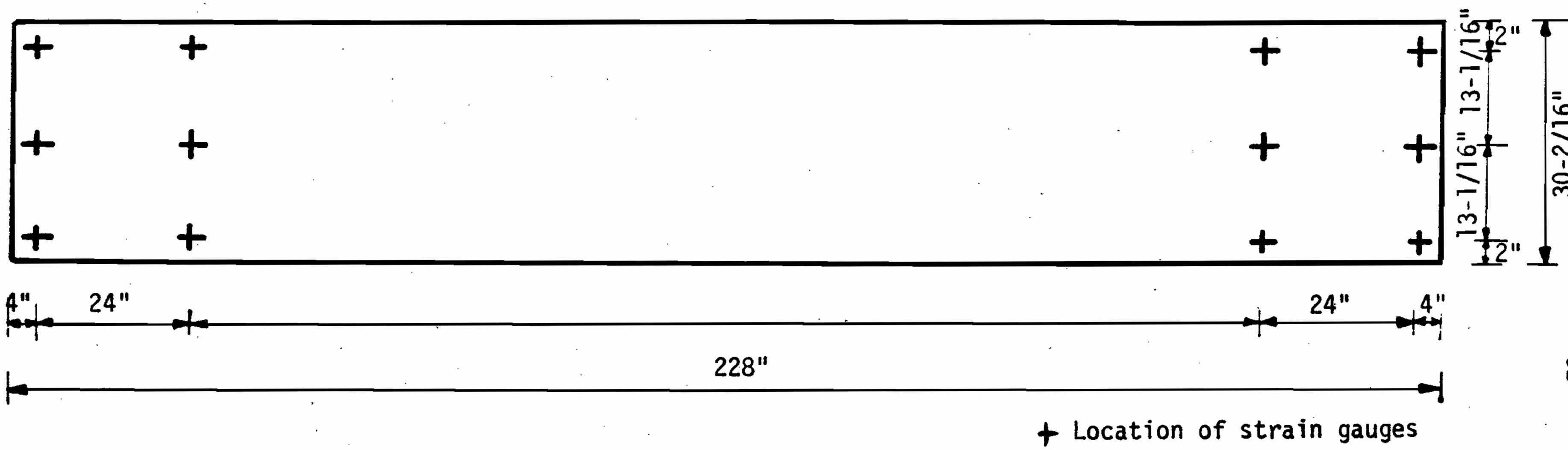

FIG. 2.22 DETAILS OF STRAIN GAUGES ON THE CONCRETE SURFACE OF THE LOWER SLAB

locations for measuring both the twist and the slope. Figure 2.23 shows the details of this inclinometer and its components. Figures 2.24 and 2.25 show the locations for measurements of twists and slopes on the top slab.

2.7.2.5 Crack Widths

Crack widths were measured at the appropriate load stages with a crack microscope to an accuracy of 0.05 mm.

2.8 Test Program

The experimental program was divided into the following three phases:

1. Dead load alone.
2. Two symmetrical point loads placed over the two webs at the midspan section (within the elastic range).
3. A concentrated load placed at the midspan section over one of the webs for the ultimate load test.

It was decided to accommodate a wide range of loading stages for each phase to determine the load-deformation relationship and response for each loading type. The load for each phase was increased at a steady rate, and was kept constant by adjusting the control valve of the jacks while the readings were being taken. On the average, each load stage required about 35 minutes for all observations.

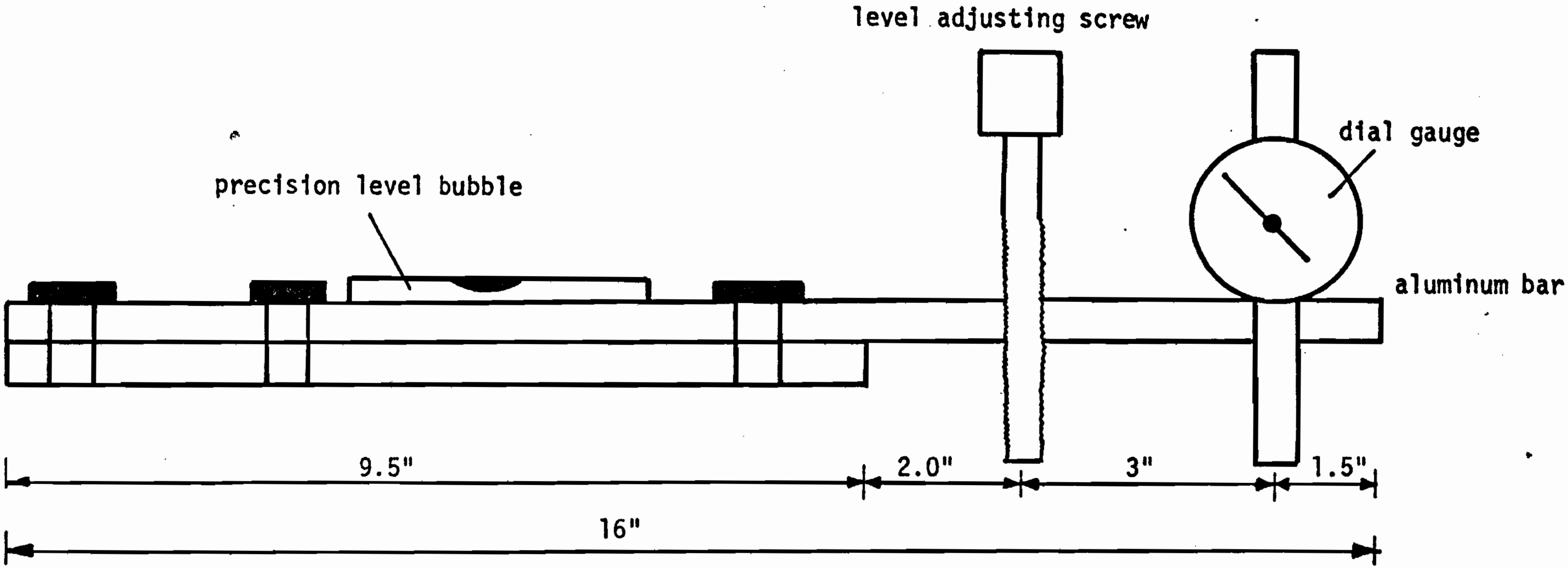

FIG. 2.23 DETAILS OF THE INCLINOMETER USED FOR MEASURING ROTATIONS AND TWISTS

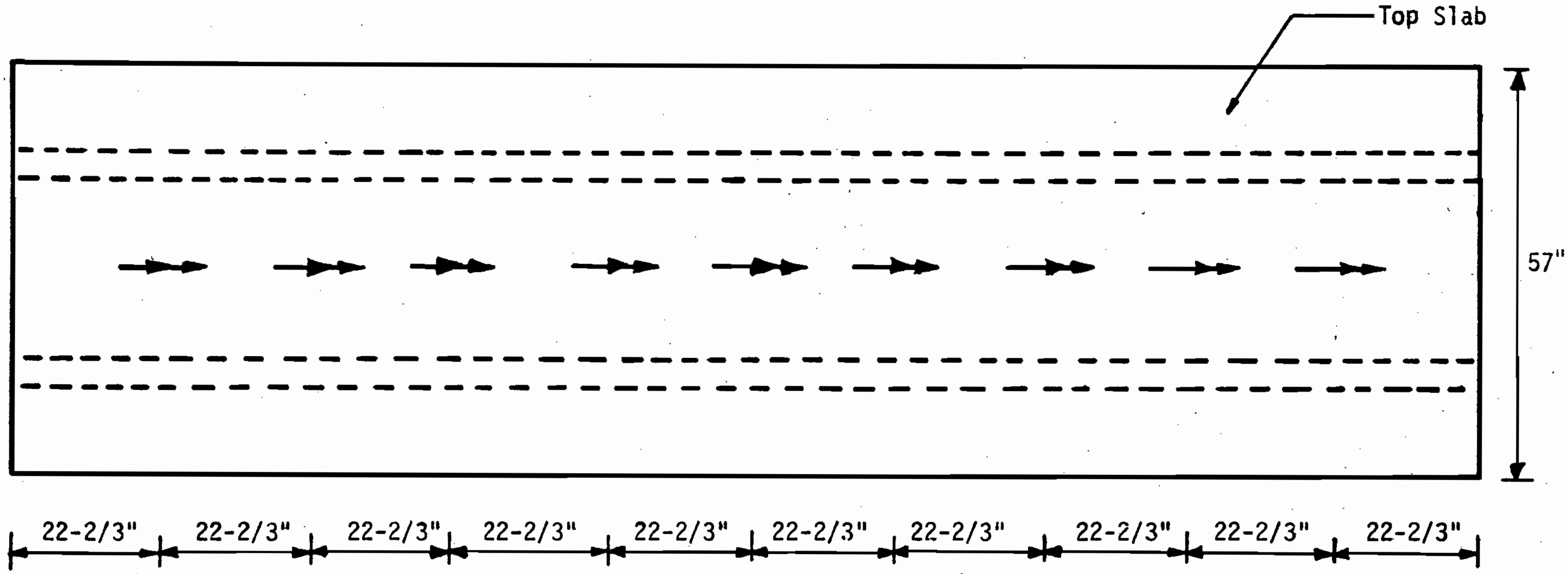

FIG. 2.24 LOCATIONS FOR MEASURING TWISTS OF THE BOX SECTION

The first phase consisted of the effects of the dead load alone. The strains and deformations of this phase were taken as the differences in the recorded readings before and after the removal of the five steel beams which were acting as a temporary support for the formwork.

The second phase consisted of ten loading increments of 1.3 kips each, up to a total load value of 13 kips, and it was removed in four instalments of 3 kips each.

The third phase consisted of fourteen loading increments of 4.2 kips each, up to a total load value of 59 kips; it was removed in five instalments of 15 kips each.

In the last stage of this phase, at a load value of 55 kips, a 1/4 in. deep local punching shear failure occurred in the top slab beneath the ram. The test was stopped at this stage and the applied load was removed in decrements as mentioned before. The damage was not serious, and it was therefore decided to repair the hole by filling it with a gypsum capping material. After fixing the hole, a 6 x 6 x 1 in. steel plate was used to cover the damaged location, and the bridge was reloaded again from zero load to failure. The loading increments used were 10 kips each, up to a total load value of 69 kips, and the decrements were 30 kips each. Again, at a load value of 69 kips a local punching shear failure occurred in the top slab beneath the steel plate under the ram. The depth of the hole was 1 in. The magnitudes of deflections, strains, twists and slopes were taken at this stage and the applied loading was removed.

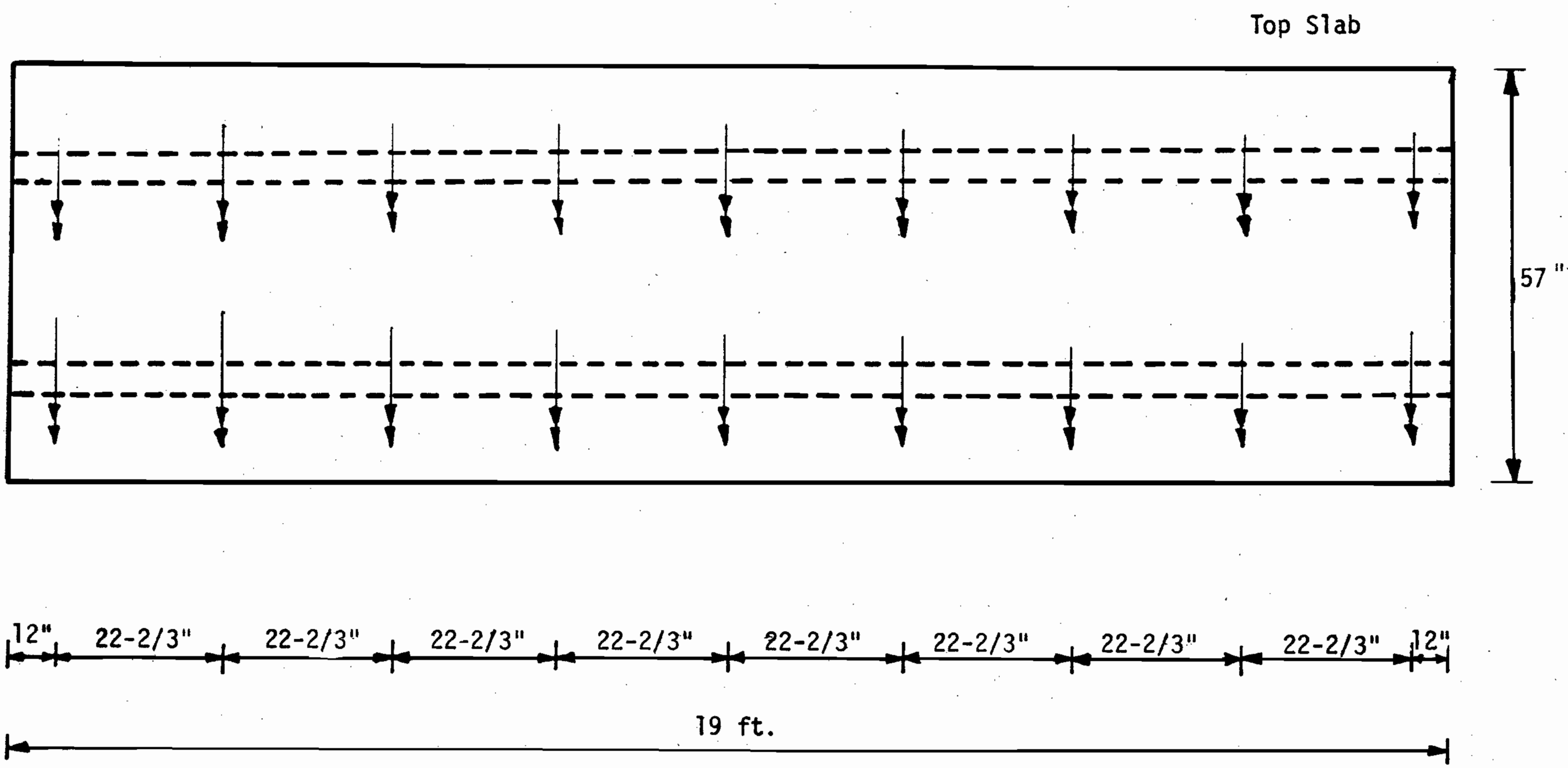

FIG. 2.25 LOCATION FOR MEASUREMENT OF SLOPES

2.9 Hydraulic Loading Jacks

Two kinds of hydraulic jacks were used to load the box girder bridge. Two 30 kips capacity jacks were used for the symmetrical loading phase, while a 100 kips capacity jack was used for the ultimate load test. The details of these hydraulic loading jacks are as follows:

Jack type	30 kips capacity (RLC-302)	100 kips capacity (RLC-1002)
Stroke (in.)	2-7/16	2-1/4
Effective area of the cylinder (in.^{2})	6.49	19.64
Maximum internal pressure (psi)	9250	10200
Outside diameter (in.)	4	6-1/2

CHAPTER 3

EXPERIMENTAL RESULTS

3.1 General

As mentioned in Chapter 2, the load tests of the bridge under investigation consisted of the following three phases:

1) Dead load

2) Symmetrical loading test (two point loads symmetrically placed over the two webs at the midspan section)

3) Unsymmetrical loading test (a point load placed over one web at the midspan section).

Wherever possible, the experimental results were compared with the values calculated from the simple beam theory [85], the Knittel method [24], the Kollbrunner and Hajdin method [86], and the method of beam-on-elastic-foundation [87]. Details of these methods and the computer program developed, including input data, output data and listing of the program, are presented in Appendix A.

3.2 Dead Load Stresses

After removal of the form work the bridge was supported on the underside by five cross-beams which were removed just before testing. The central deflection of the bridge due to its own weight was observed to be 0.144 in. The self weight of the bridge was 0.7 kips per foot, including the extra weights used for dead load compensation. It was observed that the longitudinal stresses in the top slab reinforcement were not uniform across the slab width; the maximum values occurred at the web-flange junction (Fig. 3.1). This is due to the shear lag resulting from the change in the shear deformations in the plane of flanges with respect to the longitudinal forces and therefore the resulting stresses at the web-flange junction are higher than those between the webs or at the cantilever tips. The steel stresses calculated from the measured strain values in the top slab reinforcement over the webs were approximately 20 and 30 per cent larger than the stresses at locations between the webs at midspan and at the support sections, respectively. The maximum steel stresses in the top slab reinforcements at the midspan and support sections were -2.6 ksi and 2.1 ksi respectively. Here the negative sign indicates that these stresses are compression.

As is evident from the measured strains, the longitudinal concrete stresses across the top slab were not uniform. Over the webs, they were approximately 40 to 50 per cent larger than the stress values at points between the webs or at the cantilever tips (Fig. 3.2).

The steel stresses in the lower slab reinforcement as calculated from the measured strain values showed a similar behaviour of higher stresses at the web-flange junction than at locations between the webs. This difference was 10 per cent at the support and 40 per cent at the midspan sections. As shown in Figure 3.3, the steel stresses in the

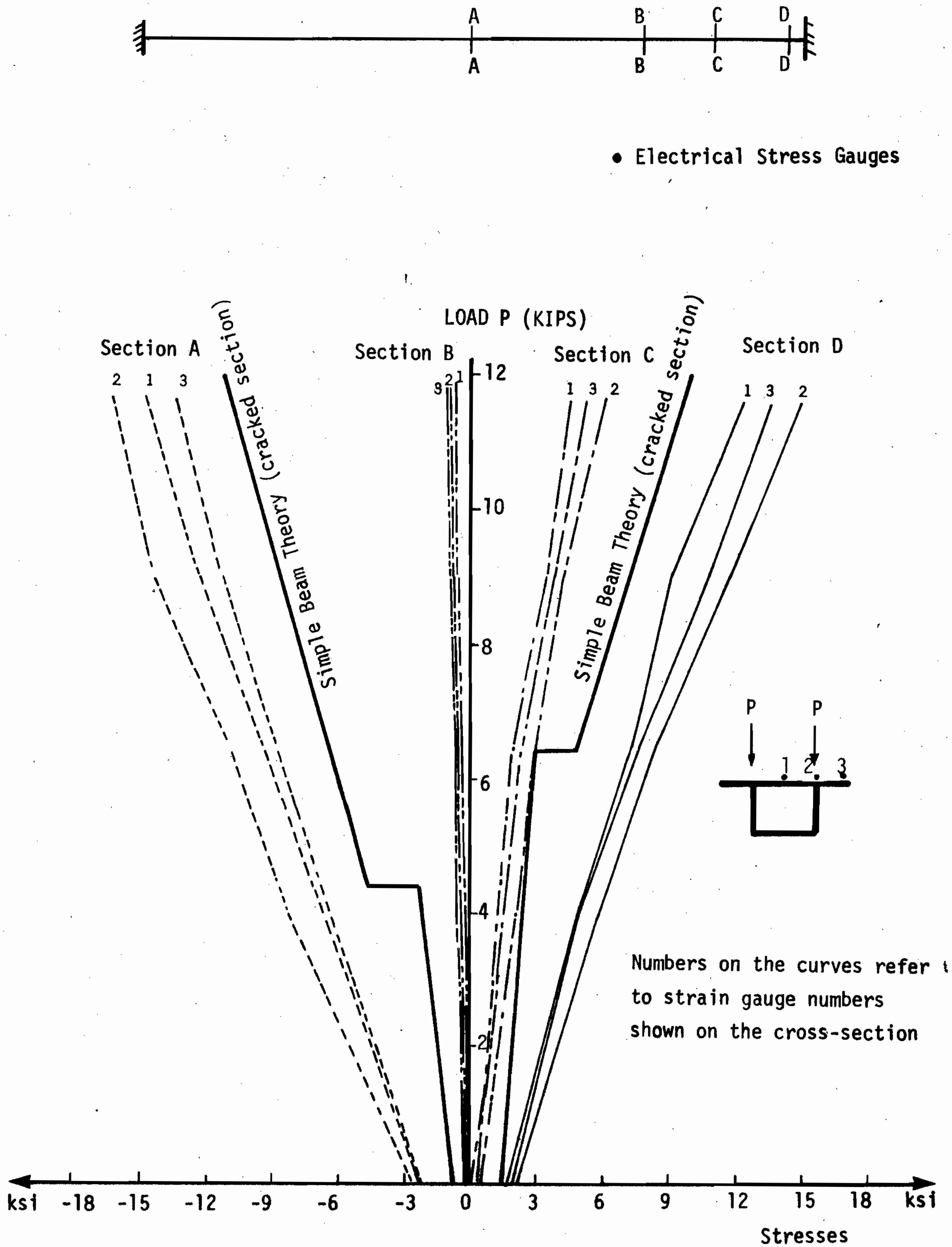

FIG. 3.1 LONGITUDINAL STRESSES IN THE TOP SLAB REINFORCEMENT (SYMMETRICAL LOADING CASE)

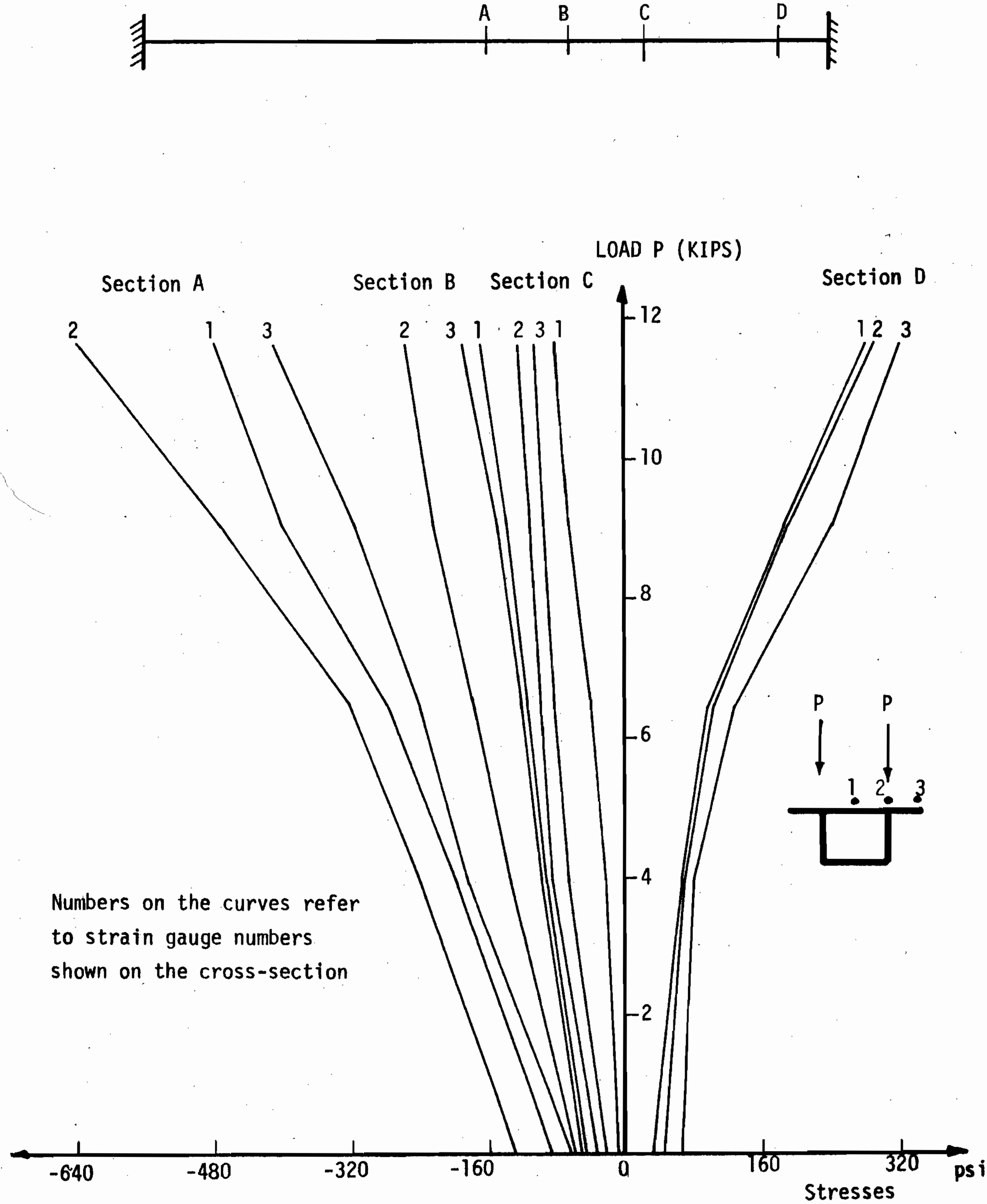

FIG. 3.2 LONGITUDINAL STRESSES IN THE TOP SLAB CONCRETE
(SYMMETRICAL LOADING CASE)

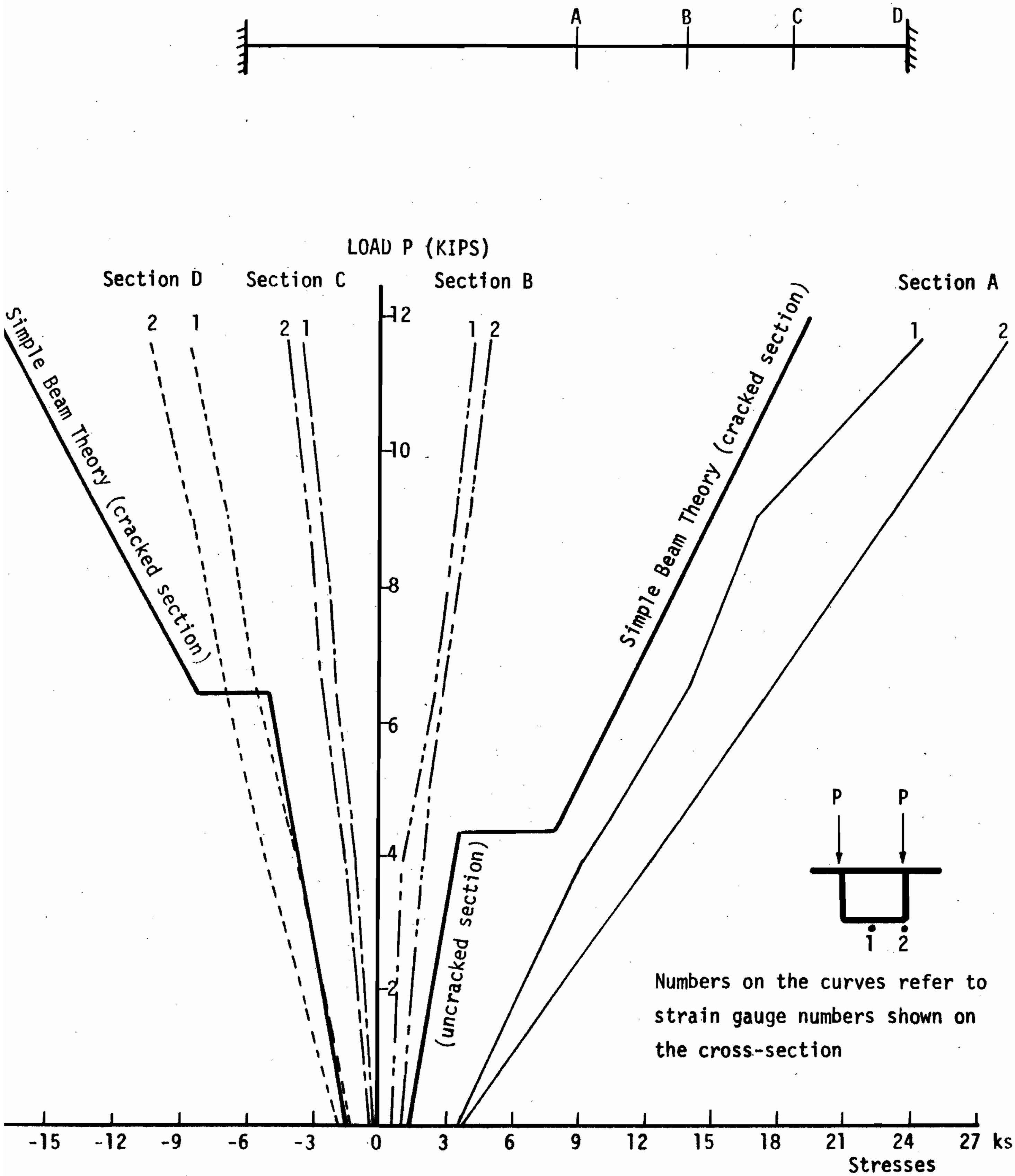

FIG. 3.3 LONGITUDINAL STRESSES OF THE BOTTOM SLAB REINFORCEMENT (SYMMETRICAL LOADING CASE)

lower slab reinforcements had maximum values of 3.6 ksi and -2.1 ksi at the midspan and support sections, respectively. The longitudinal concrete stresses in the lower slab were also generally small and were 50 per cent higher than the corresponding stress values at locations between the webs for both the support and midspan sections. The transverse steel and concrete stresses in both the top and bottom slabs throughout the bridge span were approximately 10 per cent of the corresponding longitudinal stresses at the same locations. No significant strains, and therefore stresses, were noted in the stirrups for the case of dead load alone.

3.3 Symmetrical Loading Test

3.3.1 Deflections

The load increments used in this loading case were 1.32 kips each. The experimental load-deflection curve (Fig. 3.4) shows that the bridge behaved linearly up to a load value of 4 kips on each web when cracks were first observed in the bottom slab near midspan. The tensile stresses in the concrete as calculated from the measured strain values were approximately 417 psi. Figure 3.5 shows the variation of vertical deflections along the bridge span at load values of 3.9, 7.8 and 11.7 kips. These curves represent the average deflections for the left and right webs (the difference between the two sets of deflection readings was less than 4%). As shown in Fig. 3.4, the

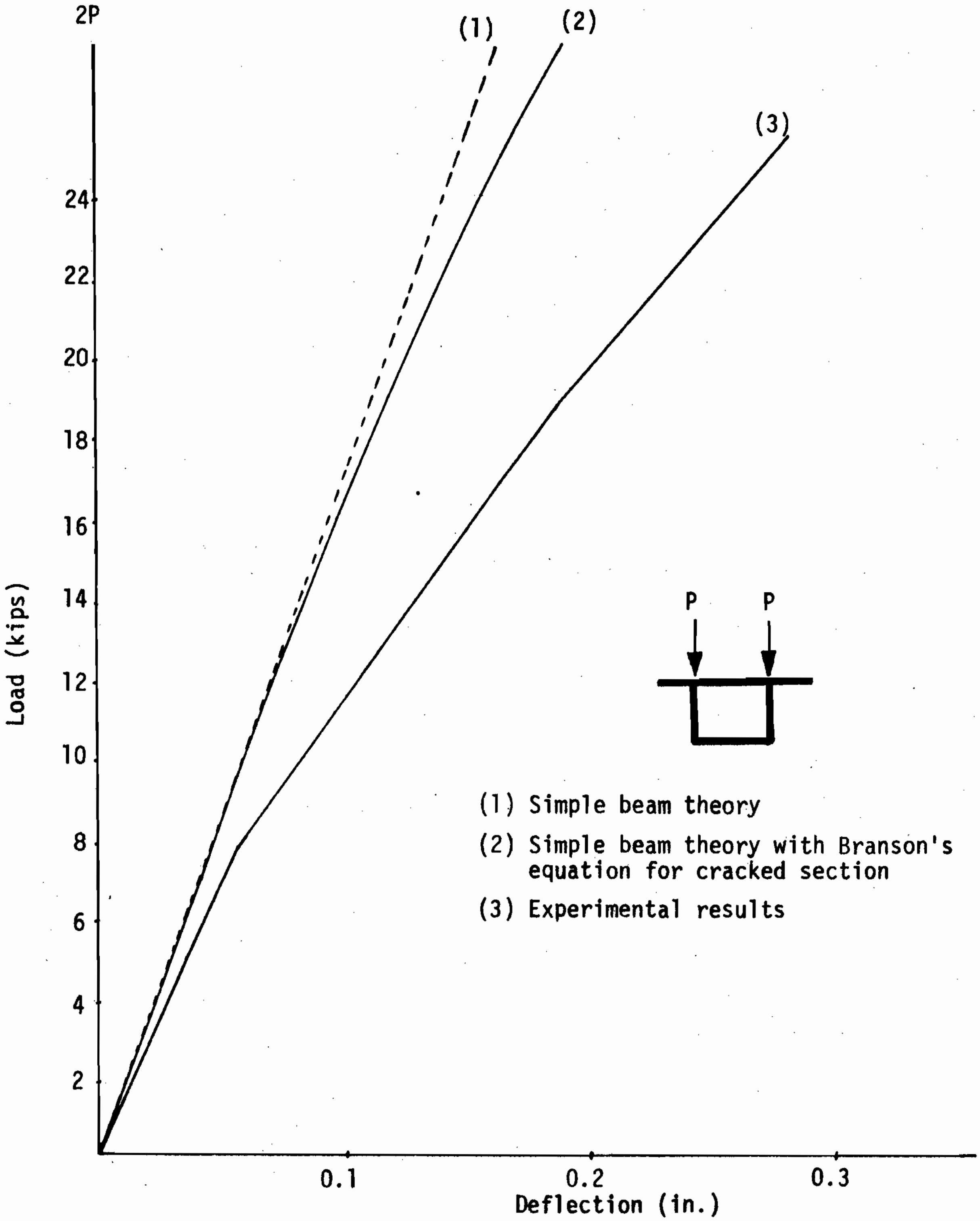

FIG. 3.4 LOAD-MIDSPAN DEFLECTION (SYMMETRICAL LOADING CASE)

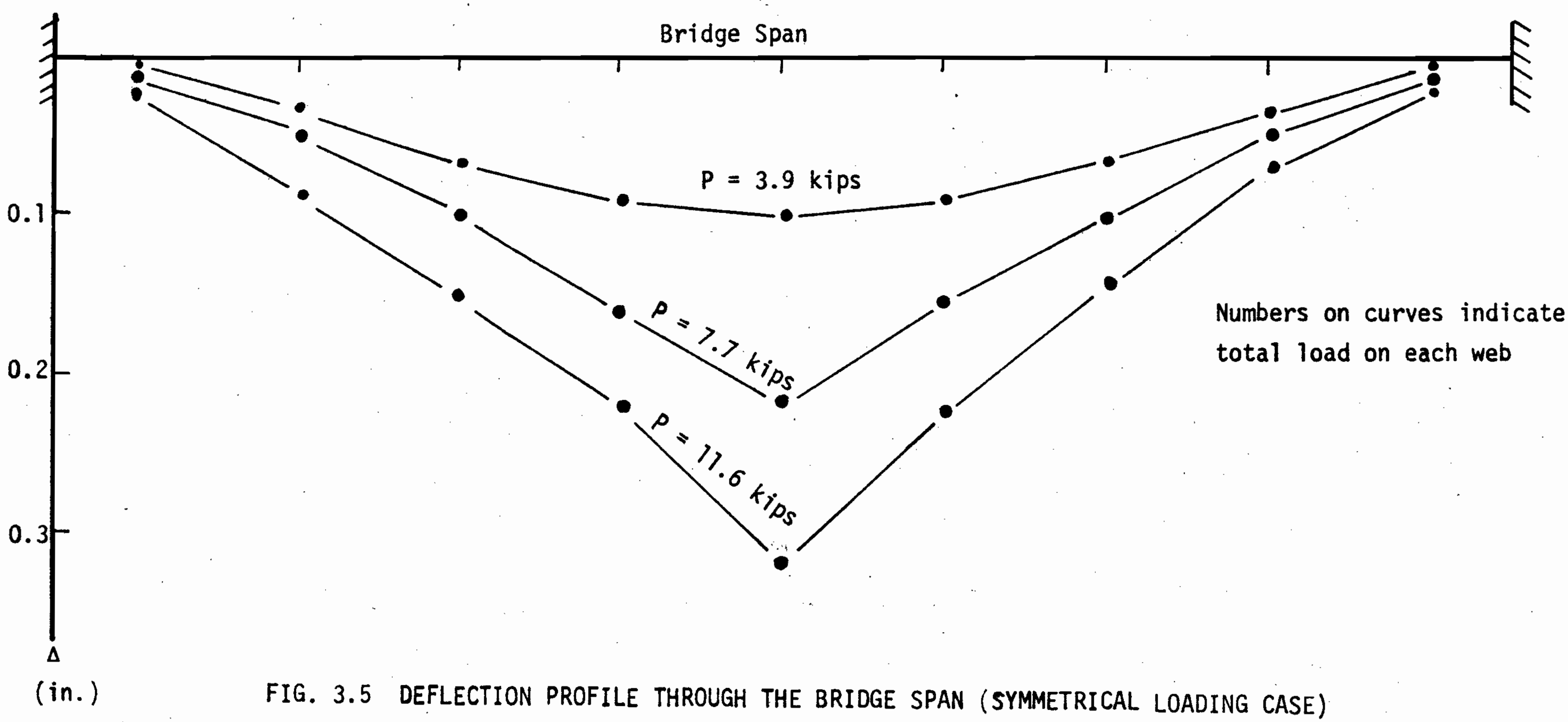

FIG. 3.5 DEFLECTION PROFILE THROUGH THE BRIDGE SPAN (SYMMETRICAL LOADING CASE)

initial stiffness of the bridge, which is the slope of the load-deflection curve, is 17 per cent less than the value calculated from the simple beam theory which does not account for the cracking of the concrete.

Using Branson's equation which accounts for the cracking of concrete [88], the effective moment of inertia of the bridge was calculated. This led to an increase of approximately 20 per cent in the calculated deflections and showed an improved agreement with the experimental load-deflection curve (Fig. 3.4). Thus, use of Branson's equation which accounts for the cracking of concrete, gives better assessment of the bridge deflections than the simple beam theory. The deflection profile along the span of the bridge (Fig. 3.5) shows that the end regions of the specimen was fixed-ended as stipulated in the design of the experiment.

3.3.2 Longitudinal Steel and Concrete Stresses

3.3.2.1 Top Slab

Figure 3.1 shows the variation of the longitudinal stresses in the top slab reinforcement with load at different locations through the span of the bridge. The steel stress values calculated from the measured strains at both the midspan and support sections were larger than those calculated using the simple beam theory for the uncracked and the cracked sections. At a load value of 4.5 kips, the steel stresses over the webs were approximately -8 ksi and 6 ksi at both the midspan and support sections, respectively. These stresses were approximately two to three times larger than those calculated from the simple beam theory based on the uncracked section at both the mid-span and support sections. As shown in Figure 3.1, the calculated stress values considering the section to be cracked gives better agreement with the stress values calculated from measured strains. In this case, the longitudinal stresses in the steel reinforcement over the webs at a load value of 8 kips were approximately -13 ksi and 11 ksi at the midspan and support sections, respectively. These stresses were approximately 66 per cent larger than those predicted from the simple beam theory at both the midspan and support sections.

Figures 3.6 through 3.9 show the longitudinal steel stresses across the width of the top slab at different locations through the bridge span at load values of 3.4, 6.5, 9.0 and 11.6 kips. The stress variation throughout half of the bridge span at a load value of 11.6 kips is shown in Figure 3.10. These figures show that the steel stresses across the width of the top slab of the bridge are not uniform. At the web-flange junction these stresses were higher than those at the cantilever tips or at points between the webs. The fluctuation in these stresses and their higher values at the web-flange junction are due to the effect of shear lag phenomena as mentioned earlier. The effect of shear lag was more pronounced in the midspan region than near the supports mainly due to the local effect of the support end block.

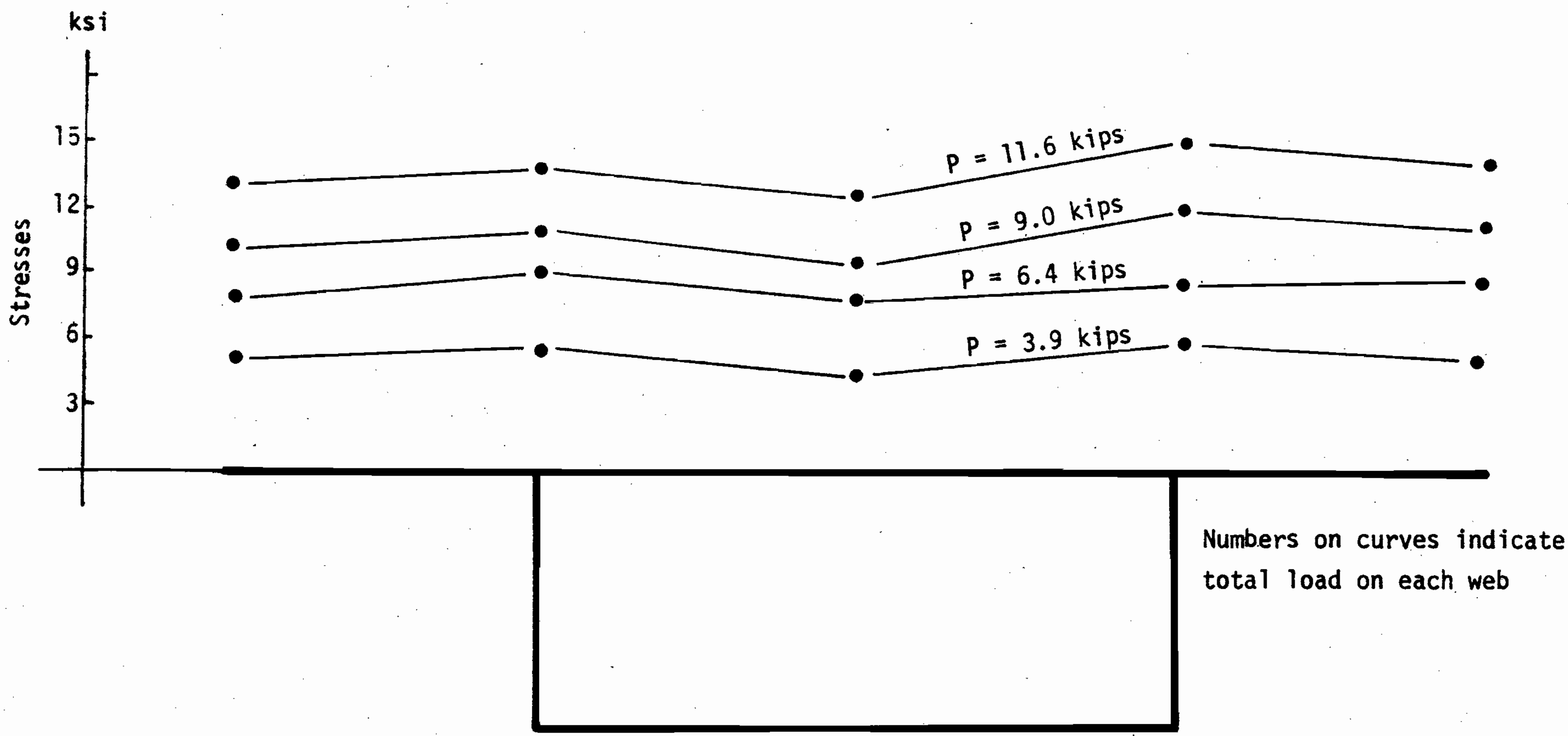

FIG. 3.6 LONGITUDINAL STEEL STRESS VARIATION ACROSS THE TOP SLAB WIDTH (SECTION AT 4" FROM SUPPORT)
(SYMMETRICAL LOADING CASE)

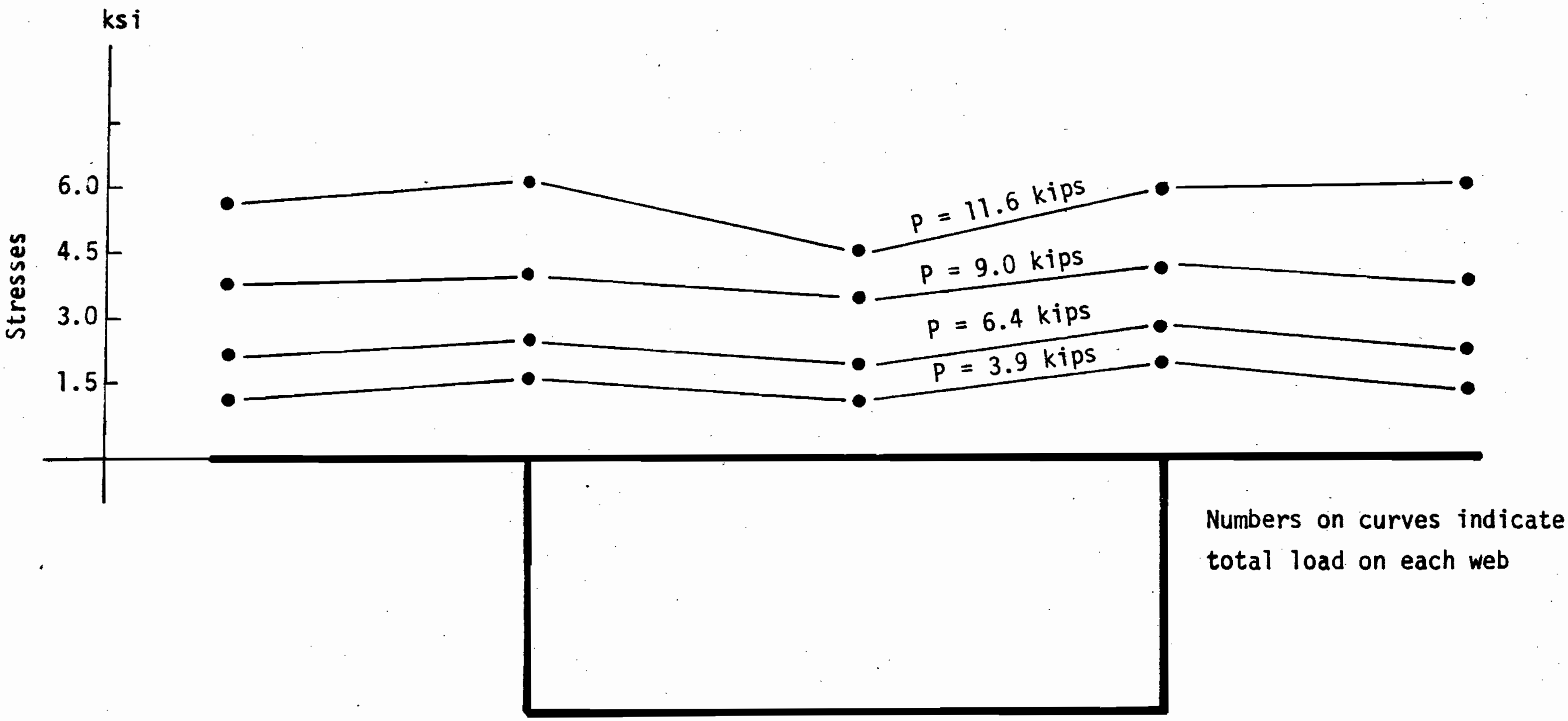

FIG. 3.7 LONGITUDINAL STEEL STRESS VARIATION ACROSS THE TOP SLAB WIDTH (SECTION AT 28" FROM SUPPORT) (SYMMETRICAL LOADING CASE)

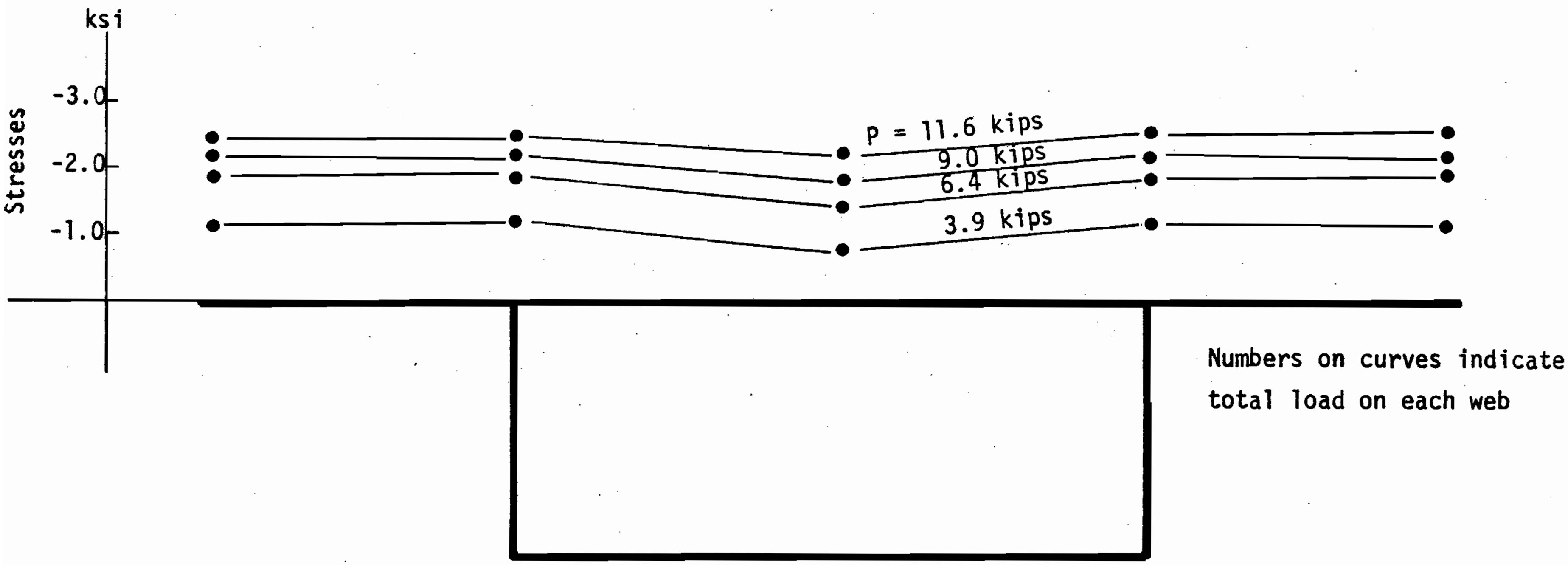

FIG. 3.8 LONGITUDINAL STEEL STRESS VARIATION ACROSS THE TOP SLAB WIDTH (SECTION AT 54" FROM SUPPORT)
(SYMMETRICAL LOADING CASE)

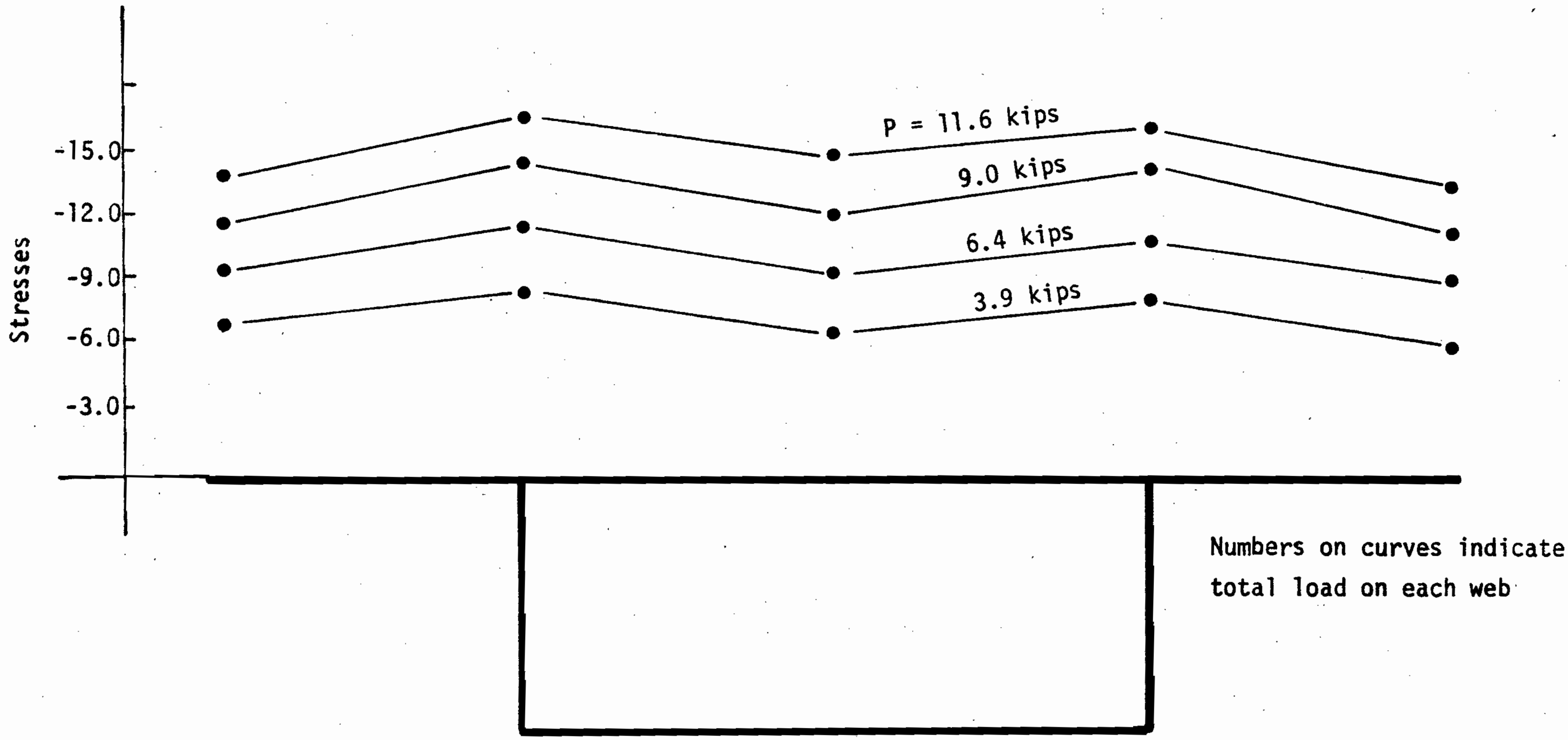

FIG. 3.9 LONGITUDINAL STEEL STRESS VARIATION ACROSS THE TOP SLAB WIDTH (SECTION AT MIDSPAN)
(SYMMETRICAL LOADING CASE)

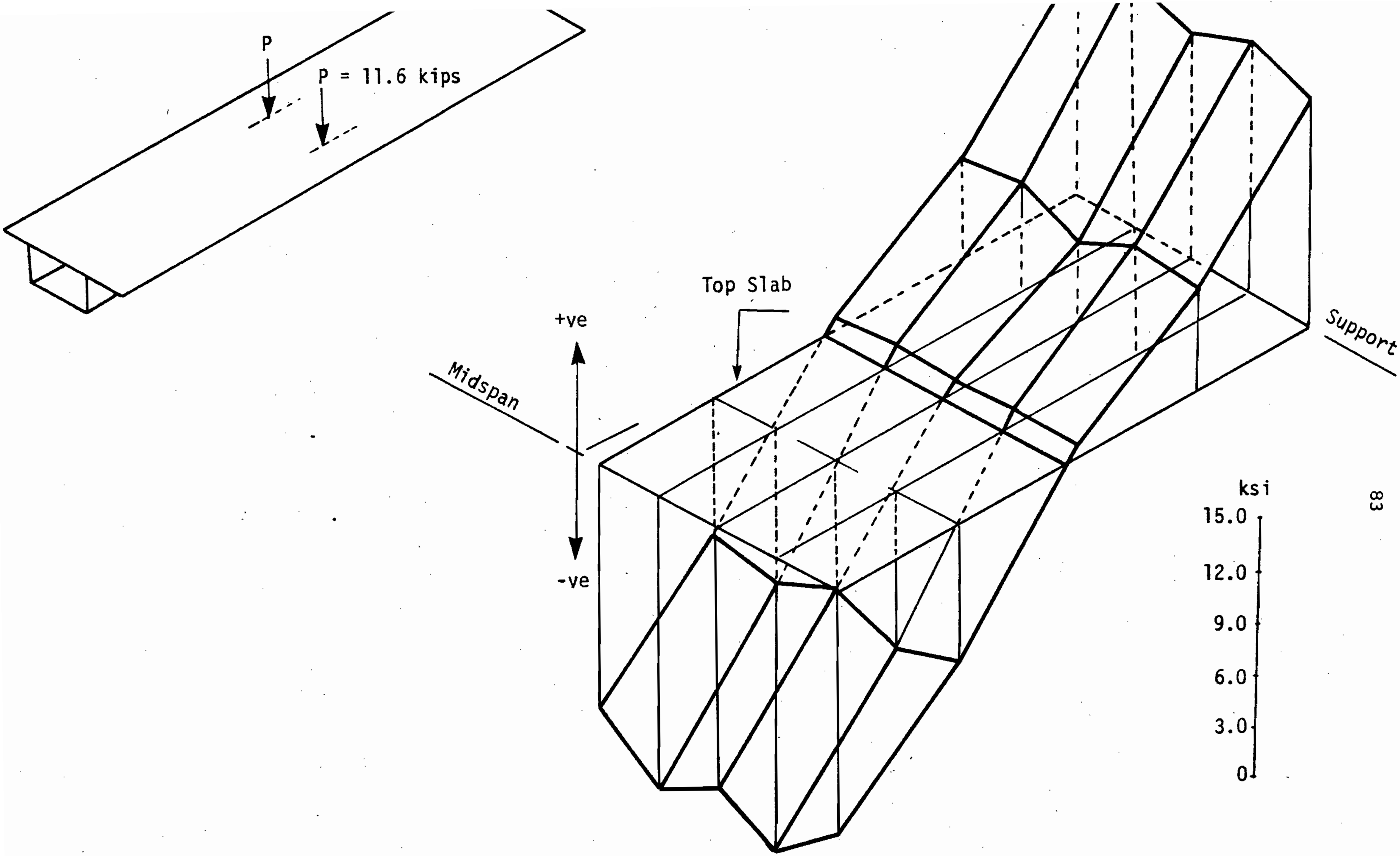

FIG. 3.10 LONGITUDINAL STEEL STRESS ENVELOPE THROUGH HALF THE BRIDGE SPAN (LOAD P = 11.6 KIPS]
(SYMMETRICAL LOADING CASE)

At a load value of 6 kips on each web, the longitudinal steel stresses over the webs at the midspan section were approximately -10 ksi, while those between the webs were approximately -8 ksi. At the support section, for the same load level, these longitudinal stresses over the webs were approximately 8 ksi, while those between the webs were 7 ksi.

The longitudinal concrete stresses across the top slab varied in a manner similar to the longitudinal steel stresses. The variation of the longitudinal concrete stresses on the top slab with load at different locations through the span of the bridge is shown in Figure 3.2. Figures 3.11 through 3.14 show the distribution of the concrete longitudinal stresses across the width of the top slab at different locations throughout the span of the bridge at load values of 3.9, 6.5, 9.0 and 11.6 kips. Also, the variation of the longitudinal concrete stresses in half of the bridge span is shown in Figure 3.15. As shown in these figures, the shear lag phenomenon caused an increase of approximately 30 per cent in the stresses at the web-flange junction above those at the cantilever tips or at points between the webs. At a load value of 10 kips, the concrete longitudinal stresses over the webs at the midspan section were approximately 530 psi, while those between the webs were approximately 420 psi. The simple beam theory is not capable of predicting the varying stress distribution within the box section.

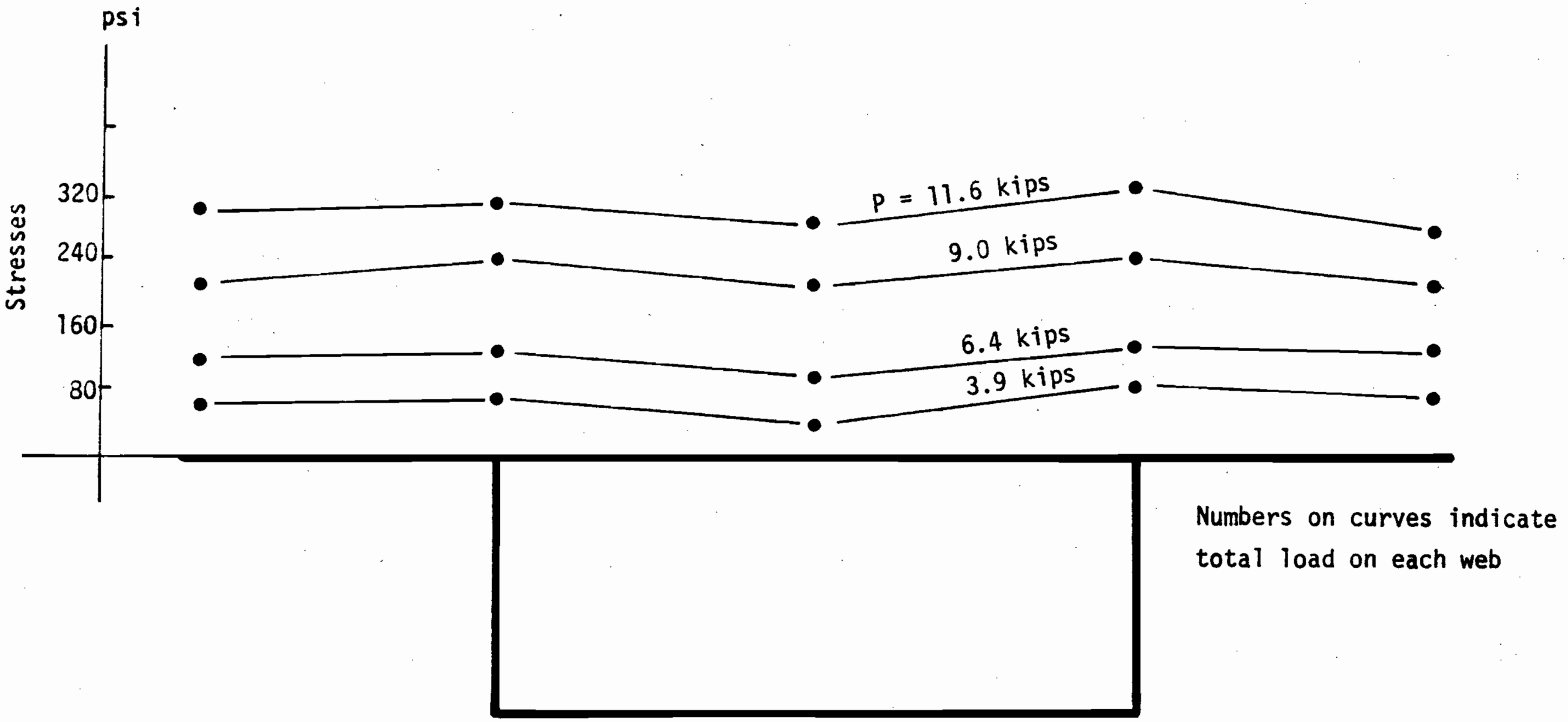

FIG. 3.11 LONGITUDINAL CONCRETE STRESS VARIATION ACROSS THE TOP SLAB WIDTH (SECTION AT 17" FROM SUPPORT) (SYMMETRICAL LOADING CASE)

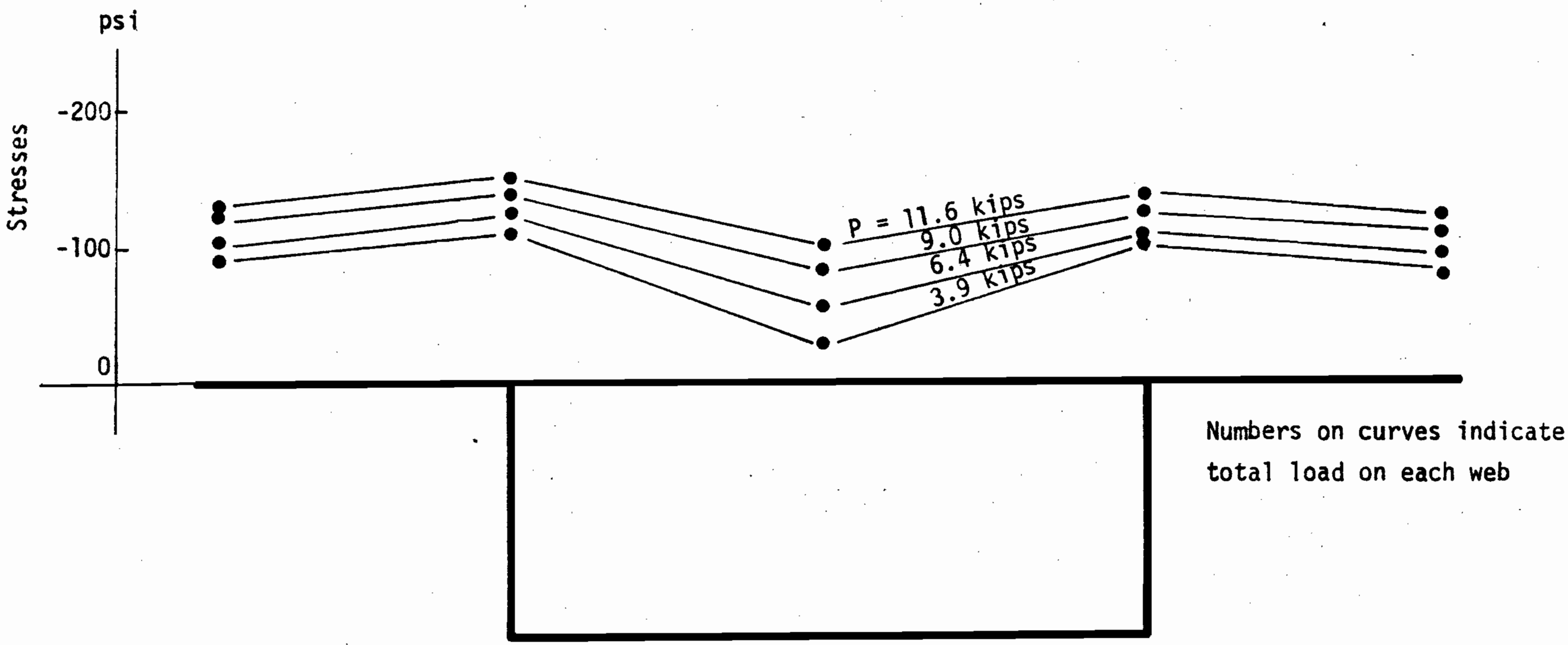

FIG. 3.12 LONGITUDINAL CONCRETE STRESS VARIATION ACROSS THE TOP SLAB WIDTH (SECTION AT 63" FROM SUPPORT)
(SYMMETRICAL LOADING CASE)

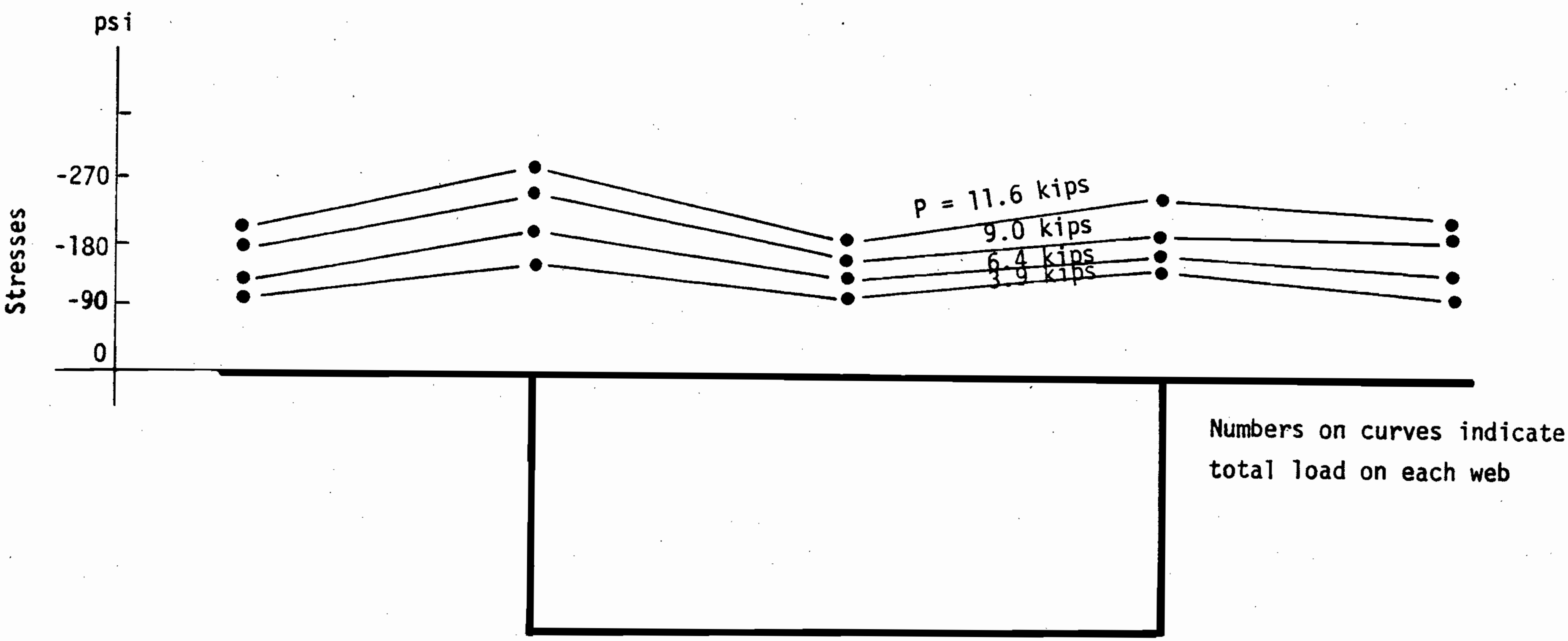

FIG. 3.13 LONGITUDINAL CONCRETE STRESS VARIATION ACROSS THE TOP SLAB WIDTH (SECTION AT 86" FROM SUPPORT)
(SYMMETRICAL LOADING CASE)

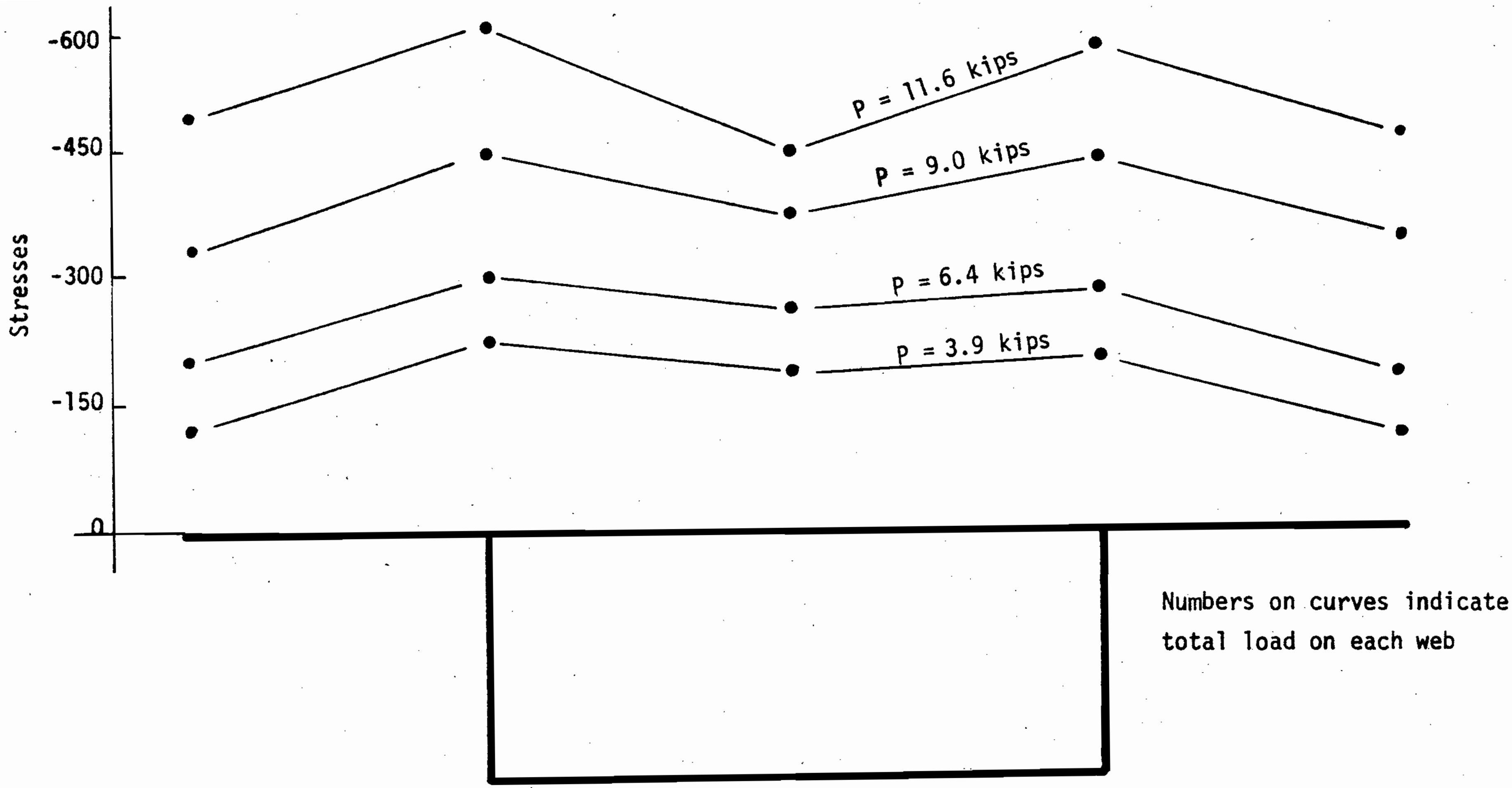

FIG. 3.14 LONGITUDINAL CONCRETE STRESS VARIATION ACROSS THE TOP SLAB WIDTH (SECTION AT MIDSPAN) (SYMMETRICAL LOADING CASE)

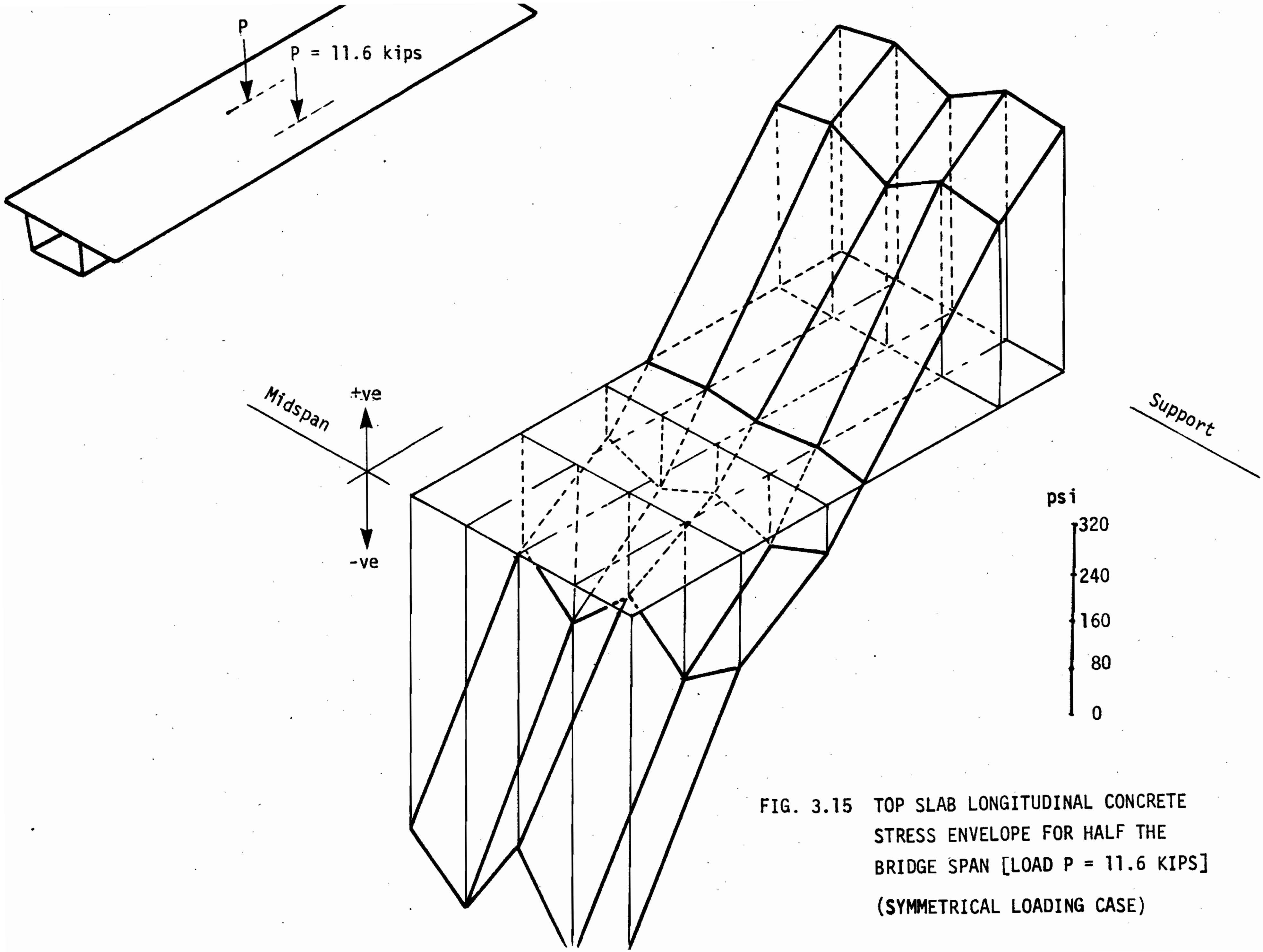

FIG. 3.15 TOP SLAB LONGITUDINAL CONCRETE STRESS ENVELOPE FOR HALF THE BRIDGE SPAN [LOAD P = 11.6 KIPS]

(SYMMETRICAL LOADING CASE)

3.3.2.2 Lower Slab

Figure 3.3 shows the variation of longitudinal steel stresses in the lower slab at various cross-sections through the bridge span. At the midspan section, these longitudinal stresses were higher than those predicted from the simple beam theory. Just before cracking, at a load value of 4 kips, the longitudinal steel stresses at the midspan section were 12 ksi, which is approximately 2.5 times larger than those calculated from the simple beam theory assuming that the section was uncracked. However, calculated values based on an assumed cracked section give better agreement with the experimental results. At a load value of 10 kips, these stresses were approximately 25 ksi, which is about 1.5 times larger than the calculated stress based on a cracked section analysis. The distribution of the longitudinal steel stresses across the lower slab at different locations through the bridge span for different load values is shown in Appendix C. The envelope of these longitudinal stresses through half of the bridge span is shown in Figure 3.16. Again, the effect of the shear lag phenomenon on the longitudinal stresses of the lower slab reinforcement at both the midspan and support sections is quite evident. The longitudinal steel stresses at the web-flange junction of the lower slab were higher than those between the webs at both the midspan and support sections. At a load value of 10 kips, the steel stresses beneath the web at the midspan section were approximately 26 ksi, while between the webs they were

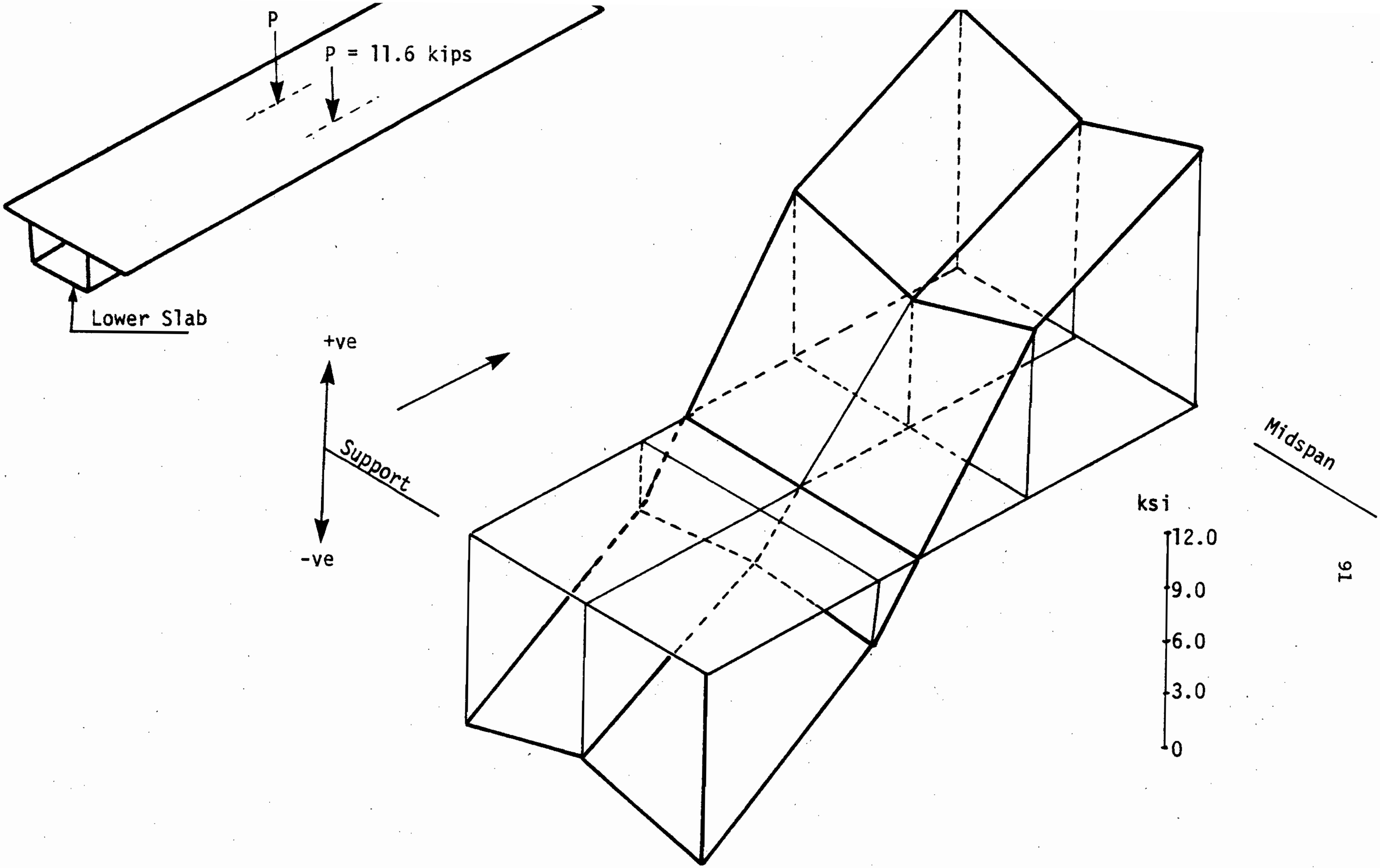

FIG. 3.16 LONGITUDINAL STRESS ENVELOPE FOR THE LOWER SLAB REINFORCEMENT [LOAD P = 11.6 KIPS]
(SYMMETRICAL LOADING CASE)

19 ksi. At the support section, at the same load level, these stresses were -9 ksi and -7.5 ksi beneath and between the webs, respectively. The restraining effect of the end blocks at the support section caused a decrease in the differences between the stresses beneath the webs and those between it. Again, as shown in Figure 3.3, the simple beam theory is incapable of predicting the stress distributions within the box section. It underestimates the stresses for both the uncracked and the cracked conditions.

Figure 3.17 shows the concrete stress variation with load at different points across the width of the lower slab. The longitudinal concrete stress distribution across the width of the lower slab and its variation with load is shown in Appendix C. Again, the shear lag considerably influences the longitudinal concrete stresses. At the support section, at a load value of 10 kips, the longitudinal concrete stresses beneath the webs were approximately 1100 psi, while those between the webs were 850 psi.

3.3.3 Transverse Stresses in Top and Bottom Slab Reinforcements

Figure 3.18 shows the stress variation in the transverse top slab reinforcement as calculated from the measured strains at different cross-sections through the span of the bridge. The transverse stresses in the top and bottom slab reinforcements were approximately constant between the two webs, and decreased toward the ends of the cantilevers

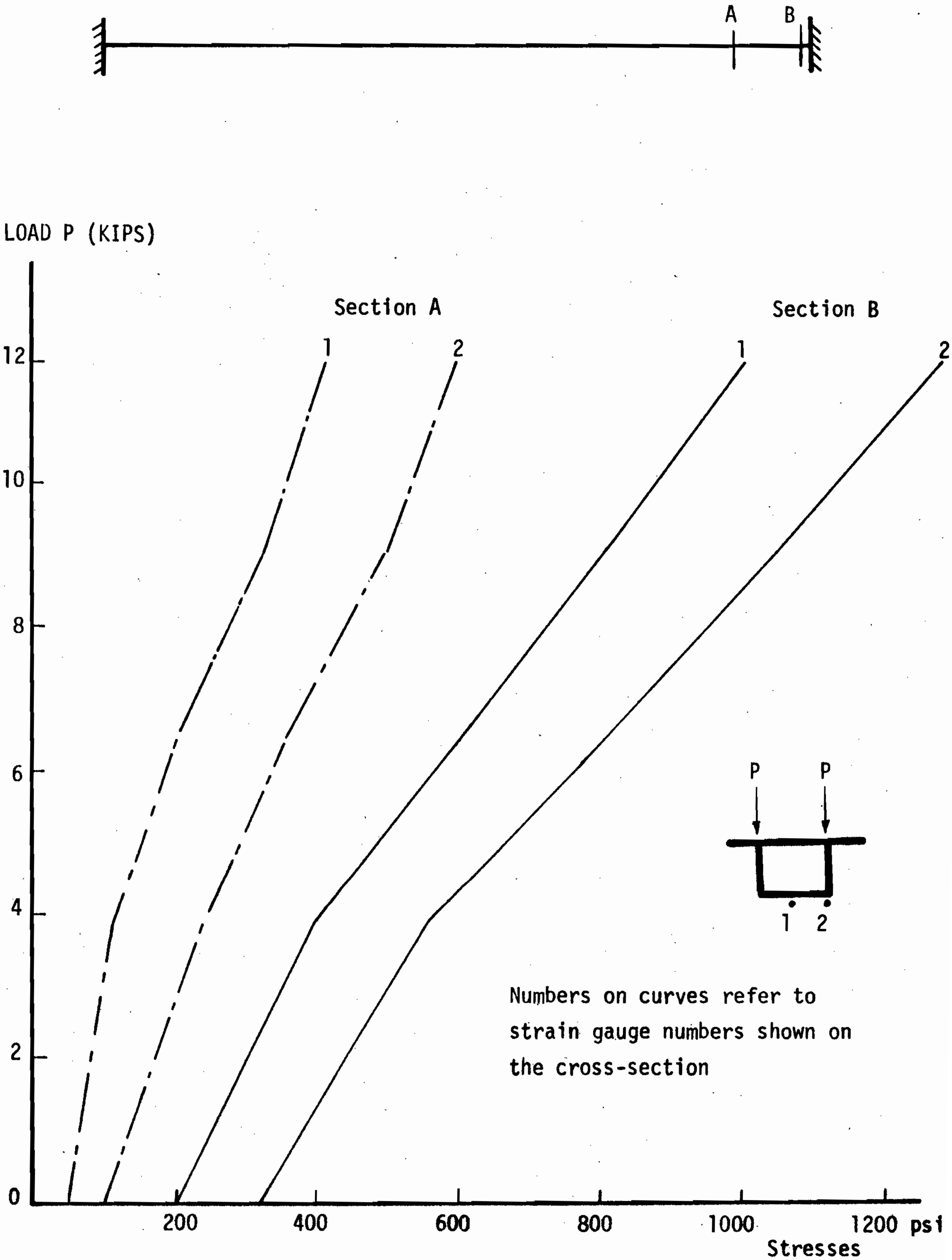

FIG.3.17 LONGITUDINAL CONCRETE STRESSES IN THE LOWER SLAB
(SYMMETRICAL LOADING CASE)

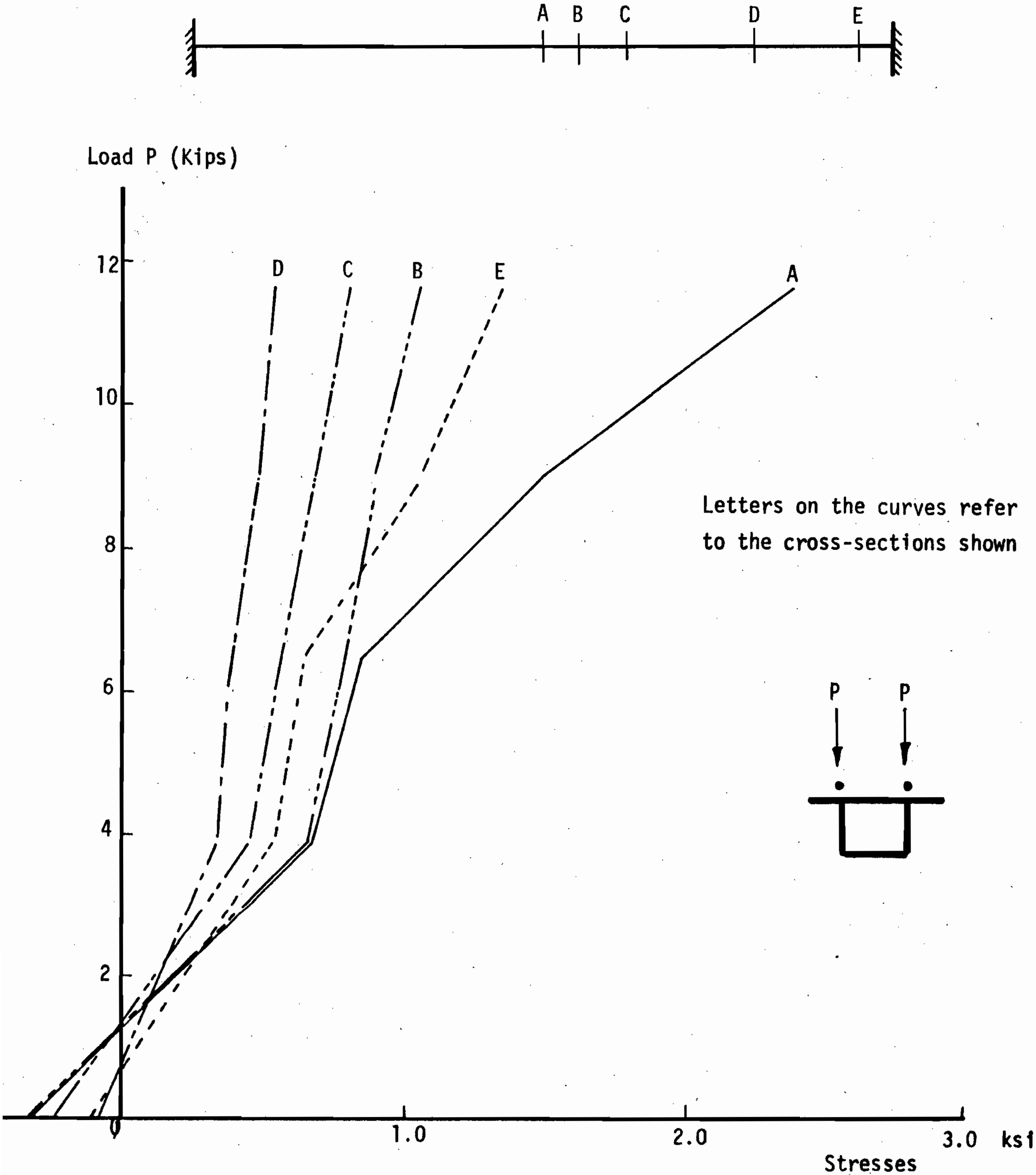

FIG. 3.18 TRANSVERSE STEEL STRESSES IN THE TOP SLAB REINFORCEMENT (SYMMETRICAL LOADING CASE)

on the top slab. The transverse stresses in both the top and bottom slab reinforcements were approximately 30 per cent of the longitudinal stresses at the same location, with a maximum value at the midspan section. The transverse stresses across the width of the top slab at different bridge sections for different load values are detailed in Appendix C. At a load value of 10 kips these steel stresses in the upper transverse reinforcement layer at the midspan section were approximately 2 ksi. Initially, the transverse steel stresses on the top slab were compressive and small; however, with a loading increase these stresses reversed in nature and became tensile. As mentioned in Chapter 2, there were two layers of reinforcement in both the upper and lower slabs. The stresses in the transverse steel in the upper reinforcement layer showed an increase of 50 per cent above those in the lower layer. Similarly, the stress in the transverse steel of the lower layer showed a similar increase of 50 per cent above those observed in the upper layer at the same location. These increases can be attributed to the Poisson effect.

The transverse concrete stresses, as calculated from the measured strain values in the top slab of the bridge, were approximately uniform between the webs and decreased toward the cantilever tips. In the midspan region, at a load value of 10 kips, the transverse tensile stresses over the webs were approximately 120 psi which were approximately 20 per cent of the longitudinal concrete stresses at the same location. Figure 3.19 shows the load-concrete transverse stresses

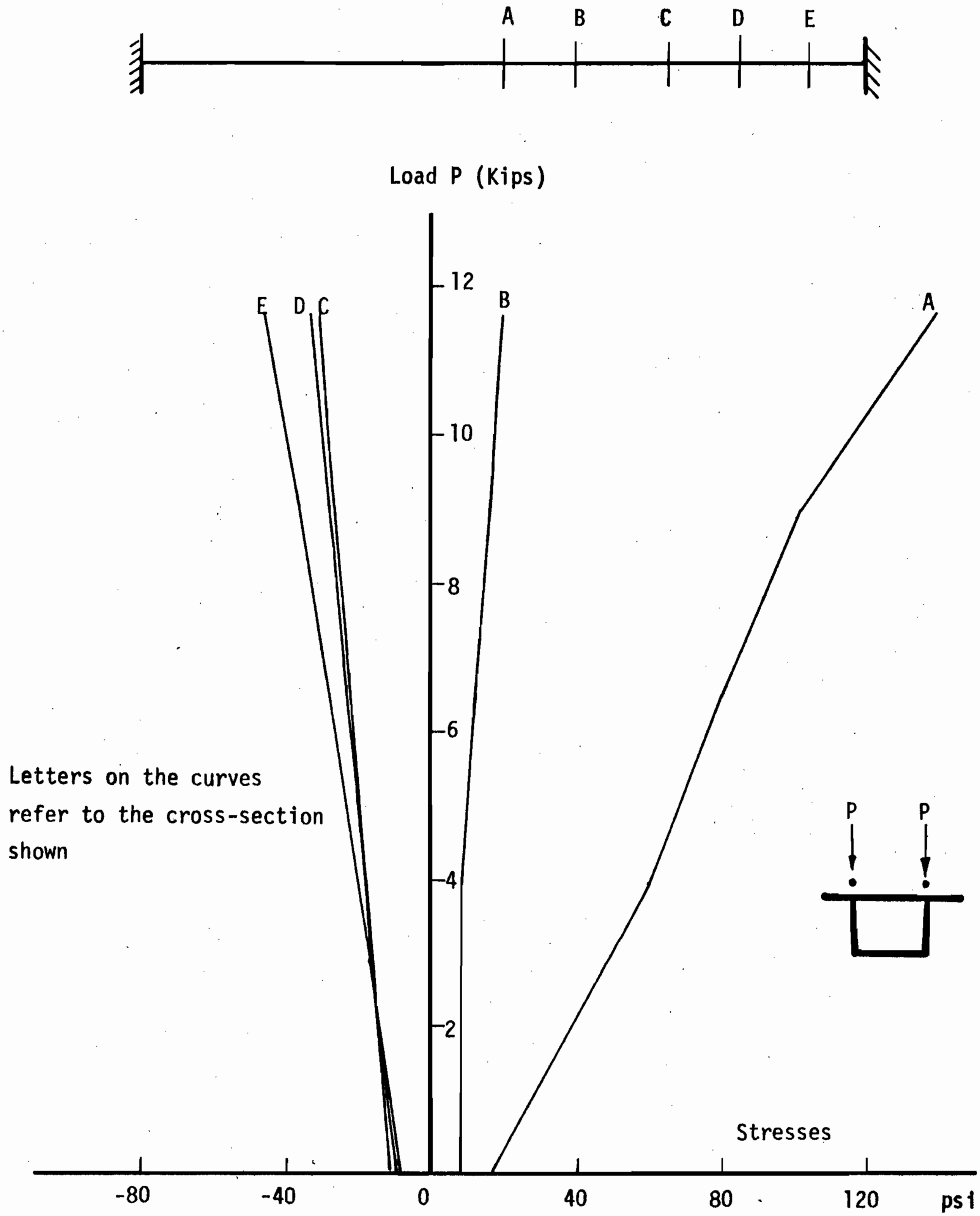

FIG. 3.19 TRANSVERSE CONCRETE STRESSES IN THE TOP SLAB
(SYMMETRICAL LOADING CASE)

at different cross-sections through the span of the bridge. The maximum deformations take place at midspan and therefore the maximum transverse stresses also occur at midspan. These transverse stresses decrease towards the cantilever tips as well as towards the end supports. The transverse concrete stresses across the width of the top slab at different locations through the bridge span for different load values are detailed in Appendix C. The transverse concrete stress envelope through half the bridge span at a load value of 11.7 kips is shown in Figure 3.20. It should be mentioned that the simple beam theory does not account for the transverse stresses in this type of structure.

At a load value of 10 kips, the transverse stresses in the top slab at the midspan section, calculated using Knittel's method [24], were approximately 80 psi. This value is approximately 8 per cent of the longitudinal concrete stresses at the same location. These calculated stresses are less than those measured at the same location and approximately half those predicted from the Poisson's ratio effect.

These observations show that the transverse stresses within the box section, in some cases, can reach values which are larger than those predicted from the Poisson's ratio effect or with any available analytical method, therefore a better method of analysis is needed to predict these stresses in reinforced concrete box section structures.

3.3.4 Stresses in the Web Reinforcement

The web reinforcement of the box section consisted of vertical closed stirrups as recommended by the ACI Code and AASHTO Specifications [89, 66]. As a result of some detailed investigations [90, 91, 92],

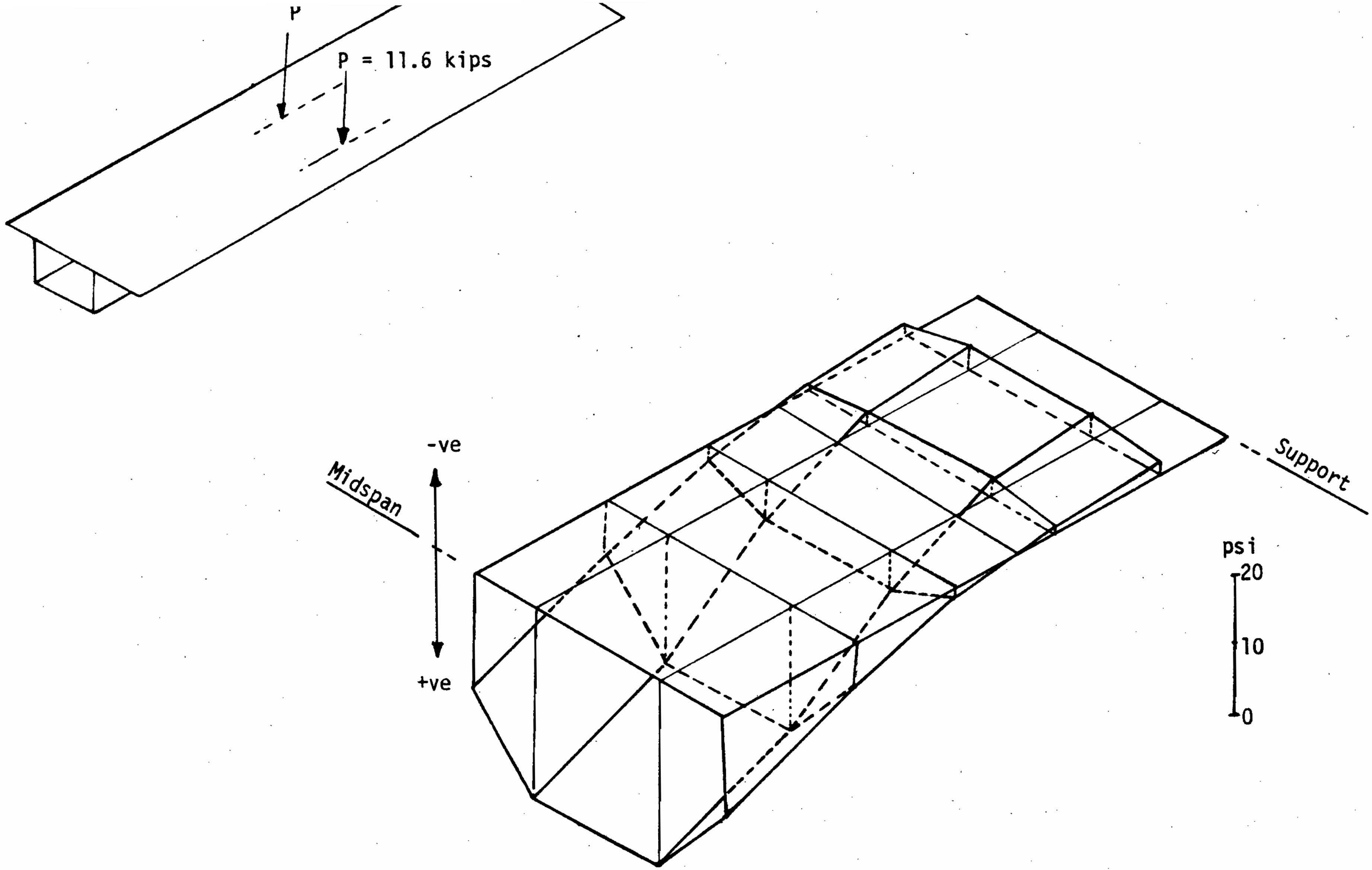

FIG. 3.20 TRANSVERSE CONCRETE STRESS ENVELOPE FOR THE TOP SLAB THROUGH HALF THE BRIDGE SPAN [LOAD P = 11.6 KIPS] (SYMMETRICAL LOADING CASE)

it has now been established that the shear capacity of a reinforced concrete simply-supported beam with a rectangular cross-section consists of the resistance provided by (1) the compression zone, (2) the aggregate interlock at the cracks, (3) the dowel action of the longitudinal reinforcement, and (4) the contribution of the web reinforcement and its interaction with the other components. However, a similar qualitative breakdown of the shear and torsional resistance of the box section has not yet been attempted.

The ACI and the AASHTO shear and torsion design equations are empirical in nature and consider the strength to consist of two components - the strength contribution of the concrete section and the strength contribution of the reinforcement. This simplified philosophy was used for the analysis of stirrup stress in the present study. The contribution of concrete is given by

$$V_c = 2\sqrt{f'_c}\,(2\,b_w\,d)$$

$$= 4\sqrt{f'_c}\;b_w\,d \tag{3.1}$$

where b_w is the thickness of the web

d is the depth of the cross-section

f'_c the compressive strength of concrete.

The contribution of the web reinforcement is given by

$$V_s = \frac{f_y A_v d}{s} \tag{3.2}$$

where f_y is the yield stress of the web reinforcement.

By combining equations (3.1) and (3.2), as in the ACI Code and the AASHTO Specifications

$$V_u = V_c + V_s \tag{3.3}$$

and dividing by the web area $(2\ b_w\ d)$

$$v_u = v_c + v_s \tag{3.4}$$

By simplification of equation (3.4), and substituting from equations (3.1) and (3.2), and by replacing f_y by f_s, the stirrup steel stress is given by

$$f_s = \frac{2\ (v_u - v_c)\ b_w\ s}{A_v} \tag{3.5}$$

It must be noted that the stress in the stirrup steel is almost negligible before the section cracks and since according to the ACI Code 318.77 [74] and the AASHTO Specifications [89], V_c represents the load at which the concrete section cracks, equation (3.5) was used to calculate the stirrup steel stress after the section cracked. No calculations were made for the stirrup steel stress for loading stages before the cracking of the section.

The experimental load-calculated stirrup stresses at different locations through the bridge span are shown in Figure 3.21. As shown, the stirrup stresses at the midspan section before cracking were small. However, after cracking at a load value of 4.3 kips on each web, the stirrup stresses increased significantly and were 1.3 ksi and 0.2 ksi at the midspan and support sections, respectively. The stirrup stress envelope for half the bridge span is shown in Figure 3.22 at a load of 11.7 kips on each web.

3.4 Unsymmetrical Loading Test

3.4.1 Deflections

The vertical deflections were measured under both the loaded and the unloaded webs through the span of the bridge at 23-inch intervals. The following six curves for the midspan vertical deflection are shown in Figure 3.23:

1. Deflection of the loaded web
2. Deflection of the unloaded web
3. Deflection of the longitudinal centreline of the bridge for the unsymmetrical loading test

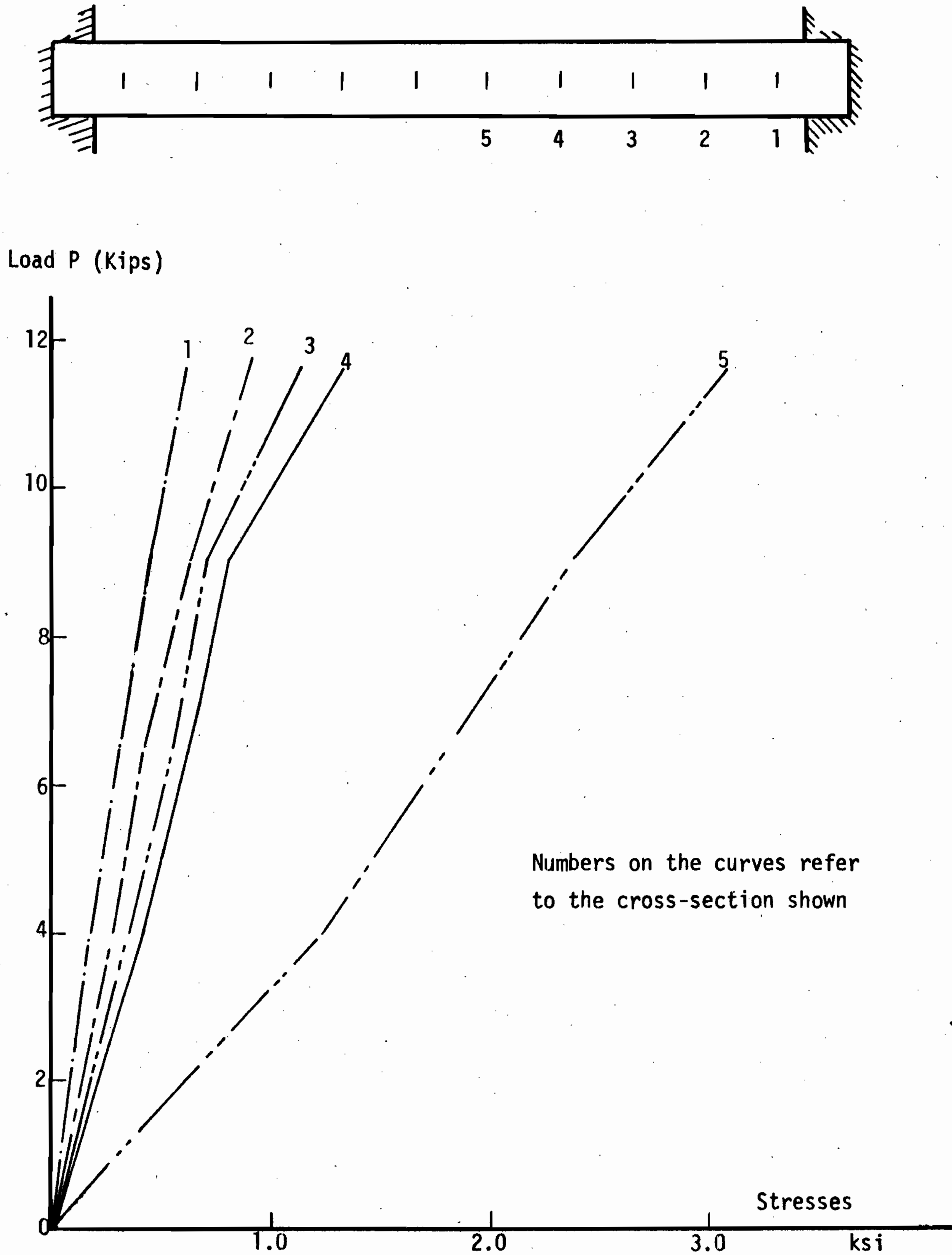

FIG. 3.21 VARIATION OF STIRRUP STRESSES WITH LOAD (SYMMETRICAL LOADING CASE)

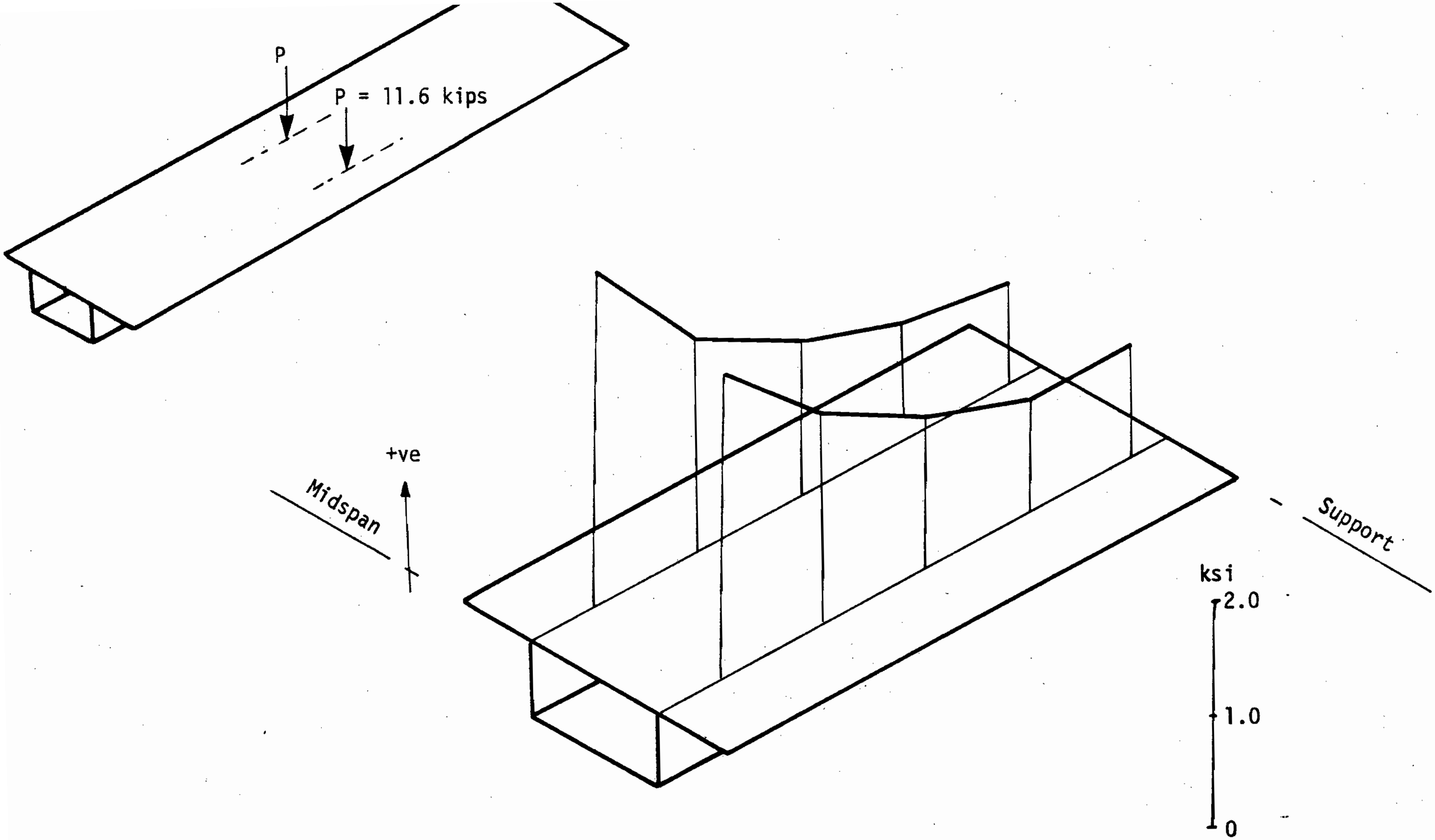

FIG. 3.22 STIRRUP STRESS ENVELOPE FOR HALF THE BRIDGE SPAN [LOAD P = 11.6 KIPS]
(SYMMETRICAL LOADING CASE)

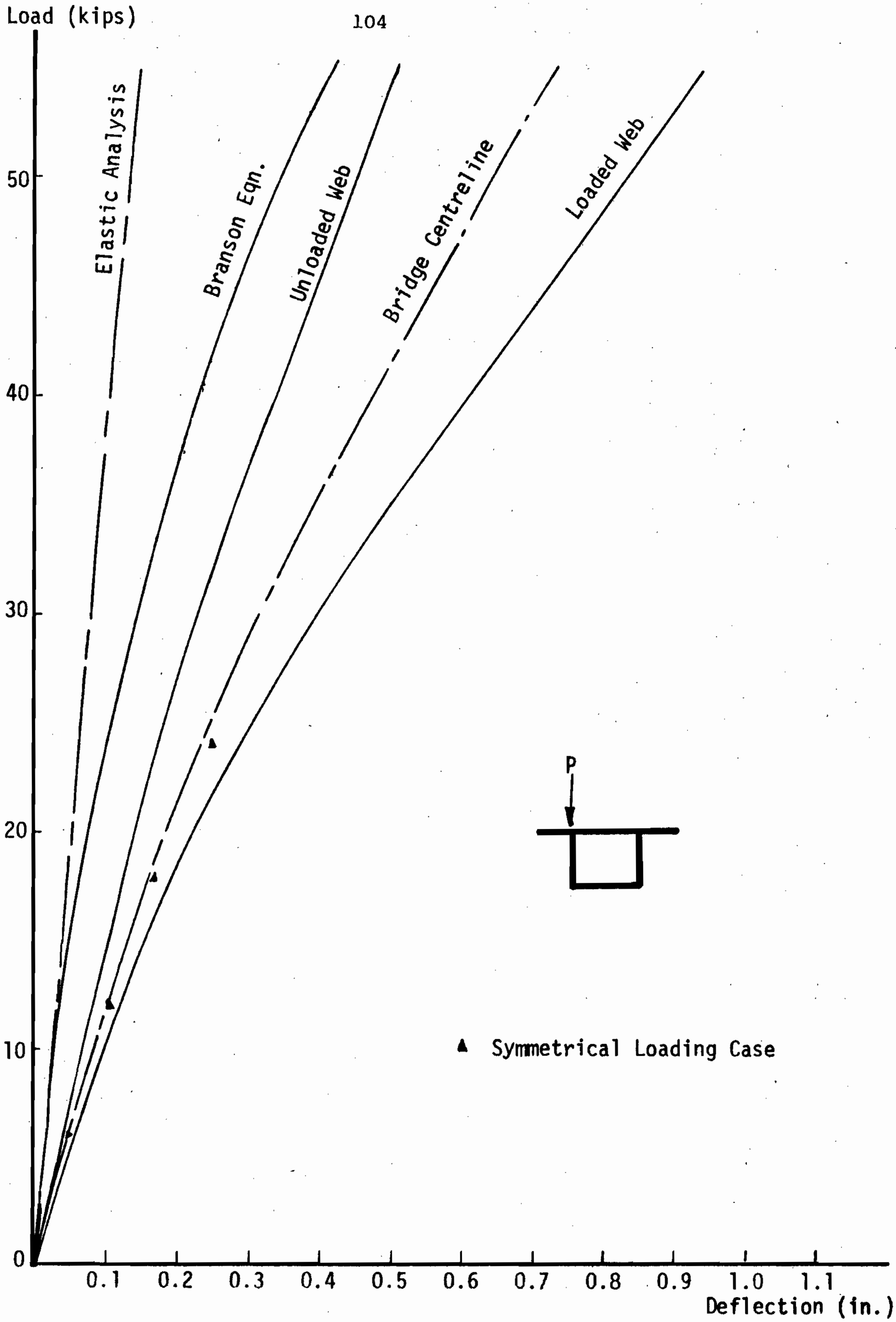

FIG.3.23 LOAD-MIDSPAN DEFLECTION CURVES (UNSYMMETRICAL LOADING CASE)

4. Deflection of the longitudinal centreline of the bridge for the symmetrical loading test
5. Elastic deflection from the simple beam theory using the uncracked cross-section
6. Deflection values obtained by incorporating Branson's equation to account for the cracking of the cross-section in simple beam theory.

These curves are plotted for the case of the concentrated load only. The dead load deflection at the midspan section was 0.144 in. and must be taken into consideration in calculating the total deflection at any load level.

Due to the combined effect of torsion, shear and bending in the box girder bridge, the loaded web showed higher deflection values than the unloaded web.

The midspan deflection at a load value of 20 kips was 0.24 in. under the loaded web, 0.15 in. under the unloaded web, and 0.19 in. at location midway between the webs.

As shown in these curves (Fig. 3.23), the deviation from linearity is clearly observed at a load value of approximately 20 kips for the loaded web and 28 kips for the unloaded web. The deflection values calculated using the simple beam theory were the lowest deflection values. At the midspan section for a load value of 20 kips, the calculated deflection value obtained from the simple beam theory was approximately 0.05 in. which is about 25 per cent of the measured deflection value of the bridge centreline. However, the use of Branson's equation in this analysis increased the calculated deflection value to about 0.1 in. These deflection values are approximately 60 and 40 per cent respectively compared with the measured deflection values under the unloaded and loaded webs respectively.

As shown in Figure 3.23, up to a load value of 16 kips for the unsymmetrical loading case, the measured deflection values of the bridge centreline were close to those for the symmetrical loading test. Therefore it can be concluded that at the early stages of loadings below approximately 0.2 of the ultimate load, the torsional and shear deformations have a negligible effect on the deflection and the overall behaviour of the bridge. However, these deformations have a significant influence in the bridge response beyond this load level, mainly due to the formation of inclined cracks around the box section and the propagation of these cracks with an increase of load.

Lateral displacement of the top slab at different locations along the span are shown in Figure 3.24 for load values of 9.7, 19.4, 29.0, 38.7 and 55.0 kips. The maximum lateral displacement occurred at the midspan section for all load levels. At a load value of 55 kips, the measured lateral displacement at the midspan section was 0.0425 in.

Figure 3.25 shows the longitudinal displacement of the cantilever tips through the bridge span at different load values of 9.7, 19.4, 29.0, 38.7 and 55.0 kips. As can be noted from Figure 3.25,

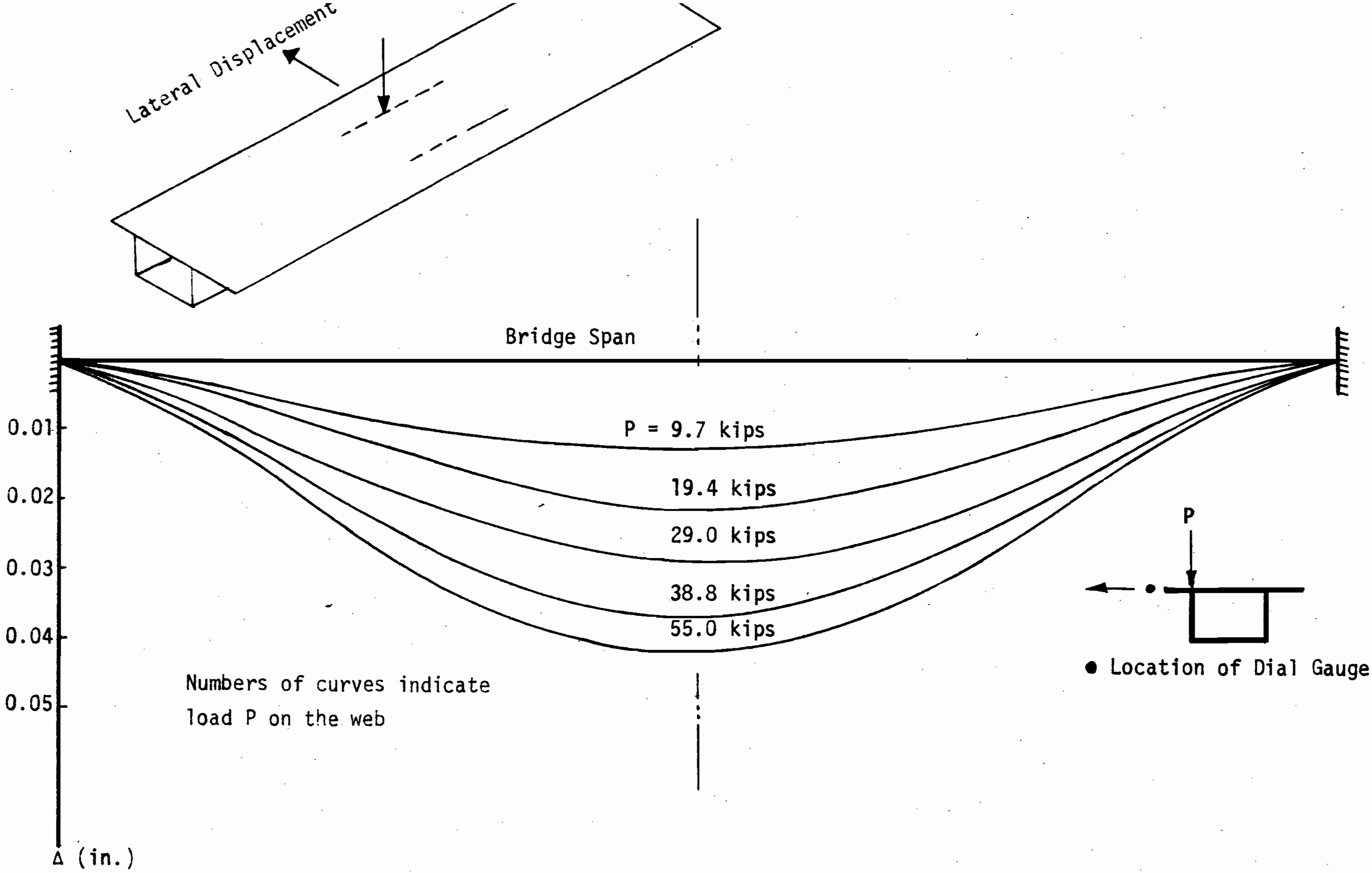

FIG. 3.24 PROFILE OF LATERAL DISPLACEMENT THROUGH THE BRIDGE SPAN
(UNSYMMETRICAL LOADING CASE)

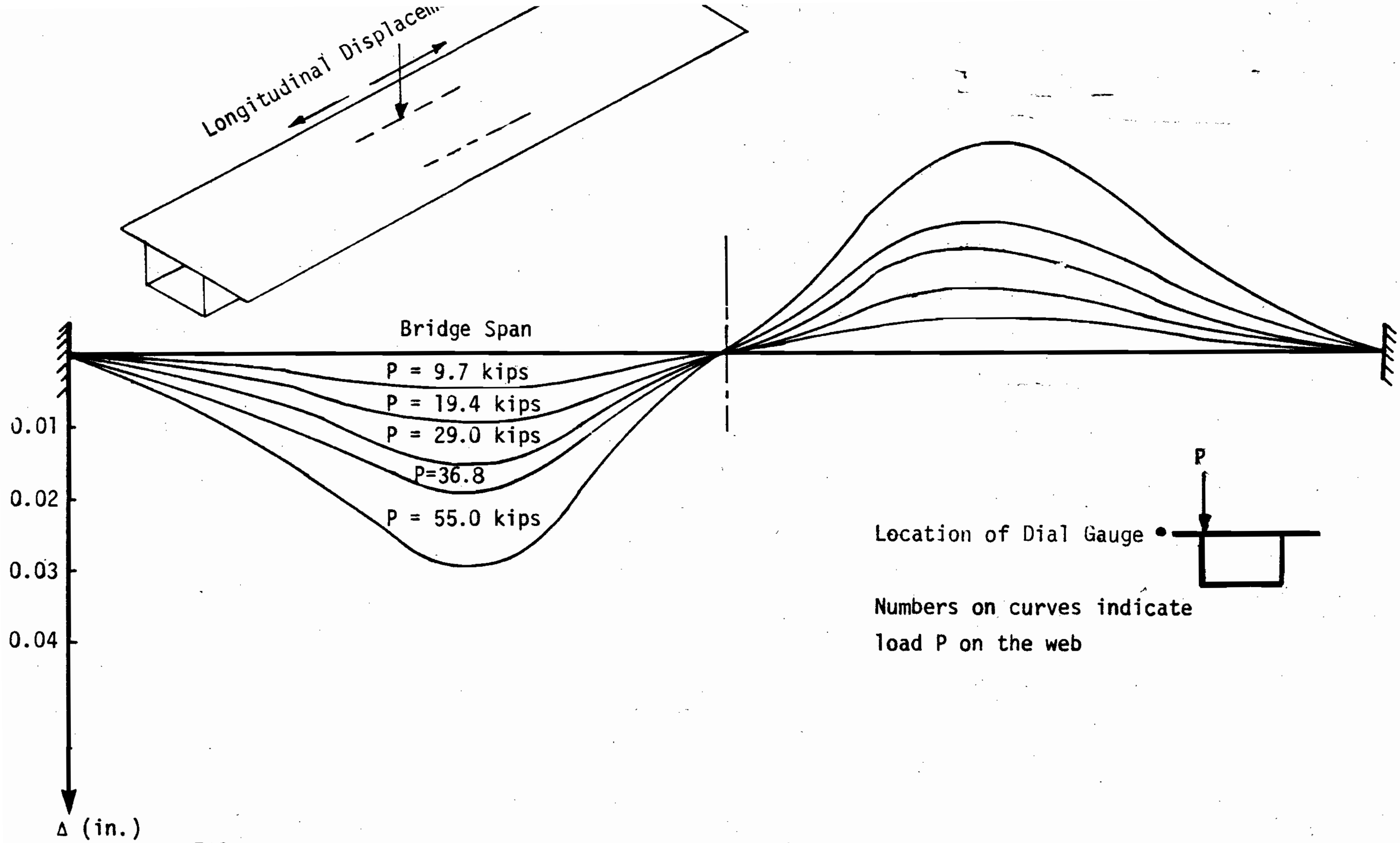

FIG. 3.25 PROFILE OF LONGITUDINAL DISPLACEMENT THROUGH THE BRIDGE SPAN
(UNSYMMETRICAL LOADING CASE)

the maximum measured longitudinal displacement occurred approximately at the quarter span section of the bridge. These deformation patterns can be attributed to torsional and distortional deformations in the box section through the bridge span due to the applied unsymmetrical loads. The measured longitudinal displacement of the cantilever tips at the quarter span section was 0.03 in. at a load value of 55 kips which is approximately 4 and 6 per cent of the measured vertical deflection at the midspan section for the loaded and the unloaded webs, respectively.

The longitudinal displacements of both the left and the right webs for the applied eccentric load through half the bridge span are shown in Figure 3.25. It can be noted that the loaded web moves outwards at the midspan section, while the unloaded web moves inwards. It must be observed that the bridge deflection profiles shown in Figures 3.24 and 3.25 confirm that the end regions of the bridge were fixed as stipulated in the design of the experiment.

3.4.2 Angle of Twist

The angle of twist "θ" of the midspan section, relative to the fixed end section, ignoring the warping restraint, can be calculated from the following formula [9]

$$\theta = \frac{M_T \ell}{J_{eq} G} \tag{3.6}$$

Figure 3.26 shows the load-measured angle of twist relationship along with the curves obtained using the above beam formula and the diagonal compression field theory. This theory has been developed for the analysis of concrete sections under pure torsion. The longitudinal and transverse reinforcements are considered to act as ties or tensile members, while the concrete between the cracks is assumed to behave as compression struts. The equations from the latter theory used in the computer program are detailed in Appendix B. Detailed derivation of these equations can be found in Reference [93].

As shown in Figure 3.26, the load versus measured angle of twist relationship is linear up to a load value of 16 kips and approximately the same as the curve obtained using the diagonal compression field theory. Beyond this limit, due to the formation of cracks, the torsional stiffness of the box section, as noted from the slope of the measured load-angle of twist, decreased to a value of approximately one-third of the initial value. Beyond a load value of 30 kips, the

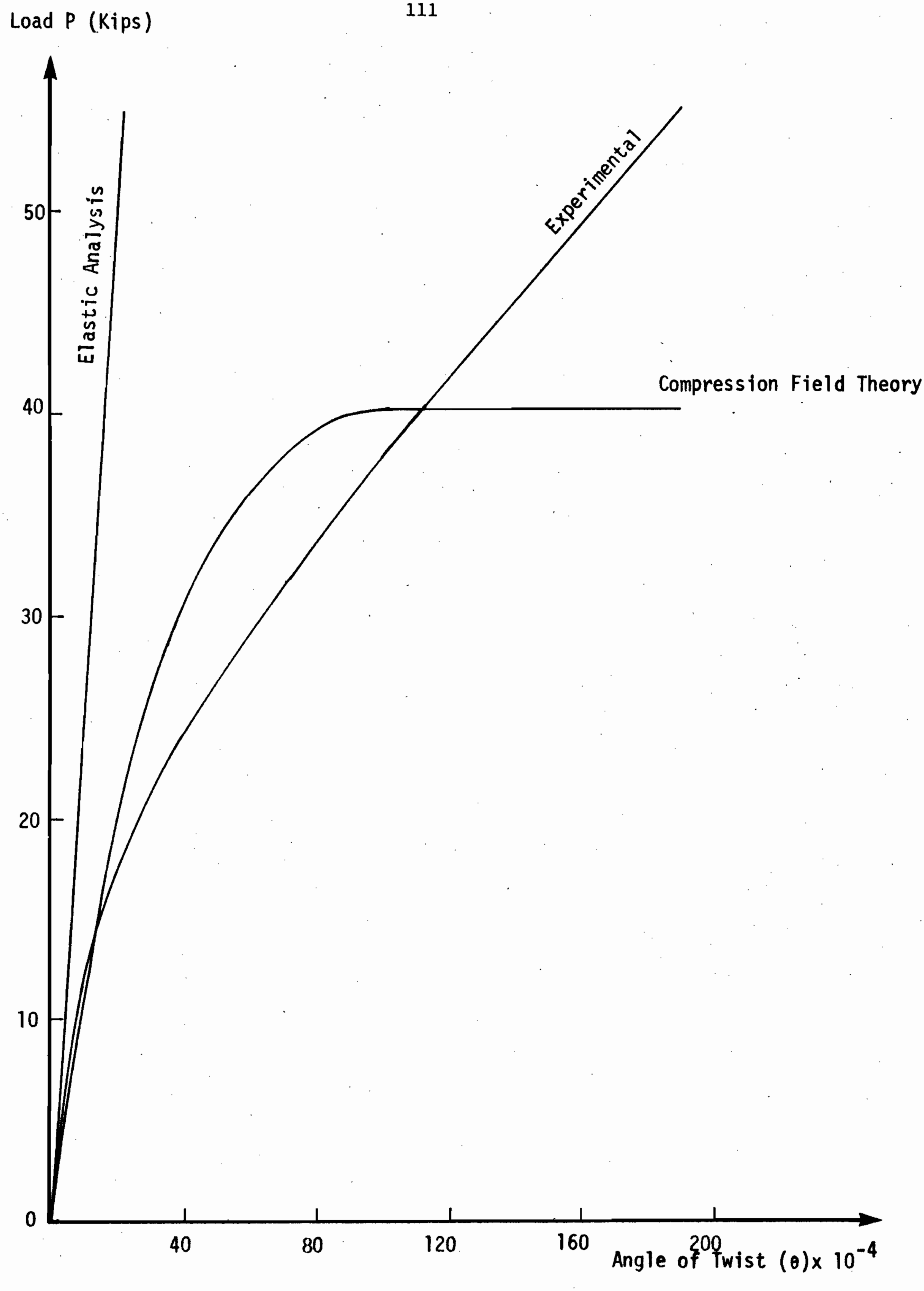

FIG. 3.26 LOAD-ANGLE OF TWIST VARIATION AT MIDSPAN SECTION
(UNSYMMETRICAL LOADING CASE)

torsional stiffness of the bridge decreased to about 20 per cent of its initial value, and it remained approximately constant up to the ultimate load level. This observation shows the serious effect of the formation and propagation of cracks within the box section in decreasing its torsional stiffness.

The beam formula yields the stiffest load-twist relationship, and as shown, a serious deviation between the measured and the calculated values occurs at a load value of 10 kips. At a load value of 30 kips, the measured angle of twist value was 90×10^{-4} radian, while the beam formula indicated angle of twist of 20×10^{-4}. It must be noted that the beam formula is valid only for homogeneous and linearly elastic elements and can be used only for the analysis of the box section before cracking. There is no justification for the use of this equation for load stages beyond cracking because of the large discrepancy with the experimental values.

The diagonal compression field theory can be used to analyse the concrete element of any cross-sectional shape in pure torsion. As mentioned before, the measured and the calculated values from this method were approximately the same up to a load value of 16 kips. Beyond this load value and up to a load value of 40 kips, the measured angle of twist was larger than the calculated value. At a load value of 25 kips, the measured angle of twist was approximately 40×10^{-4} radian, and the calculated value was 35×10^{-4} radian which is reasonably close. At another load value of 35 kips, the measured angle of twist was 90×10^{-4} radian, while the calculated value was 70×10^{-4} radian. Thus the experimental value starts showing departure from the calculated values. Beyond a load value of 40 kips, the calculated angle of twists increased more rapidly (Fig. 3.26) on account of yielding of the reinforcing steel in the cross-section. The distribution of the angle of twists through the bridge span for different load levels is shown in Figure 3.27.

It must be noted that, as mentioned earlier, the compression field theory was derived for the case of pure torsion only and does not account for any interaction with shear and possible stiffening of the section on account of bending. This may have caused the deviation between the theoretical and the experimental curves.

Details of the compression field theory and the computer program used in this analysis (input data, output data, and listing of the program) are presented briefly in Appendix B. The extension of compression field theory to include the influence of bending and shear are also presented in Appendix B.

3.4.3 Longitudinal Steel and Concrete Stresses

3.4.3.1 Top Slab

The longitudinal steel stresses in the top slab reinforcement as obtained from the measured steel strain and the values calculated using the simple beam theory across the bridge width at different locations along the bridge span are shown in Figure 3.28. As shown, the steel stresses across the width of the top slab were not uniform, with the maximum values occurring over the loaded web. These stresses

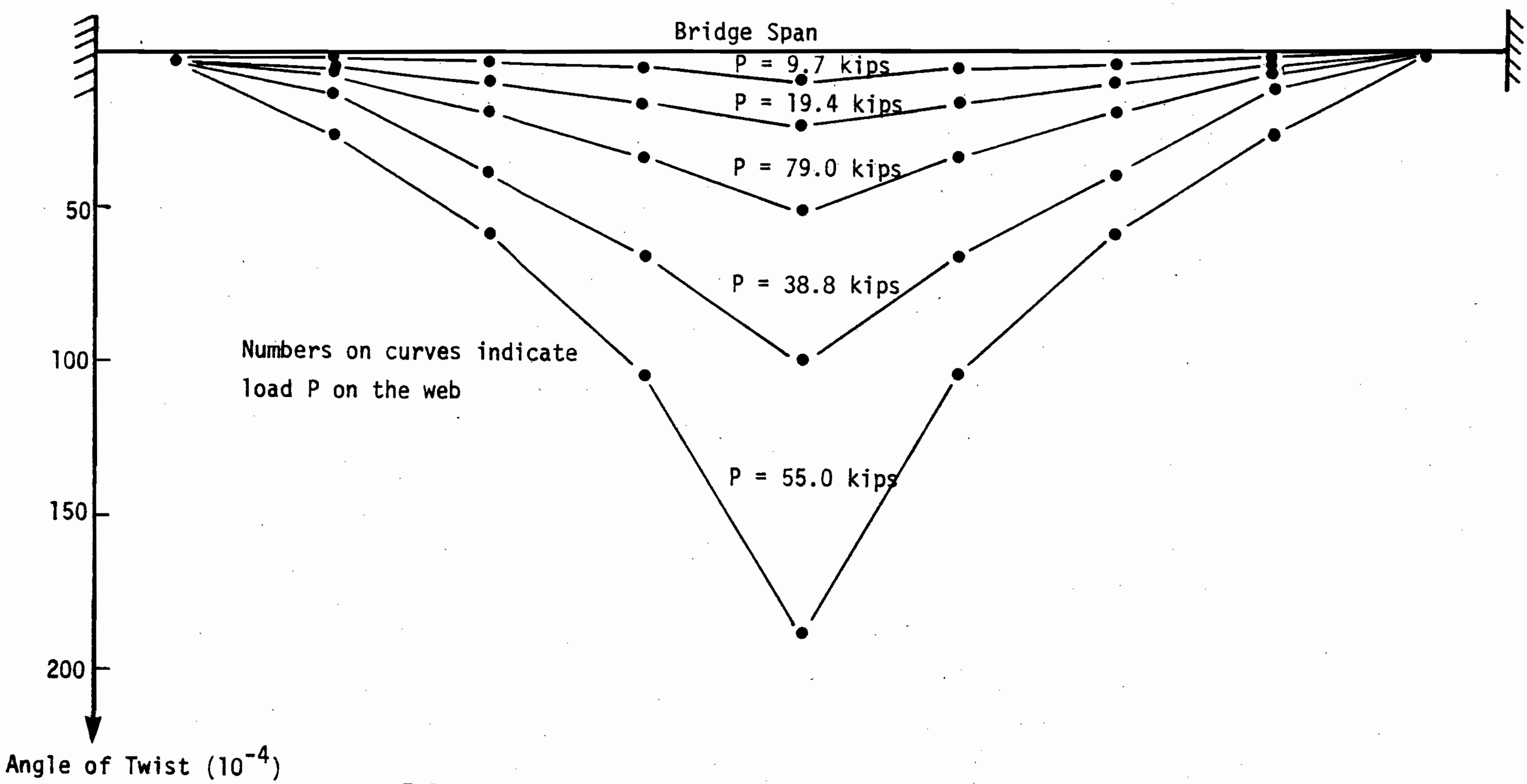

FIG. 3.27 VARIATION OF ANGLE OF TWIST THROUGH THE BRIDGE SPAN (UNSYMMETRICAL LOADING CASE)

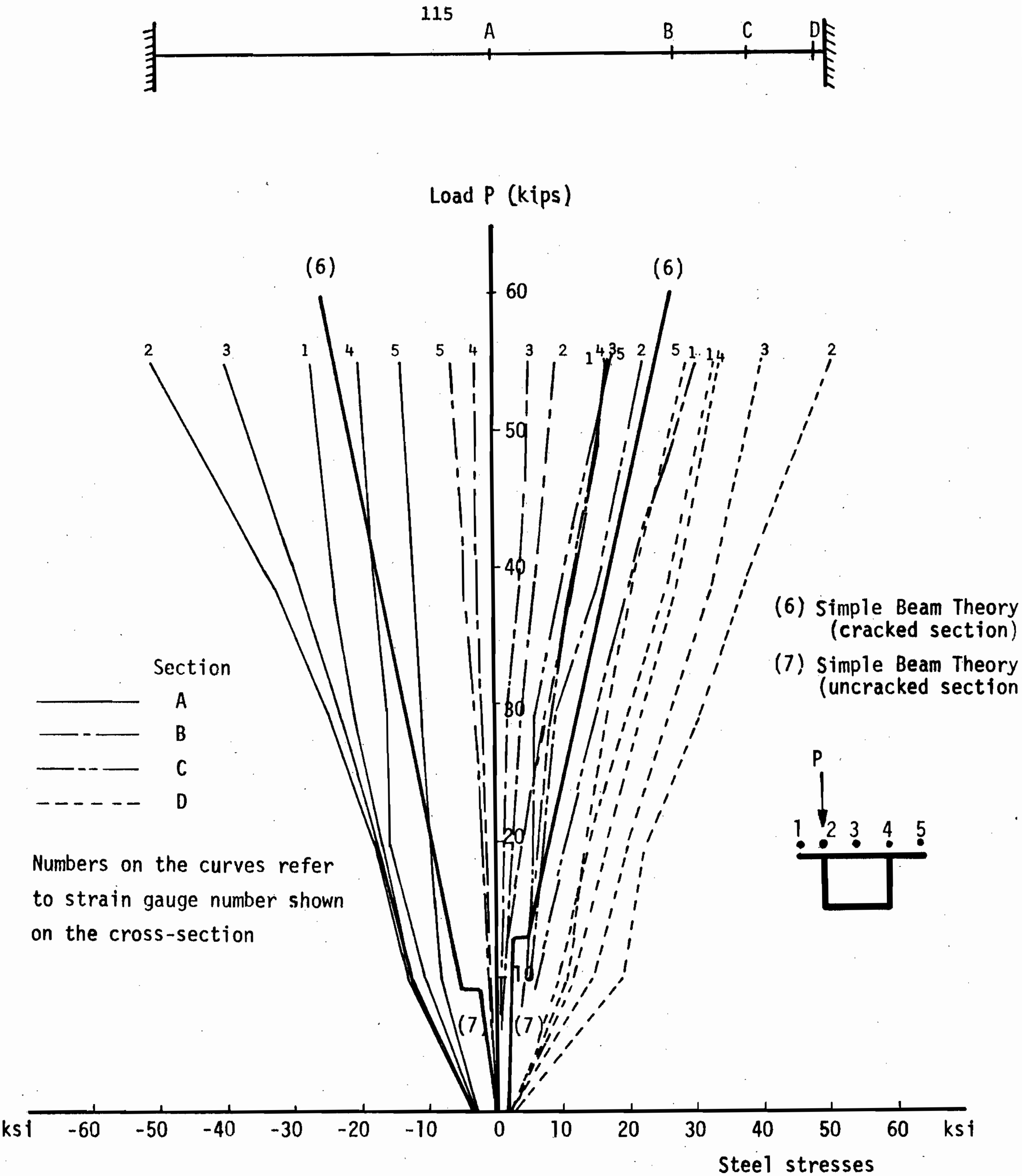

FIG. 3.28 LONGITUDINAL STRESSES IN THE TOP SLAB REINFORCEMENT (UNSYMMETRICAL LOADING CASE)

decreased towards the cantilever ends. At the midspan section, for a load value of 40 kips, the longitudinal steel stresses over the loaded web was approximately -35 ksi, while the minimum value at the cantilever end was -12 ksi. At the support section, for the same load level, the longitudinal steel stress over the loaded web was approximately 40 ksi, while that at the cantilever end was 20 ksi. Figures 3.29 and 3.30 show the envelope of the longitudinal steel stresses through half the bridge span at load values of 19.4 and 55.0 kips. As can be seen, the maximum steel stress values at these load levels were 24 ksi and 52 ksi, respectively.

For years the American Association of State Highway and Transportation Officials (AASHTO) [66] and the California State Department of Highways [94] have used the simple beam theory as a design tool for the box section structures. In the present study, the longitudinal steel stresses calculated from the simple beam theory for both the uncracked and the cracked section analyses were lower than the measured stresses. These differences are due to the effect of warping restraint in increasing these stresses (Fig. 3.28). The longitudinal torsional and the distorsional warping stresses in the longitudinal steel and the concrete in the loaded web at both the midspan and support sections were calculated using the following methods and their combinations for load levels of 20 and 40 kips, respectively:

1. Simple beam theory based on uncracked section analysis.
2. Simple beam theory based on cracked section analysis.

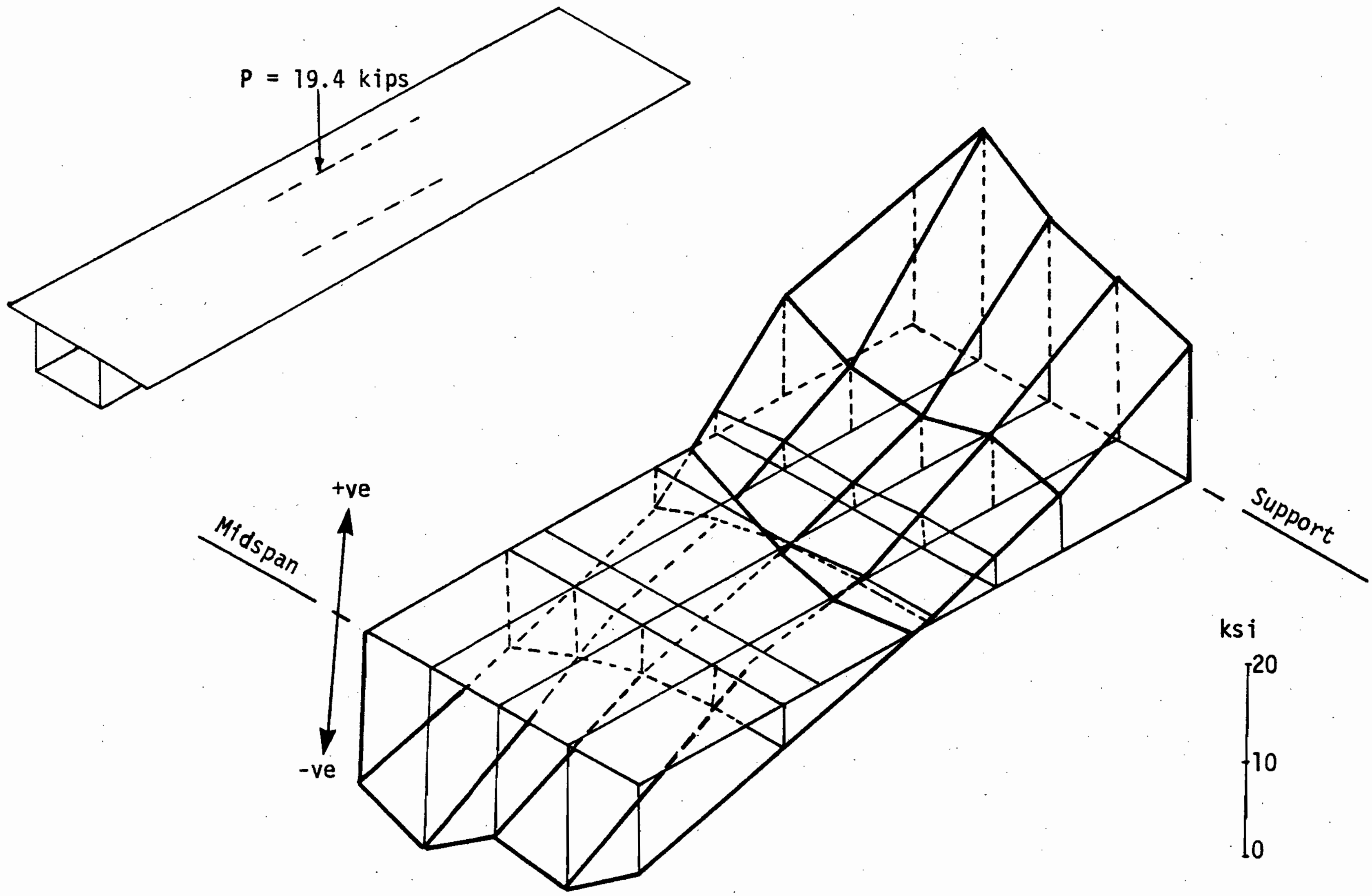

FIG. 3.29 LONGITUDINAL STEEL STRESS ENVELOPE FOR HALF THE BRIDGE SPAN [LOAD P = 19.4 KIPS]
(UNSYMMETRICAL LOADING CASE)

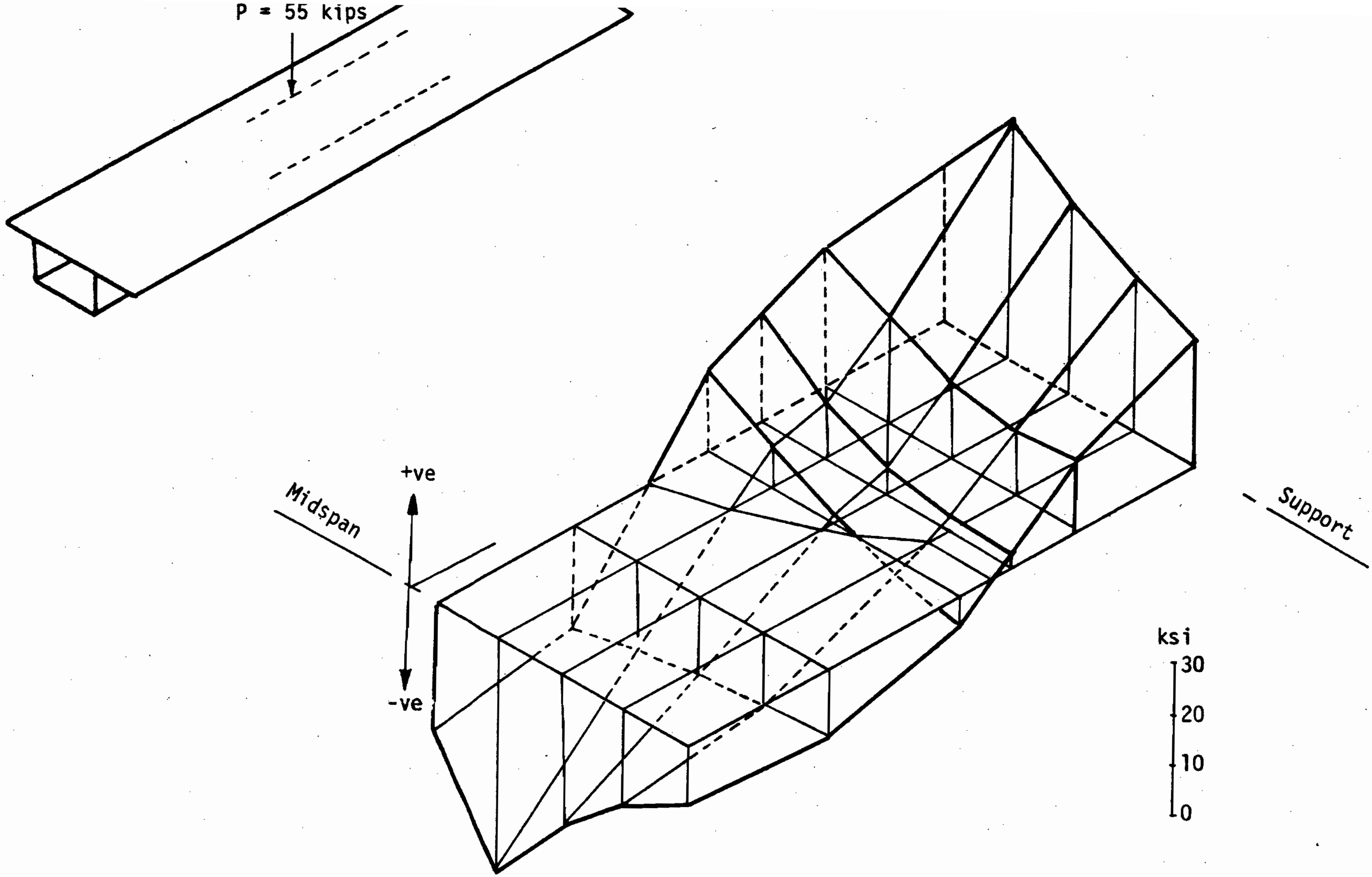

FIG. 3.30 LONGITUDINAL STEEL STRESS ENVELOPE FOR HALF THE BRIDGE SPAN [LOAD P = 55 KIPS]
(UNSYMMETRICAL LOADING CASE)

3. Simple beam theory + longitudinal torsional stresses from the Kollbrunner and Hajdin method.
4. Simple beam theory + longitudinal distorsional stresses from the beam-on-elastic-foundation method.
5. Simple beam theory (uncracked section) + longitudinal torsional stresses from the Kollbrunner and Hajdin method + longitudinal distorsional stresses from the beam-on-elastic-foundation method.
6. Simple beam theory (cracked section) + longitudinal torsional stresses from the Kollbrunner and Hajdin method + longitudinal distorsional stresses from the beam-on-elastic-foundation method.

The calculated values of the concrete and steel stresses are shown in Table 3.1. The experimental longitudinal steel stresses of the top slab were higher than the values calculated using the simple beam theory for both uncracked and cracked sections. However, the addition of the longitudinal torsional and distorsional warping stresses from the Kollbrunner and Hajdin method and the beam-on-elastic-foundation method to the simple beam theory (cracked section analysis) caused the calculated stresses to increase by 30 per cent (Table 3.1). The differences between the experimental and the calculated longitudinal stresses (including the torsional and distortional longitudinal warping stresses) increased with an increase in the applied load.

Table 3.1

Unsymmetrical Load Test

Longitudinal Steel and Concrete Stresses for Load at Midspan of 20 and 40 kips

Load	Bridge cross-section	Element	Steel(s) or concrete(c)	Stress value calculated from measured strains (ksi)	Calculated stress values - ksi: Simple beam theory: Uncracked section (1)	Cracked section (2)	Kollbrunner & Hajdin's method (3)	Beam-on-elastic-foundation method (4)	(1)+(3)+(4) (5)	(2)+(3)+(4) (6)
20 kips	Midspan section	Top slab	s	-18.4	-4.5	-9.5	-1.45	-1.6	-7.55	-12.55
			c	- 0.32	-0.59	-1.47	-0.19	-0.21	-0.99	- 1.87
		Lower slab	s	36.6	6.5	16.0	1.3	1.45	9.25	18.75
			c	-	-	-	-	-	-	-
	Support section	Top slab	s	23.1	3.2	8.1	1.42	1.7	6.32	11.22
			c	0.14	-	-	-	-	-	-
		Lower slab	s	-11.5	-6.5	-14.0	-0.9	-1.05	-8.45	-15.95
			c	-	-1.04	- 2.6	-0.12	-0.14	-1.3	- 2.86
40 kips	Midspan section	Top slab	s	-34.5	-8.6	-17.5	-2.9	-3.2	-15.1	-23.1
			c	- 1.0	-1.07	- 2.5	-0.38	-0.42	- 1.87	- 3.3
		Lower slab	s	60	12.2	31	2.6	2.9	17.7	36.5
			c	-	-	-	-	-	-	-
	Support section	Top slab	s	38.5	4.5	17.5	2.8	3.4	10.75	23.7
			c	-	-	-	-	-	-	-
		Lower slab	s	-21.1	-11	-31	-1.8	-2.1	-14.9	-34.9
			c	- 2.1	- 1.76	- 3.7	-0.24	-0.28	- 2.28	- 4.22

As shown in Table 3.1, these differences were approximately 40 per cent at a load value of 20 kips, and reached a value of approximately 60 per cent at a load value of 40 kips. It should be mentioned that at a load of 10 kips, this difference was less than 20 per cent. Since these methods were developed for elastic homogeneous box sections, it is not surprising to note a large discrepancy between the experimental and the calculated stresses, especially when the section cracks.

The distributions of longitudinal stress in the top slab reinforcement at different bridge sections for different load levels are detailed in Appendix C.

The longitudinal concrete stresses in the top slab in the midspan region behaved in a manner similar to those of the top slab reinforcement at the same location. The non-uniform variation of longitudinal concrete stresses with load in the top slab at different bridge sections is shown in Figure 3.31. At a load value of 40 kips, the maximum longitudinal concrete stress over the loaded web at the midspan section was approximately -1000 psi while the minimum stress at the cantilever tips was approximately -460 psi. The envelopes of the longitudinal concrete stresses in the top slab through half of the bridge span at load values of 19.4 and 55.0 kips respectively are shown in Figures 3.32 and 3.33. Again, as expected, the simple beam theory overestimates the resulting longitudinal concrete stresses within the box section. Table 3.1 shows a comparison between the experimental longitudinal concrete stresses and those obtained from the simple beam

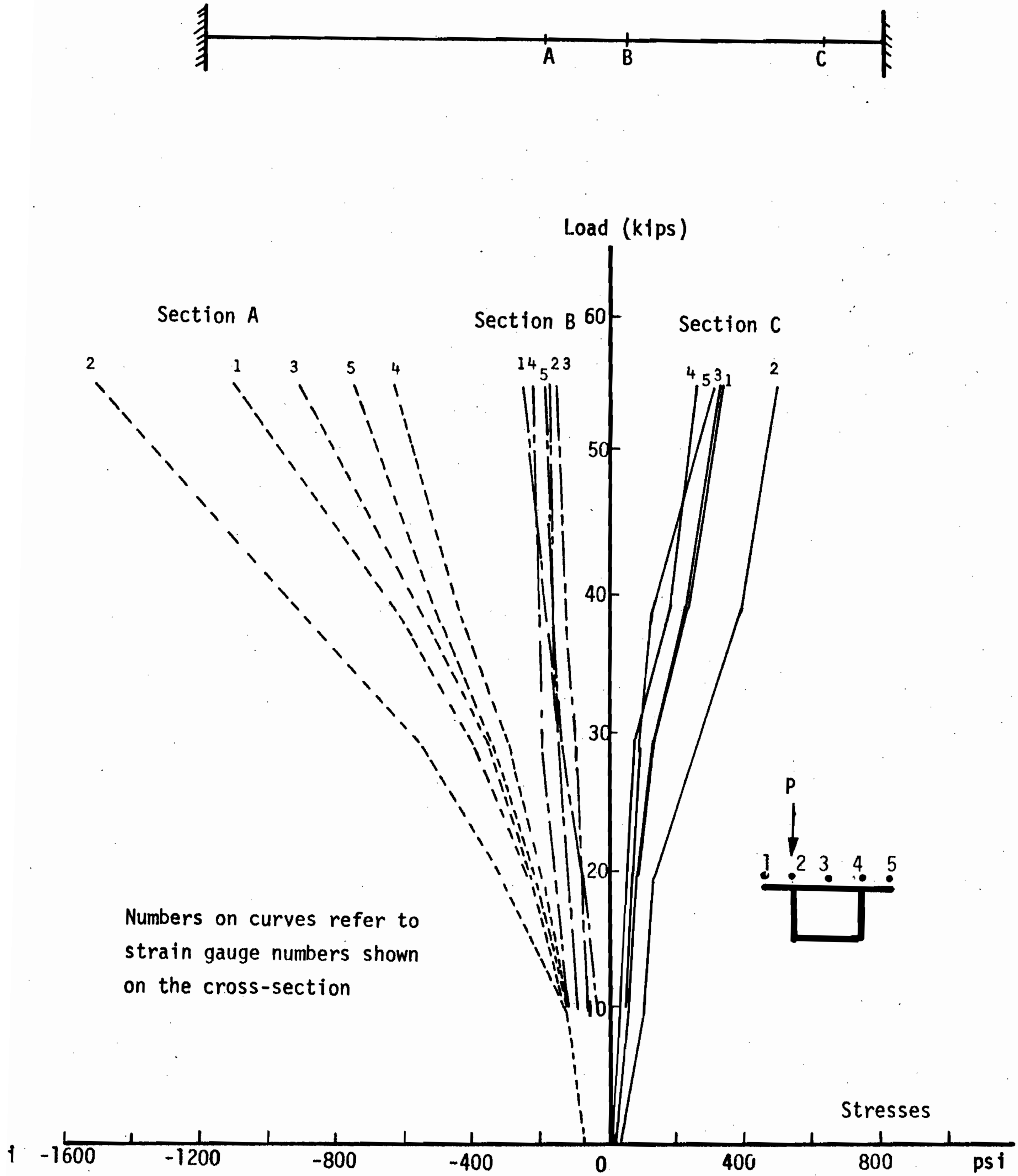

FIG. 3.31 LONGITUDINAL CONCRETE STRESSES ON THE TOP SLAB (UNSYMMETRICAL LOADING CASE)

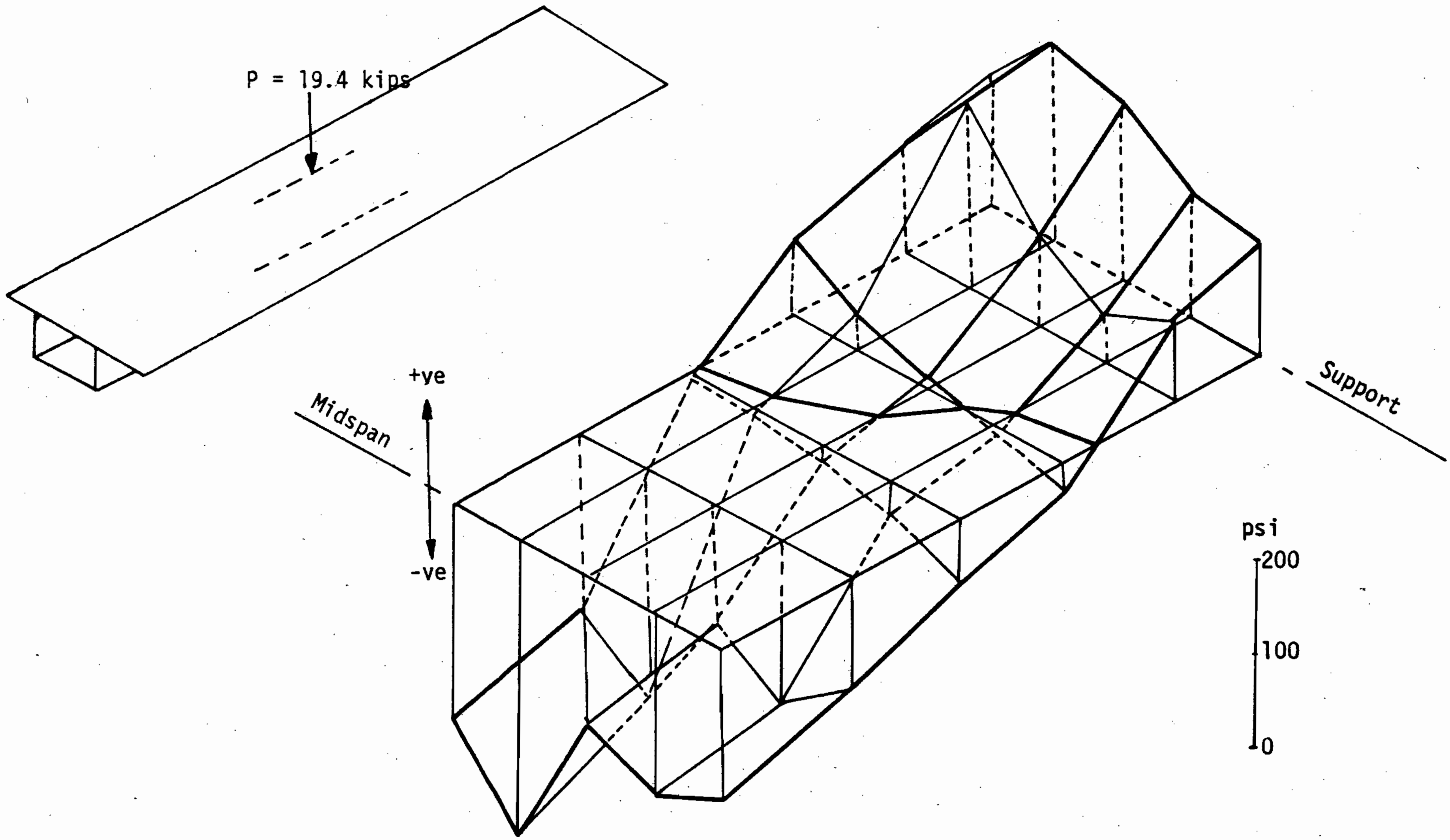

FIG. 3.32 TOP SLAB LONGITUDINAL CONCRETE STRESS ENVELOPE FOR HALF THE BRIDGE SPAN [LOAD P = 19.4 KIPS] (UNSYMMETRICAL LOADING CASE)

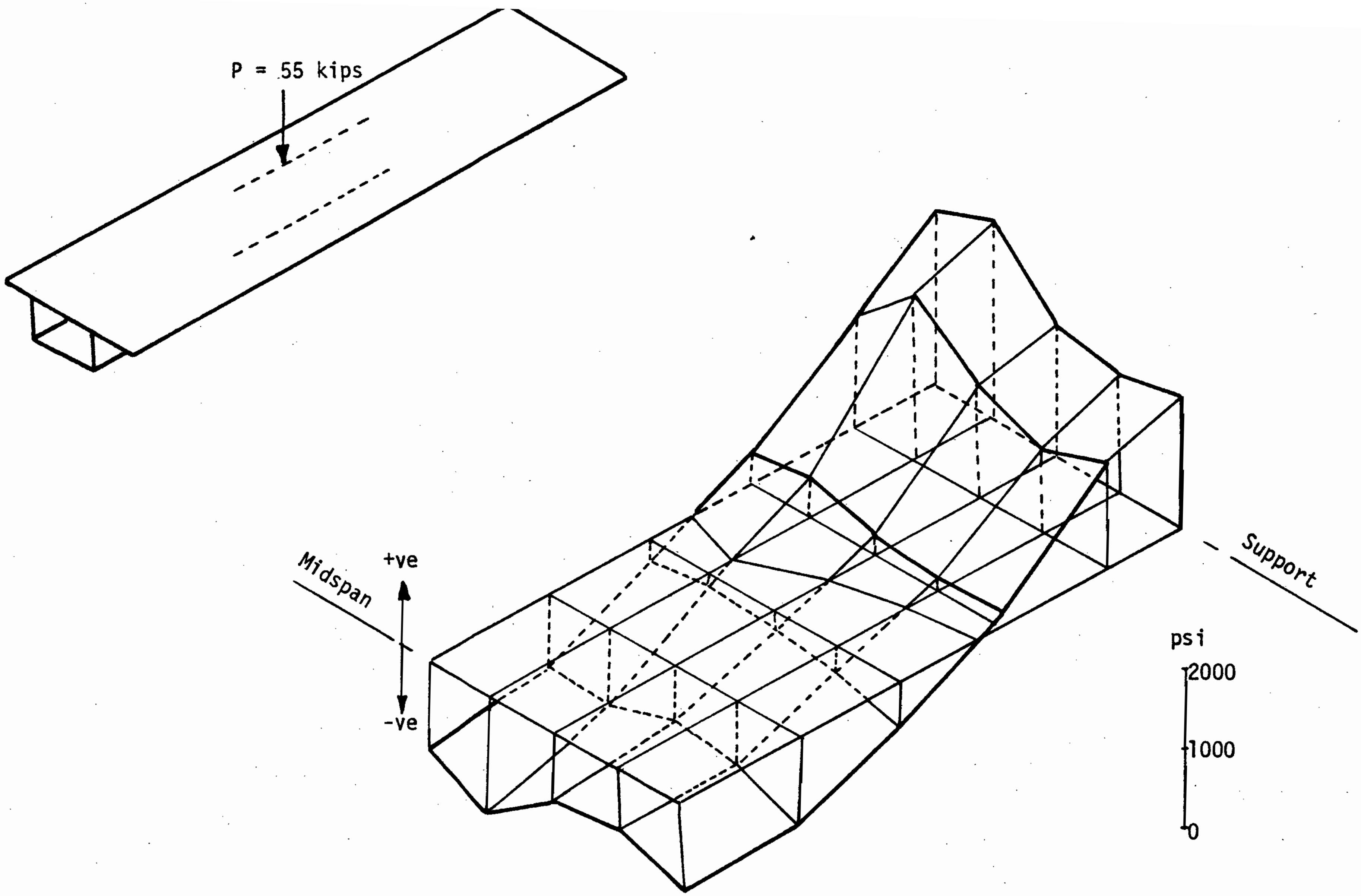

FIG. 3.33 TOP SLAB LONGITUDINAL CONCRETE STRESS ENVELOPE FOR HALF THE BRIDGE SPAN
[LOAD P = 55 KIPS] (UNSYMMETRICAL LOADING CASE)

theory for both uncracked and cracked sections. As shown, the simple beam theory based on the cracked section analysis gave a concrete stress value of -2500 psi over the loaded web at the midspan section, while the experimental stress value was approximately -1000 psi. The incorporation of the longitudinal torsional and distorsional warping stresses in these analyses has increased the predicted values from the simple beam theory for both uncracked and cracked sections by approximately 15 to 30 per cent. The addition of the torsional and distorsional warping stresses in the slab steel to the stress values calculated from the simple beam theory using a cracked section, showed convergence towards the measured values at both the midspan and support sections (Table 3.1). The calculated longitudinal concrete stresses do not show the same convergence to the measured values as the steel stresses. The longitudinal concrete stresses at different bridge sections for different load values are detailed in Appendix C.

3.4.3.2 Lower Slab

Variation of the longitudinal stresses in the lower slab reinforcement at different locations through the bridge span is shown in Figure 3.34. Again, the distribution of the longitudinal stresses in the lower slab reinforcement was not uniform across the lower slab width. At the midspan section, for a load value of 40 kips, the maximum steel stress occurred under the loaded web and was approximately 60 ksi, while the minimum stress occurred beneath the unloaded web and

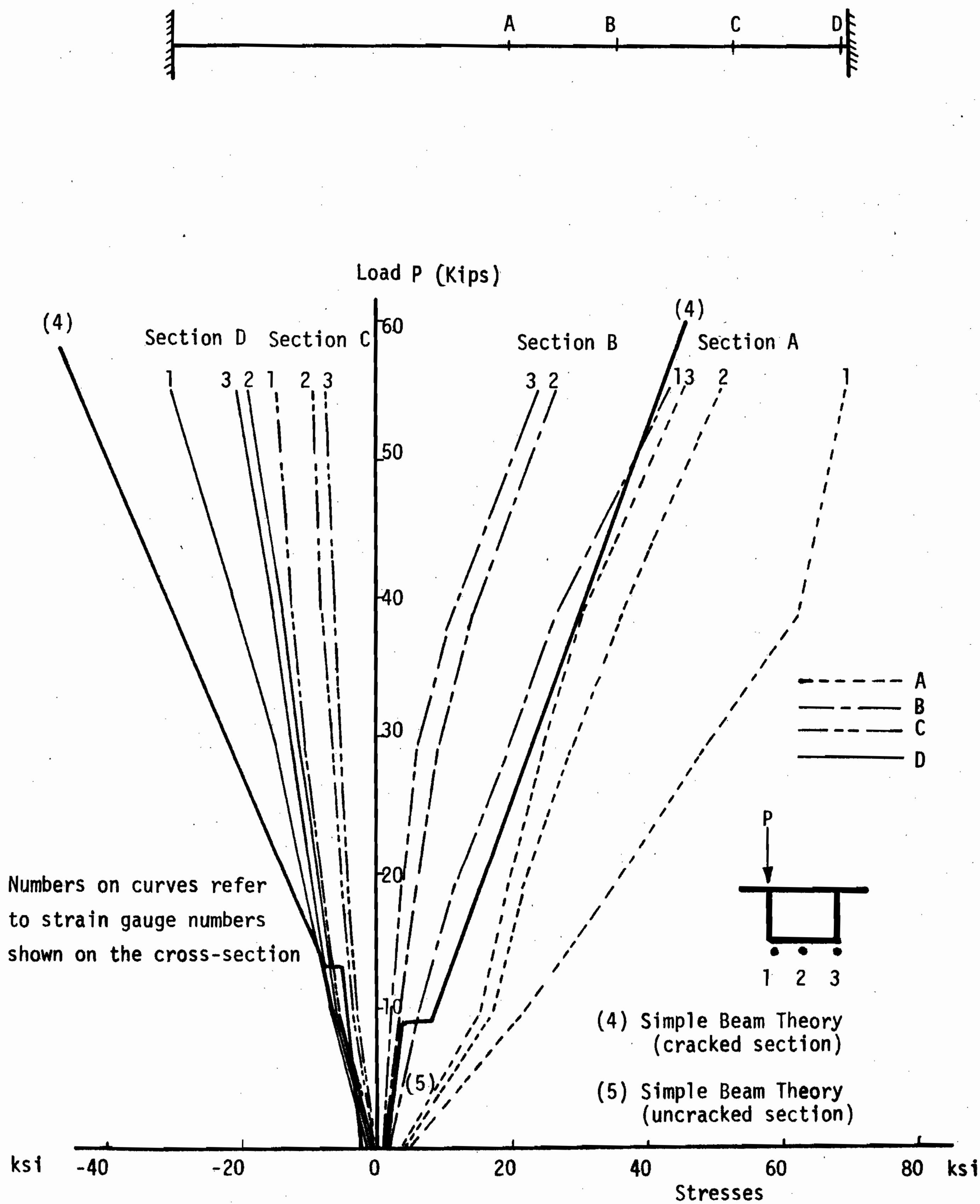

FIG. 3.34 LONGITUDINAL STRESSES OF THE LOWER SLAB REINFORCEMENT (UNSYMMETRICAL LOADING CASE)

was approximately 32 ksi. At the support section, for the same load level, the steel stresses beneath the loaded and unloaded webs were approximately -21 ksi and -14 ksi, respectively. Here the negative sign indicates that these stresses are compressive.

The envelopes of the longitudinal steel stresses in the lower slab through half the bridge span at load values of 19.4 and 55.0 kips are shown in Figures 3.35 and 3.36 respectively. The longitudinal steel stresses at different bridge sections for different load values are detailed in Appendix C.

A comparison between the measured and the calculated steel stresses in the lower slab at both the midspan and support sections for load values of 20 and 40 kips are shown in Table 3.1. As shown in this table, the measured longitudinal steel stresses in the lower slab at the midspan section were higher than the calculated values, even after accounting for the contribution of the torsional and distorsional warping stresses. However, at the support section, the measured stresses were higher than those calculated using the uncracked section analysis and were lower than those based on the cracked section analysis. This difference is due to the warping of the section.

The longitudinal concrete stresses in the lower slab behaved in a manner similar to the longitudinal stresses in the lower slab reinforcement at the same location. As shown in Table 3.1, the measured longitudinal concrete stresses were higher than those predicted from the simple beam theory based on an uncracked section, and lower than those based on a cracked section. However, the inclusion of the torsional

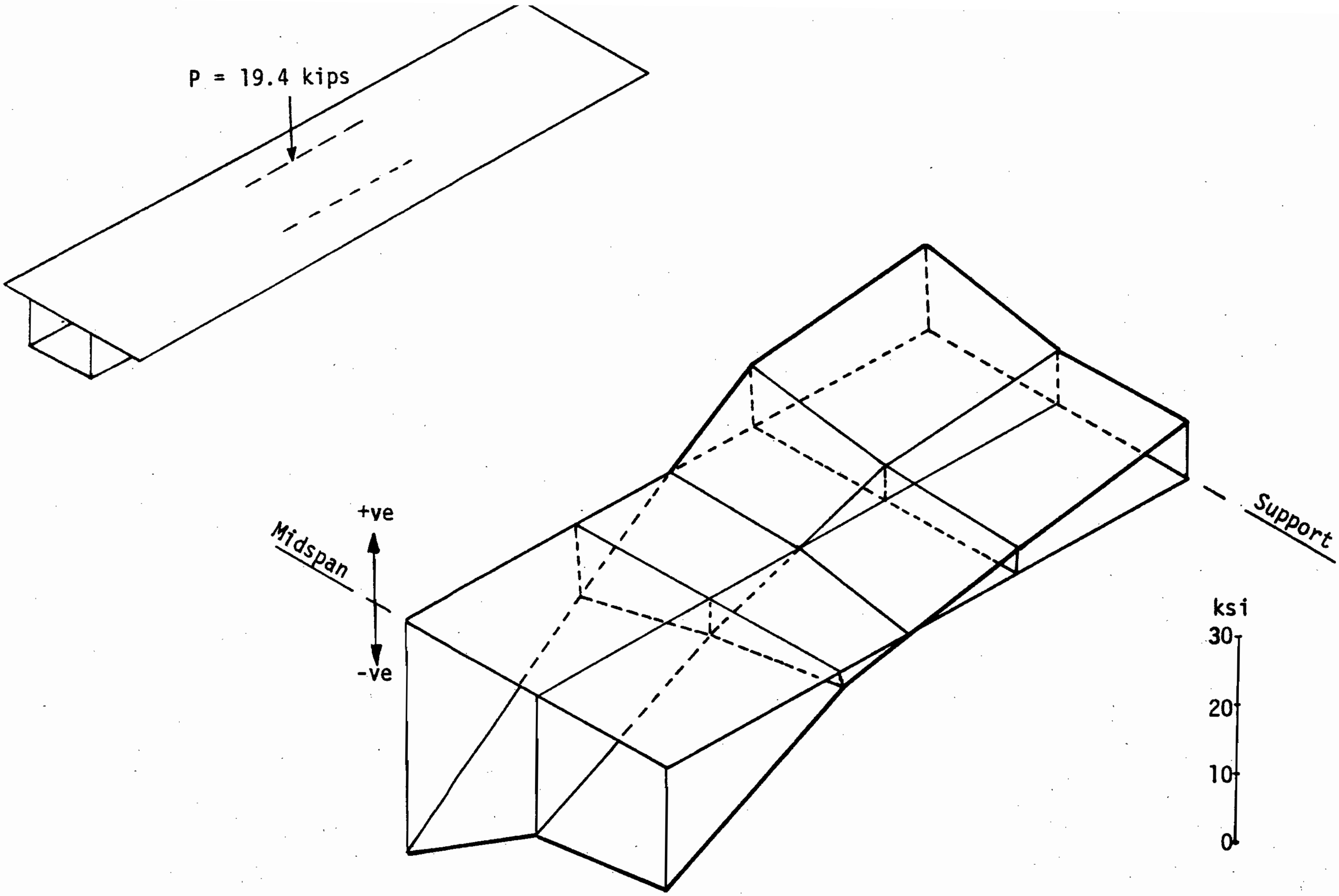

FIG. 3.35 LONGITUDINAL STRESS ENVELOPE FOR THE LOWER SLAB REINFORCEMENT THROUGH HALF THE BRIDGE SPAN [LOAD P = 19.4 KIPS] (UNSYMMETRICAL LOADING CASE)

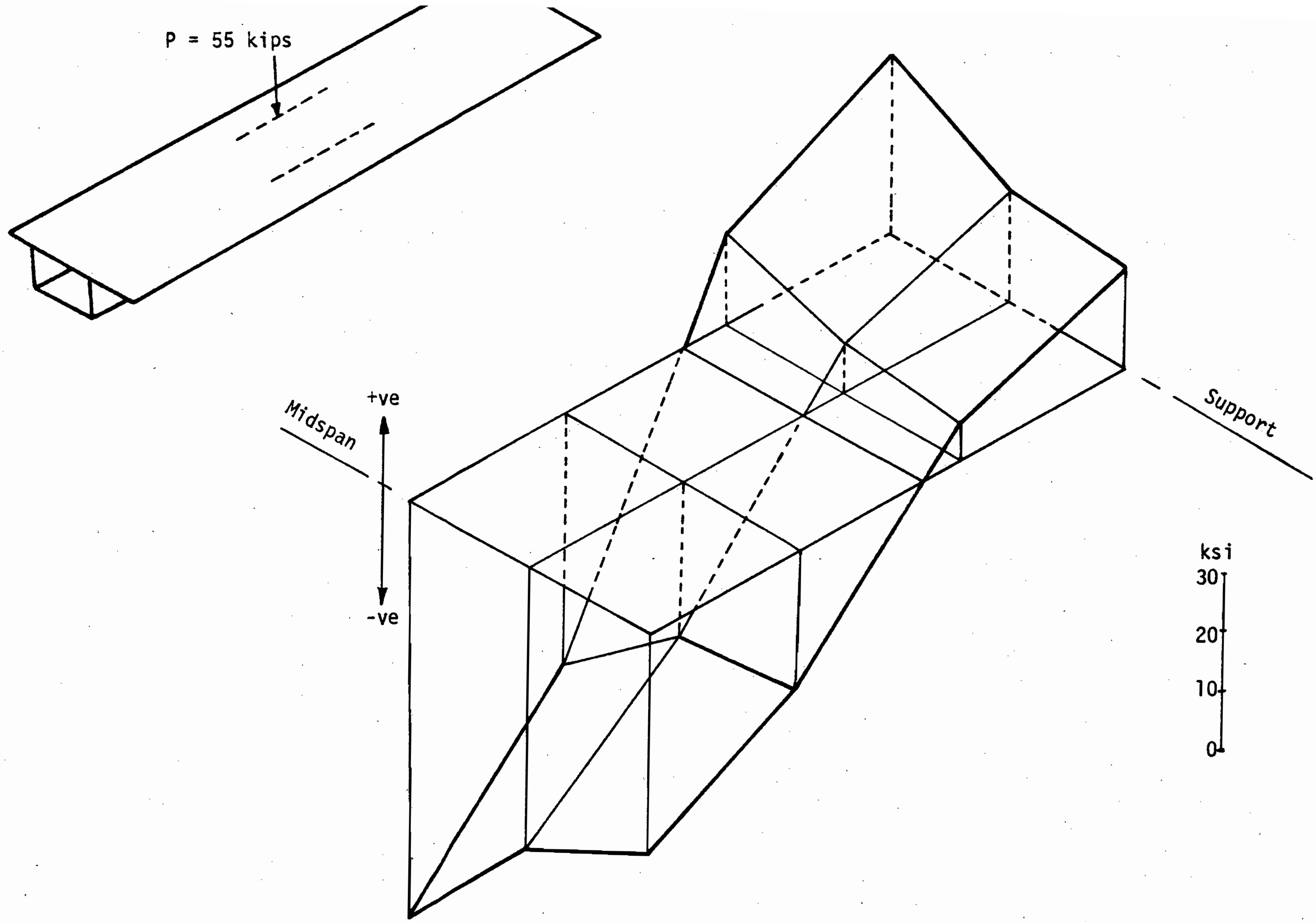

FIG. 3.36 LONGITUDINAL STRESS ENVELOPE FOR THE LOWER SLAB REINFORCEMENT THROUGH HALF THE BRIDGE SPAN [LOAD P = 55 KIPS] (UNSYMMETRICAL LOADING CASE)

and distorsional warping stresses in the calculation (column (5)) gave better agreement with the measured values. Again, the differences are due to the combined effect of the longitudinal flexural and warping stresses in this region, in addition to the redistribution of forces within the box section resulting from the cracking of concrete.

3.4.3.3 Cracks in the Top Slab

Flexural cracks first formed in the top slab near the support at a load value of 22 kips. These cracks were perpendicular to the longitudinal axis of the bridge. A few cracks were formed through the thickness of the cantilever slab on the loaded web side. As the load was increased, these cracks extended horizontally in the cantilever slab until they intersected the loaded web before propagating into the lower slab. As expected, these cracks were concentrated in the loaded web more than those in the unloaded web. Figure 3.37 shows the crack pattern in the top slab.

At a load value of 48 kips, an inclined crack formed in the top slab over both webs near the quarter span region of the bridge. With the increase in the applied load, these cracks extended into the webs and the top slab until they intersected the longitudinal cracks formed over the unloaded web due to the transverse tensile stresses in this region. In the vicinity of the applied load at the midspan section, a curved longitudinal crack formed as shown in Figure 3.37.

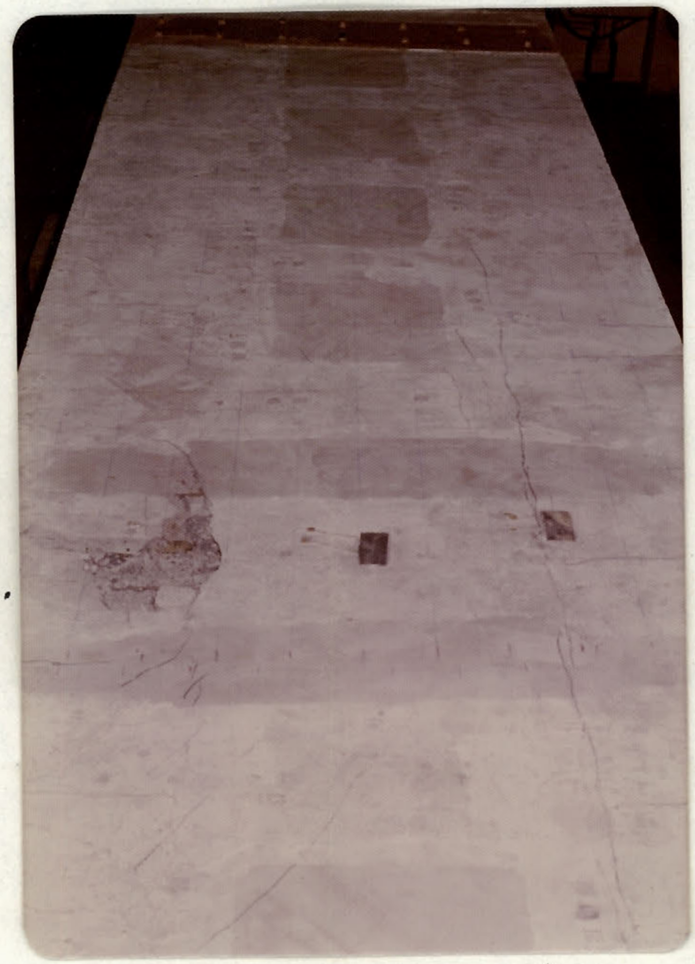

FIG. 3.37 CRACK PATTERN FOR THE TOP SLAB
(UNSYMMETRICAL LOADING CASE)

At a load value of 58 kips, a local punching shear failure occurred beneath the applied load; the depth of the punched region was about 3/16 in.

Figure 3.38 shows the average variation of the crack width with load in the top slab at both support and midspan sections.

As shown in Figure 3.39, the cracks in the cantilever slabs were perpendicular to the longitudinal axis of the bridge; there were no inclined cracks in this region. This shows that the side cantilevers in a box section do not contribute to its torsional behaviour.

3.4.3.4 Cracks in the Lower Slab

At a load value of 10 kips, flexural cracks first formed in the lower slab at the midspan section under the applied load. The number of cracks in the lower slab increased as the applied load was increased. These cracks were concentrated beneath the loaded web, perpendicular to the longitudinal axis of the bridge, and confined within a distance of approximately 4 ft. in the midspan region. In the quarter span region, diagonal cracks formed, inclined at approximately 40° to 45° to the horizontal axis of the bridge.

At a load value of 48 kips, a set of transverse cracks formed in the lower slab at the midspan section and were perpendicular to the longitudinal cracks in this region. These cracks were concentrated beneath the loaded web and extended over the middle third of the bridge span. These cracks decreased in number, length and width towards the

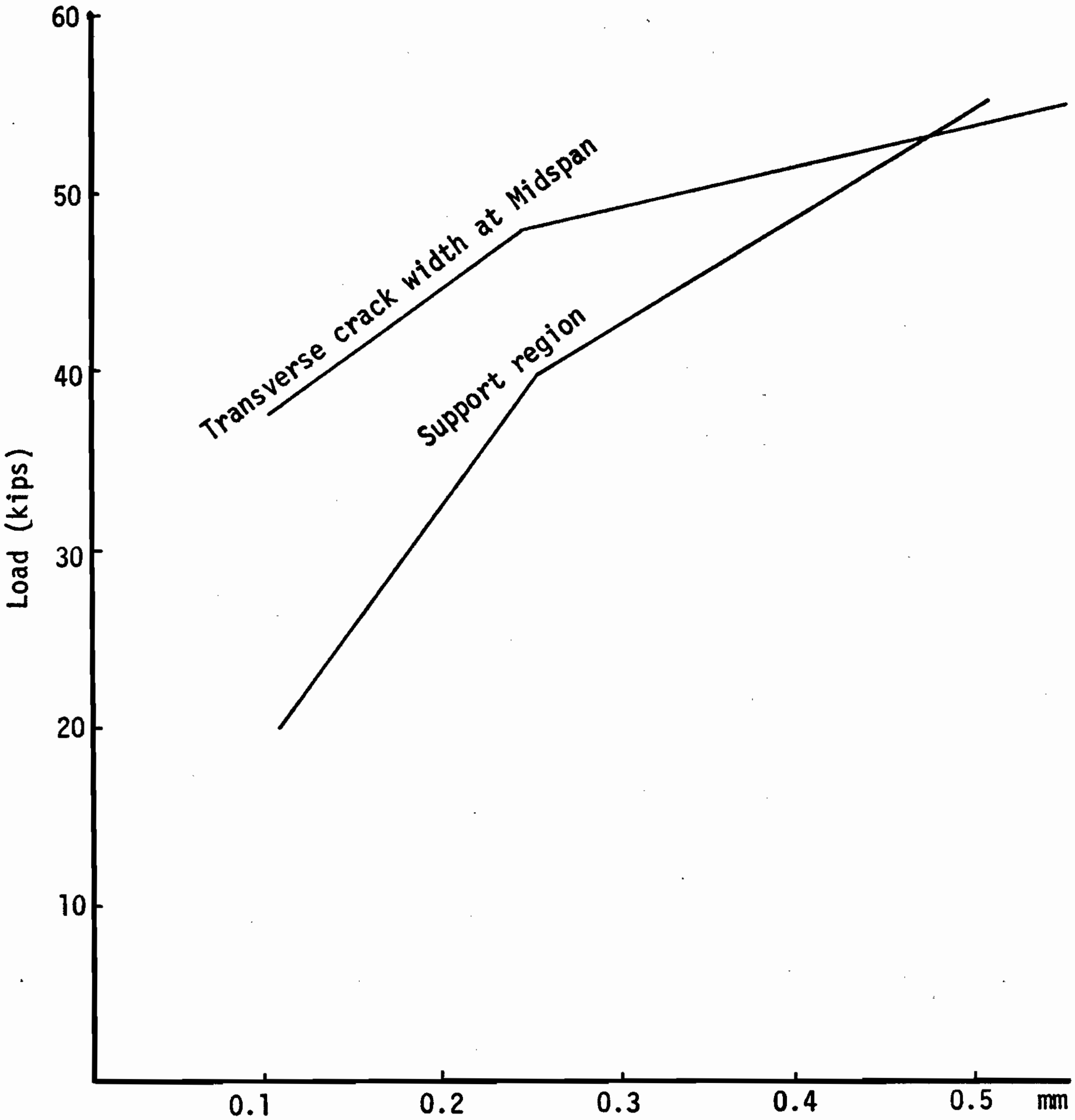

FIG. 3.38 LOAD-AVERAGE CRACK WIDTH VARIATION FOR THE TOP SLAB (UNSYMMETRICAL LOADING CASE)

FIG. 3.39 CRACK PATTERN IN THE CANTILEVER SLAB
(UNSYMMETRICAL LOADING CASE)

unloaded web and towards the support regions. The inclined cracks in the lower slab were the horizontal extension of the shear cracks from both the loaded and the unloaded webs. Figure 3.40 shows the load-crack width variation in the lower slab beneath the loaded and the unloaded webs in the vicinity of the midspan section.

3.4.4 Transverse Steel and Concrete Stresses

3.4.4.1 Transverse Stresses in Top and Bottom Slab Reinforcement

For the symmetrical loading case, the transverse reinforcement was subjected to transverse stresses which were approximately 30 per cent of the longitudinal steel stresses at the same location. In the unsymmetrical loading case, the transverse reinforcement played a significant part in resisting the applied eccentric loads. These transverse stresses were approximately of the same order as the longitudinal stresses at the same location. Figure 3.41 shows the experimental load-transverse stresses for the top slab reinforcement over the loaded and unloaded webs at different locations through the bridge span.

A study of the experimental data shows that the tensile stresses in the top slab transverse reinforcement were concentrated over the unloaded web in the midspan region of the bridge, while transverse compressive stresses existed over the loaded web at the same section. The reason for the change in the sign of the transverse stresses between the loaded and the unloaded webs is that the concentrated load causes a

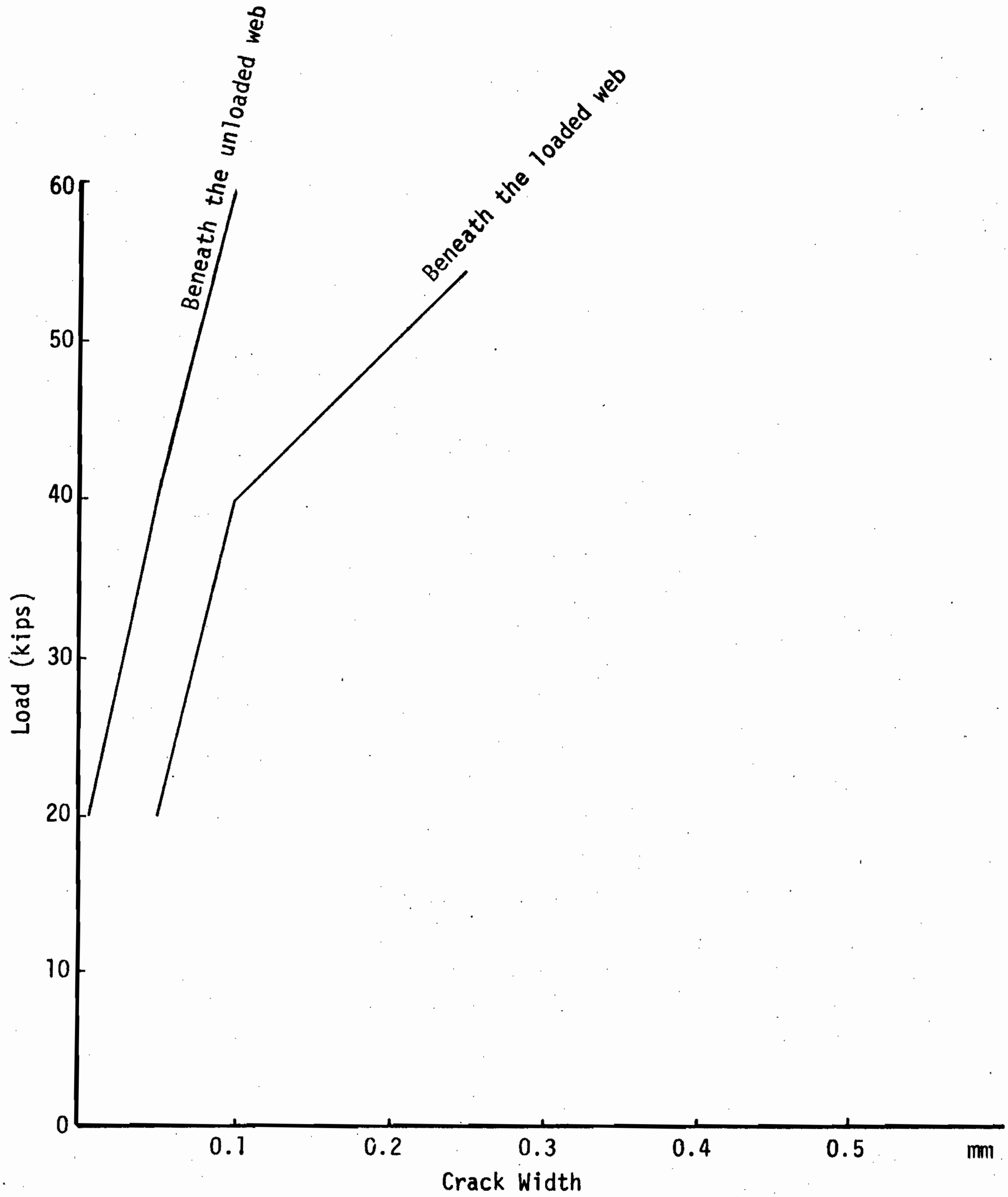

FIG. 3.40 LOAD AVERAGE CRACK WIDTH FOR THE BOTTOM SLAB
(UNSYMMETRICAL LOADING CASE)

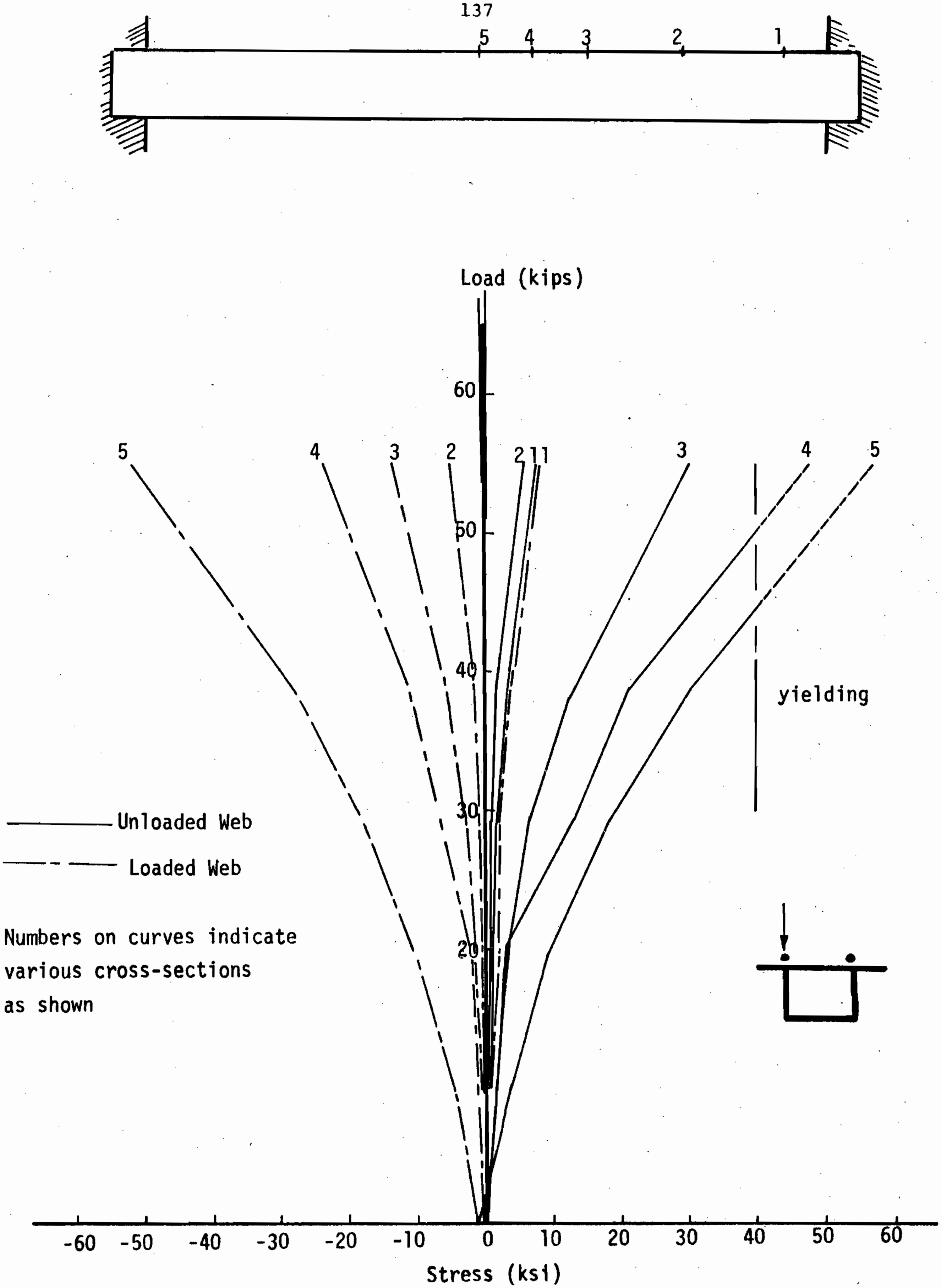

FIG. 3.41 STEEL STRESS VARIATION IN THE TOP SLAB TRANSVERSE REINFORCEMENT (UNSYMMETRICAL LOADING CASE)

sagging transverse bending at the top of the loaded web and hogging transverse bending at the top of the unloaded web. Consequently the stresses due to the concentrated load oppose the stresses due to dead load at the loaded web and are additive to these stresses at the unloaded web resulting in this increase.

Figures 3.42 and 3.43 show the envelope of the steel stresses of the transverse reinforcement in the top slab through half of the bridge span at load values of 19.4 and 55 kips, respectively. The transverse steel stresses in the loaded and unloaded webs at the midspan section were -11 ksi and 9 ksi respectively at 19.4 kips, and -47 ksi and 46 ksi respectively at 55 kips. These stresses were approximately of the same order as the longitudinal stresses in the top slab reinforcement at the same location. These observations show that for the eccentric load test the transverse stresses in the top slab are higher than those predicted from the Poisson effect. This is due to the combined effect of shear and torsional stresses in the transverse direction, along with the contribution of the longitudinal stresses in that direction through the Poisson effect. The transverse reinforcement over the unloaded and the loaded webs in the top slab at the midspan section yielded at load values of 43 and 46 kips, respectively.

For homogeneous, elastic bodies the following well known equation [9] was developed to calculate the transverse stresses in thin-walled open or closed sections:

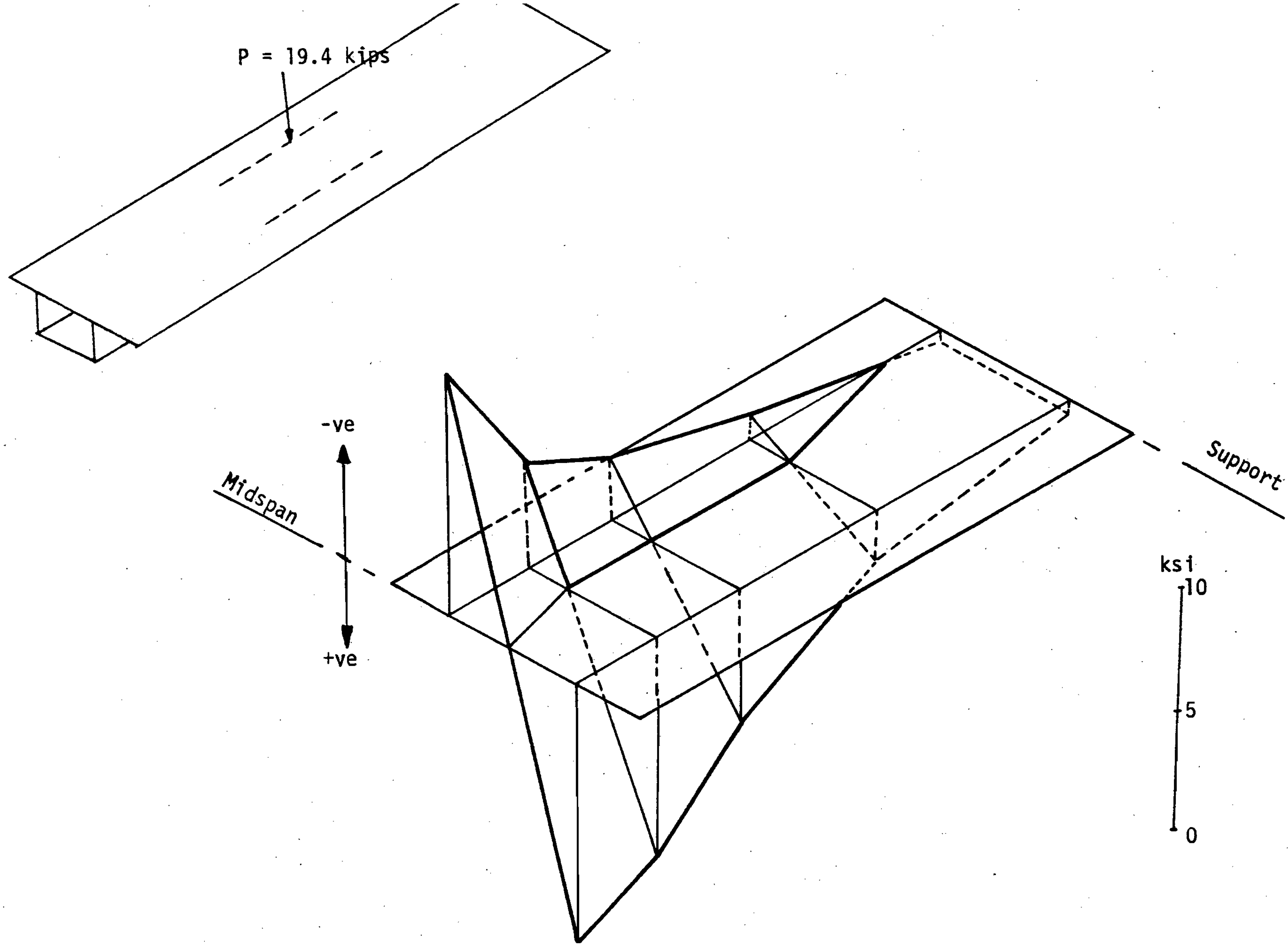

FIG. 3.42 TRANSVERSE ENVELOPE FOR THE TOP SLAB TRANSVERSE REINFORCEMENT THROUGH HALF THE BRIDGE SPAN [LOAD P = 19.4 KIPS] (UNSYMMETRICAL LOADING CASE)

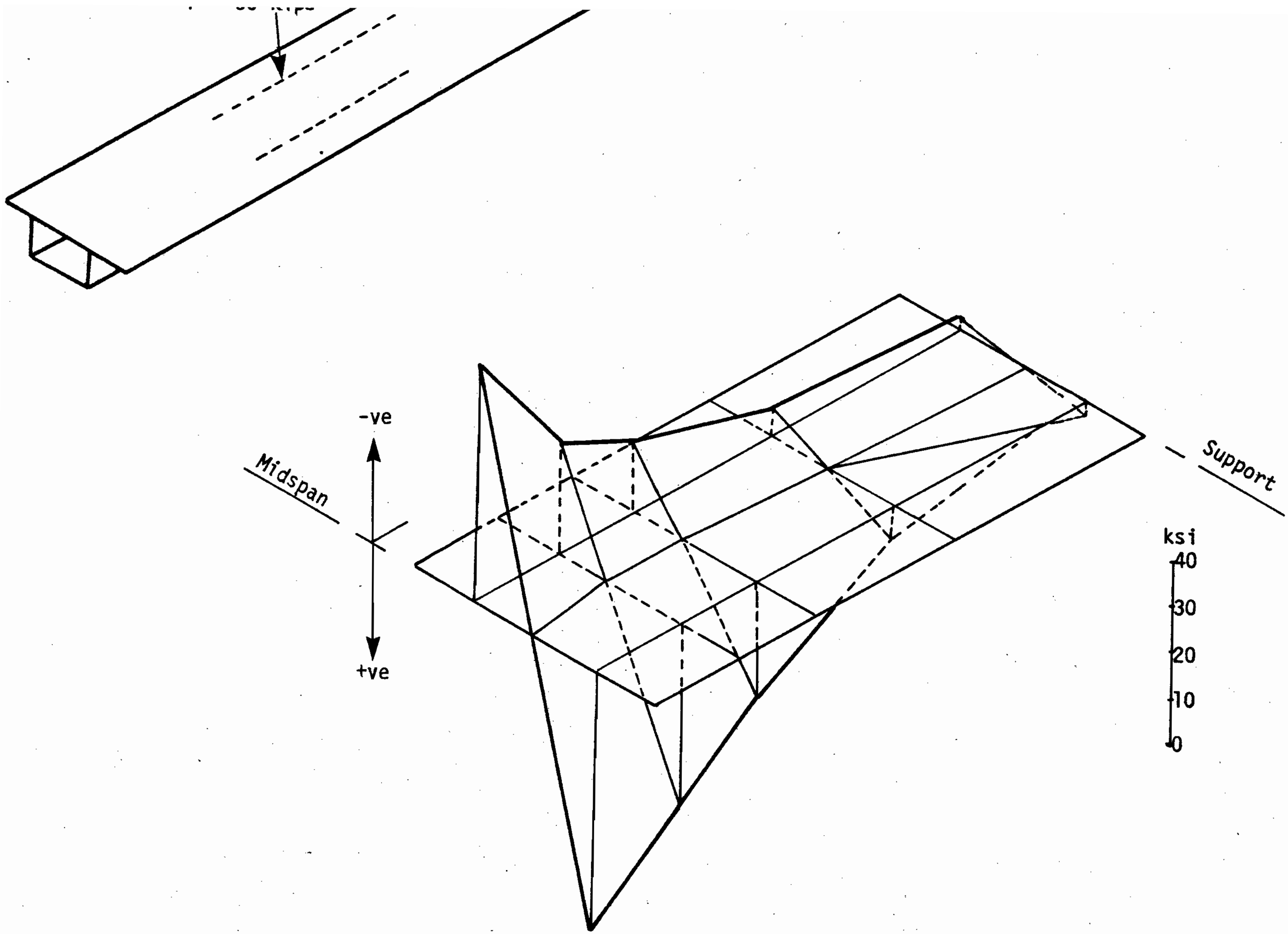

FIG. 3.43 ENVELOPE FOR THE TOP SLAB TRANSVERSE REINFORCEMENT THROUGH HALF THE BRIDGE SPAN [LOAD P = 55 KIPS] (UNSYMMETRICAL LOADING CASE)

$$\tau = \frac{M_T}{2 A_{enc} t} \tag{3.7}$$

where τ = shear stress at the centreline of the flange

M_T = torsional moment at the cross-section

A_{enc} = area enclosed by centreline of wall of closed portion of the cross-section

t = flange thickness.

The experimental results were much higher than the values predicted from this equation. It is therefore obvious that equations developed for linear elastic systems cannot be used for analysis of a box section structure and there is a need for a suitable analysis method to calculate these transverse stresses in such types of structures, which will account for nonlinearities of behaviour resulting from inelasticity of concrete, yielding of steel and cracking.

The transverse stresses in the lower slab reinforcement at the midspan section were also higher than the values predicted from equation 3.7 (Fig. 3.44). The measured transverse steel stresses for a load value of 20 kips were 12 ksi and 9 ksi under the unloaded and loaded webs respectively, while the calculated value was approximately 2 ksi. As shown in Figure 3.44, the transverse stress under the unloaded web was higher than that under the loaded web. This is due to the combined influence of the Poisson effect and the transverse bending stresses at this section. As the applied load was increased,

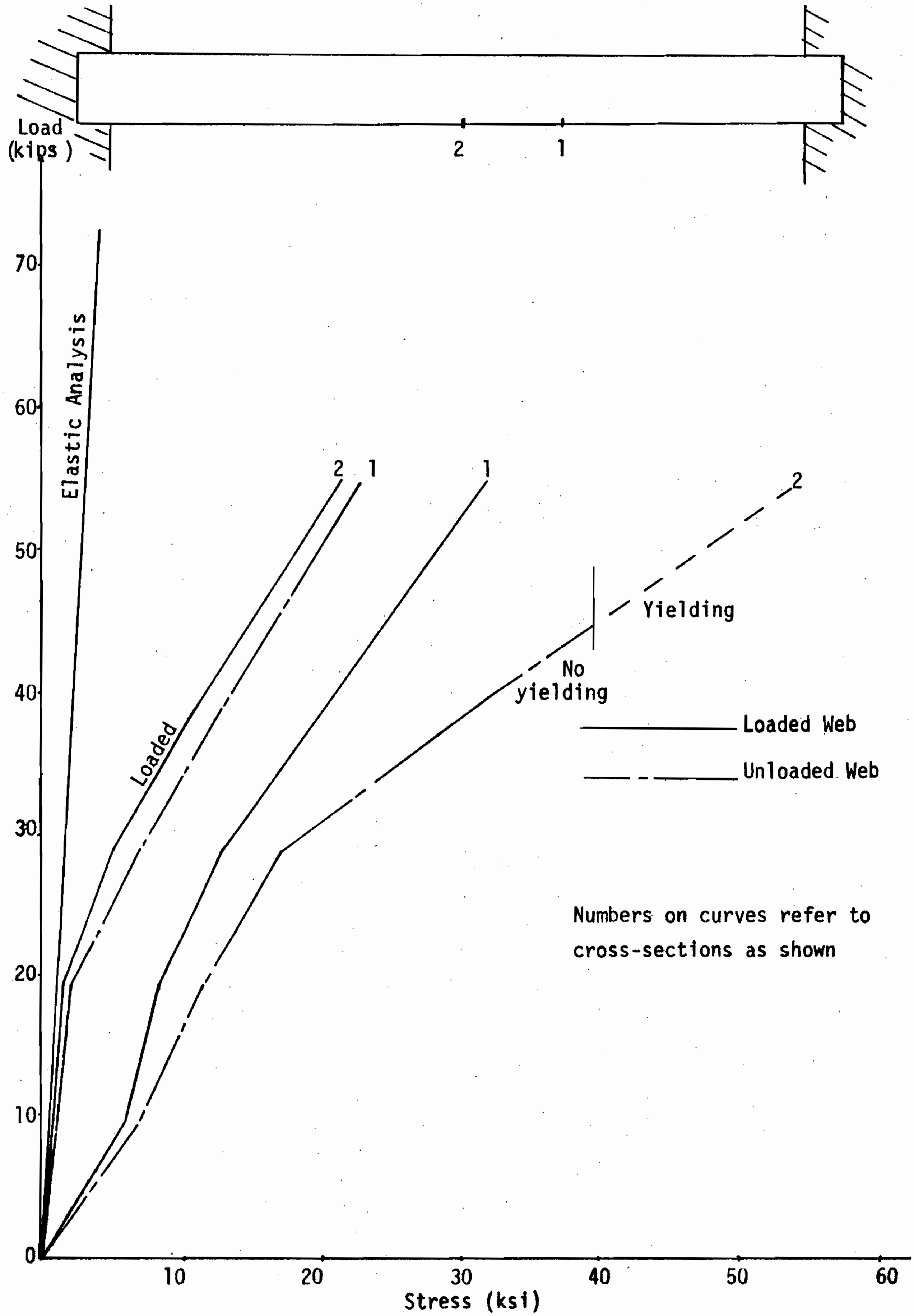

FIG. 3.44 STRESS VARIATION IN THE LOWER SLAB TRANSVERSE REINFORCEMENT (UNSYMMETRICAL LOADING CASE)

the stresses in the transfer reinforcement under the unloaded web increased significantly until it yielded at a load value of 45 kips.

The transverse steel stresses through half of the bridge span at load values of 19.4 and 55 kips are shown in Figures 3.45 and 3.46. The transverse stress distribution in the top and bottom slab reinforcements at different bridge sections for different load values is shown in Appendix C.

3.4.4.2 Transverse Concrete Stresses in Top and Bottom Slabs

The experimental transverse concrete stresses in the top slab over the loaded and the unloaded webs at different locations through the bridge span are shown in Figure 3.47.

Significant transverse tensile and compressive concrete stresses were observed over the unloaded and the loaded webs respectively. Over the unloaded web, these transverse stresses are due to the Poisson effect from the longitudinal direction, in addition to the stresses resulting from the load distribution across the width of the box section. Over the loaded web, these compressive transverse stresses result from the transverse distribution of loads across the width of the box section, as well as the stress concentration in the vicinity of the applied load. At a load value of 38.8 kips, the tensile stresses in the concrete over the unloaded web at the midspan section exceeded the tensile strength of concrete (f'_t = 450 psi), causing a longitudinal crack in the top slab at the unloaded web parallel to the bridge longitudinal axis. These

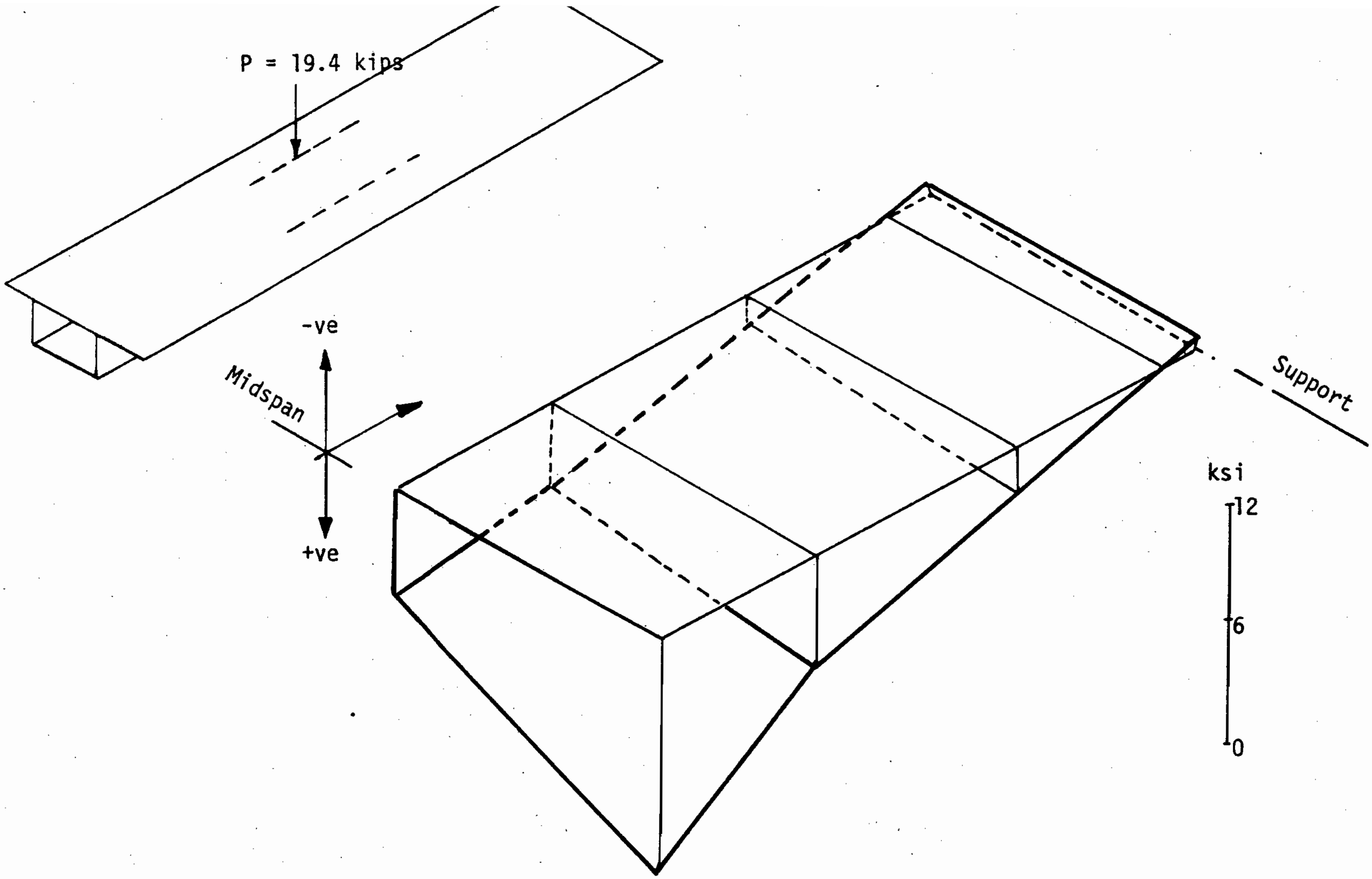

FIG. 3.45 STRESS ENVELOPE FOR THE LOWER SLAB TRANSVERSE REINFORCEMENT THROUGH HALF THE BRIDGE SPAN [LOAD P = 19.4 KIPS] (UNSYMMETRICAL LOADING CASE)

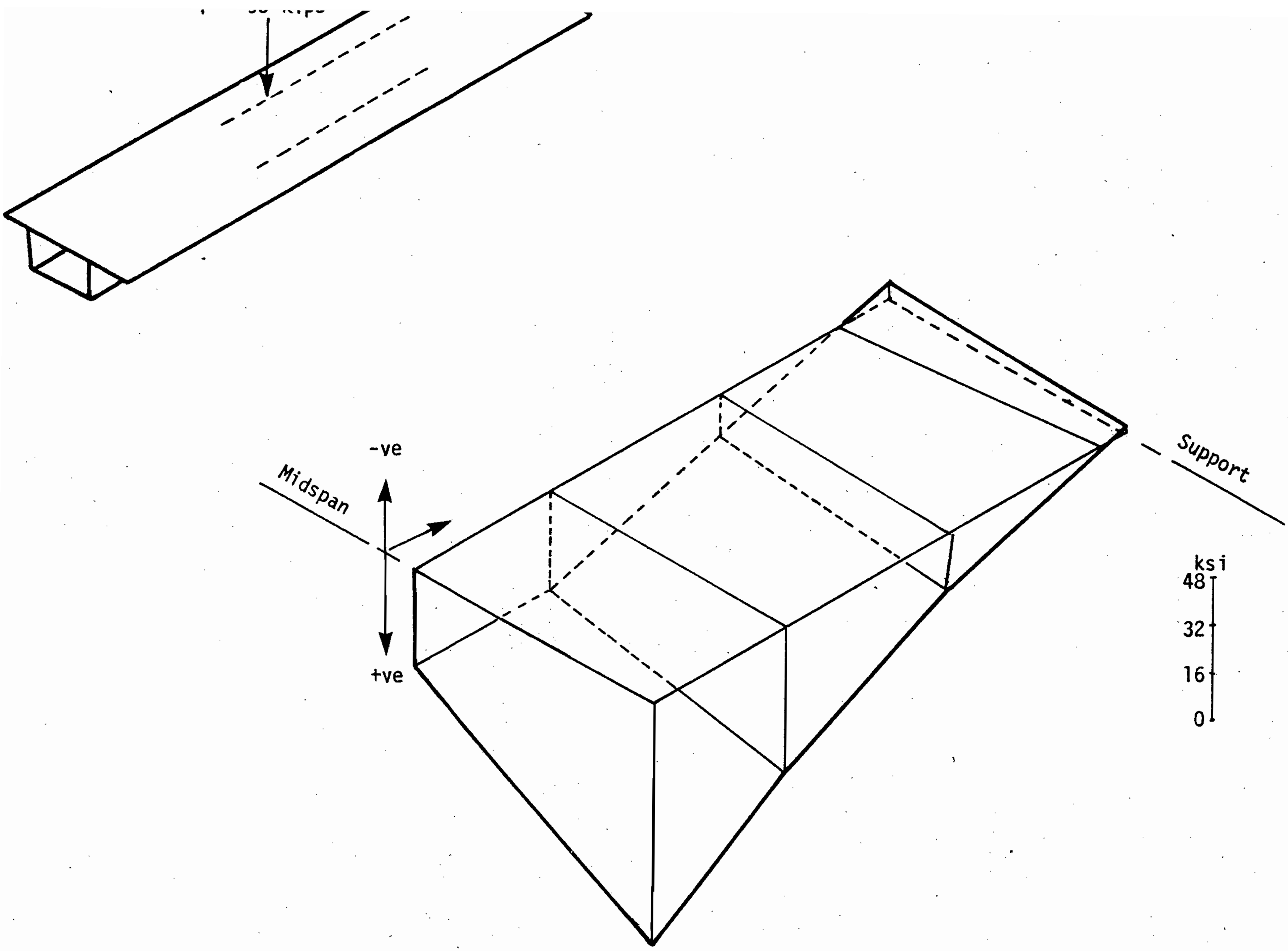

FIG. 3.46 STRESS ENVELOPE FOR THE LOWER SLAB TRANSVERSE REINFORCEMENT THROUGH HALF THE BRIDGE SPAN [LOAD P = 55 KIPS] (UNSYMMETRICAL LOADING CASE)

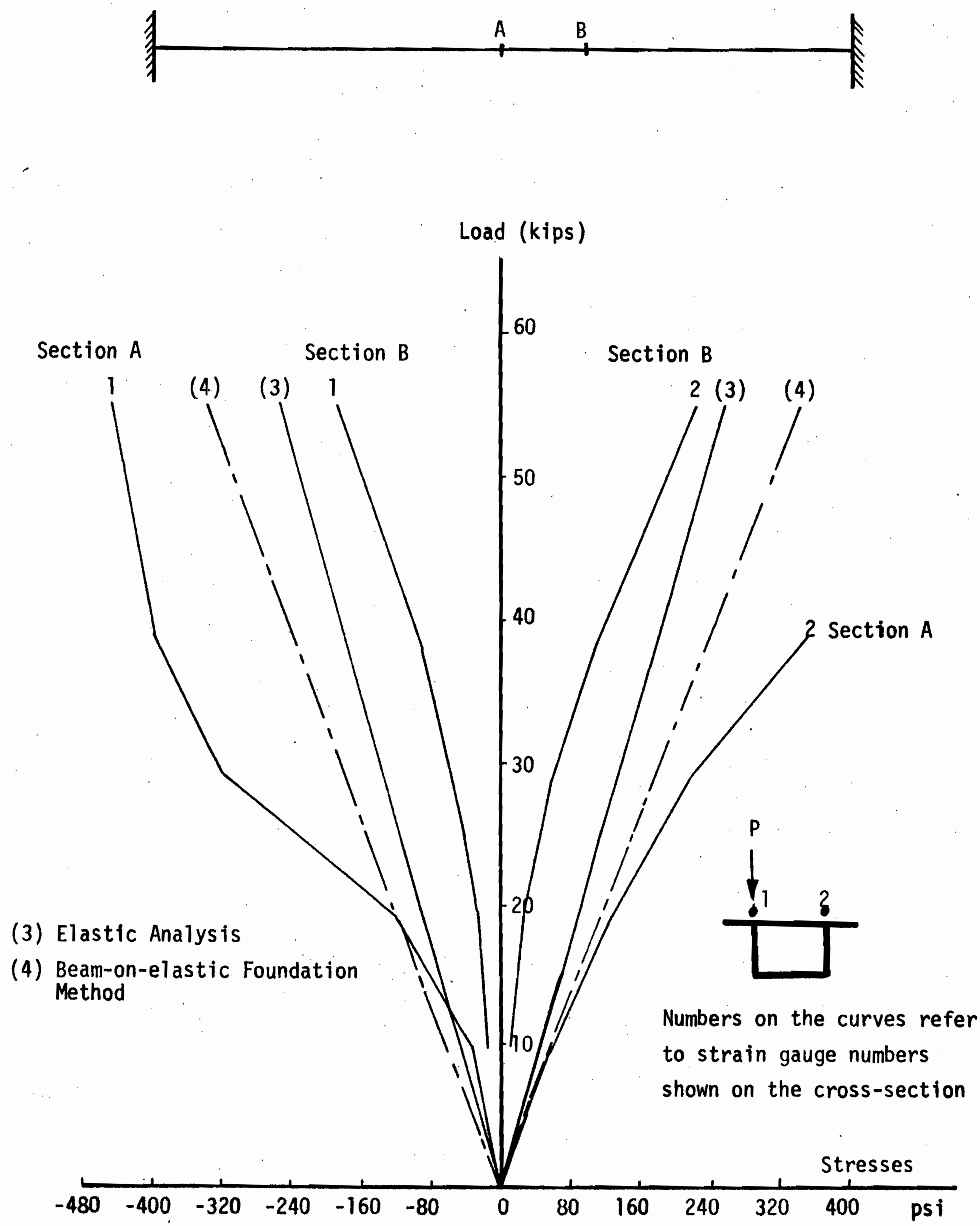

FIG. 3.47 TRANSVERSE CONCRETE STRESSES ON THE TOP SLAB (UNSYMMETRICAL LOADING CASE)

cracks were concentrated over the unloaded web and increased rapidly in length and number as the applied load was increased. The distribution of the transverse concrete stresses in the top slab through half of the bridge span is shown in Figures 3.48 and 3.49 for load values of 19.4 and 55 kips. The maximum transverse concrete stresses over the loaded and the unloaded webs at the midspan section were -150 psi and 150 psi respectively for a load value of 19.4 kips. For a load value of 55 kips, the transverse concrete stresses were -450 psi over the loaded web while the unloaded web showed a significant crack parallel to the longitudinal axis of the bridge. These transverse stresses were approximately 30 and 40 per cent from the longitudinal concrete stresses at the same location for the 19.4 and 55 kips load values respectively. The distribution of the transverse concrete stresses across the width of the top slab at different locations through the bridge span for different load values is shown in Appendix C.
The transverse concrete stress values calculated from the Knittel method, the beam-on-elastic foundation method, and the Kollbrunner and Basler method along with the transverse stresses calculated from the measured strain values are shown in Table 3.2. It can be seen that the experimental stress values were approximately 25 to 40 per cent higher than the calculated values at the working load level (20 kips). However, near the ultimate load level, the experimental transverse stresses were approximately 50 to 60 per cent higher than the calculated values. It must be noted that these methods are valid only for homogeneous and linearly elastic bodies and can be used only for analysis of the box

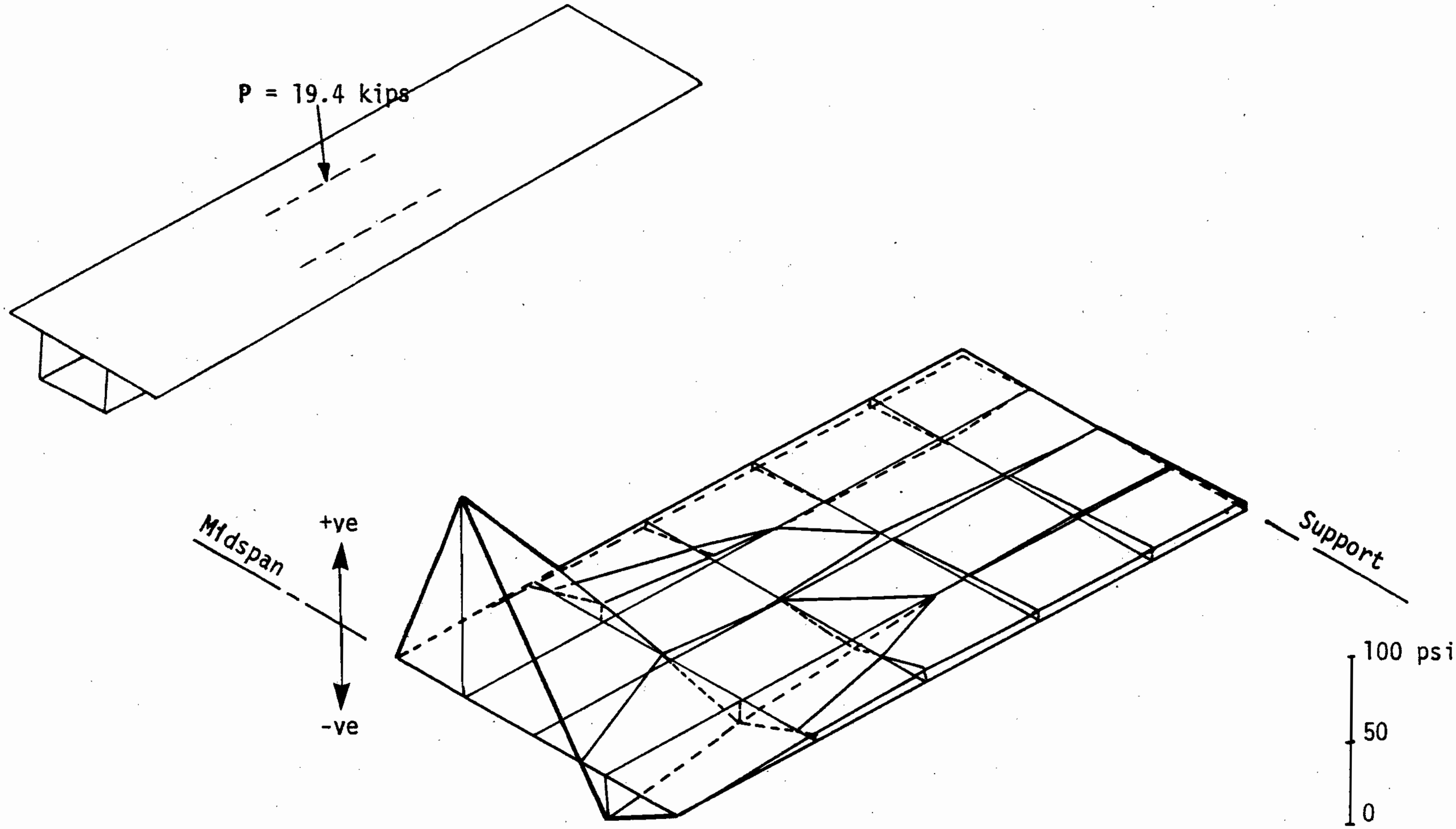

FIG. 3.48 ENVELOPE FOR TRANSVERSE CONCRETE STRESS IN THE TOP SLAB THROUGH HALF THE BRIDGE SPAN [LOAD P = 19.4 KIPS] (UNSYMMETRICAL LOADING CASE)

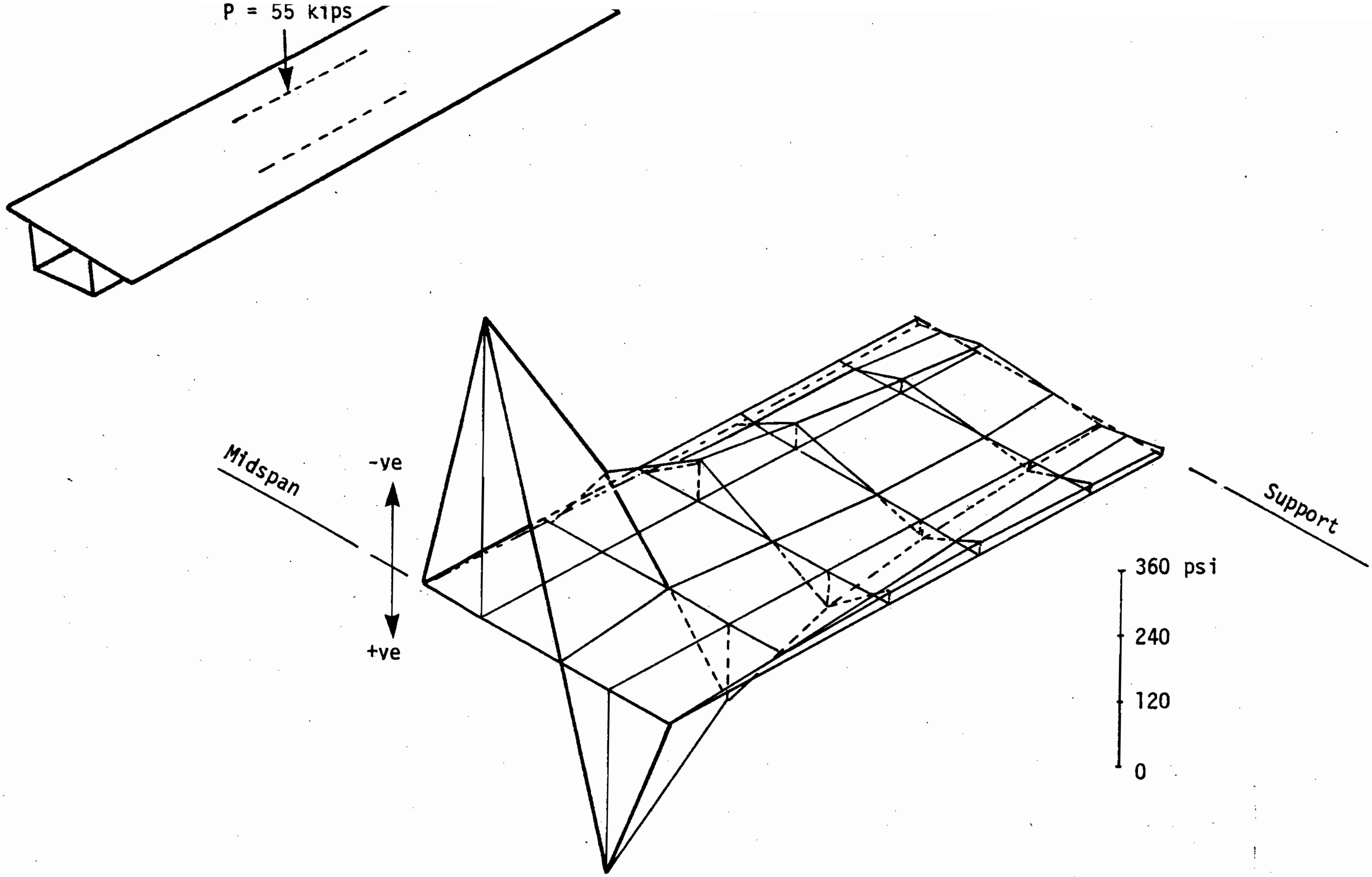

FIG. 3.49 ENVELOPE FOR TRANSVERSE CONCRETE STRESS IN THE TOP SLAB THROUGH HALF THE BRIDGE SPAN [LOAD P = 55 KIPS] (UNSYMMETRICAL LOADING CASE)

Table 3.2

Unsymmetrical Load Test

Transverse Concrete Stresses in Top Slab at Midspan Section

Load (kips)	Stress values calculated from measured strains (psi)		Calculated stresses (psi)					
			Kollbrunner & Basler method		Knittel method		Beam-on-elastic-foundation method	
	Loaded web	Unloaded web	Loaded web	Unloaded web	Loaded web	Unloaded web	Loaded web	Unloaded web
20	-125	140	-100	100	-92	92	-118	118
40	-400	-	-200	200	-184	184	-236	236

section within the working load level. This is the reason for the discrepancy between the calculated and the experimental transverse stresses near the ultimate load levels. Therefore, there is need for a suitable analysis method to account for nonlinearities of behaviour at higher load levels.

3.4.5 Stresses in Web Reinforcement

3.4.5.1 Stirrup Steel Stresses

For a beam loaded with a pure torsional moment, diagonal tensile stresses result on all four beam faces; however, they are in opposing direction on the parallel faces. For a beam subjected to a transverse shear force V, diagonal tensile stresses result on both vertical faces and these are in the same direction. Consequently, for a beam loaded in combined torsion and shear, the diagonal tensile stresses are additive on one of the vertical faces and subtractive on the other. On the beam horizontal faces, the diagonal tensile stress exists due to torsion alone.

Upon removal of the loads for the symmetrical loading case, the residual stresses in the vertical stirrups were very small and therefore they have been neglected. As observed by several investigators in tests for shear strength of reinforced concrete beams, the stirrup stresses increased significantly only after the formation of cracks. Figure 3.50 shows the experimental load-stirrup stresses for both the loaded and unloaded webs at different bridge sections.

As explained before in Section 3.3.4, the theoretical stirrup steel stresses in one web can be calculated by the following equation:

$$f_s = \frac{v\, b_w\, s}{A_v} \tag{3.8}$$

where v is the algebraic sum of the shear stresses due to the shearing force V and the torsional moment M_T. After reducing the contribution of concrete cross-section in resisting the shear stress as follows:

$$v = v_V + v_T - v_c$$

Therefore for the loaded web this equation gives:

$$v = \frac{V}{2\, b_w\, d} + \frac{M_T}{2\, A_{enc}\, b_w} - v_c \tag{3.9}$$

and for the unloaded web

$$v = \frac{V}{2\, b_w\, d} - \frac{M_T}{2\, A_{enc}\, b_w} - v_c \tag{3.10}$$

As shown in Figure 3.50, up to a load value of approximately 20 kips the stirrups were not significantly stressed.

At a load value of 20 kips, at the midspan section, the stirrup stresses of both loaded and unloaded webs were approximately 5 ksi and 2 ksi respectively. The calculated stirrup stresses for this load level were 12 ksi and 7.5 ksi respectively. At a load

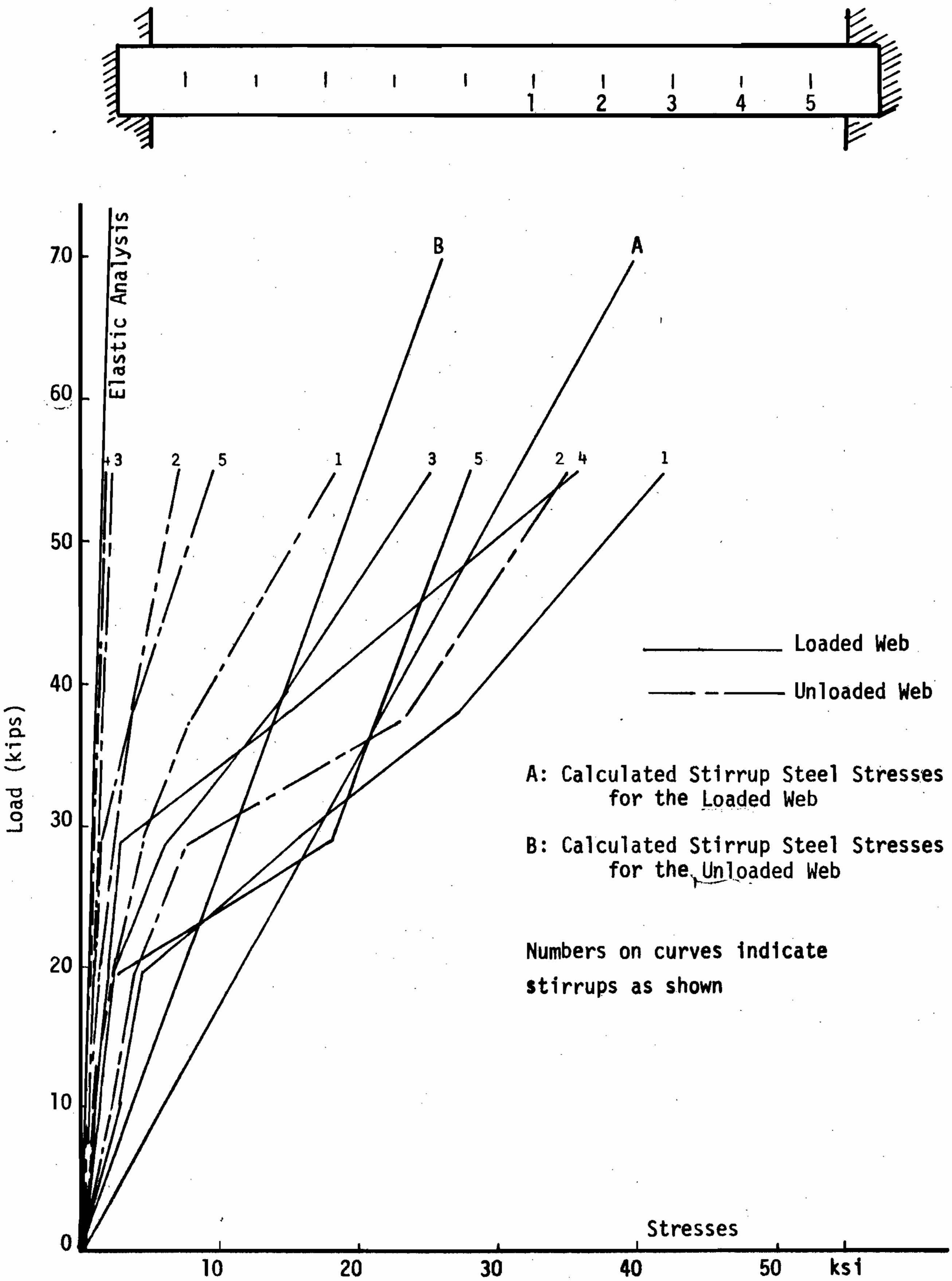

FIG 3.50 STRESS VARIATION IN STEEL STIRRUPS FOR THE LOADED AND UNLOADED WEBS (UNSYMMETRICAL LOADING CASE)

value of approximately 26 kips, the cracks formed at the midspan of the loaded web. Beyond this load level, the stirrups of the loaded web started to show significant stresses, especially in the vicinity of the point of application of the load. These stirrups yielded at a load value of 52 kips. The stress in the stirrups of the unloaded web at the midspan section for the same load level was approximately 18 ksi.

As mentioned earlier, the stirrup stresses for both the loaded and the unloaded webs through the bridge span were lower than those calculated from equations 3.8 and 3.9 up to a load value of approximately 24 kips. Beyond this load level, and after the formation of web cracks, this trend changed and the experimental stress values for the loaded web stirrups were higher than the calculated values.

However, at a load value of 45 kips, the stirrup stresses of the loaded and the unloaded webs were 33 ksi and 12.5 ksi respectively, and the corresponding calculated stresses were approximately 25 ksi and 15 ksi respectively. As shown in Figure 3.50, the stresses in the unloaded web stirrups at higher load levels were approximately 20 per cent lower than the calculated values.

The difference in the stirrup stresses between the loaded and the unloaded webs is due to the earlier formation of cracks in the loaded web. At a load value of 38.8 kips, the stirrup stresses in the loaded web were approximately three times larger than those in the unloaded web. However, at a load value of 50 kips, the stirrup stresses of the loaded web were approximately double those of the unloaded web, sharing commencement of inelastic behaviour in the unloaded web. However, it is not possible to make a direct comparison between the experimental and the calculated values of stresses in the stirrups because there is no such analysis, which accounts for the combined effect of bending, shear and torsion after the formation of cracks, at present available. The stirrup steel stress envelopes for the loaded and the unloaded webs through half of the bridge span for load values of 19.4 and 55.0 kips are shown in Figures 3.51 and 3.52.

The unsymmetrical load test of the bridge was stopped at a load value of 55 kips due to a shear punching failure under the hydraulic jack over the loaded web. The resulting damage was repaired and the bridge was prepared again for the final loading test. Results of the final load test are presented in Section 3.5.

3.4.5.2 Web Cracks

Cracks first appeared in the loaded web at a load value of 20 kips after formation of flexural cracks at the midspan section of the lower slab. With further increase in load, these cracks increased in number and extended vertically to the point of application of the applied load. At a load value of 38 kips, inclined cracks formed in the quarter span region of the loaded web and in the loaded web at the support region. These cracks were inclined at approximately 40° to 45° with the longitudinal axis. Near the midspan region, the shear

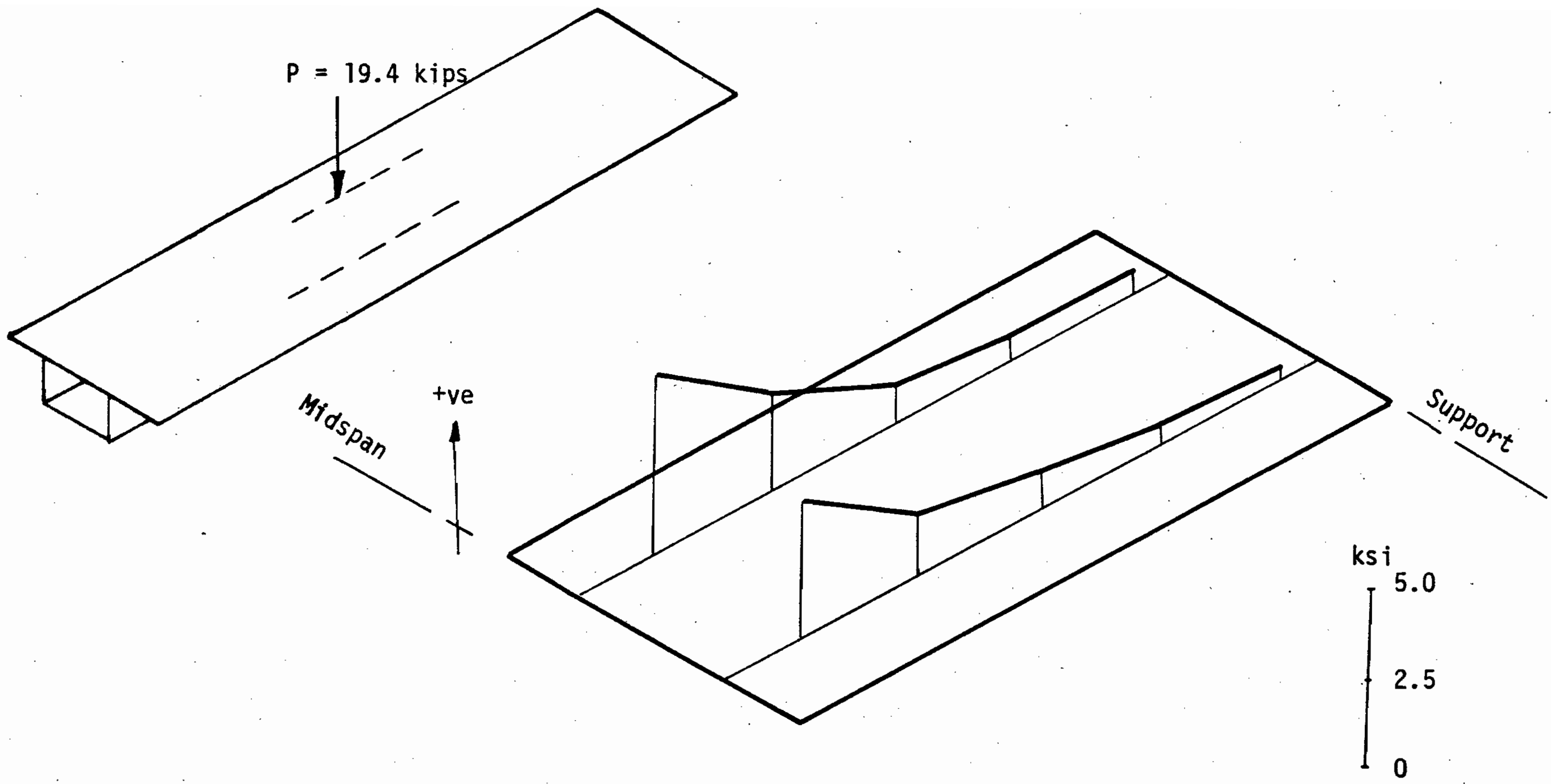

FIG. 3.51 STIRRUP STEEL STRESS ENVELOPE THROUGH HALF THE BRIDGE SPAN [LOAD P = 19.4 KIPS]
(UNSYMMETRICAL LOADING CASE)

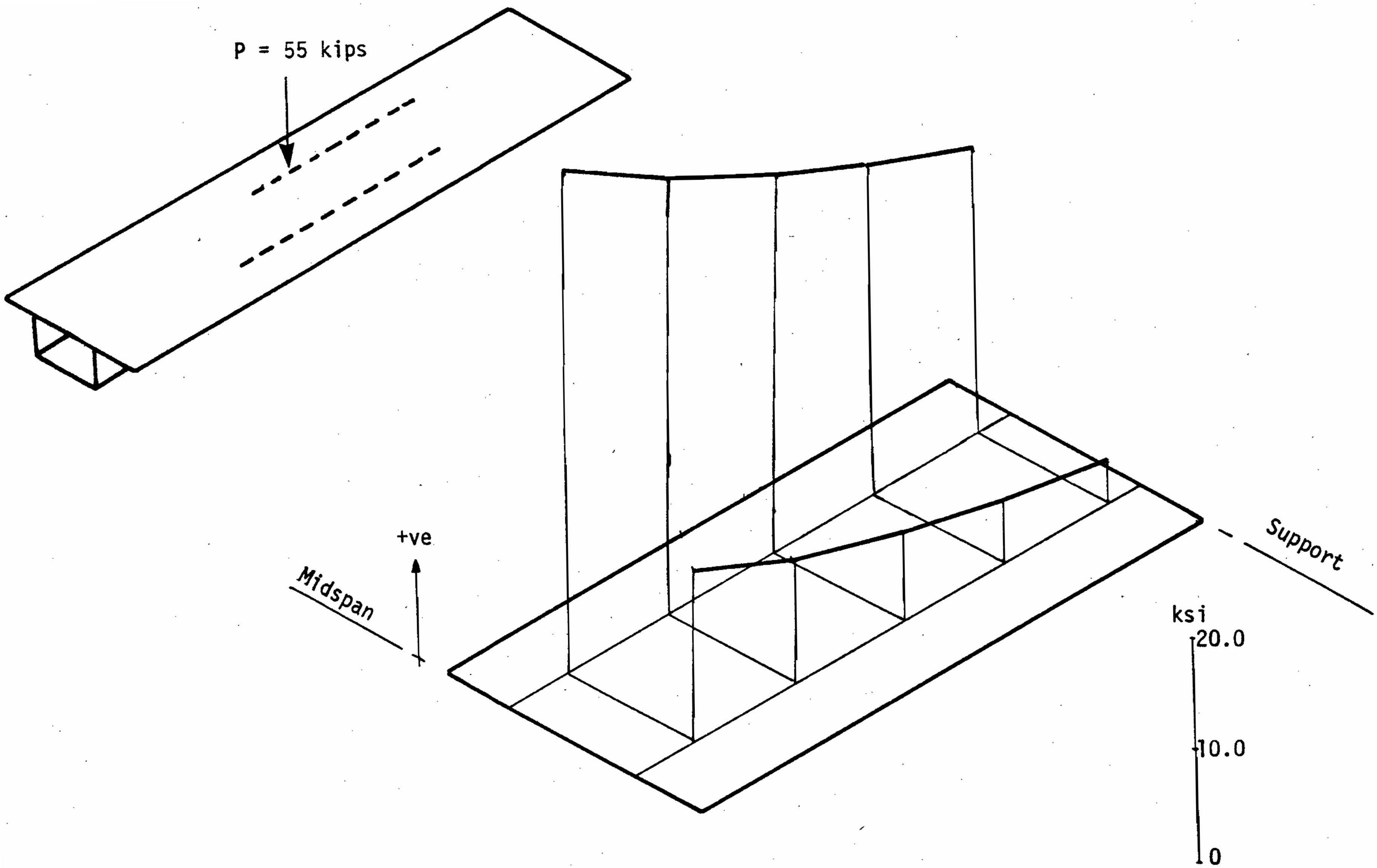

FIG. 3.52 STIRRUP STEEL STRESS ENVELOPE THROUGH HALF THE BRIDGE SPAN [LOAD P = 55 KIPS]
(UNSYMMETRICAL LOADING CASE)

cracks intersected the flexural cracks, and secondary cracks formed as the applied load was increased. Near the support region, the flexural cracks were observed at a load value of 22 kips, followed by shear and torsion cracks near the mid depth of the loaded web. These cracks extended toward the top and bottom slabs as the applied load was increased. The crack spacing was approximately of 4 inches with an average crack width of 0.5 mm and 0.11 mm for the loaded and unloaded webs respectively, at a load value of 55 kips.

The cracks appeared in the unloaded web at a load value of 28 kips. These cracks started as flexural cracks from the lower slab and as the load was increased the cracks extended vertically toward the upper slab.

In the quarter span region of the bridge, vertical cracks were observed in the unloaded web at a load value of 42 kips. No inclined cracks due to the combined effect óf shear and torsion were observed in this region as these were in opposite directions on this web. The loaded web showed more diagonal cracks as the shear and torsional effects were additive in that web.

The crack patterns in both the loaded and unloaded webs of the bridge are shown in Figures 3.53 and 3.54. Figure 3.55 shows the average variation of the crack width with load in the loaded and unloaded webs at the support and midspan sections.

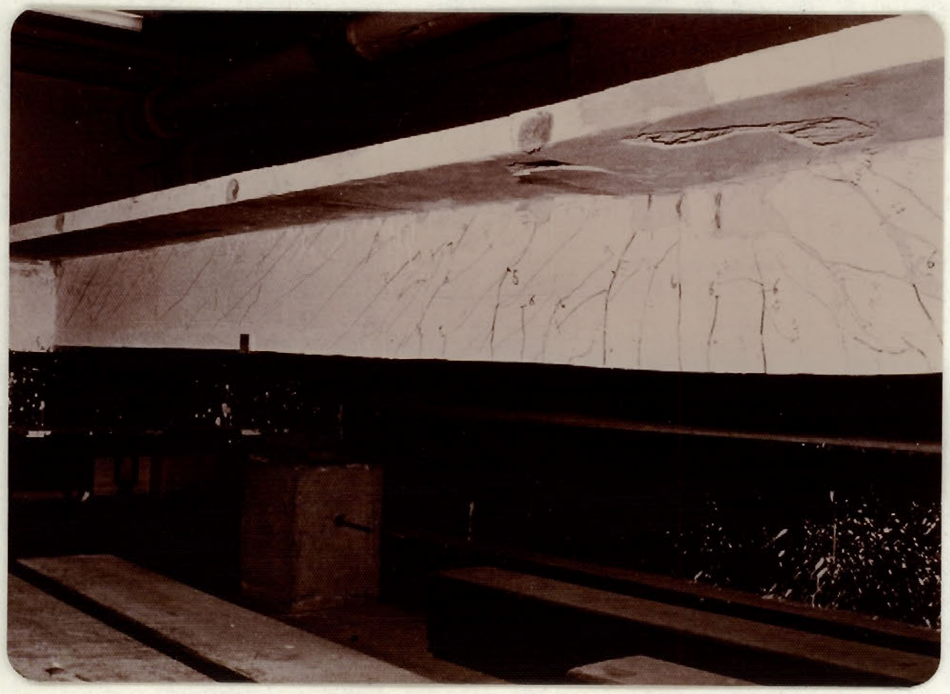

FIG. 3.53 CRACK PATTERN FOR THE LOADED WEB
(UNSYMMETRICAL LOADING CASE)

FIG. 3.54 CRACK PATTERN FOR THE UNLOADED WEB
(UNSYMMETRICAL LOADING CASE)

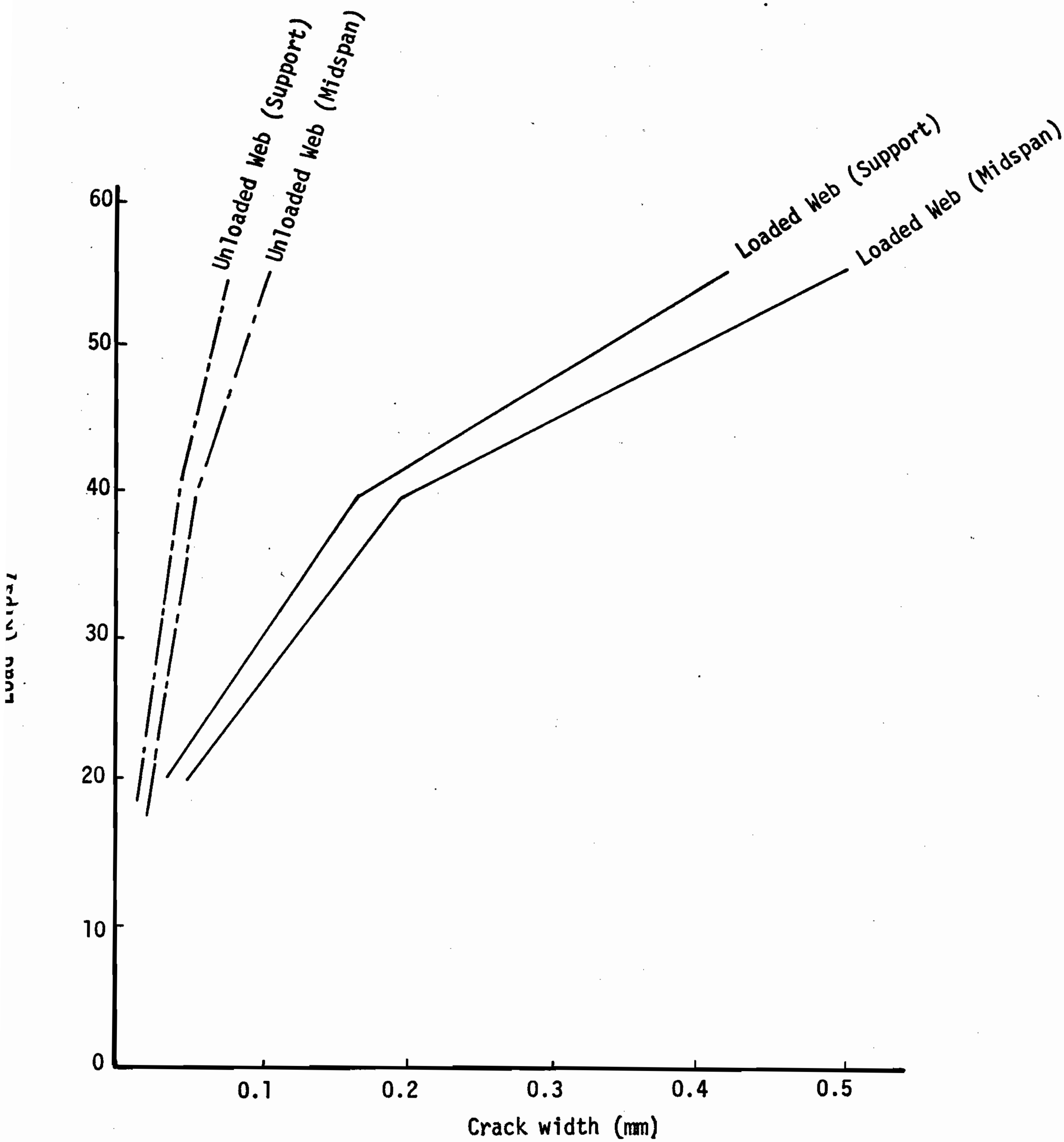

FIG. 3.55 LOAD-AVERAGE CRACK WIDTH FOR THE LOADED AND UNLOADED WEBS (UNSYMMETRICAL LOADING CASE).

3.5 Ultimate Loading Case

After repairing the partial shear punching failure which occurred at the end of the previous unsymmetrical loading case, the bridge was loaded in an identical manner to the last test, in loading increments of 10 kips each until failure. The instrumentation used was similar to that used for the last test.

3.5.1 Deflections

The experimental load-deflection curves of the loaded and unloaded webs are shown in Figure 3.56. The deflection due to the dead load (0.144 in.) should be added to these values to obtain the total deflection at any load level. The residual deflection resulting from the previous loading test is also shown in Figure 3.56.

The nonlinear response for both the loaded and the unloaded webs through the entire loading test is shown in Figure 3.56. This nonlinearity in the behaviour is due to the cracks which had already formed in the bridge from the previous loading test. At a load value of 15 kips, the cracks in the loaded web opened and a significant decrease was observed in the stiffness of the loaded web. At a load value of 23 kips, the unloaded web also showed a decrease in stiffness due to the opening of the cracks. The measured deflection values of the loaded and the unloaded webs at a load value of 20 kips were approximately 0.5 in. and 0.3 in., respectively. These values are approximately 35 per cent larger than those obtained in the previous load test at a similar load level.

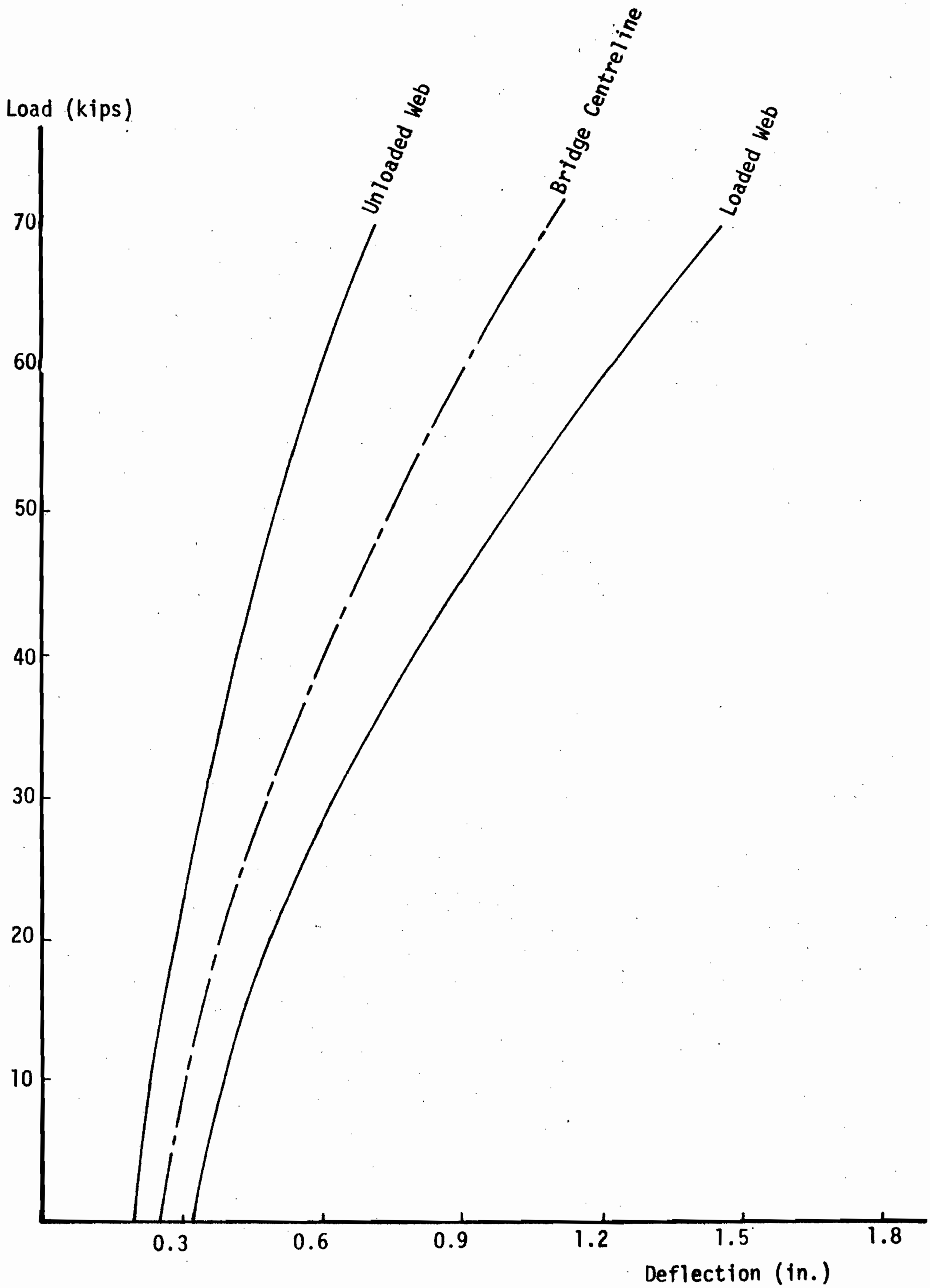

FIG. 3.56 LOAD-MIDSPAN DEFLECTION CURVES
(UNSYMMETRICAL LOADING CASE)

The initial stiffnesses of both the loaded and the unloaded webs were approximately 20 per cent and 50 per cent, respectively, less than those observed in the previous loading test.

The lateral displacements of the cantilever tips through the bridge span are shown in Figure 3.57 for different load values of 19.6, 39.2, 58.8 and 68.6 kips. The maximum lateral displacements occurred at the midspan section and were 0.056 in. and 0.062 in. for load values of 58.8 and 68.6 kips, respectively. These displacement values were approximately 25 per cent higher than those obtained at the same load level from the previous loading test.

Figure 3.58 shows the longitudinal displacement of the cantilever slab tips through the bridge span at load values of 19.2, 39.2, 58.8 and 68.6 kips. The location of the maximum longitudinal displacement was coincident with that of the previous loading test. The measured longitudinal displacements of the cantilever tips at the quarter span section were 0.042 in. and 0.051 in. for load values of 58.8 and 68.6 kips, respectively. These longitudinal displacement values were approximately 30 per cent higher than those obtained from the previous loading test. This is due to the opening of the cracks which had previously formed in the bridge.

3.5.2 Angle of Twist

As explained in Section 3.2, the angle of twist of the box section relative to the fixed end, ignoring the warping restraint, can be calculated using the formula:

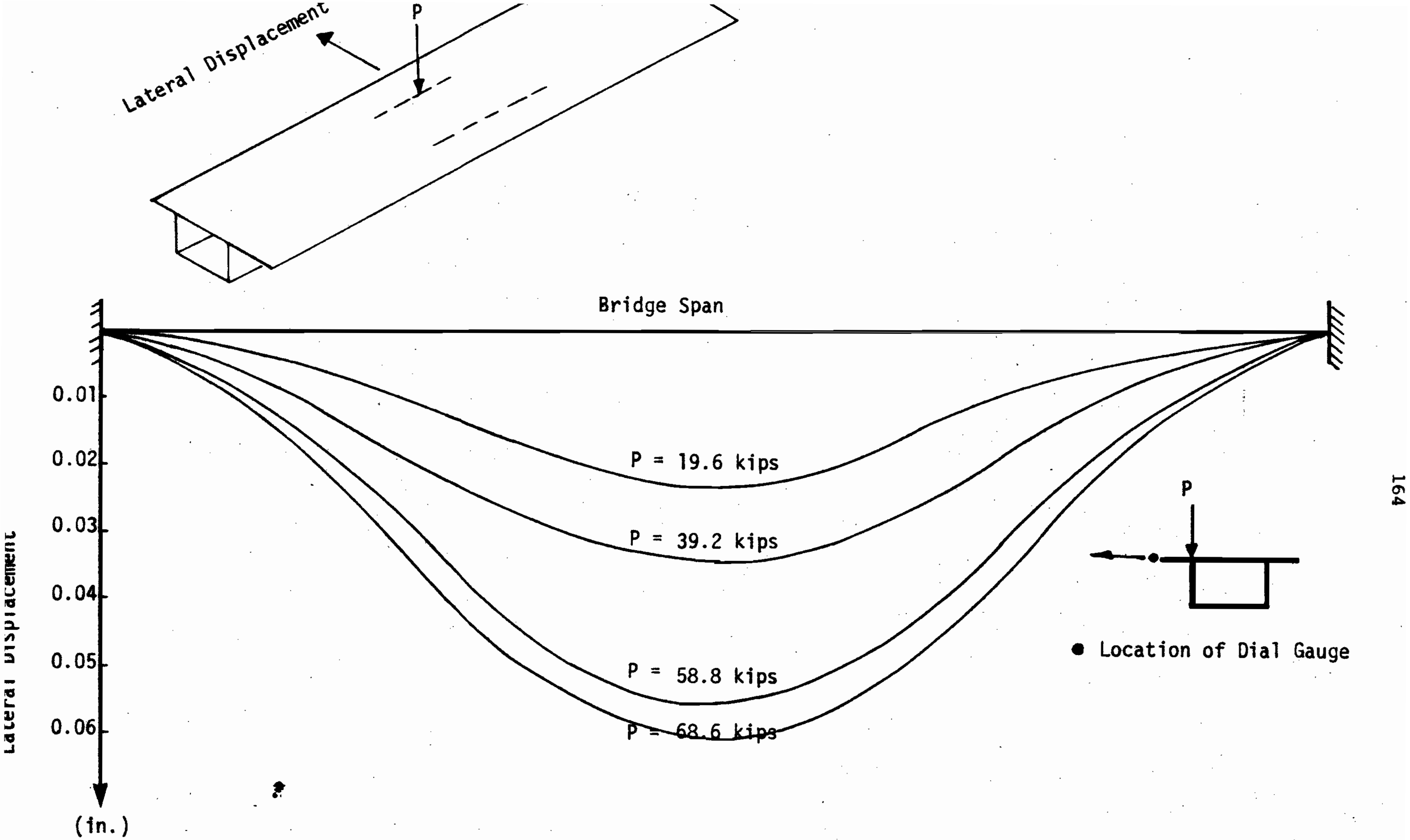

FIG. 3.57 PROFILE OF LATERAL DISPLACEMENT ALONG THE BRIDGE SPAN
(UNSYMMETRICAL LOADING CASE)

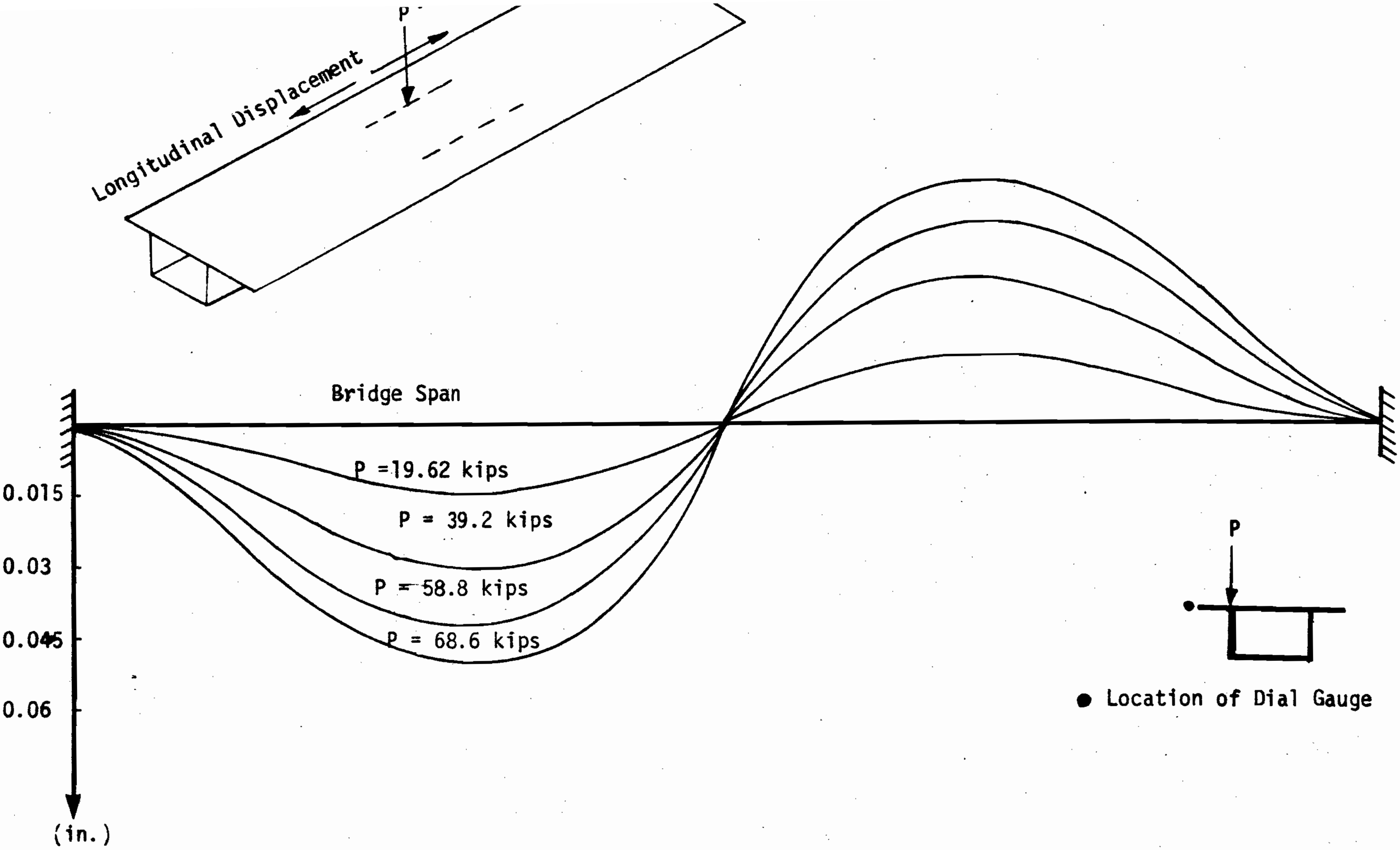

FIG. 3.58 PROFILE OF LONGITUDINAL DISPLACEMENTS THROUGH THE BRIDGE SPAN
(UNSYMMETRICAL LOADING CASE)

$$\theta = \frac{M_T \ell}{J_{eq} G} \tag{3.6}$$

The load versus angle-of-twist relationship at the midspan section of the bridge is shown in Figure 3.59. It can be noted that the measured load-angle of twist relationship was linear up to a load value of 15 kips after which it started to deviate from linearity - this is due to the opening of the cracks formed in the previous loading test which decreased the torsional stiffnesses at the zero and ultimate load levels to approximatley 20 per cent and 25 per cent, respectively, lower than those observed in the previous loading test. The measured angle of twist at load value of 20 kips was 85 x 10^{-4}. This value was three times larger than that obtained at the same load level for the previous loading test. At a load value of 50 kips, the measured angle of twist was 200 x 10^{-4} radian which was 25 per cent larger than that obtained in the previous loading test.

At a load value of 60 kips, the torsional stiffness as observed from the slope of the load-angle of twist relationship was approximately 500 kips in^2; this value remained constant beyond this load level until the ultimate load stage. The angle of twist at the 60 kips load level was 300 x 10^{-4} radian.

3.5.3 Longitudinal Steel and Concrete Stresses

3.5.3.1 Top Slab

The distribution of the stresses in the top slab reinforcement of the present loading test was similar to that in the previous loading

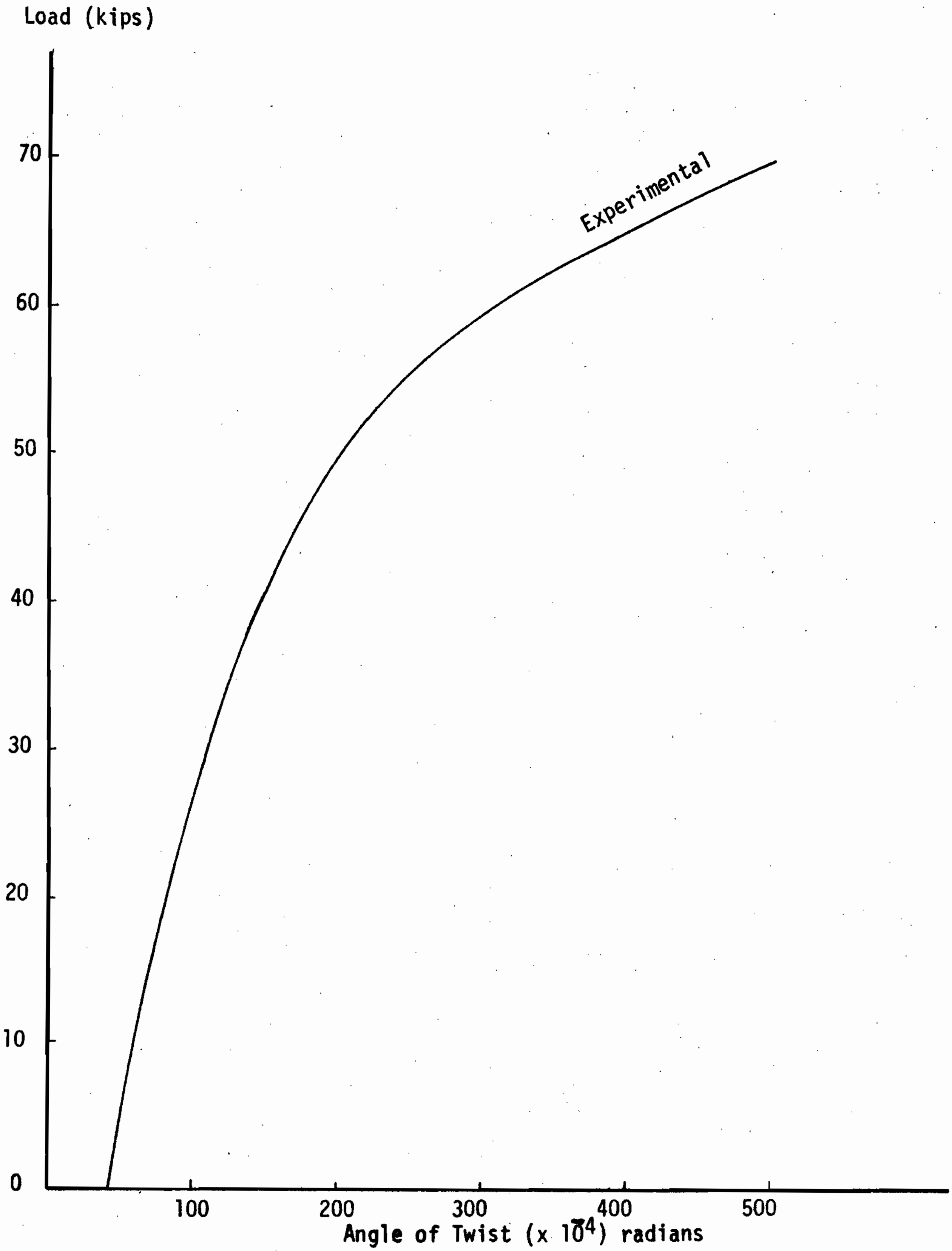

FIG. 3.59 LOAD-ANGLE OF TWIST VARIATION AT THE MIDSPAN SECTION (UNSYMMETRICAL LOADING CASE)

test. Figure 3.60 shows the load-longitudinal steel stresses of the top slab reinforcement at different locations through the span of the bridge. The non-uniformity of the steel stresses across the width of the top slab can be noted from this figure. At the support section, for a load value of 65 kips, the maximum longitudinal steel stress over the loaded web was approximately 52 ksi, while that over the unloaded web was approximately 38 ksi. The minimum stress in this case occurred at the cantilever tips and was approximately 31.5 ksi. At the midspan section, for the 65 kips load level, the longitudinal steel reinforcement over the loaded web yielded, while the longitudinal steel stresses over the unloaded web were approximately -22.5 ksi. The minimum stress in this case occurred at the cantilever tips with a value of approximately -15 ksi. It should be noted that the resulting stresses in the present load test were approximately 50 per cent higher than those obtained from the previous load test. Again, this is due to the cracks which had been formed previously and caused a redistribution of stresses within the structure.

Figure 3.61 shows the load-longitudinal concrete stresses on the top slab at different locations through the span of the bridge. These stresses were non-uniform across the width of the top slab. It shows also that the longitudinal stresses over the loaded web are much higher than those over the unloaded web. At a load value of 65 kips, the maximum longitudinal concrete stresses over the loaded web at the midspan section were approximately -2400 psi while those over the unloaded web were approximately -680 psi. However, the longitudinal

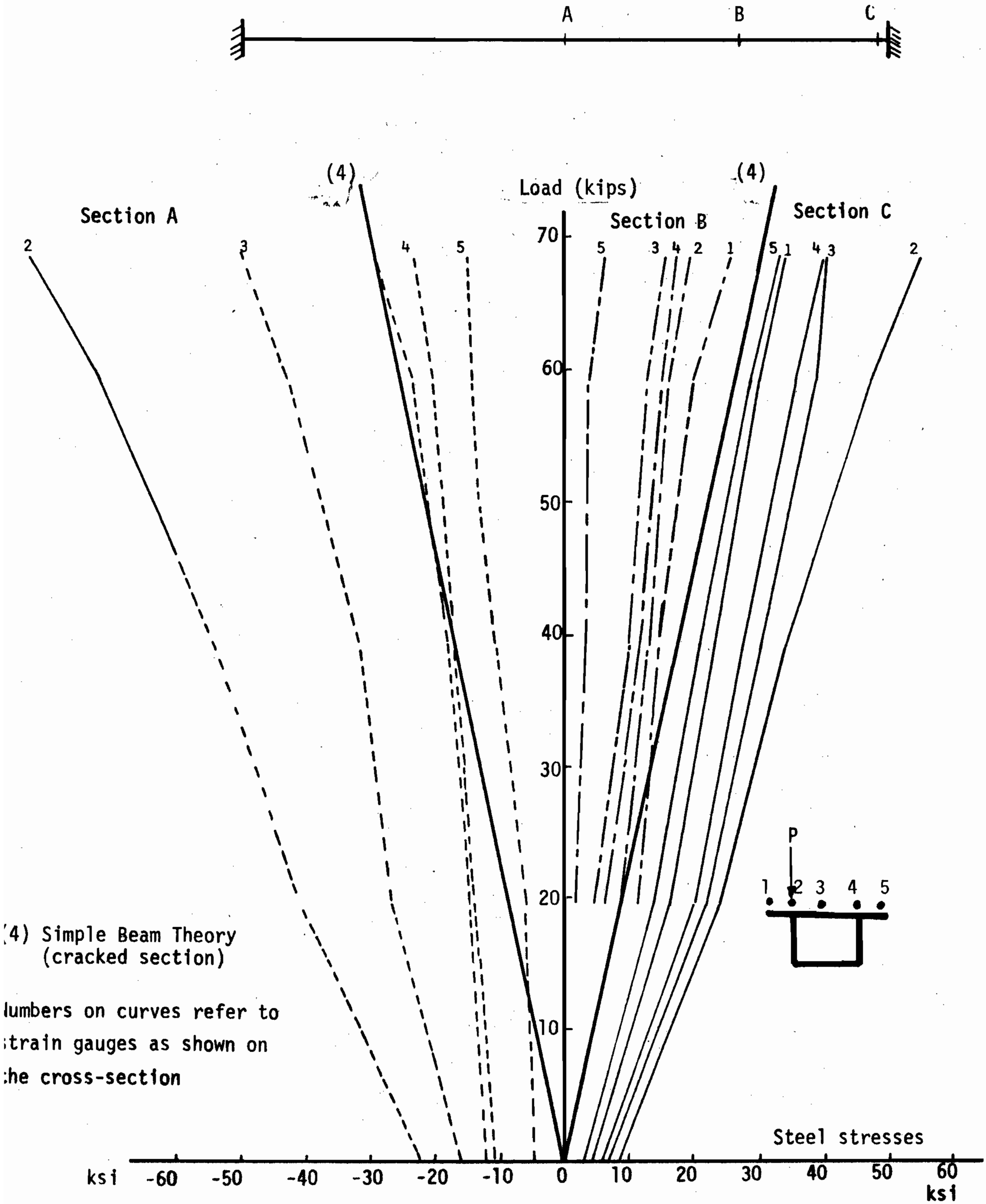

FIG. 3.60 LONGITUDINAL STRESSES IN THE TOP SLAB REINFORCEMENT
(UNSYMMETRICAL LOADING CASE)

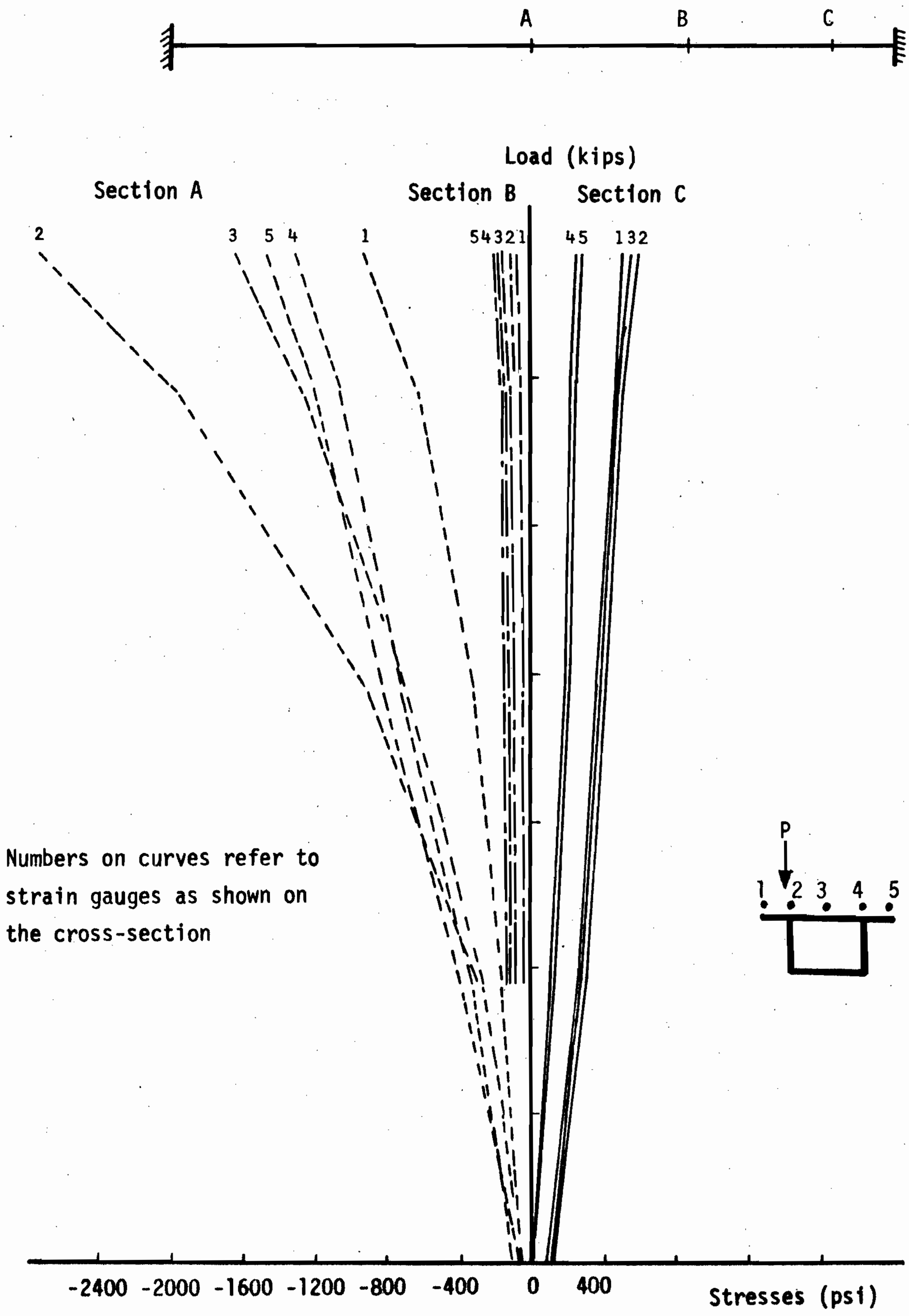

FIG. 3.61 LONGITUDINAL CONCRETE STRESSES IN THE TOP SLAB (UNSYMMETRICAL LOADING CASE)

concrete stresses in this load test were approximately 10 per cent larger than those obtained from the previous load test. This increase is due to the redistribution of stresses within the box section and through the bridge span due to the further propagation of previously formed cracks and the new cracks which were formed in the present load test.

3.5.3.2 Lower Slab

The distribution of the longitudinal stresses in the lower slab reinforcement was not uniform across the slab width (Figure 3.62). At a load value of 60 kips, the maximum stress under the loaded web at the midspan section was approximately 38 ksi while that under the unloaded web was approximately 30 ksi. At the support section these stresses were -35 ksi and -19 ksi for the loaded and the unloaded webs respectively. At the same load level, the calculated longitudinal stresses from the simple beam theory based on a cracked section analysis were 40 per cent and 25 per cent larger than the values calculated from the measured strains at the support and midspan sections respectively. The ability of the box section to distribute the loads in the transverse direction in addition to the combined effect of both the flexural and the warping stresses are the cause of these differences.

Figure 3.63 shows the load-longitudinal concrete stresses in the lower slab at different locations throughout the span of the bridge. As shown, the longitudinal stresses at the loaded web are higher than those for the unloaded web. At a load of 60 kips, the longitudinal

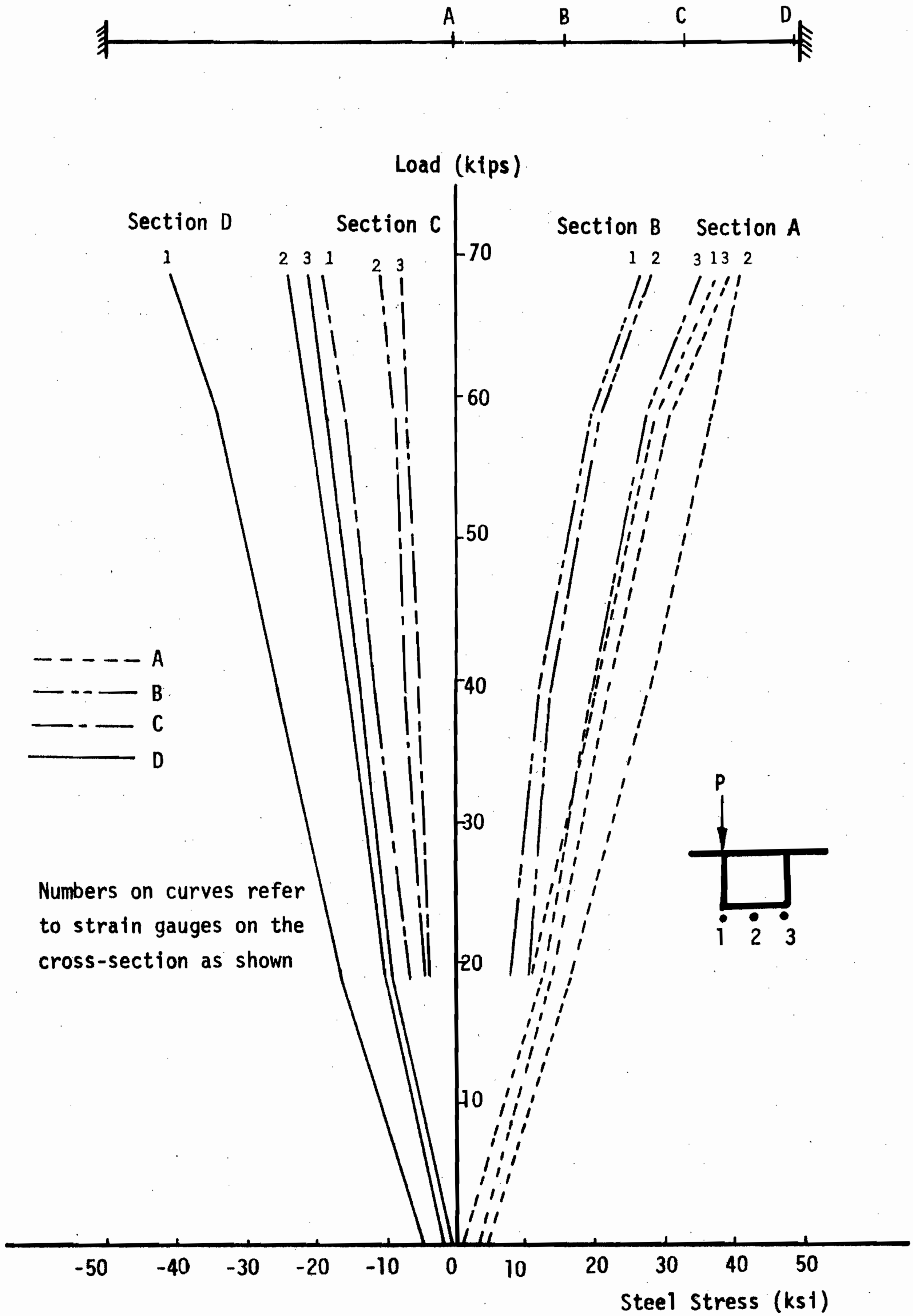

FIG. 3.62 LONGITUDINAL STRESSES IN THE LOWER SLAB REINFORCEMENT (UNSYMMETRICAL LOADING CASE)

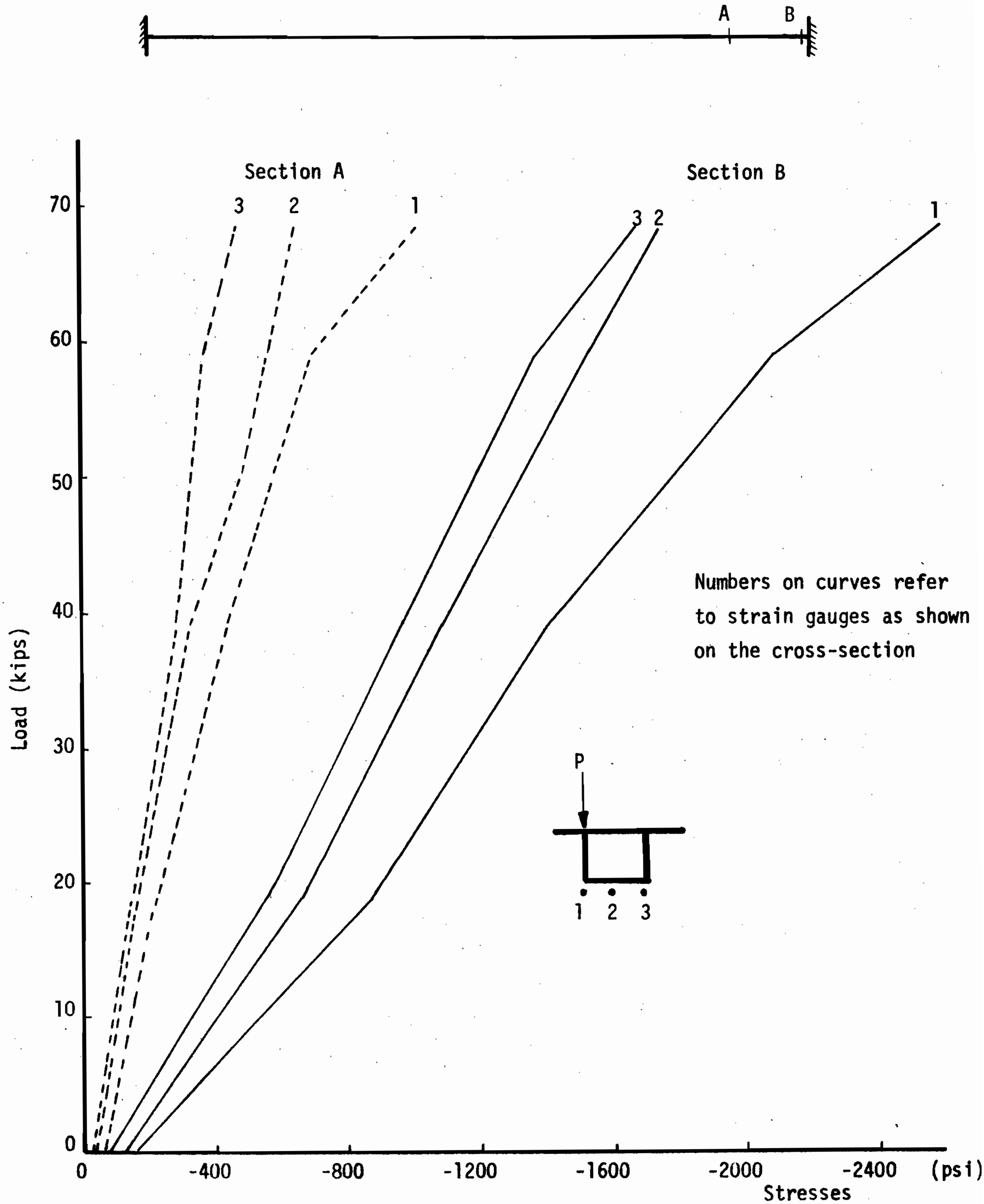

FIG. 3.63 LONGITUDINAL CONCRETE STRESSES IN THE LOWER SLAB (UNSYMMETRICAL LOADING CASE)

stresses of the loaded web were 55 per cent higher than those for the unloaded web. Also, the non-uniformity of these stresses across the slab width was more pronounced.

3.5.4 Transverse Stresses in Top and Bottom Slab Reinforcement

Figure 3.64 shows the variation of transverse stresses with load for the top slab reinforcement at different locations through the span of the bridge. As shown, the transverse tensile stresses were concentrated over the unloaded web with maximum values at the midspan section in the vicinity of the applied load. At a load value of 40 kips, the transverse tensile steel stresses at the midspan section over the unloaded web were approximately 36 ksi, while the transverse compressive steel stresses over the loaded web were 18 ksi. These transverse tensile stresses were approximately 10 per cent higher than those obtained in the previous load test, while the transverse compressive stresses were approximately 50 per cent less than those obtained in the previous test. At a load value of 55 kips, the transverse tensile steel stresses over the unloaded web were approximately twice the transverse compressive steel stresses over the loaded web. The transverse steel over the unloaded web at the midspan section yielded at a load value of 46 kips. However, the transverse steel stress over the loaded web at this load level was -20 ksi,which is approximately 50 per cent less than that obtained at the same load in the previous loading test. The local punching shear failure which occurred beneath the applied load over the loaded web in the previous loading test caused

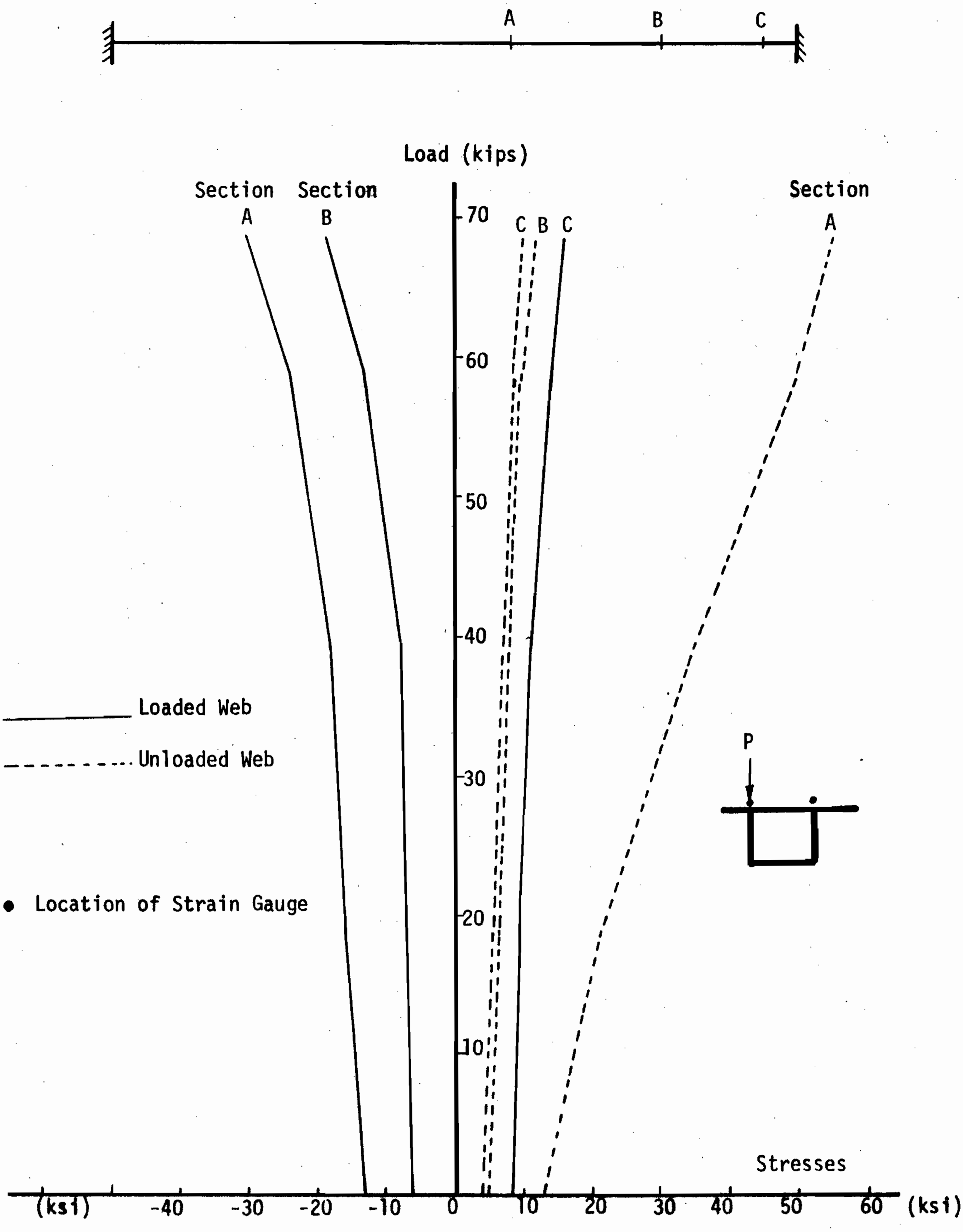

FIG. 3.64 STRESS VARIATION IN THE TOP SLAB TRANSVERSE REINFORCEMENT (UNSYMMETRICAL LOADING CASE)

a release in the compressive stresses in the vicinity of the applied load causing this reduction.

Figure 3.65 shows the load-transverse concrete stresses in the top slab of the bridge at different locations through the bridge span. The distribution of these transverse stresses across the width of the top slab is similar to those obtained from the steel reinforcement of the top slab.

As shown in Figure 3.65, the transverse compressive concrete stresses over the loaded web were approximately 50 per cent less than those obtained from the previous load test. Again, the cracks and the punching shear at the midspan section led to a redistribution of the stresses in this region.

Figure 3.66 shows the variation of transverse stresses with load for the lower slab reinforcement. As shown in this figure, the transverse stresses at section "A" under the unloaded web at a load value of 40 kips were 50 per cent higher than those at the loaded web. This is due to the combined effect of the longitudinal and the resulting transverse stresses, in addition to the torsional and distortional transverse warping stresses in this region. The steel bars under the unloaded web at section A yielded at a load value of 66 kips. Unfortunately, the strain gauges at the midspan section had ceased functioning at the end of the previous loading test, therefore no comparison can be made between the steel stresses of section A with those at the midspan section.

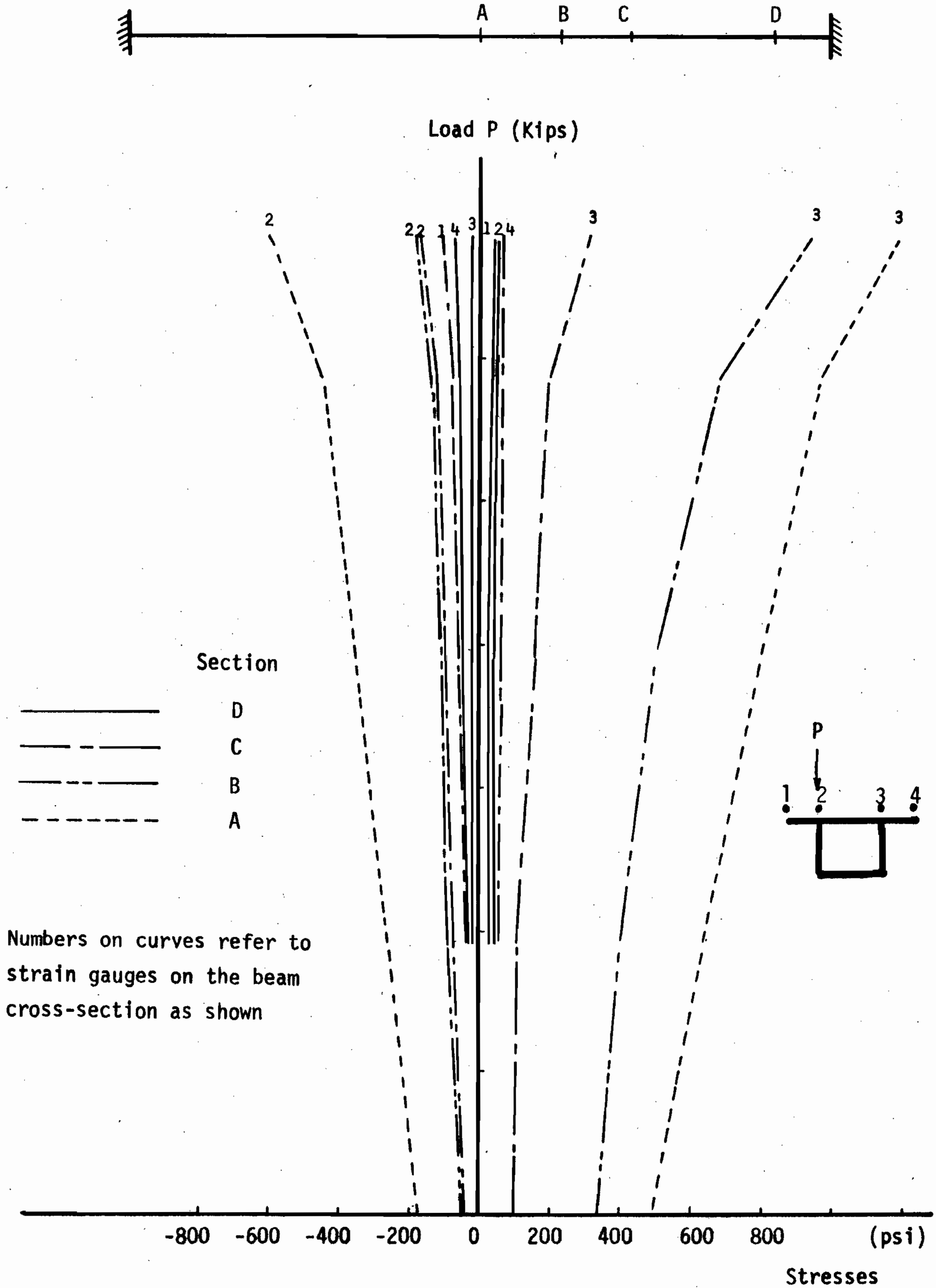

FIG.3.65 TRANSVERSE CONCRETE STRESSES IN THE TOP SLAB
(UNSYMMETRICAL LOADING CASE)

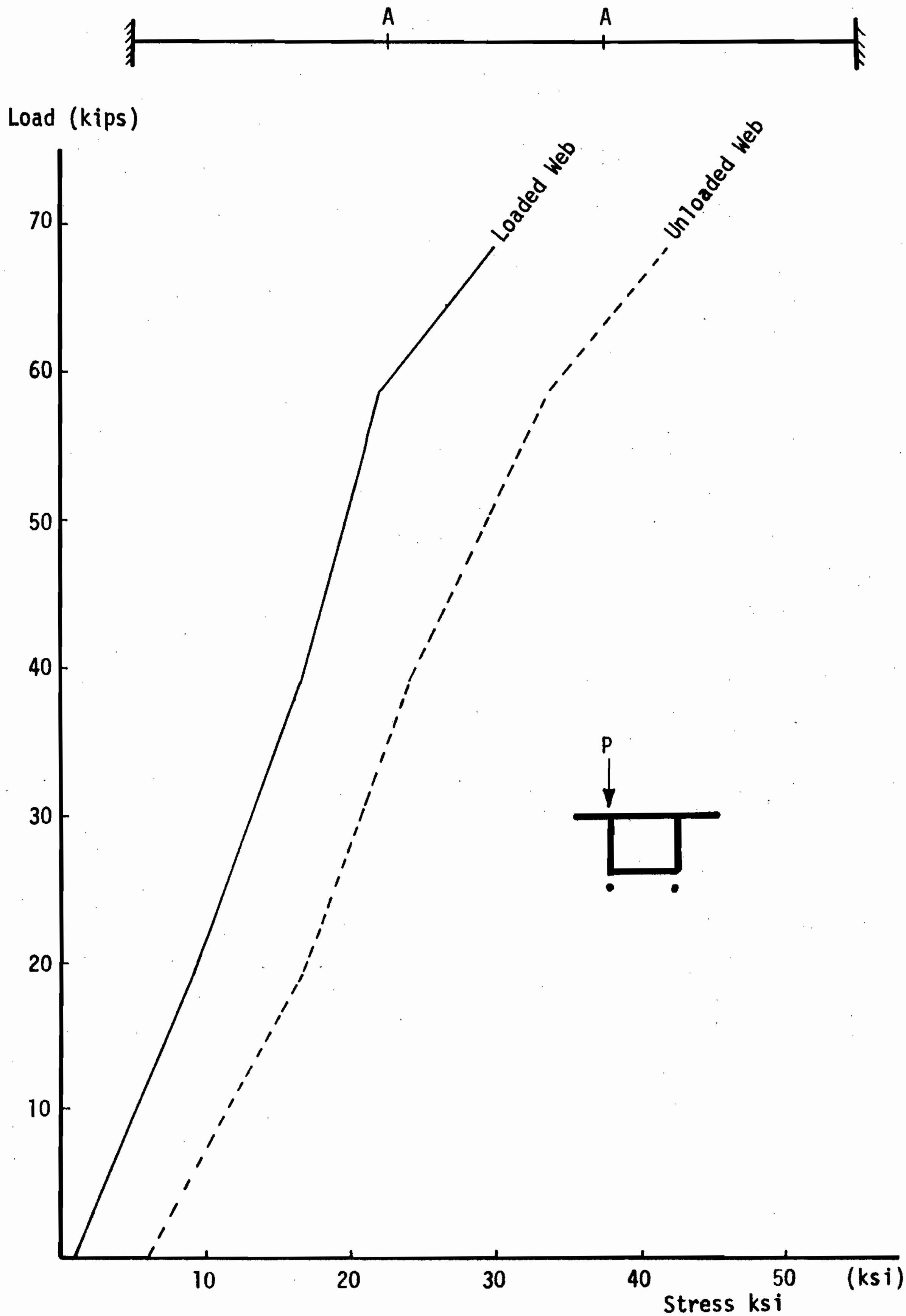

FIG. 3.66 STRESS VARIATION IN THE LOWER SLAB TRANSVERSE REINFORCEMENT (UNSYMMETRICAL LOADING CASE)

3.5.5 Stresses in the Web Reinforcement

The experimental load-stirrup stresses at different locations through the span of the bridge for both the loaded and the unloaded webs are shown in Figure 3.67. Initially, there were some residual stresses from the previous test, with values of 15 ksi and 5 ksi for both the loaded and the unloaded webs, respectively. These values form approximately 28 per cent of the maximum stirrup stresses obtained in the previous load test. However, the behaviour of the stirrup stresses in the present test was similar to that in the previous load test. The loaded web stirrups showed higher stresses than those of the unloaded web. At a load value of 40 kips the stirrup stress in the loaded web at the midspan section was 33 ksi, while those in the unloaded web had a stress of 12 ksi. The experimental stirrup steel stresses in the present load test were 10 per cent and 20 per cent higher than those obtained in the previous test for the unloaded and loaded webs, respectively. This can be attributed to the residual stresses from the previous test.

As shown in Figure 3.67, beyond a load value of 47 kips, most of the stirrups in the loaded web had yielded. At this load level, the stress in the stirrups of the unloaded web at the midspan section was only 15 ksi.

Again, although the shear force was maximum at the support section, the maximum stirrup stresses occurred in the vicinity of the applied load at the midspan section.

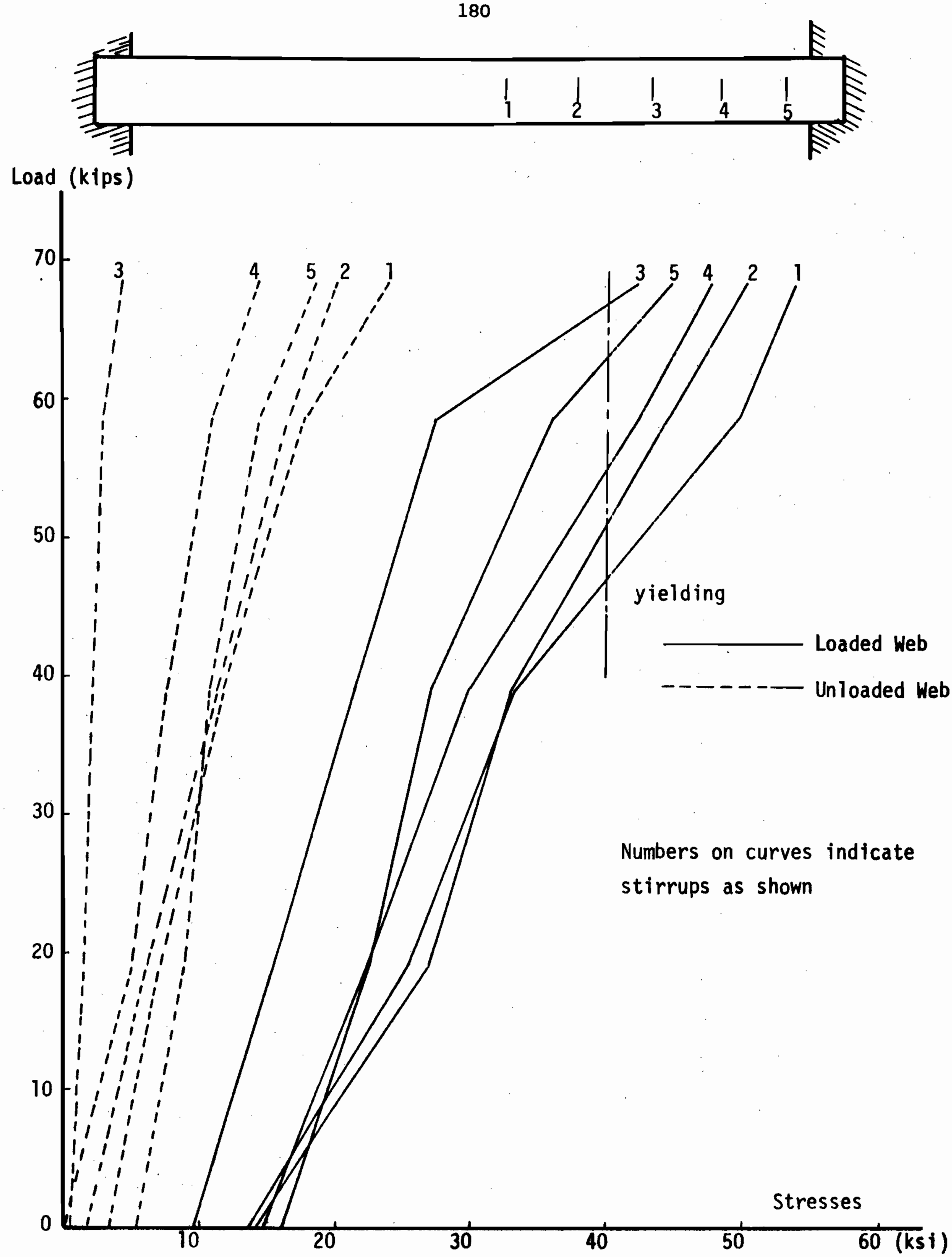

FIG. 3.67 VARIATION OF STIRRUP STEEL STRESSES IN THE LOADED AND THE UNLOADED WEBS (UNSYMMETRICAL LOADING CASE)

Because of the existence of cracks which had formed during the previous loading test, the sudden changes in the load-stirrup stresses which occurred in the previous test did not occur in the present test (see Figure 3.67).

The cause of failure, however, can be considered to be due to the failure of the loaded web beneath the applied load at the midspan section at a load of approximately 70 kips. The principal compressive stresses in the webs at the midspan section exceeded the allowable limits of 5000 psi causing the crushing of the concrete strut between the diagonal cracks at this location, followed by yielding and buckling of the web reinforcement.

3.6 Summary of Experimental Observations

3.6.1 Deflections

The measured deflection values were generally higher than those calculated from the simple beam theory. Also, for the unsymmetrical loading test, the loaded web showed higher deflections than the unloaded web. Tables 3.3 and 3.4 show the measured flexural and torsional rigidities as percentages of the rigidities EI_g and GJ_g based on the gross cross-section, and also as percentages of the experimental initial rigidities EI_{int} and GJ_{int} at different load levels. As shown in these tables, the flexural rigidity EI of the bridge was less than the rigidity based on the gross cross-section mainly due to the cracking of the concrete. The flexural and torsional rigidities decreased significantly

Table 3.3

Flexural Rigidities at the Midspan Section
for Different Load Levels

Load (kips)	Loaded Web			Unloaded Web		
	$\frac{EI}{EI_g}$	$\frac{EI}{EI_{int}}$	$\frac{EI}{EI_{cr}}$	$\frac{EI}{EI_g}$	$\frac{EI}{EI_{int}}$	$\frac{EI}{EI_{cr}}$
0	0.45	1.0	1.45	0.6	1.0	2.32
10	0.35	0.9	1.3	0.6	1.0	2.11
20	0.28	0.7	1.0	0.46	0.9	1.19
35	0.2	0.5	0.71	0.3	0.6	0.83
55	0.17	0.45	0.64	0.22	0.57	0.80

Table 3.4

Torsional Rigidities at the Midspan Section
for Different Load Levels

Load (kips)	$\frac{GJ}{GJ_g}$	$\frac{GJ}{GJ_{int}}$
0	0.5	1.0
10		
10	0.4	0.8
20	0.2	0.4
35	0.11	0.22
55	0.11	0.22

and gradually after the occurrence of cracks and with further increase in applied load. The load deflection curves of the loaded and the unloaded webs were linear up to load values of 15 kips and 22 kips respectively, while the load-angle of twist curve was linear up to a load value of approximately 12 kips. At the working load level, the torsional rigidity decreased to about 0.4 of the initial torsional rigidity value; however, the flexural rigidities of the loaded and unloaded webs were about 0.7 and 0.9, respectively, of the initial flexural rigidity values.

Due to the unsymmetrical formation of cracks in both webs and flanges, the shear centre of the box section moved away from the axis of symmetry of the section. This forced the bridge to move horizontally in the lateral direction. Therefore the reduction in the stiffness of the box section should be considered in the calculation of deformations in this type of structure.

The maximum lateral displacement occurred at the midspan of the top side of the loaded web.

Regarding the longitudinal displacement, the lower side of the loaded web showed larger displacements than the top side. This is because the neutral axis is situated nearer the upper slab which is also stronger and stiffer than the lower slab. The maximum longitudinal displacement occurred approximately in the quarter span region of the bridge.

3.6.2 Longitudinal Stresses

For both the symmetrical and the unsymmetrical loading cases, the longitudinal stresses in both the upper and the lower slabs were not uniform across the slab width. The differences in these stresses were about 30 per cent for the symmetrical loading case and 70 per cent for the unsymmetrical loading case.

For the symmetrical loading case the shear lag phenomenon caused a 30 per cent increase in the stresses at the web-flange junction above the stresses in the region between the webs. The measured longitudinal stresses at the midspan and support sections were 50 per cent and 60 per cent higher than the values calculated from the simple beam theory for the symmetrical loading case, respectively, and were approximately twice the calculated values for the unsymmetrical loading case. This is due to the effect of warping restraint in increasing these longitudinal stresses. However, the calculated longitudinal stresses increased by approximately 30 per cent above those obtained from the simple beam theory for both the uncracked and the cracked section analyses by consideration of the torsional and distortional longitudinal warping stresses using the Kollbrunner and Hajdin method and the method of the beam-on-elastic foundation.

In the unsymmetrical loading cases, the longitudinal stresses of the loaded web were approximately twice those of the unloaded web at the midspan section, while at the support section this increase was approximately 50 per cetn.

Bending moments at midspan and support sections evaluated integrating the measured longitudinal stresses for the symmetrical and the unsymmetrical loading cases were within 5 and 10 respectively of the total statical bending moment, thus establishing the reliability of the measured values.

3.6.3 Transverse Stresses

Although the transverse stresses were small in the symmetrical loading case, it plays a significant part in resisting the applied eccentric loads. In the symmetrical loading case, these transverse stresses were about 20 per cent to 40 per cent from the longitudinal stresses at the same location. In the unsymmetrical loading case, these transverse stresses were approximately of the same order as the longitudinal stresses. There were significant transverse tensile stresses over the unloaded web, and this caused a longitudinal crack on the top and bottom slabs. Therefore special consideration should be given to the details of the longitudinal and transverse reinforcements of box girder bridges at the web-flange junctions.

The stirrup stresses increased significantly after the formation and propagation of cracks. Before the formation of cracks, in the unsymmetrical loading cases, these stresses were 30 per cent less than the calculated values (Section 3.4.5), taking both the shear force and the torsional moment into consideration. However, after the formation of cracks, these stresses were about 35 per cent higher than the calculated values. The stirrup stresses in the loaded web showed higher values than those in the unloaded web.

3.6.4 Cracking

In addition to the flexural cracks from the symmetrical load case, shear and torsional cracks formed in the unsymmetrical loading case.

The loaded web showed more severe cracks than the unloaded web due to the combined effects of shear force, bending moment and torsional moment. In the top and bottom slabs, in addition to the flexural cracks, the torsional cracks were observed in the vicinity of the webs. These cracks can be considered to be the horizontal extension of the shear cracks from the webs.

The cracks in the cantilever slabs were mainly flexural cracks all through the bridge span. Therefore, the contribution of the cantilever slabs in the torsional stiffness of the box girder can be neglected. A vertical crack was observed through the thickness of the cantilever slabs especially in the quarter span region and at the support region. These cracks were due to the torsional and the distortional warping stresses.

CHAPTER 4

FINITE ELEMENT ANALYSIS

4.1 Introduction

The behaviour of reinforced concrete box girder bridges has received considerable attention particularly with respect to the distribution of internal forces within the linear elastic range. Even at these lower load levels the response of the structure is rather difficult to predict analytically because of the complications arising from shear lag, warping and distortion phenomena. These difficulties are compounded at load levels beyond the cracking load as sudden localized changes in stiffness cause changes in the deformation and stress distributions. With the propagation and widening of these cracks with increases in the applied load, these deformations and stress distributions get modified further until failure is reached. The performance of the structure in these latter stages is of particular importance to designers working within a 'limit states' framework.

Of the analytical methods available to the designer, the classical approaches of simple bending theory and torsional theory of closed sections are generally used to yield a prediction of the stresses in concrete box girder bridges [87,94]. Although these methods are reliable within the working stress range, their use beyond the cracking load is questionable, especially in a research program where the main objective is to achieve a better understanding of the structural behaviour at all load levels. Limit load theories are also under a severe handicap in the present context because of the inherent difficulty to include the effects of membrane forces. It would seem that the only reliable method which is also general enough to deal with the complexities of the present problem is the Finite Element Method. Although the cost of applying such a technique may be prohibitive in the design process, the results of the present study based on linear and nonlinear finite element analyses should be valuable to the designer and researchers. The quasi nonlinear finite element analysis presented in this chapter provides a good inexpensive tool for studying the effect of key variables which influence the response of structure.

The Finite Element Method has been used quite extensively in the analysis of reinforced concrete structures and the literature is too voluminous to be reviewed comprehensively in this chapter. However, contributions that relate directly to the present work can be found in References [95, 96].

4.2 Finite Element Modeling

In the development of the finite element model of a reinforced concrete element, the following factors are of primary concern:

(a) the treatment of steel reinforcement

(b) cracking of the concrete

(c) shear transfer across cracks

(d) element refinement.

4.2.1 Steel Reinforcement

Two main approaches are at present available to the analyst in treating the idealization of reinforcing steel in the concrete. Firstly, one-dimensional members possessing only axial stiffness can be used to represent each bar. This approach is appropriate in treating beams, but for plates and shells the large number of bars will lead to an extremely fine element mesh making a solution of the problem virtually impossible because of the high computer cost. The second approach, which is much more feasible in the present study, is the treatment of steel as a membrane located at the level of the bars, with orthotropic material properties chosen to match the stiffness in the direction of the reinforcement.

4.2.2 Concrete Cracking

The cracking of any reinforced concrete element can be classified as flexural or membrane. The former occurs when extreme fiber stresses exceed the modulus of rupture of concrete, and the latter when the average stress through the plate thickness exceeds the tensile strength of the concrete. The technique used for introducing the cracks in the finite element model depends on the type of the structure. For example, for beams and shear walls, the cracks have been introduced by assigning a separate node on each side of the crack. As a crack is introduced at a given load level based on the experimental crack configuration, its width is zero to start with and the crack width increases as the load is increased [97]. This approach is not feasible for the type of structure involved in the present study because of the very large number of cracks at higher load levels, especially near the ultimate load. Therefore in the finite element analysis of such structures, it is easier to deal simultaneously with cracked and uncracked elements by modifying the material compliance matrix to account for the varying element properties parallel and perpendicular to the cracks rather than introducing cracks between discrete elements. This technique has provided considerable versatility in studying the effects of the coupling terms in the elasticity matrix on the total behaviour of the box girder bridge under investigation.

The elasticity matrix [D] of an isotropic homogeneous, linearly elastic material (uncracked element) is given by

$$[D] = \begin{bmatrix} E_c & \nu E_c & 0 \\ \nu E_c & E_c & 0 \\ 0 & 0 & G \end{bmatrix} \tag{4.1}$$

where ν is the Poisson's ratio and E_c is the modulus of elasticity of the concrete given by the equation:

$$E_c = 33\ W^{1.5}\ \sqrt{f'_c} \qquad (4.2)$$

where W is the weight of one cubic foot of concrete and f'_c is the compressive strength of concrete.

In an element, when the principal tensile stress exceeds the flexural tensile strength of concrete ($7.5\sqrt{f'_c}$), cracks are introduced along these principal planes. Once the element cracks, the Poisson effect is neglected, and the modulus of elasticity of the concrete perpendicular to the direction of the crack and the shear force transferred across the crack are altered depending on the load level, the crack width and spacing, the concrete cover and the cross-sectional areas of concrete and steel [90 , 91]. These two factors are important in formulating the constitutive relationship to account for the material nonlinearity of concrete in any future finite element analysis. These two phenomena have been handled differently by many researchers as follows.

4.2.2.1 Modulus of Elasticity of Concrete in the Direction Perpendicular to Crack "E_p"

For simplicity, many researchers have recommended the use of a zero value for E_p [72], but Berg [98] has suggested that a non-zero value can yield results that are closer to experimental response. He proposed the following equation to evaluate E_p:

$$E_p = 0.4\ \left(\frac{0.0001}{\varepsilon}\right)^2\ E_c \qquad (4.3)$$

where ε is the concrete strain at the cracking level. However, since the mechanism of the force transfer between cracks is dependent on the steel reinforcement and to some extent on the concrete between the cracks and the concrete cover, the value selected for E_p must account for these factors.

A value for E_p is recommended based on the properties of the uncracked and the cracked sections and the elastic modulus of concrete as follows [99]

$$E_p = \frac{E_c \, I_{cr}}{I_g} \tag{4.4}$$

where E_c is the modulus of elasticity of the uncracked concrete,

I_{cr} is the moment of inertia of a strip of unit width after cracking,

and I_g is the moment of inertia of a strip of unit width before cracking.

Both zero and non-zero values for E_p, calculated using Equation (4.4), have been investigated in the present study to determine the sensitivity of the finite element analysis results to this factor.

4.2.2.2 Shear Transfer Across Cracks

The presence of cracks through the concrete plate causes an immediate reduction in the shear stiffness. The fact that the plate has any stiffness at all in this mode is due to the ability of the concrete to transmit shear forces across the cracks by means of aggregate interlock. This phenomenon has been studied by Houde and Mirza [90], Fenwick [91], and by Taylor [92]. Houde and Mirza observed that the influence of the maximum aggregate size was negligible compared with the effect of the crack width and the concrete strength. They observed that the shear transfer across the crack is basically a function of the crack width and continues to diminish as the crack widens. They showed the shear modulus of the cracked concrete, βG, with the inverse of the crack width C, in Figure 4.1.
It must be noted that G is the shear modulus of elasticity or the modulus of rigidity of the uncracked concrete, and β is a reduction factor which decreases the effective shear modulus to account for the crack width. The term G in the elasticity matrix is therefore replaced by βG to account for the reduced shear transfer across the cracks. For simplicity, most of the investigators have neglected this factor in finite element analyses of reinforced concrete. However, Agrawal [100] has arbitrarily used a value of 0.5 for the reduction factor β to account for the shear transfer across the crack.

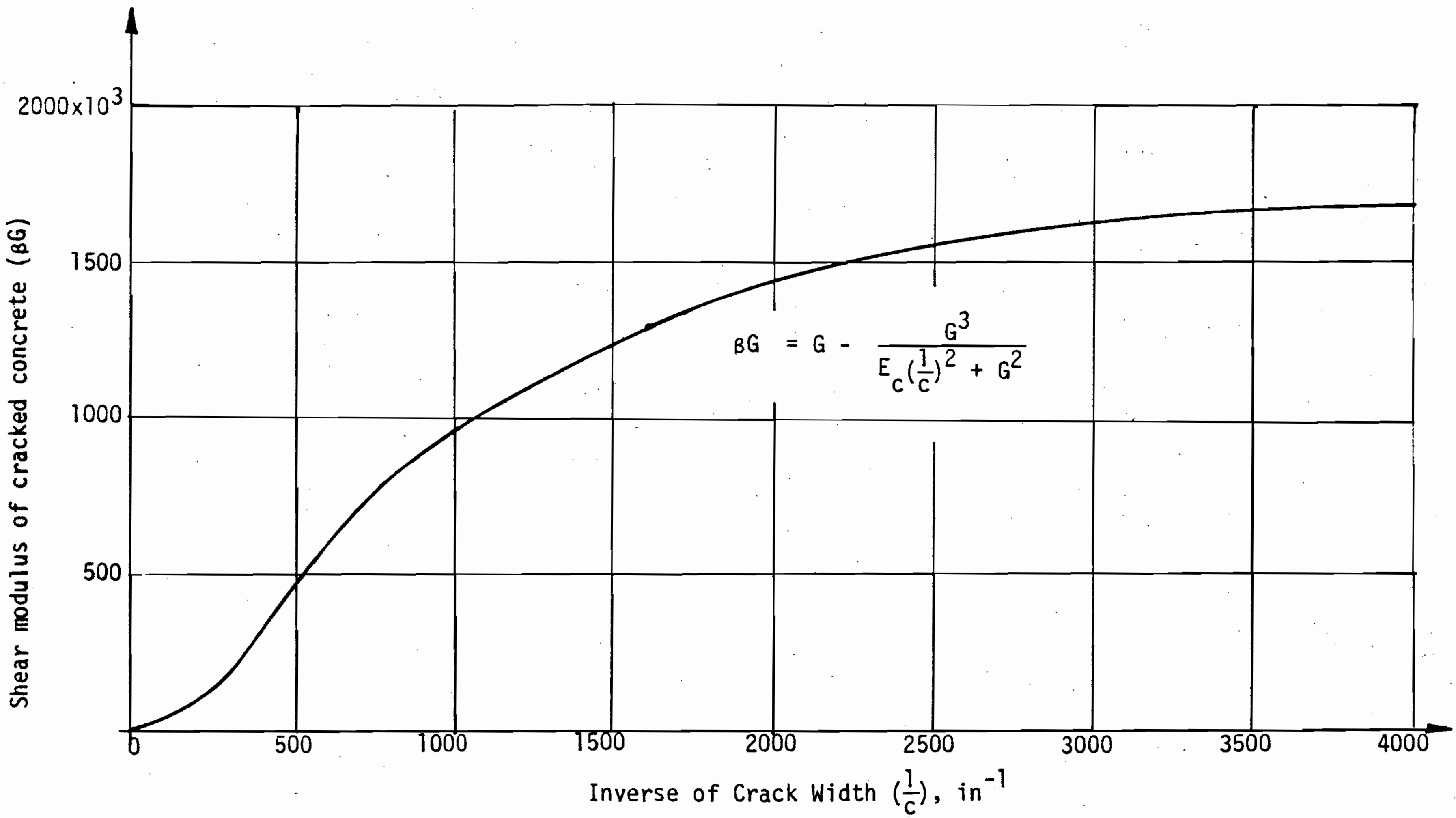

FIG. 4.1 INFLUENCE OF THE CRACK WIDTH ON THE SHEAR MODULUS [90]

The implications of the findings of Houde and Mirza on the behaviour of box girder bridges have been considered in the present study. Based on their findings, a parametric study has been conducted for difference values of the reduction factor, "β", namely, 0, 25%, 50% and 75% which correspond to crack widths of 0.0, 0.015 mm, 0.03 mm and 0.05 mm respectively. Again, it must be noted that the effects of this factor 'β' and that of the modulus of elasticity perpendicular to the crack E_p, are important in developing a nonlinear finite element analysis of reinforced concrete.

The modified elasticity matrix [D] of a cracked element in its u-v local axis will then be as follows:

$$[D]_{uv} = \begin{bmatrix} E_c & 0 & 0 \\ 0 & E_p & 0 \\ 0 & 0 & \beta G \end{bmatrix} \qquad (4.5)$$

This matrix can be transferred to the global x-y axis by the following equation

$$[D_{xy}] = [C]^T \ [D_{uv}] \ [C] \qquad (4.6)$$

where [C] is the transformation matrix as follows:

$$[C] = \begin{bmatrix} \cos^2\alpha & \sin^2\alpha & \sin\alpha\cos\alpha \\ \sin^2\alpha & \cos^2\alpha & -\sin\alpha\cos\alpha \\ -2\sin\alpha\cos\alpha & 2\sin\alpha\cos\alpha & \cos^2\alpha-\sin^2\alpha \end{bmatrix} \qquad (4.7)$$

where α is the angle between the direction of the crack and the x-axis as shown in Figure 4.2.

For the case of two orthogonal cracks appearing in an element, the elasticity matrix [D] is set equal to zero.

4.2.3 Element Mesh

The finite element analysis in the present study has been conducted using the thin-shell element of the SAP IV Computer Program [64]. This element was developed by Clough and Fellipa and it is a quadrilateral of arbitrary geometry formed from four compatible triangles [101]. As shown in Figure 4.3, the central node is located at the average of the coordinates of the four corner nodes. The element has six interior degrees of freedom which are eliminated at the element level prior to assembly, therefore the resulting quadrilateral element has twenty-four degrees of freedom, i.e., six degrees of freedom per node in the global coordinate system. In the analysis of flat plates, the stiffness associated with the rotation normal to the element surface is not defined, therefore it is not included in the analysis. One disadvantage of the element, however, is its significant 'element-form' times which results mainly because of the use of four

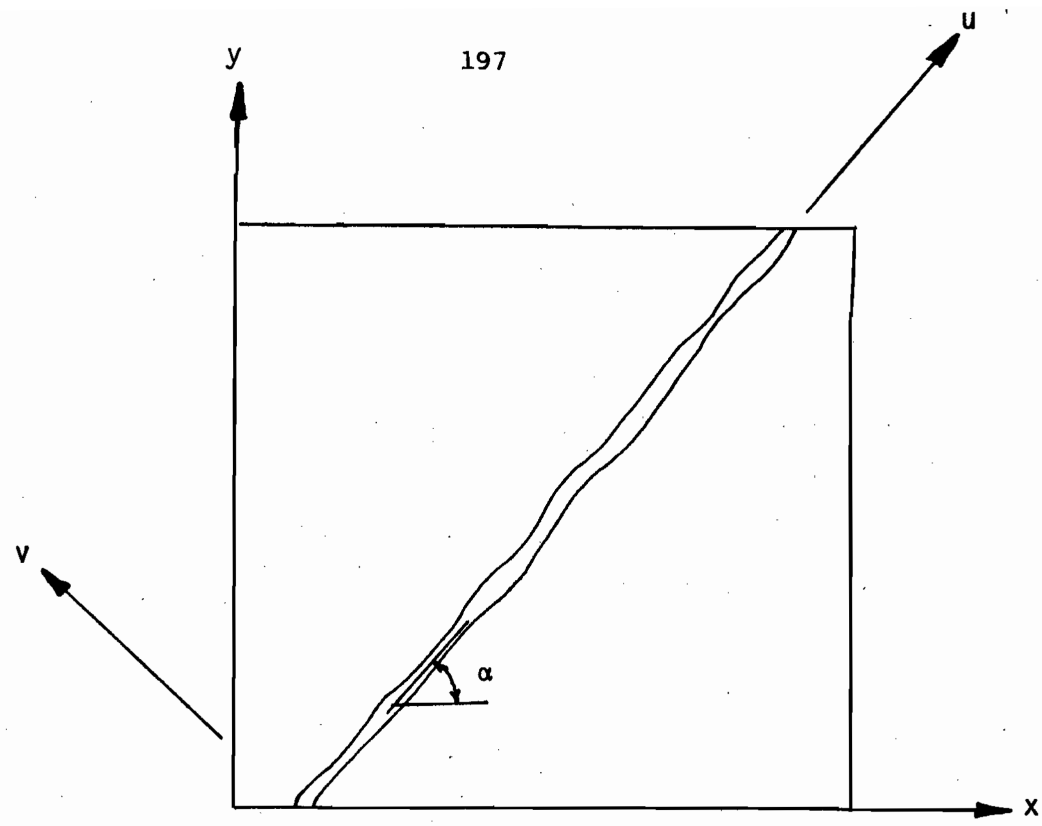

FIG. 4.2 CRACKED ELEMENT

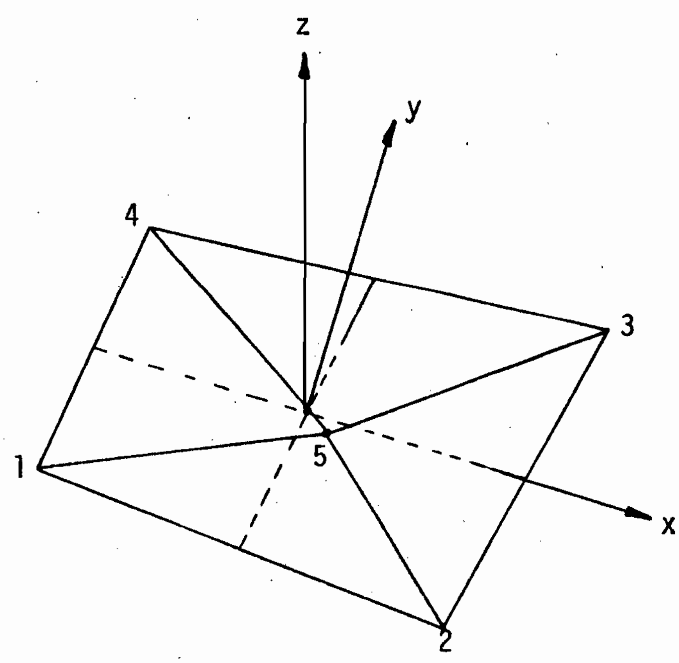

FIG. 4.3 THIN SHELL ELEMENT

subdomain triangular elements and the associated static condensation. Despite this drawback there does not seem to be a reliable alternative to this element except to use those elements utilizing higher order degrees of freedom. The severe continuity requirements of these latter elements render them all but impossible to use for the type of structure analysed herein where discontinuities in strain are expected.

Figure 4.4 shows the layout of the finite element idealization along with the associated degrees of freedom at each node. In-depth checks on the equilibrium of the stresses were obtained using this model and the associated computer costs confirmed the adequacy and economy of the grid refinement used. Once the joint rotation and displacements are evaluated, the element stresses are calculated. The results of this finite element computer program include rotations and displacements at each nodal point in addition to the membrane and bending stresses at the element centroid.

In all the analyses conducted in the present study, the nodal points at midspan of the bridge are subjected to symmetric constraints. The restraints at the support depend on whether warping is to be eliminated there. When warping is restrained, all degrees of freedom are eliminated at these nodal points. The restraint applies to all analyses with the exception of one analysis cited in the next section for which warping was unrestrained. Details of the restraints are discussed therein.

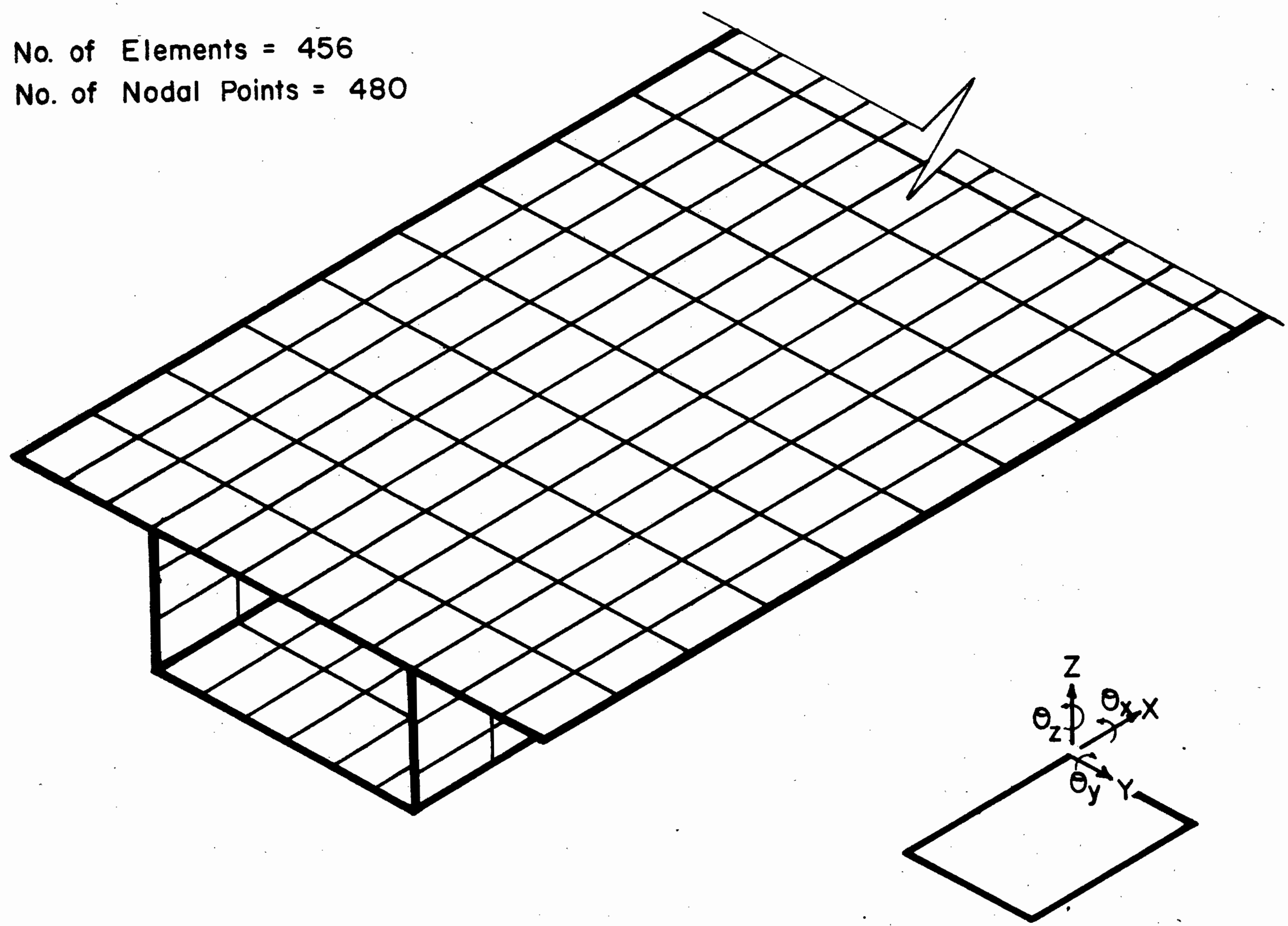

FIG. 4.4 FINITE ELEMENT IDEALIZATION

4.3 Finite Element Analysis

4.3.1 General

Finite element analysis was conducted for the self weight of the bridge model and the extra dead load used to simulate the dead weight of the prototype, in addition to the following loading conditions:

4.3.1.1 Linear Analysis

i) Two symmetrical 10 kips concentrated loads placed over the two webs at the midspan section (these were the design working loads)

ii) A 20 kips concentrated load applied at the midspan section over one web for two different analyses, one with unrestrained warping and the second one with restrained warping.

4.3.1.2 Quasi-nonlinear Analysis

Quasi-nonlinear analysis was performed for four values (20, 31, 42 and 55 kips) of concentrated load placed on one web at the midspan section for the restrained warping condition. A parametric study was conducted for this loading case to evaluate the influence of different values for the element stiffness perpendicular to the cracks,and to study the effect of the variation of the shear force transferred across the cracks for different crack widths on the deformational behaviour and strength of the box girder bridge.

4.3.2 Linear Analysis

Most box girder bridges are designed on the basis of linear analyses. It is expected that without a good understanding of the behaviour of the structure at the lower load levels, an understanding of the behaviour close to failure will not be possible. Furthermore, the performance of the structure at working loads will not depart markedly from the linear state. The element stiffnesses were calculated based on the uncracked section and the steel reinforcement was ignored.

The first part of this section deals with the results, in the form of displacements and stresses, for the box girder model bridge linear analysis. These results are then used as the basis of comparison for the results from the nonlinear analysis in the next section. The question of the effect of warping is also addressed in this section. Nonlinearities may have a quantitative influence on this effect, but probably not in any significant qualitative way.

4.3.2.1 Symmetrical Loading Case

The gravity loads of the model box girder structures have been distributed over the entire length of the bridge. Two point loads of 10 kips each are also located at midspan over the webs. The nodes at the support are completely restrained to simulate the interior support of a multispan configuration. For the boundary conditions to be exact each span would be loaded identically and diaphragms would be used at the supports.

Figure 4.5 shows the vertical displacement at midspan of the bridge. The results of the present analysis are, of course, represented by a straight line. On the same plot, also shown as a straight line, is the result of the elastic analysis based on the simple bending theory. This theory is modified by use of Branson's equation [88] to allow for the change in inertia after cracking, and the corresponding results are shown on the same plot; the experimental results are also shown. The dead load deflection of the bridge as calculated from the finite element analysis was 0.132 in. This deflection value should be added to the calculated deflection at each load level to obtain the total deflection. The experimental deflection value for the self weight of the bridge was 0.144 in. Thus good agreement was obtained between the computed and the experimental values.

As shown in Figure 4.5, all three sets of theoretical results are close to the experimental data at low loads,with the finite element results showing the best agreement. Significant reduction in stiffness is apparent at P = 8 kips. At a total load value of 20 kips, the measured deflection at the midpsan section was approximately 0.2 in., while the finite element results showed a deflection value of 0.125 in. At this load level, the measured deflection value was 0.2 in. which is approximately 74% higher than the value calculated using the simple beam theory and 48% higher than the finite element analysis value. The use of a cracked section by incorporating Branson's equation in the simple beam theory decreases the difference from 74% to 66%. Therefore it is obvious that the available elastic methods of analysis are valid only before the formation of cracks at which stage the difference between the measured and the calculated deflections increases significantly as expected.

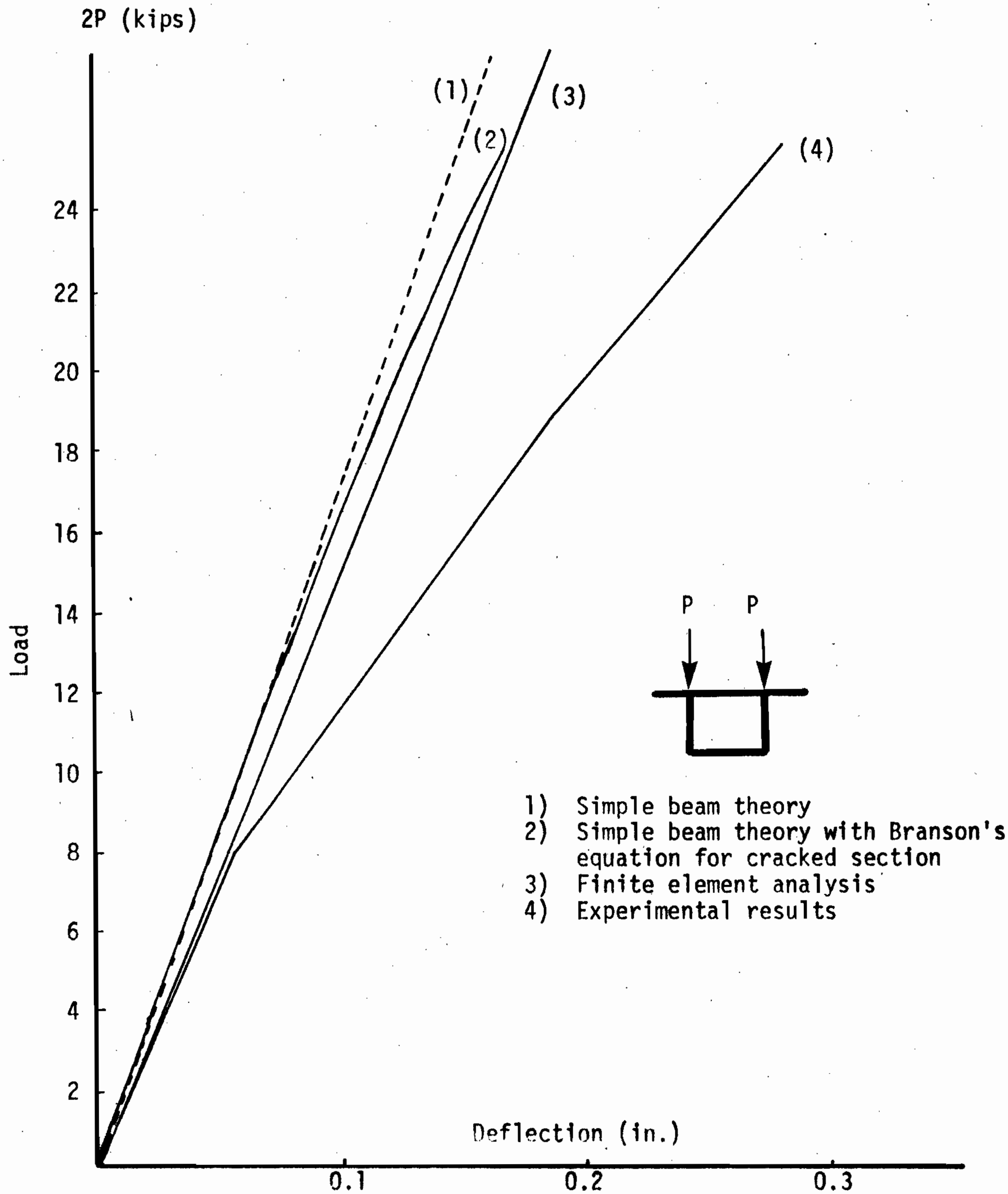

FIG. 4.5 LOAD-DEFLECTION CURVES AT THE MIDSPAN SECTION OF THE BRIDGE FOR THE SYMMETRICAL LOADING TEST

The distribution of longitudinal and transverse membrane stresses across the girder width at midspan and support sections is shown in Figure 4.6. Similarly, the variation of longitudinal and transverse bending stresses at midspan and support sections is shown in Figure 4.7. It must be noted that the longitudinal membrane and bending stresses at the web-flange junction are approximately 30% higher than those predicted from the simple beam theory. It can be seen that the membrane stresses are approximately 3 - 5 times the bending stresses.

These figures show that the largest longitudinal membrane and bending stresses within the box section occur at the web-flange junction. The differences between the largest and the smallest membranes or bending stresses across the top and the bottom slabs range between 20% and 50%. These differences result from the effect of the shear lag phenomenon in redistributing these stresses within the box section as explained in Chapter 3. The observed and the calculated transverse membrane and bending stresses within the box section are approximately constant between the webs and decrease towards the ends of the cantelever tips. These transverse stresses attain maximum values at the midspan section. At this section the transverse membrane and bending stresses are approximately of the same order.

The experimental and the calculated values of the total transverse stresses are approximately 40% of that of the total longitudinal stresses, therefore due care must be exercised in designing box section structures for transverse stresses.

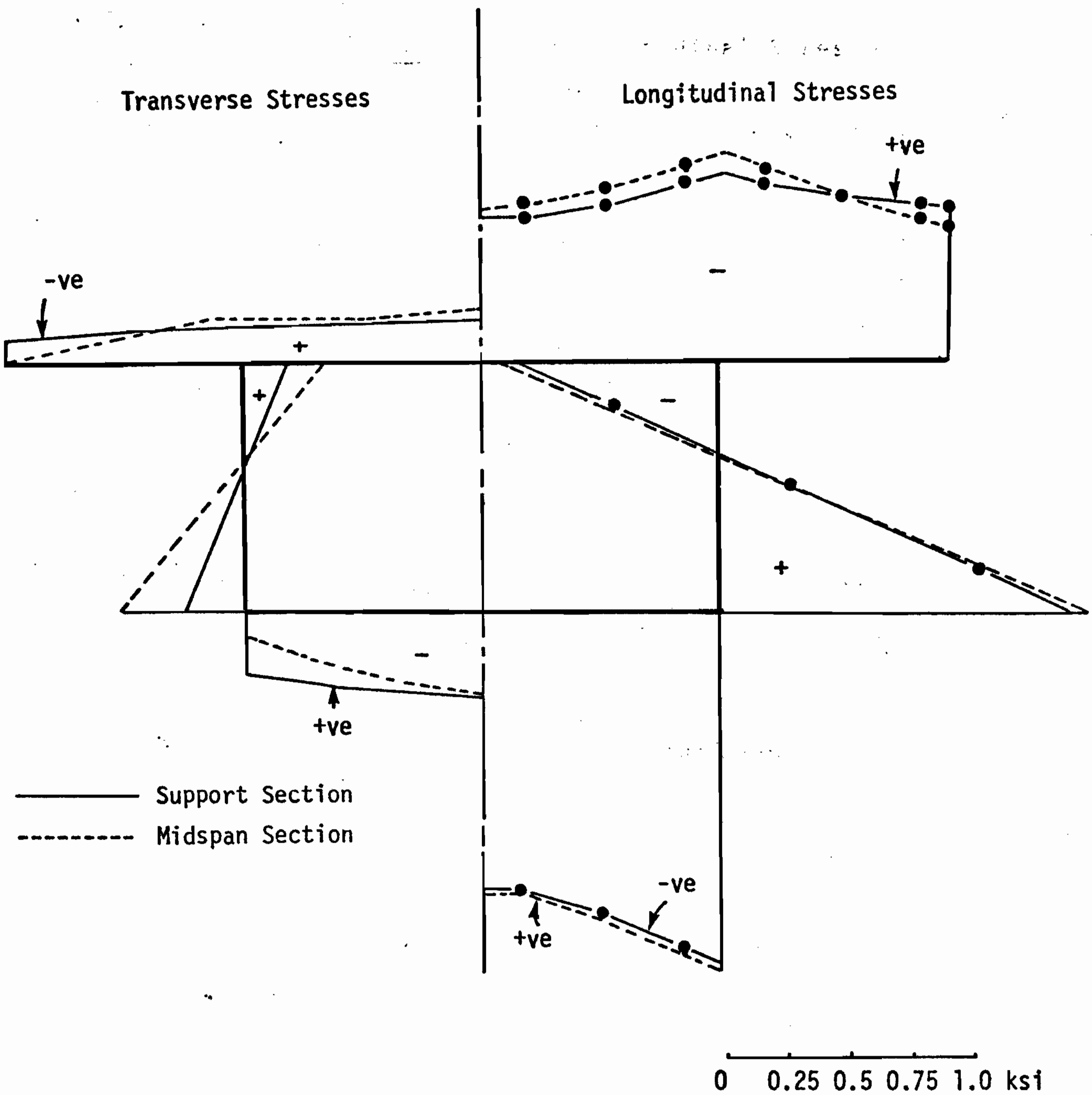

FIG. 4.6 MEMBRANE STRESSES AT MIDSPAN AND SUPPORT SECTIONS
(SYMMETRICAL LOADING CASE)

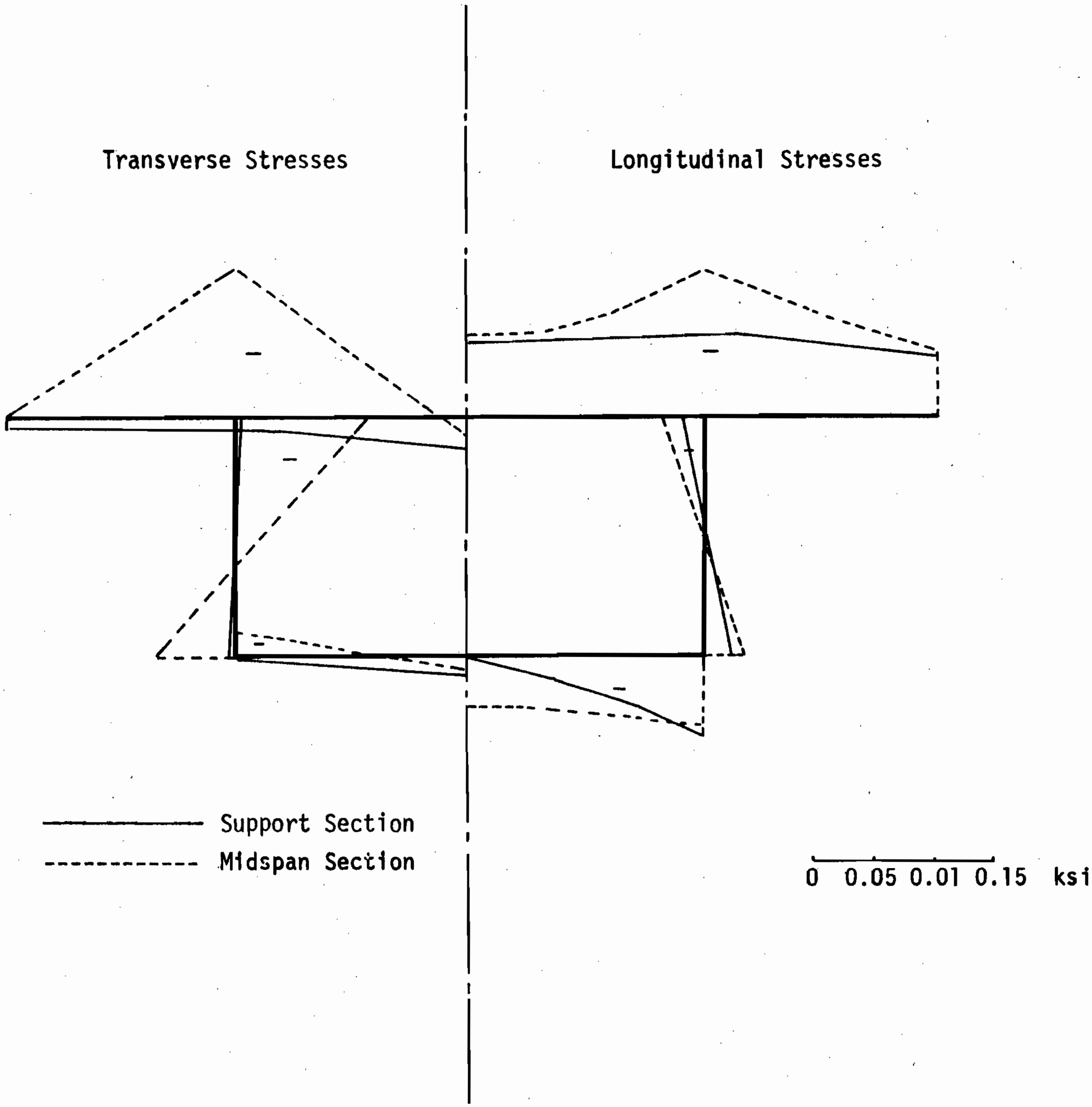

FIG. 4.7 BENDING STRESSES AT MIDSPAN AND SUPPORT SECTIONS
(SYMMETRICAL LOADING CASE)

4.3.2.2 Unsymmetrical Loading Case

(a) Behaviour With Unrestrained Warping

An elastic analysis was conducted for a total working load of 20 kips applied on one web (termed the loaded web). The unrestrained warping condition was achieved in the computer program by superposing the following two loading conditions as shown in Figure 4.8:

(i) two symmetrical loads of 10 kips on each web at midspan,

(ii) a torsional loading consisting of a downward load of 10 kips on the loaded web and an upward load of 10 kips on the other web.

Experimental and calculated values of the midspan deflection along the centerline of the bridge and the loaded and unloaded webs, calculated using the finite element analysis and the simple beam theory, are shown in Figure 4.9. As expected and verified experimentally, the deflections of the loaded web are approximately 40 - 80% higher than those of the unloaded web. As shown in Figure 4.9, the simple beam theory gives the lowest deflection value. At the load value of 20 kips, the calculated values of the centerline deflection by the simple beam theory are 0.046 and 0.088 in. for the uncracked and the cracked sections, respectively. The finite element elastic analysis resulted in deflection values of 0.1 and 0.15 in. for the unloaded and loaded webs, respectively, while the measured deflection values for the unloaded and loaded webs at the same load level are 0.134 and 0.215 in. respectively. The measured deflection values are

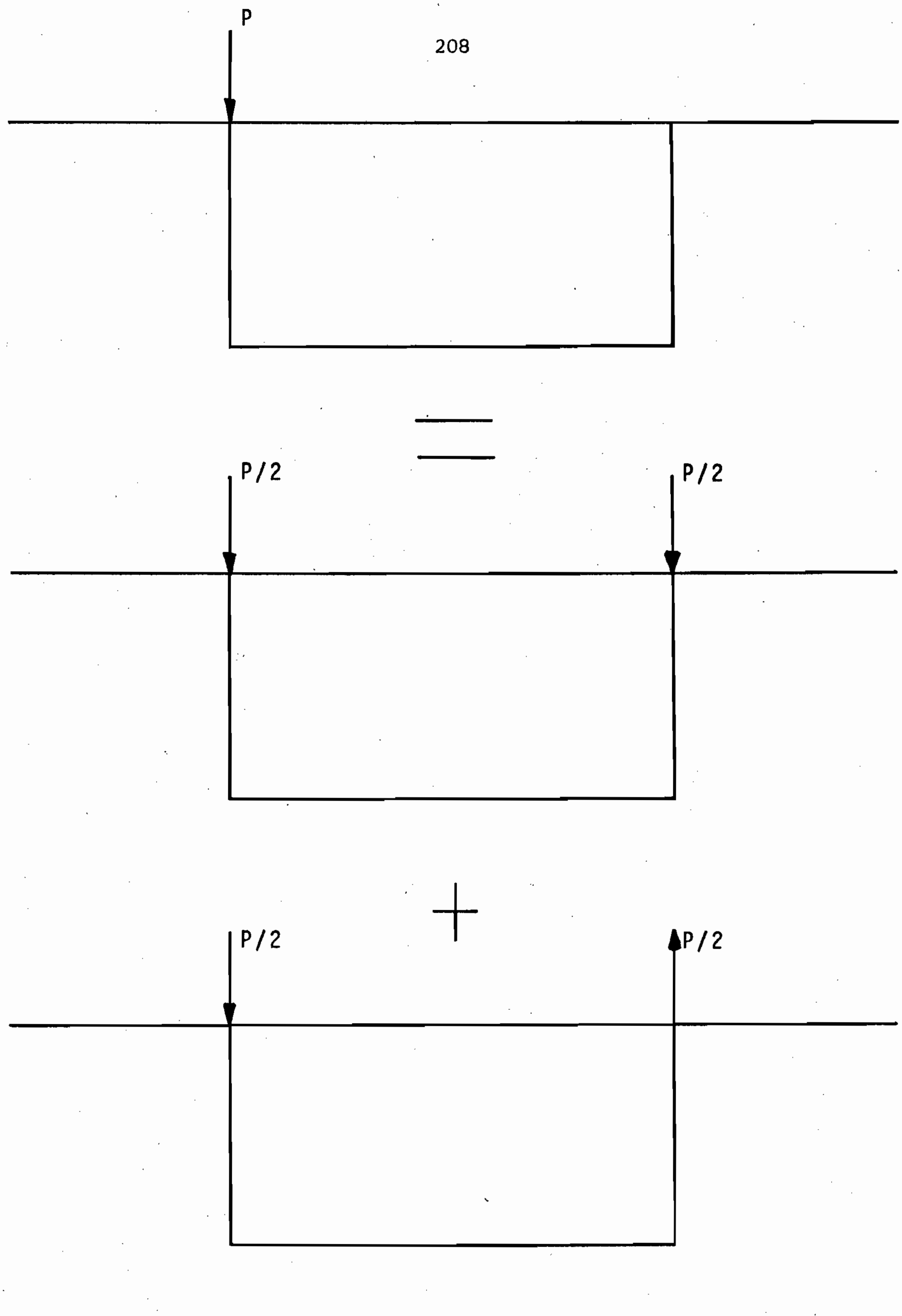

FIG. 4.8 LOAD SUPERPOSITION FOR THE UNSYMMETRICAL LOADING CASE

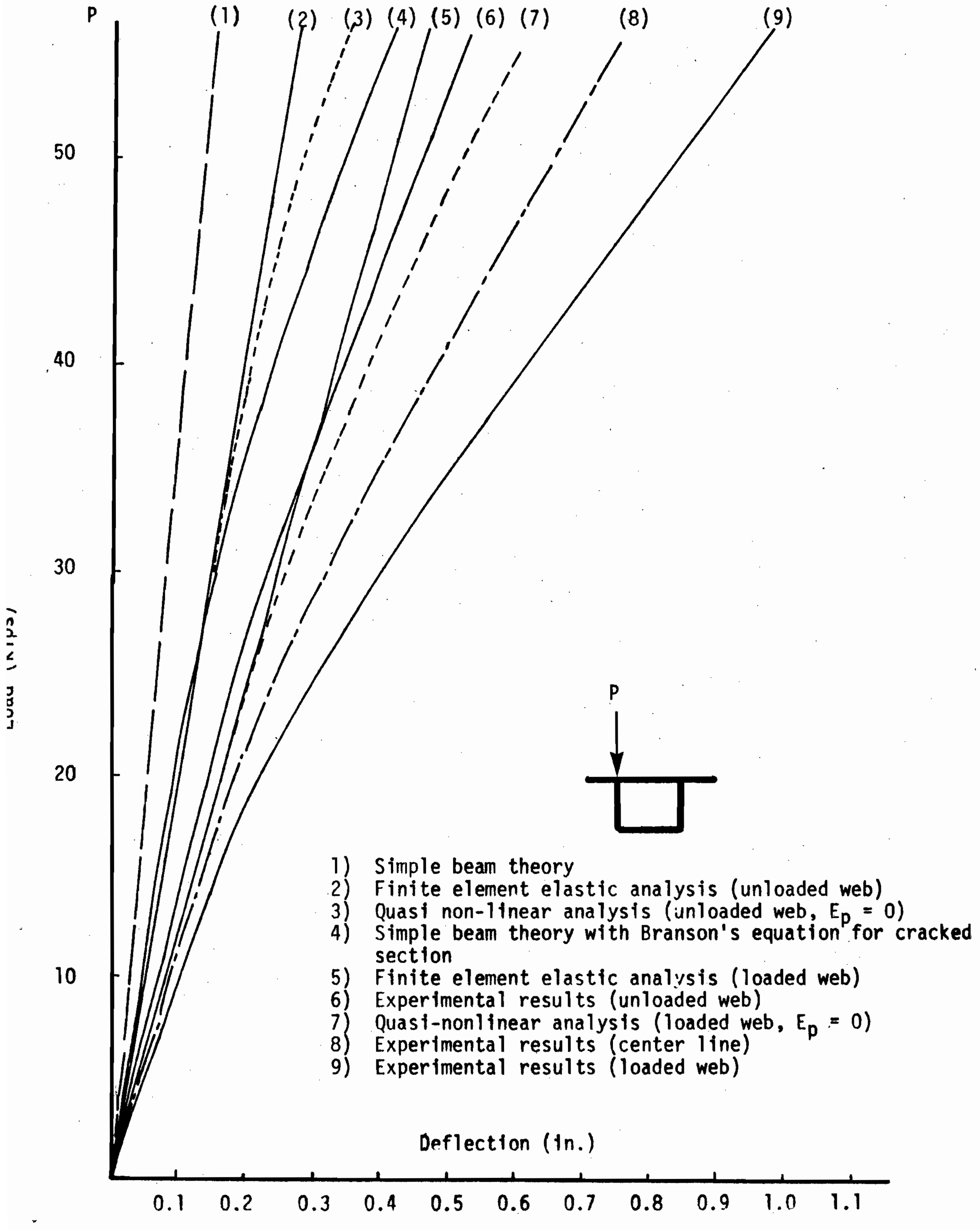

FIG. 4.9 LOAD-MIDSPAN DEFLECTION CURVES FOR THE UNSYMMETRICAL LOADING CASE

approximately 34% and 43% higher than those predicted from the elastic finite element analysis for the unloaded and the loaded webs, respectively. The measured centerline deflection value is 0.175 in. which is approximately twice that predicted from the simple beam theory using a cracked section.

Figure 4.10 shows the profile of the vertical deflection through half of the bridge span for both loaded and unloaded webs as obtained from the finite element analysis.

The load eccentricity causes the girder to twist and translate laterally. The variation of the lateral displacements of the top and the bottom of both loaded and unloaded webs along the bridge span is shown in Figure 4.11. As shown in this figure, the maximum lateral displacement of the top slab has occurred at the midspan section as expected. However, the maximum lateral displacement in the lower slab occurs near the quarter span region of the bridge. This is due to the large torsional and distorsional effects in this region as explained by the beam-on-elastic-foundation method in the previous chapter.

The longitudinal displacements of the nodes given by the finite element analysis showed larger displacements in the lower flange than in the upper flange (Figure 4.12). This was expected because the neutral axis is located near the upper flange. These displacements attain a maximum value near the quarter span of the girder. It can also be noted from Figure 4.12 that the loaded and the unloaded webs translate longitudinally in opposite directions.

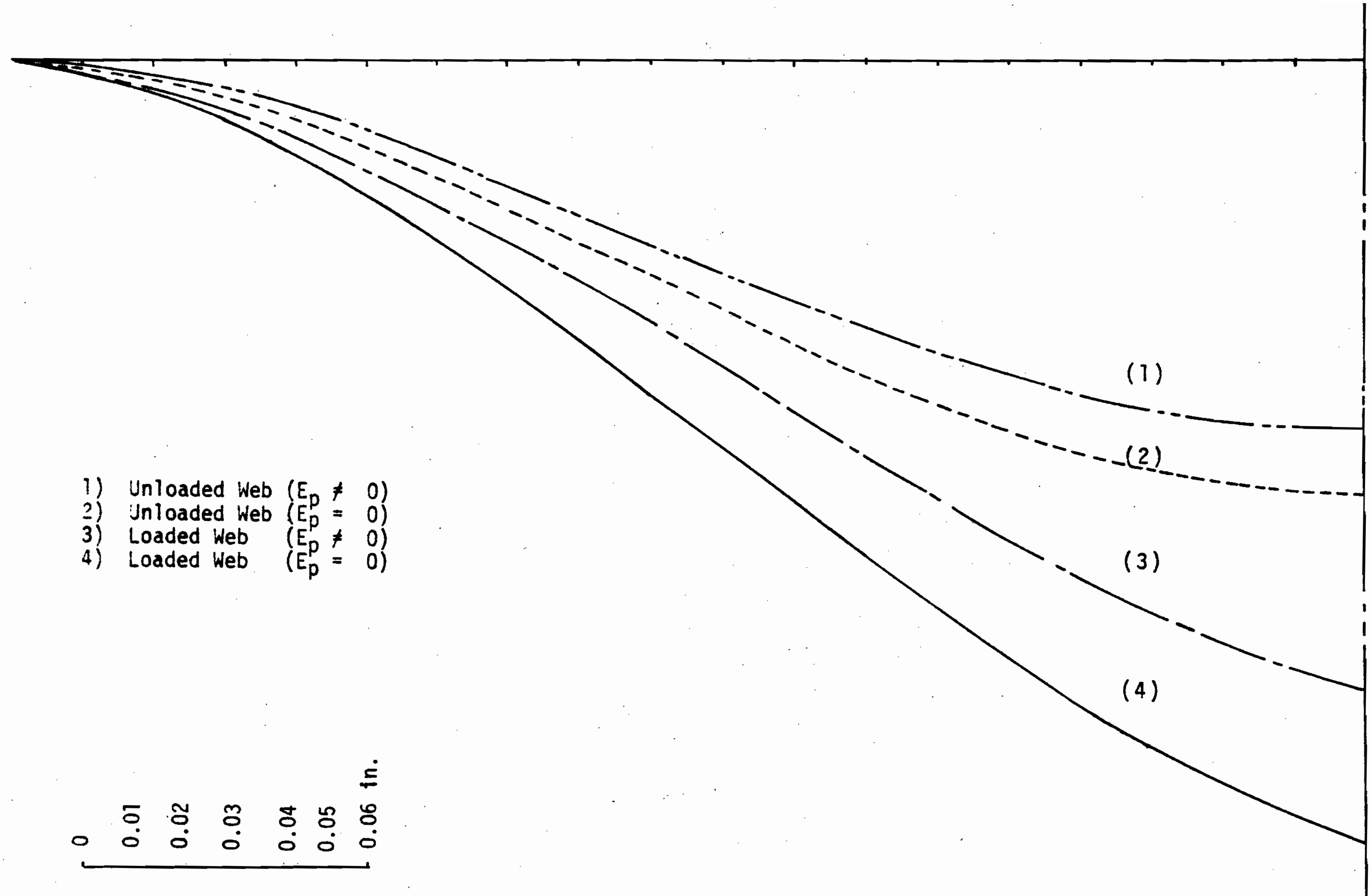

FIG. 4.10 VERTICAL DEFLECTION PROFILE FOR LOADED AND UNLOADED WEBS (UNSYMMETRICAL LOADING CASE)

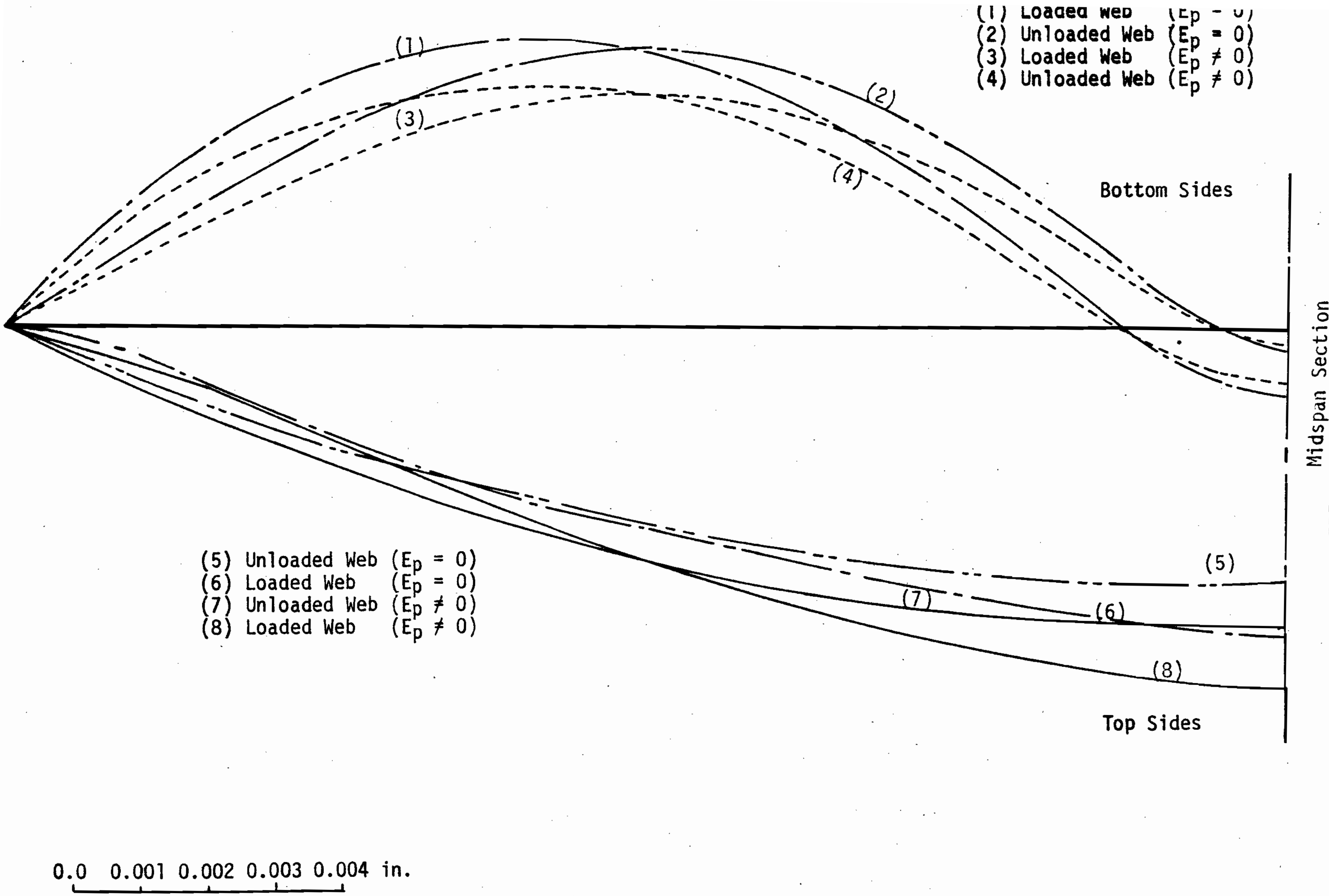

FIG. 4.11 LATERAL DISPLACEMENT PROFILE FOR LOADED AND UNLOADED WEBS (UNSYMMETRICAL LOADING CASE)

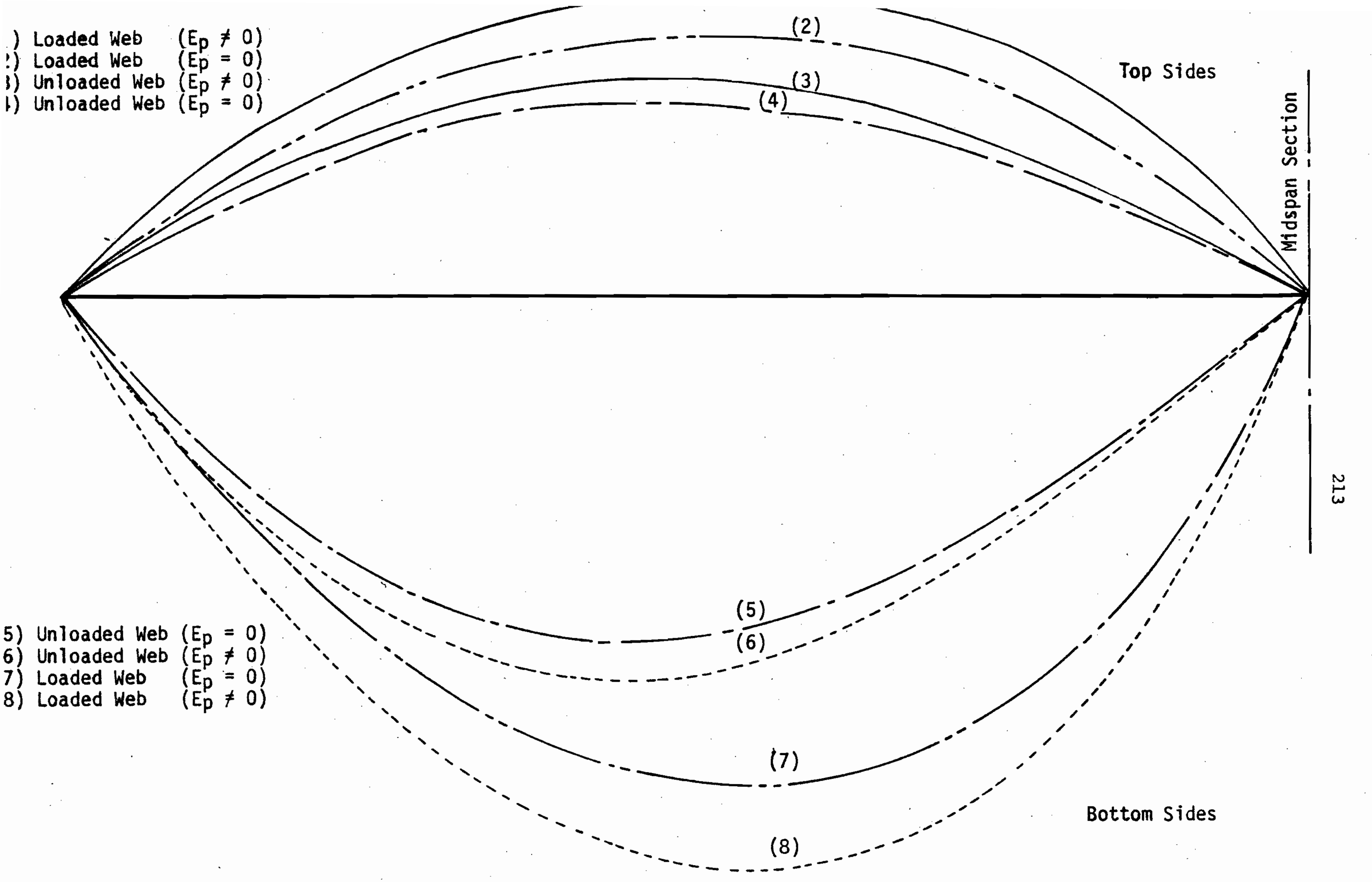

FIG. 4.12 LONGITUDINAL HORIZONTAL DISPLACEMENT FOR LOADED AND UNLOADED WEBS (UNSYMMETRICAL LOADING CASE)

Analysis results showed that the longitudinal membrane stresses were maximum at the support section while the transverse membrane and bending stresses were maximum at the midspan section. This is due to the maximum deformations which occur within the box section in the midspan region.

The variation of longitudinal membrane and bending stresses within the box section is shown in Figures 4.13 and 4.14 respectively for both midspan and support sections. As shown in these figures, the largest stresses within the box section are concentrated in the vicinity of the loaded web and decreased towards the unloaded web. The maximum deformations along the loaded and the unloaded webs are maximum at the midspan,and the maximum deflection of the loaded web is about 80% larger than the maximum deflection of the unloaded web. Therefore, the largest transverse membrane and bending stresses occur at the midspan section with different signs over the loaded and the unloaded webs due to the applied torsional load as shown in Figures 4.15 and 4.16. These transverse stresses result in significant tension over the unloaded web; this was confirmed by the tension cracks which appeared over the unloaded web during the unsymmetrical test on the bridge model, as mentioned in Chapter 3.

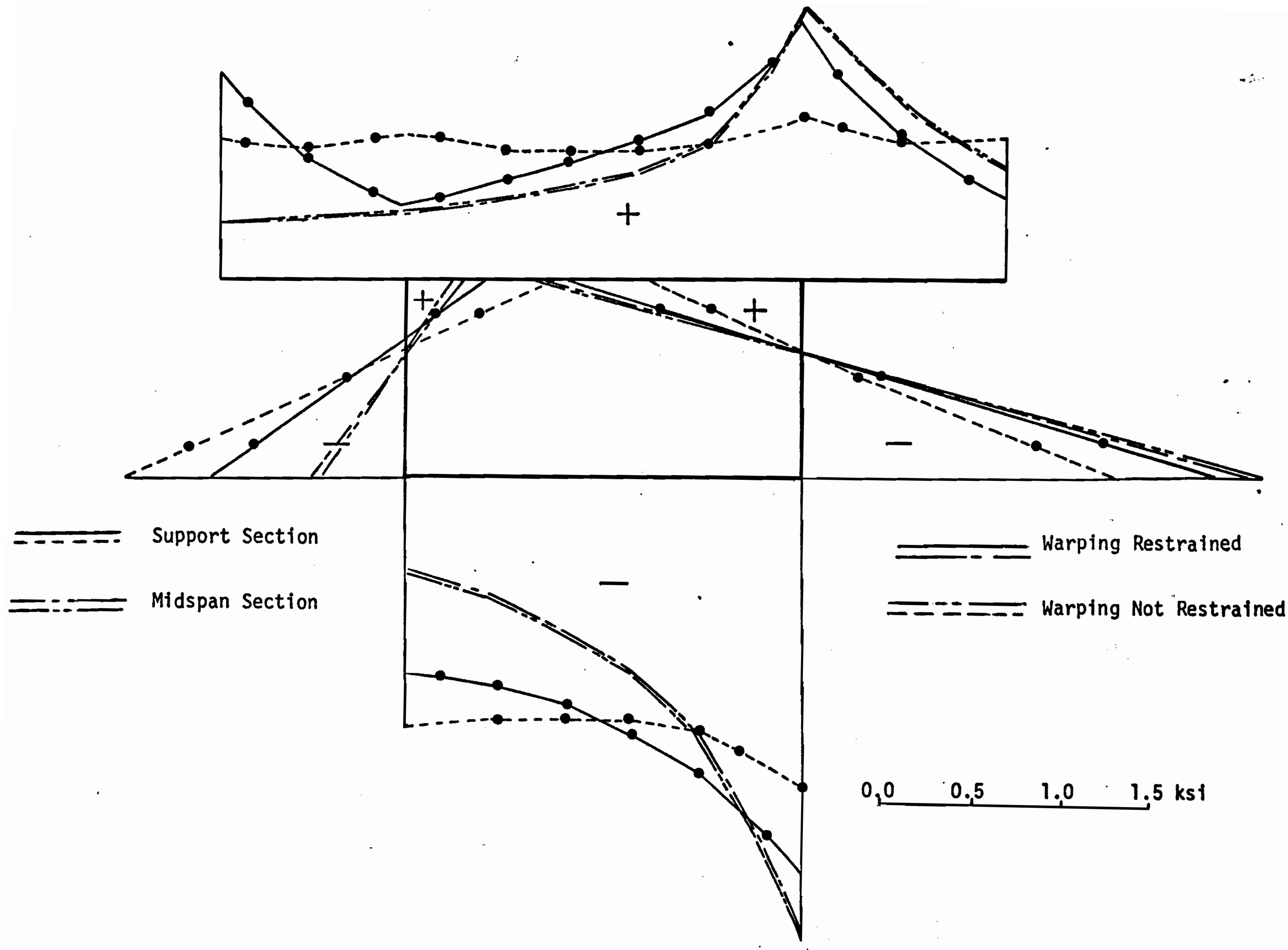

FIG. 4.13 LONGITUDINAL MEMBRANE STRESSES (UNSYMMETRICAL LOADING CASE)

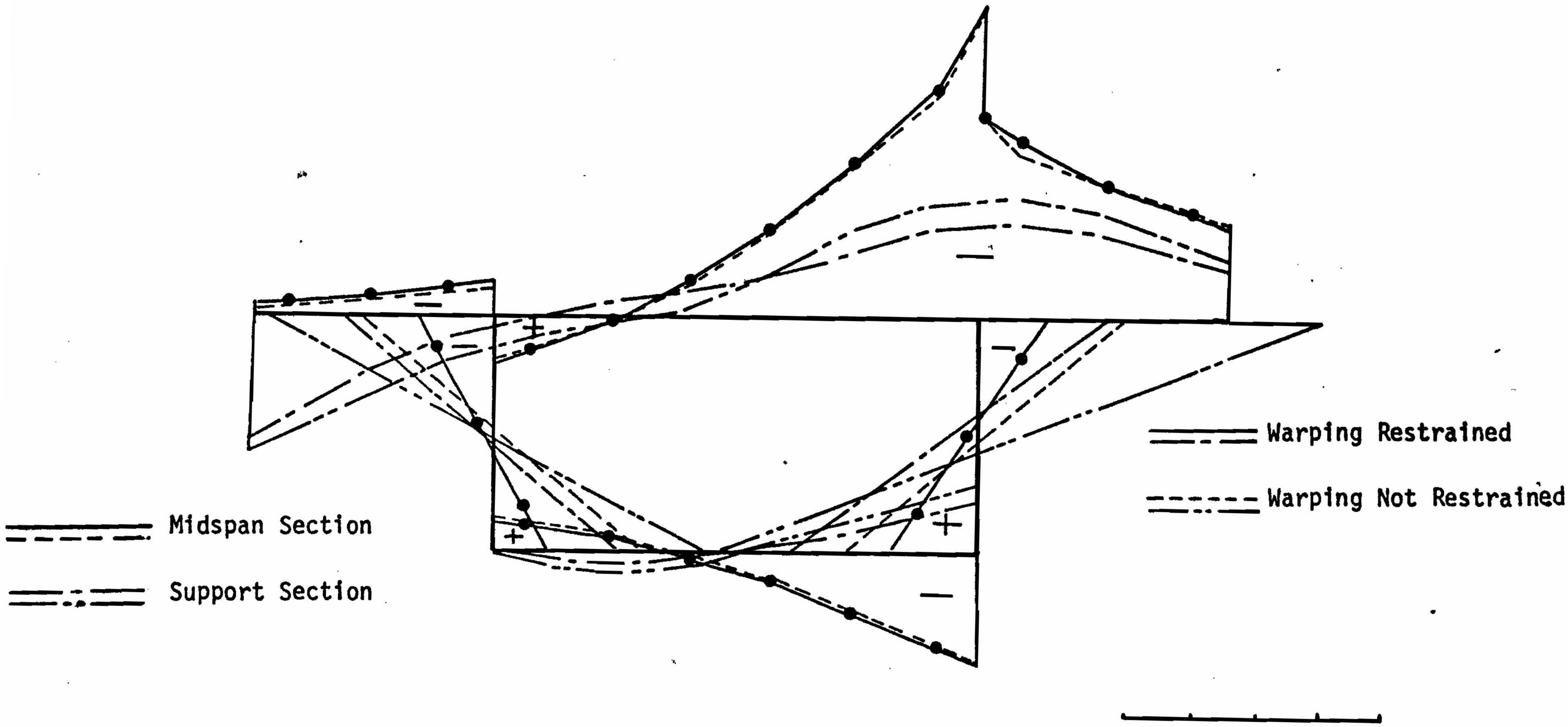

FIG. 4.14 LONGITUDINAL BENDING STRESSES (UNSYMMETRICAL LOADING CASE)

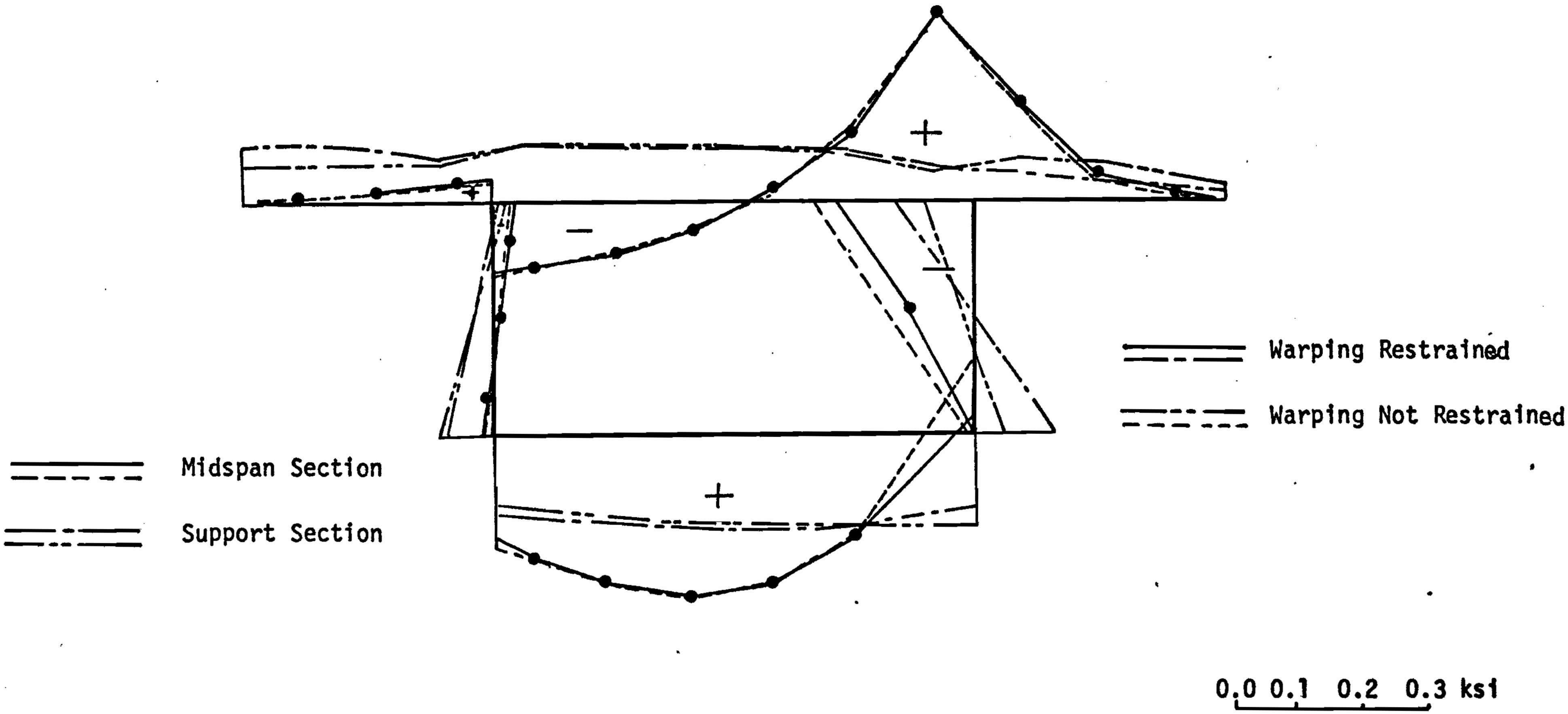

FIG. 4.15 TRANSVERSE MEMBRANE STRESSES AT MIDSPAN AND SUPPORT SECTIONS
(UNSYMMETRICAL LOADING CASE)

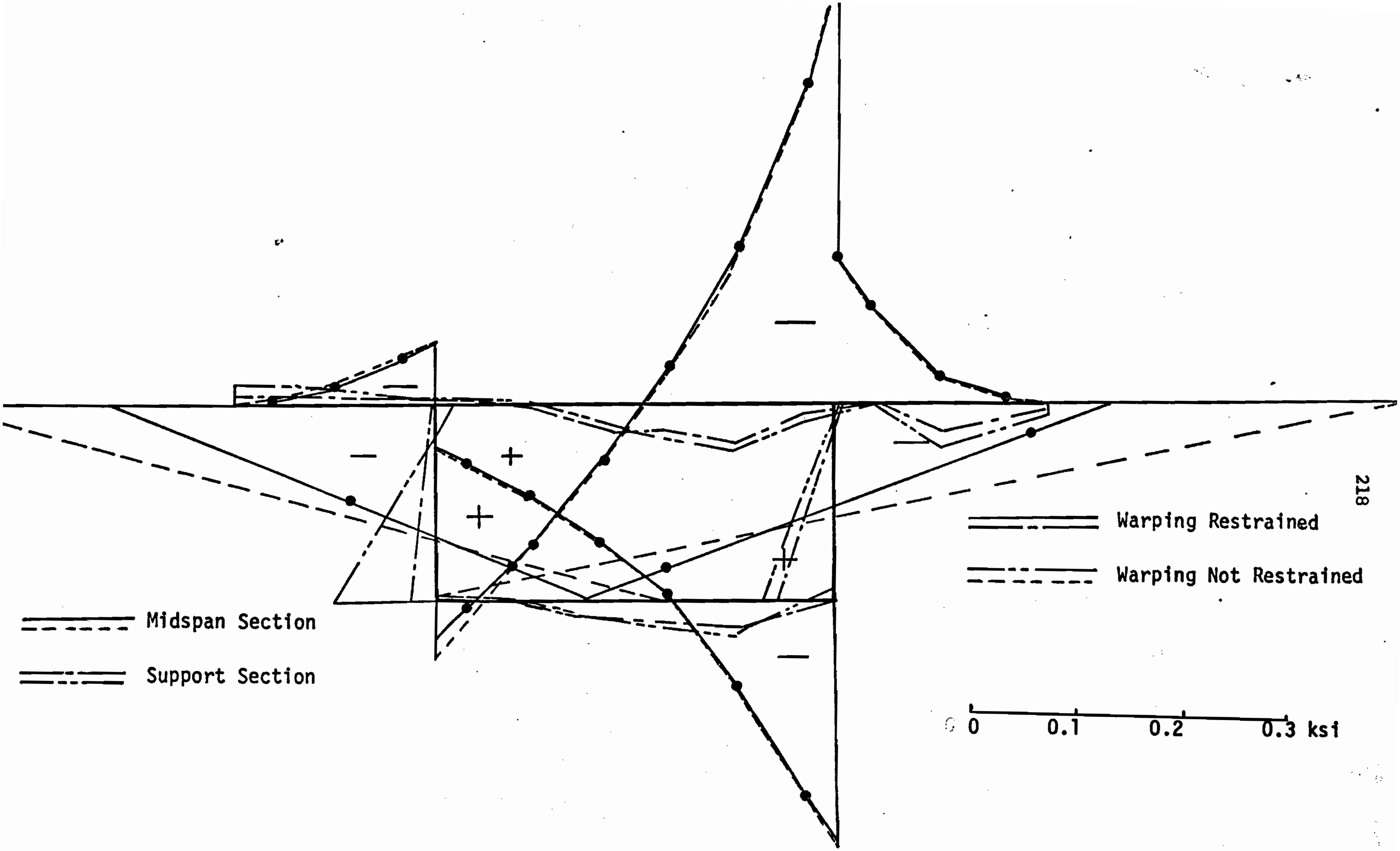

FIG. 4.16 TRANSVERSE BENDING STRESSES AT MIDSPAN AND SUPPORT SECTIONS
(UNSYMMETRICAL LOADING CASE)

(b) Behaviour With Warping Restrained

Analysis results for a total load value of 20 kips show a decrease of about 5 - 10% in the vertical and horizontal displacements when compared with the unrestrained warping case.

Figures 4.13 through 4.16 show the distribution of the longitudinal and transverse membrane and bending stresses within the box section at different bridge sections for both unrestrained and restrained warping conditions at the ends. Considerable difference was observed between these two cases,especially at the support section. The warping restraint for the unsymmetrical loading case causes the membrane stresses in the webs at the midspan section to increase by approximately 20%. However, there is no significant increase in the membrane and bending stresses in the top and bottom slabs. Moreover, there is a significant decrease in the midspan web bending stresses due to the warping restraint. The longitudinal bending stresses here have decreased by approximately 50% for both the unloaded and the loaded webs as a result of the warping restraint, while the transverse bending stresses of the webs undergo a similar decrease of 50%. However, these bending stresses are very small in comparison to the membrane stresses. No significant changes were observed in the shear stresses at the midspan section due to the warping restraint.

At the support section, for the loaded web, the warping restraint causes an increase of 25% in the longitudinal membrane stresses, and a decrease of 20% in the longitudinal and transverse bending stresses in both the top and the bottom slabs. The transverse membrane stresses at the support section showed an increase of approximately 30% due to the effect of warping restraints. Similarly, the warping restraint causes a decrease of approximately 40% in the longitudinal and transverse bending stresses in both webs at the support section; however, these stresses at this section are also very small in comparison with the membrane stresses.

In summary, the warping restraint can have a significant influence on some behavioural aspects of a box section structure. These effects become more pronounced for unsymmetrical loading cases which are more frequent and therefore restraint of warping must be carefully considered in the design of box girder bridges [102].

4.3.3 Quasi-Nonlinear Finite Element Analysis

4.3.3.1 General

A general nonlinear finite element analysis of a reinforced concrete structure which accounts for cracking and material nonlinearities with monotonically increasing loads is very expensive and time-consuming. Therefore it was not used to study the sensitivity of structural response to the various parameters examined in this study. This quasi-nonlinear analysis was conducted by incorporating the experimental data on the number, length and orientation of cracks in developing the stiffness matrix for each element. Also, the steel reinforcement in each element was idealized as an orthotropic membrane element. Eight separate computer runs were made for different combinations of values of E_p ($E_p = 0$ and $E_p \neq 0$) and four values of β to account for the crack widths ($\beta = 0.25$, 0.5, 0.75 and 1.0).

The stresses resulting from this analysis which was performed for various load levels cannot be considered "exact" or close to it because of the gross linearization utilized in this process. A conventional incremental analysis utilizing reasonably small load steps could possibly have been used to achieve this objective. However, this quasi-nonlinear approach yields semiquantitative conclusions with respect to the parameters under consideration.

A parametric study was performed for the unsymmetrical loading case to evaluate the effect of cracking in reducing the shear force transfer across the crack, and to study the effect of variation of the stiffness perpendicular to the crack direction on the stress distributions for the various loading stages. It was felt that four loading stages were sufficient to cover the entire loading history of the bridge from the cracked state through yielding of the steel reinforcing and the ultimate load. The applied eccentric load values for these loading stages were 20, 31, 42 and 55 kips, respectively. For each load stage the modulus of elasticity of concrete perpendicular to the crack was examined for the following two conditions:

(i) modulus of elasticity perpendicular to the crack $E_p = 0$

(ii) modulus of elasticity perpendicular to the crack $E_p = \frac{E_c I_{cr}}{I_g}$

For these cases, depending on the measured width of cracks, the shear force transferred across the crack was decreased by 0, 25%, 50% and 75%.

These values correspond to a coefficient β value of 1, 0.75, 0.5 and 0.25 respectively, with β = 1 representing the uncracked state. This was implemented in the finite element analysis by changing the elasticity matrix of the cracked element according to the size and the orientation of the crack as mentioned before.

The finite element meshes used for the top and bottom slabs and the webs for each load stage are shown in Figure 4.17 along with the elements which have cracked.

4.3.3.2 Analysis Results

The results of this quasi-nonlinear analysis are presented for the following:

- vertical deflection (Fig. 4.9 and 4.10)
- lateral deflection (Fig. 4.11)
- longitudinal deflection (Fig. 4.12)
- longitudinal membrane and bending stresses (Fig. 4.18 through 4.21)
- transverse membrane and bending stresses (Fig. 4.22 through 4.25).

The effect of the element stiffness perpendicular to the cracks and the effectiveness of shear transfer across the cracks are shown in all the above figures.

The experimental observation showed that most of the cracks were formed in the midspan region. These cracks formed in the lower

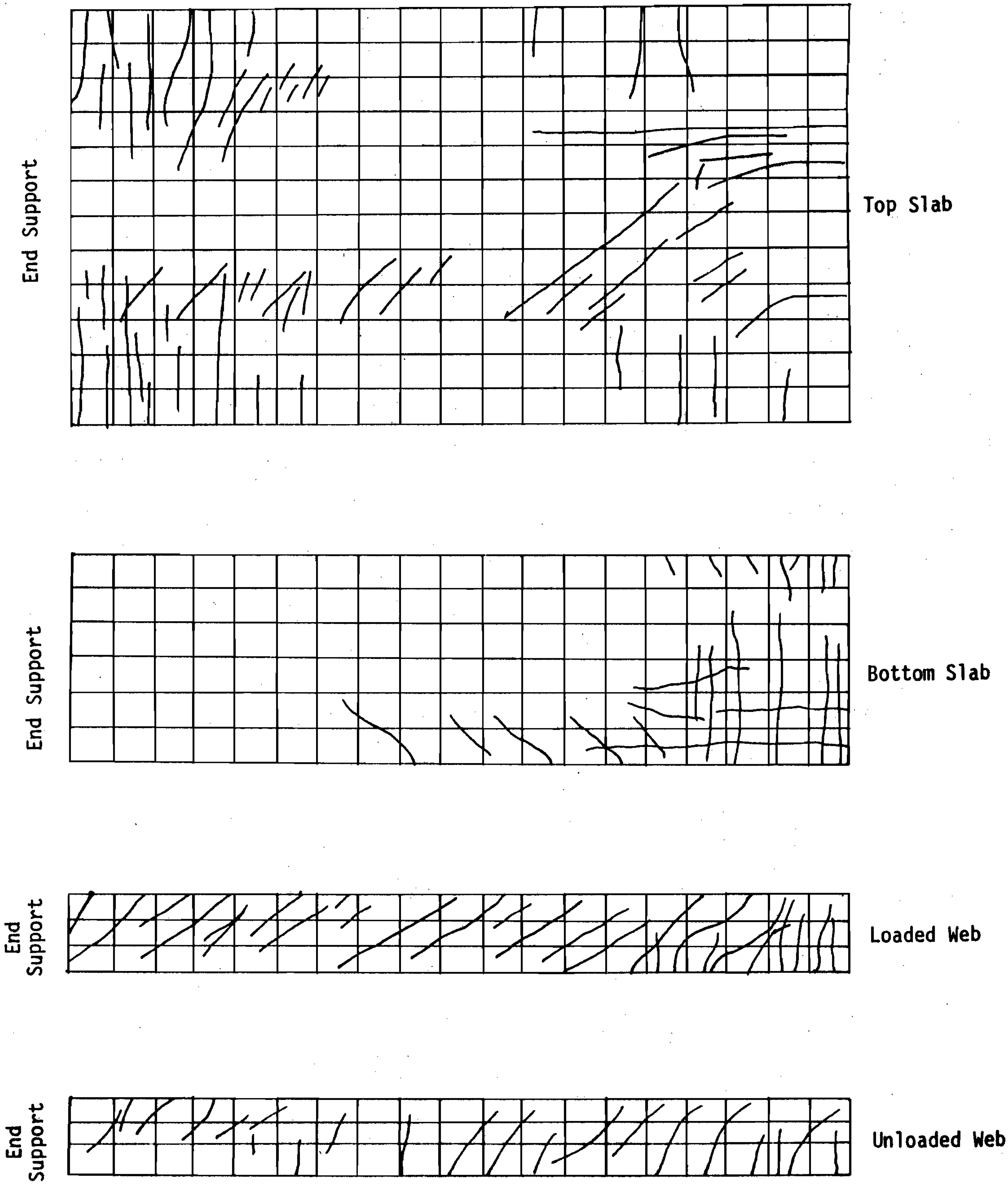

FIG. 4.17 CRACKED ELEMENTS IN THE FINITE ELEMENT IDEALIZATION [LOAD P = 42 KIPS]
(UNSYMMETRICAL LOADING CASE)

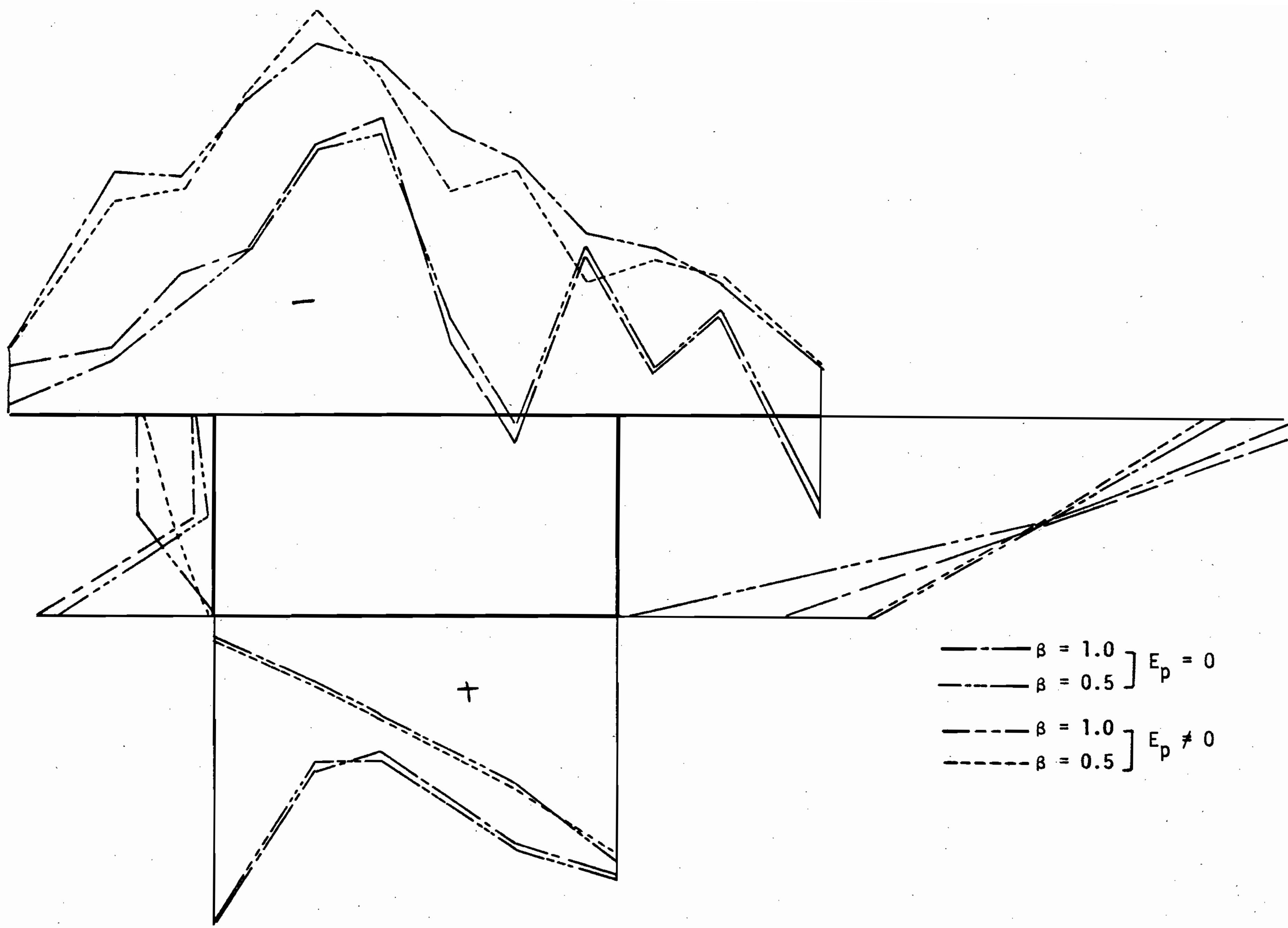

FIG. 4.18 LONGITUDINAL MEMBRANE STRESSES AT MIDSPAN SECTION
(UNSYMMETRICAL LOADING CASE - PARAMETRIC STUDY)

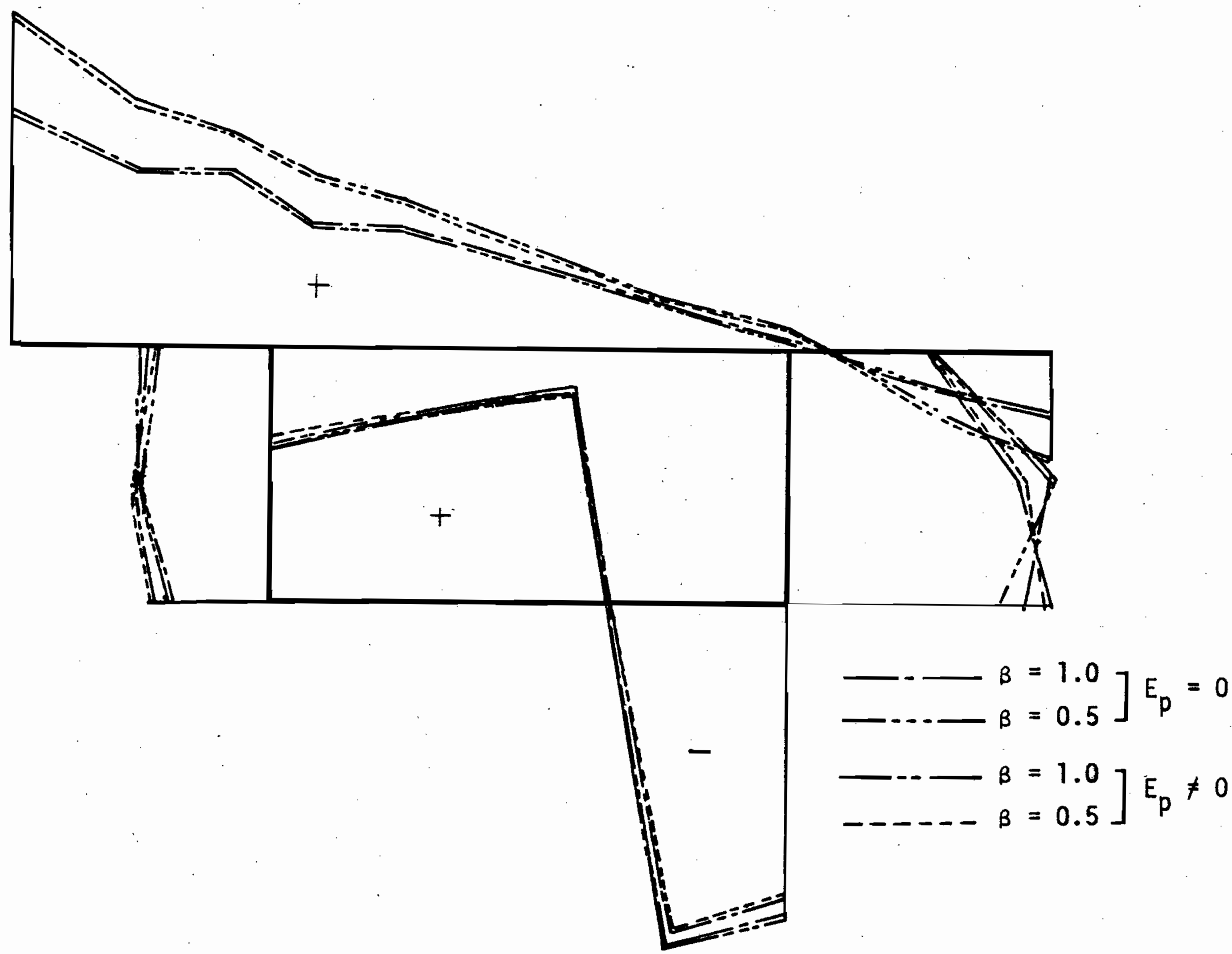

FIG. 4.19 LONGITUDINAL MEMBRANE STRESSES AT THE SUPPORT SECTION
(UNSYMMETRICAL LOADING CASE - PARAMETRIC STUDY)

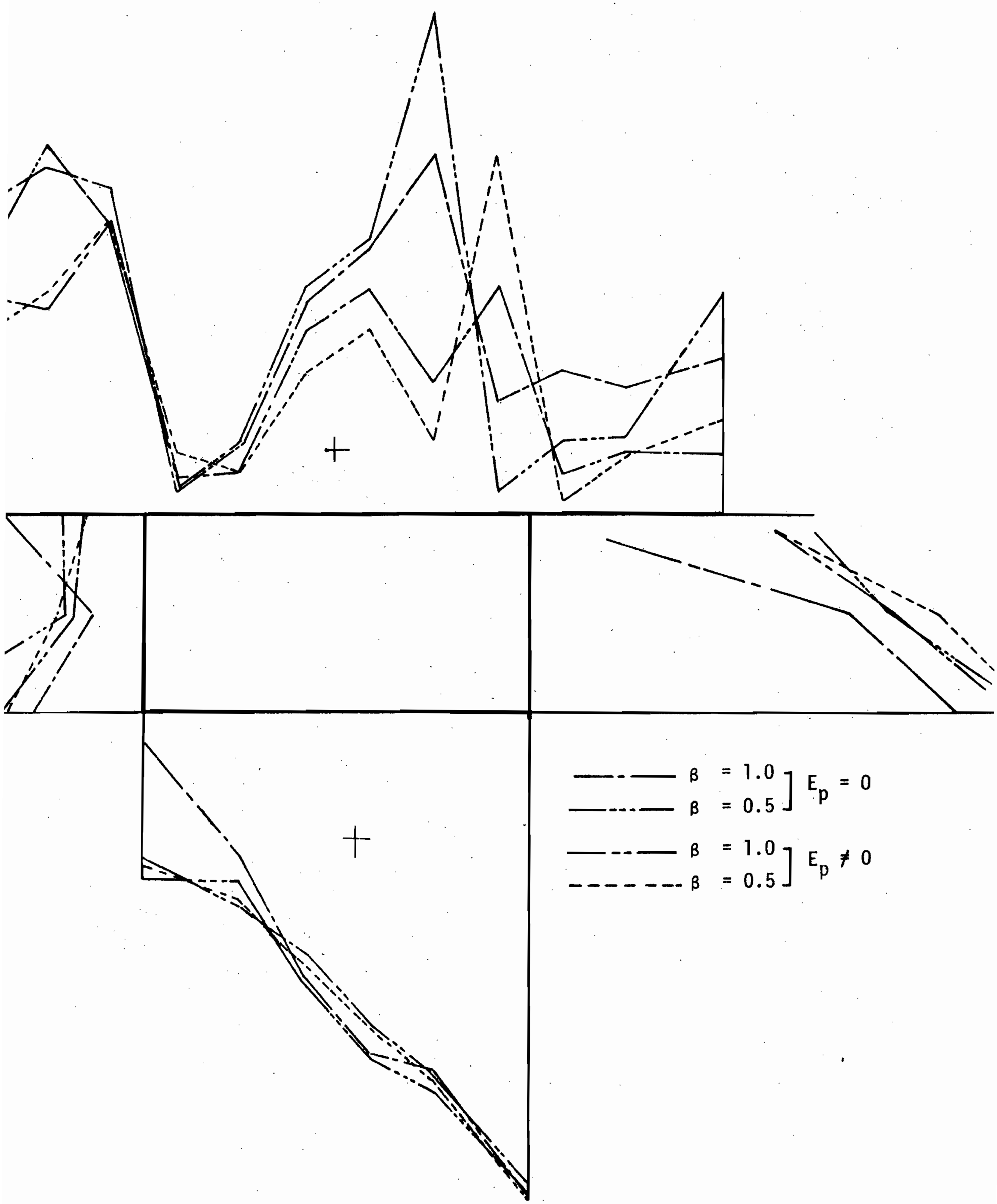

FIG. 4.20 LONGITUDINAL BENDING STRESSES AT MIDSPAN SECTION
(UNSYMMETRICAL LOADING CASE - PARAMETRIC STUDY)

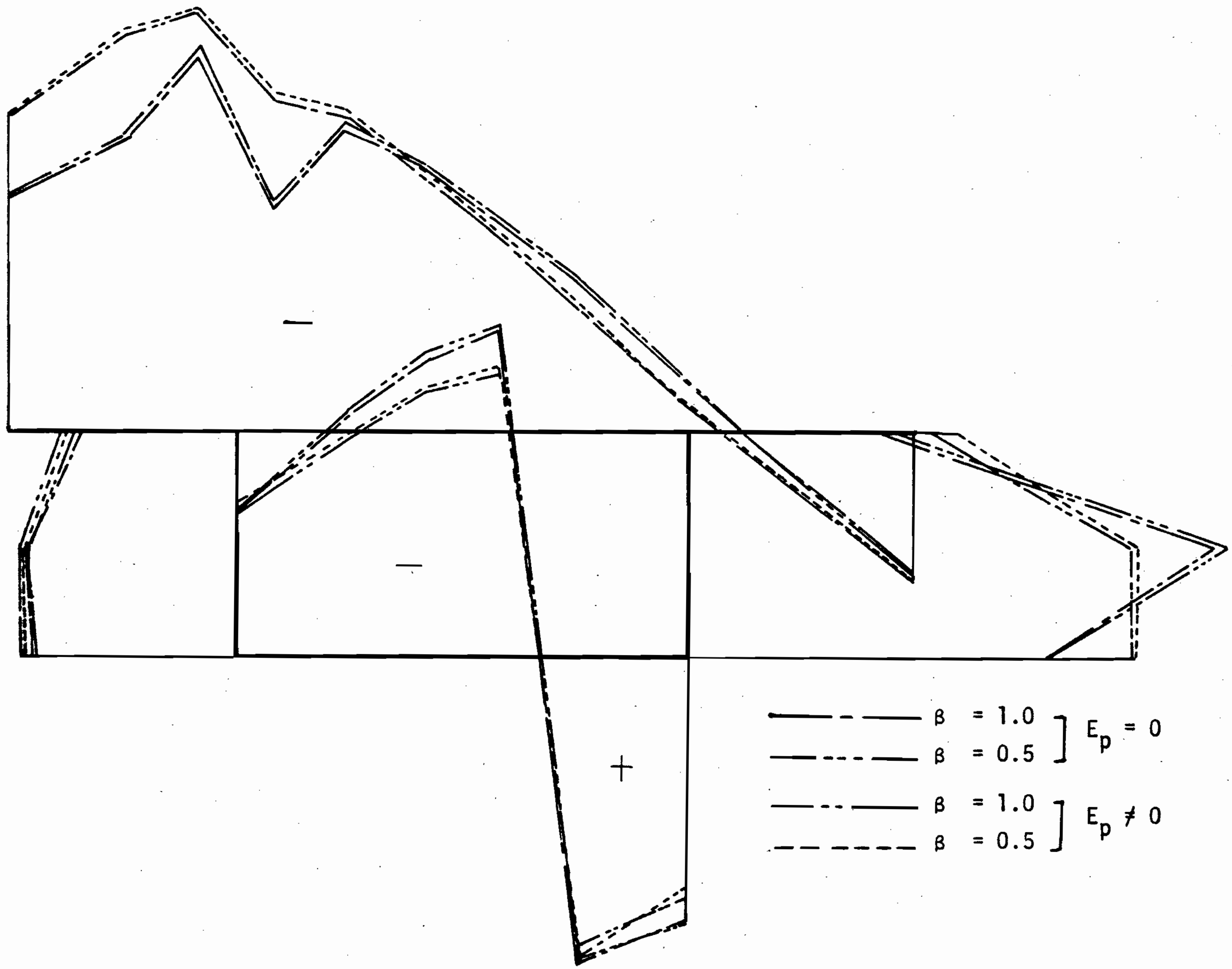

FIG. 4.21 LONGITUDINAL BENDING STRESSES AT SUPPORT SECTION (UNSYMMETRICAL LOADING CASE - PARAMETRIC STUDY)

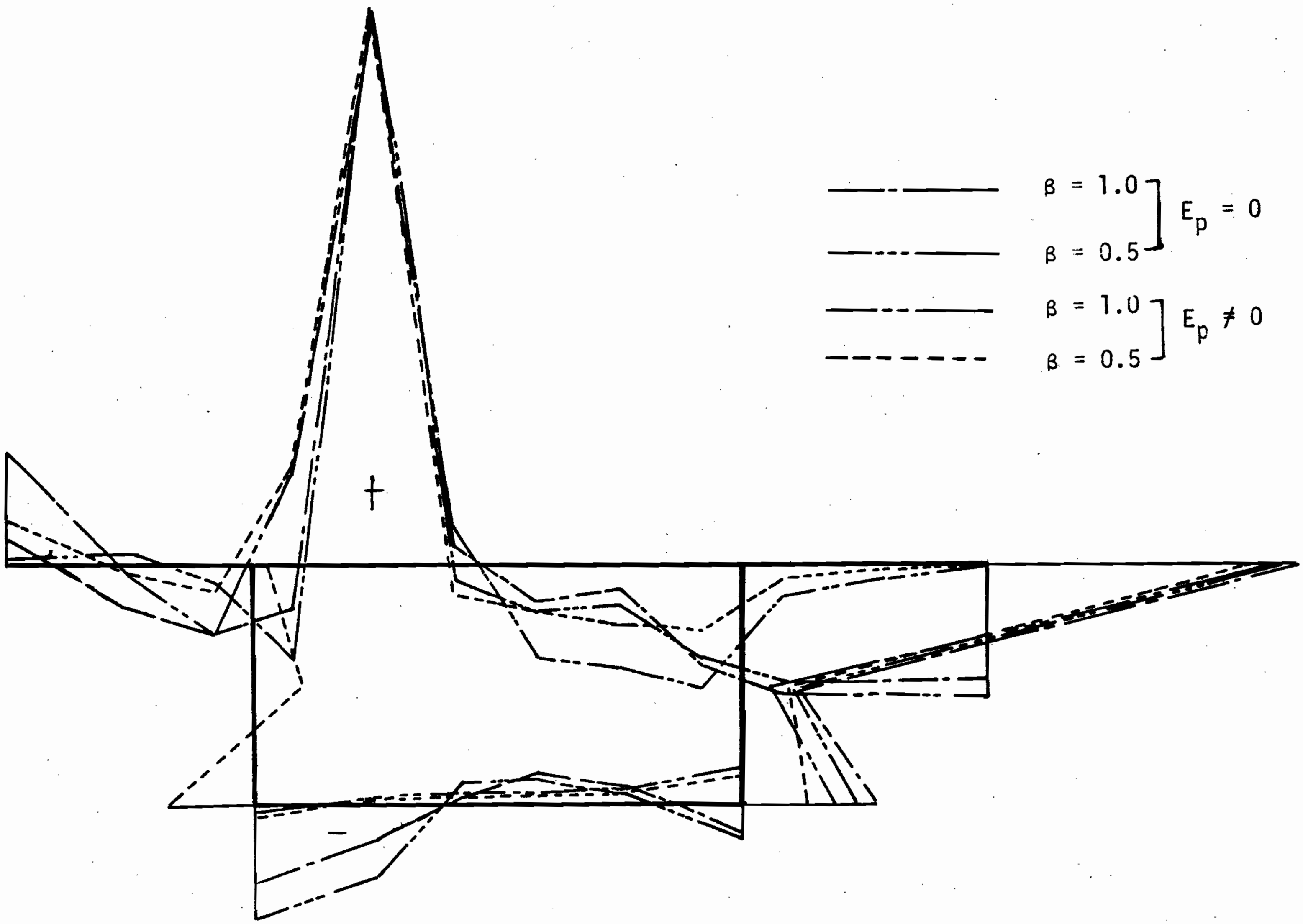

FIG. 4.22 TRANSVERSE MEMBRANE STRESSES AT MIDSPAN SECTION
(UNSYMMETRICAL LOADING CASE - PARAMETRIC STUDY)

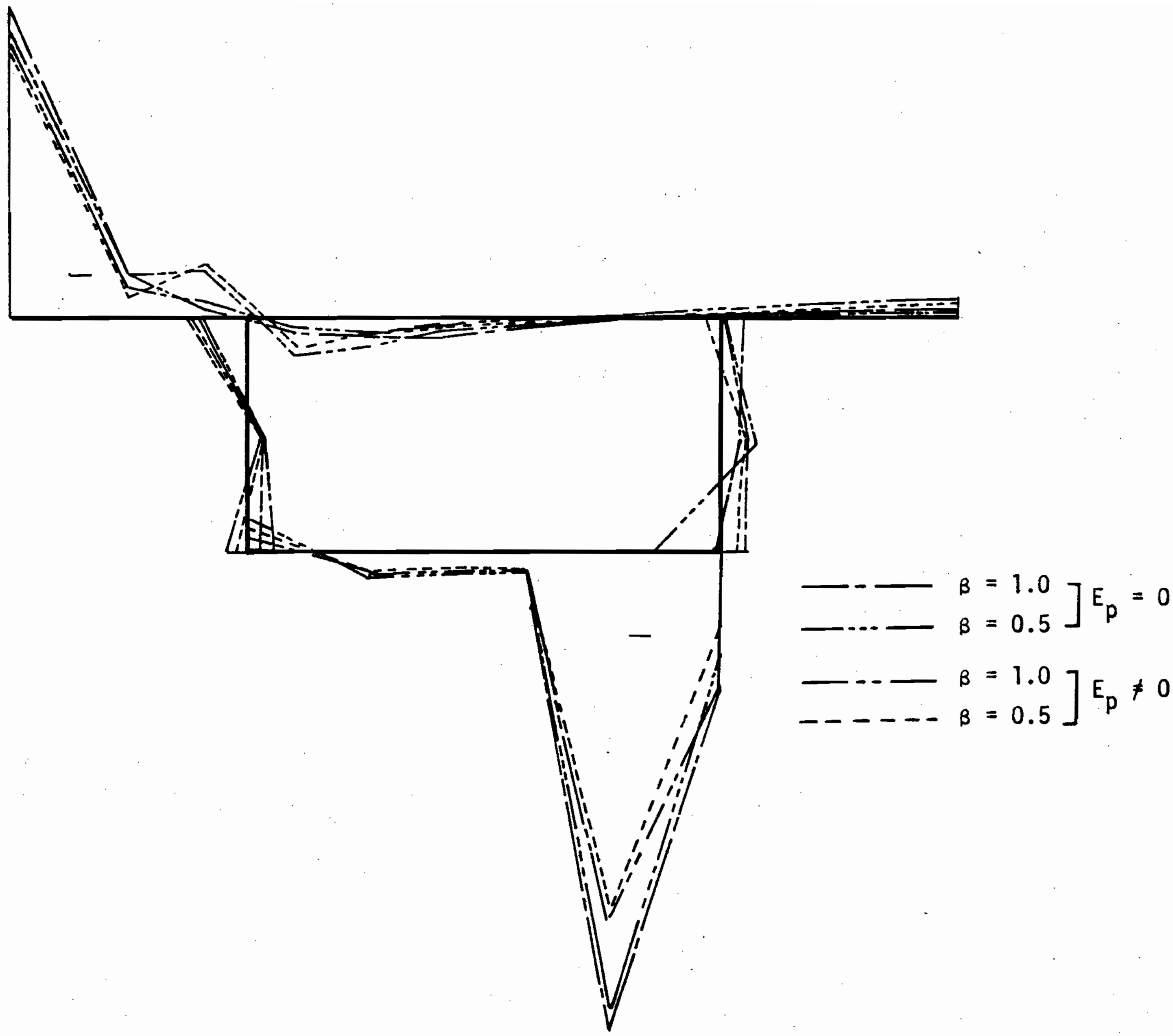

FIG. 4.23 TRANSVERSE MEMBRANE STRESSES AT SUPPORT SECTION
(UNSYMMETRICAL LOADING CASE - PARAMETRIC STUDY)

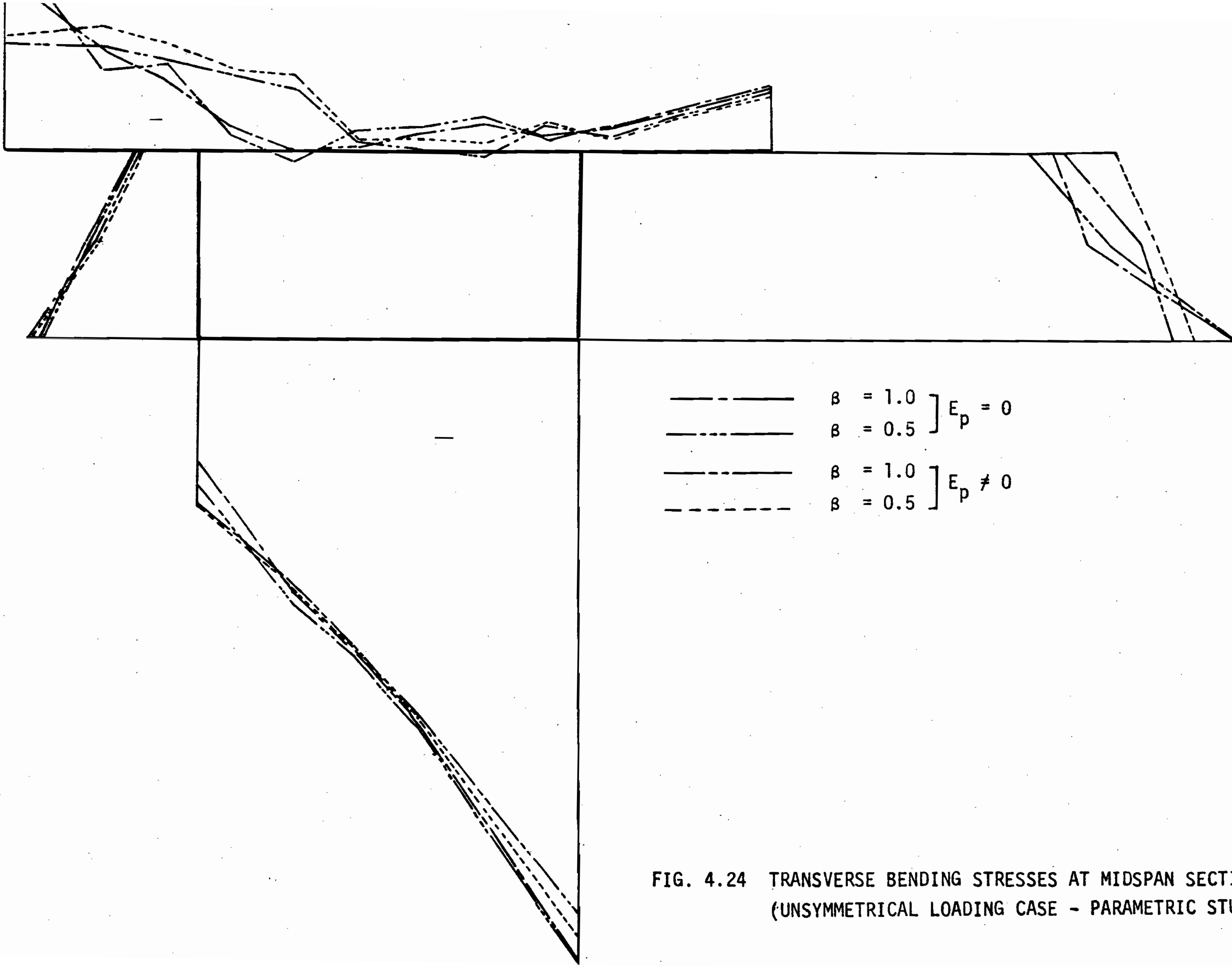

FIG. 4.24 TRANSVERSE BENDING STRESSES AT MIDSPAN SECTION (UNSYMMETRICAL LOADING CASE - PARAMETRIC STUDY)

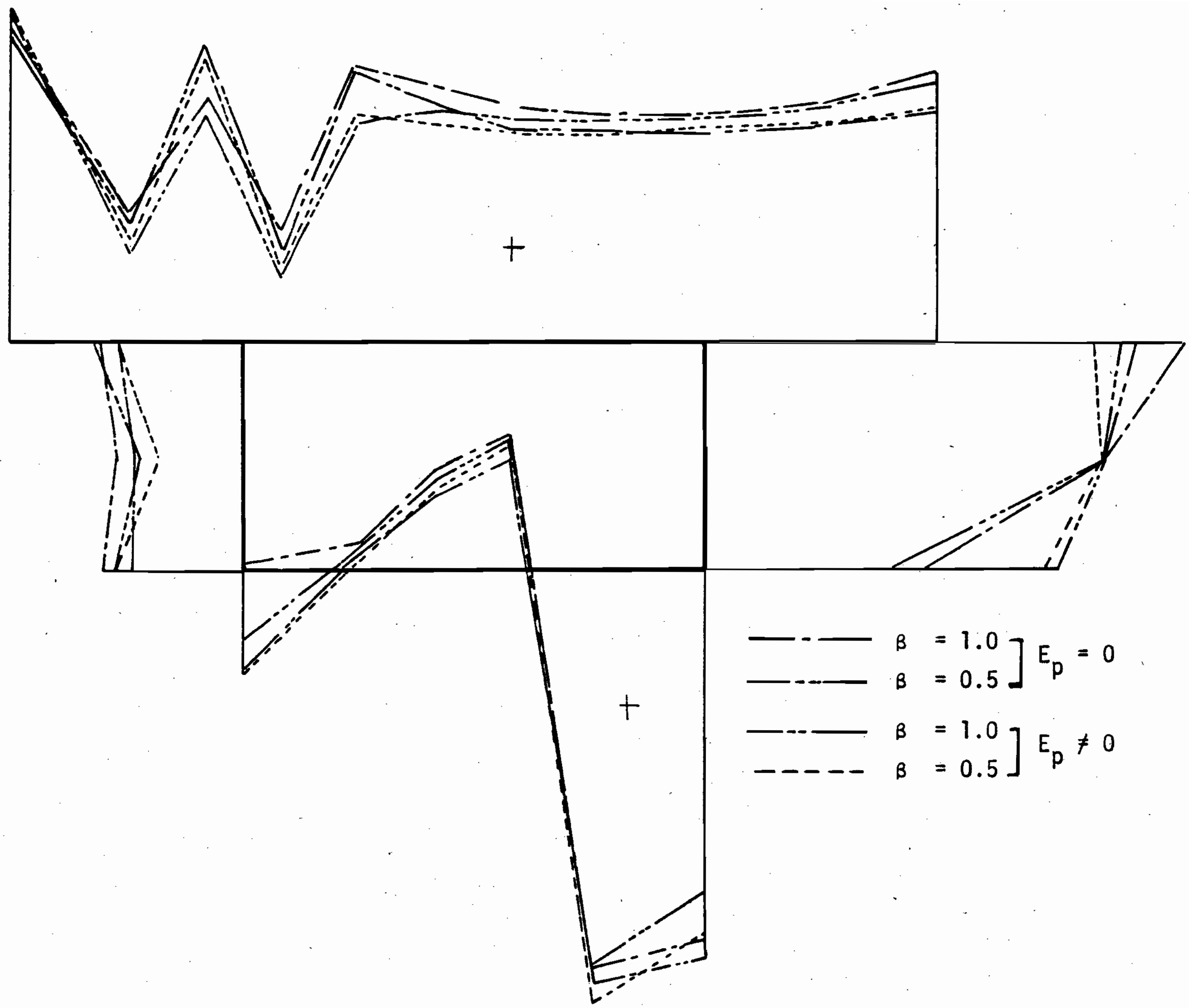

FIG. 4.25 TRANSVERSE BENDING STRESSES AT SUPPORT SECTION
(UNSYMMETRICAL LOADING CASE - PARAMETRIC STUDY)

slab in an orthogonal pattern parallel and perpendicular to the bridge centerline, while those in the top slab were formed in the longitudinal direction in the vicinity of the unloaded web. There were fewer cracks in the support region, while the least number of cracks was observed in the quarter-span region which showed the least distress compared with the support and the midspan regions. At the support section, cracks formed in the top slab in a direction perpendicular to the longitudinal axis of the bridge and they were concentrated over both webs.

The analysis results can be summarized as follows.

(a) For the second load stage (P = 32 kips), the calculated vertical deflections of the box girder bridge increased after the introduction of the cracks in the finite element model. The calculated values of these deflections showed sensitivity to the value of E_p. The computed vertical deflections for the case $E_p = 0$ were approximately 20% higher than those for $E_p \neq 0$. This is due to the under-estimation of the element stiffness resulting from assuming $E_p = 0$.

As shown in Figure 4.9, the quasi-nonlinear finite element analysis improved the deflection values obtained from the elastic analysis significantly. At the last loading stage (55 kips), the calculated deflections of the loaded and unloaded webs from the quasi-nonlinear analysis were approximately 0.6 in. and 0.3 in.

respectively, while those obtained from the elastic finite element analysis were 0.45 in. and 0.275 in. respectively. The measured deflection values at the same load level were 0.95 in. and 0.6 in. for the loaded and the unloaded webs, respectively. Thus quasi-nonlinear analysis predictions were better than those from the elastic analysis although the difference is still large.

(b) The top slab lateral deflections for the case $E_p \neq 0$ are generally 15% higher than those of $E_p = 0$, while those for the lower slab are approximately 20% smaller. These differences are due to the crack patterns in both the top and the bottom slabs. In the top slab these cracks are formed in the longitudinal direction over the unloaded web. Therefore by assigning a non-zero value for E_p, the top slab behaves as an orthotropic plate with a different stiffness in the directions parallel and perpendicular to the cracks, which causes an increase in the lateral deflections. In the lower slab these cracks are formed orthogonally, therefore the case $E_p = 0$ yields higher deflection values than the case $E_p \neq 0$.

The calculated longitudinal deflections of both the loaded and the unloaded webs showed an increase of approximately 15% for the case $E_p \neq 0$ higher than those for the case $E_p = 0$. This is again due to the different crack patterns in both webs and the corresponding increase resulting from a non-zero value of E_p as explained earlier.

(c) For the second and the third load stages (31 and 42 kips), the longitudinal membrane stresses in the top and the bottom slabs for the case $E_p \neq 0$ were respectively about 35% and 15% higher than those for the case $E_p = 0$. As mentioned before, both the top and the bottom slabs act as orthotropic plates for different values of the modulus of elasticity parallel and perpendicular to the cracks. This biaxial behaviour causes an increase in the stresses for the case $E_p \neq 0$ above those for the case $E_p = 0$.

Experimental observation showed that the bottom slab was more severely cracked than the top slab and therefore the value of E_p was close to zero and hence the smaller difference between the two cases $E_p \neq 0$ and $E_p = 0$. At the support section, this increase is approximately 20% for both the top and the bottom slabs.

(d) There is no significant difference in the transverse membrane stresses in the support region for both cases, $E_p = 0$ and $E_p \neq 0$. This is due to the small values of these stresses in this region. However, in the midspan region, the transverse membrane stresses for the case $E_p = 0$ are approximately 10% higher than those for the case $E_p \neq 0$. This is again due to the orthogonal cracks formed in this region as explained earlier.

(e) The calculated membrane shear stresses at both the midspan and the support sections showed an increase of 10% for the case $E_p \neq 0$ when compared with the values for the case $E_p = 0$.

(f) The longitudinal bending stresses in the top slab and the loaded web at the support section showed an increase of about 20% for the case $E_p \neq 0$ over those obtained for the case $E_p = 0$. This is due to the redistribution of the forces occurring in the orthotropic plate after cracking. At the midspan section, the longitudinal bending stresses of the loaded web also showed an increase of 15% for the case $E_p \neq 0$ compared with the case $E_p = 0$. The transverse bending stresses in the top slab at the support section were 12% larger for the case $E_p = 0$.
At the midspan section, the transverse bending stresses in the top slab were 20% larger for the case $E_p \neq 0$ than for the case $E_p = 0$. The crack patterns within the box section throughout the bridge span, along with the orthotropic behaviour of the individual plates, show that the bending stresses, both longitudinal and transverse, are significantly influenced by the value of the modulus of elasticity perpendicular to the cracks.

(g) As the ultimate load is approached, the calculated membrane and bending stresses become insensitive to the value of stiffness perpendicular to the cracks because, on account of the severity of cracking, the concrete between any two adjacent cracks does not remain as effective in transferring forces perpendicular to the cracks.

(i) Variation in the shear transfer coefficient β does not have a significant effect on membrane and bending stresses in earlier loading stages (20, 31 and 42 kips); however, in the later stages (42 and 55 kips) a decrease in the shear transfer coefficient β from 0.75 to 0.25 causes an increase of about 10 - 18% in the membrane and bending stresses. It is not possible to explain these trends however, with the present state of knowledge it was not possible to include the effect of dowel action in the finite element model. In conventional beam-type specimens, the dowel forces increase significantly as the ultimate load is approached, thereby increasing the contribution of the dowel action at higher load levels. More research work is needed in this area to incorporate the effect of dowel action in non-linear finite element analysis of reinforced concrete.

CHAPTER 5

CONCLUSIONS

The results of this experimental-analytical investigation of structural behaviour of box girder bridges can be summarized and conclusions drawn as follows:

1. For the unsymmetrical loading case, the flexural and torsional rigidities of the box girder decreased with an increase in the applied load due to the formation and propagation of cracks and inelasticity of concrete. At the working load level the flexural rigidities of the loaded and unloaded webs were approximately 0.7 and 0.9, respectively, of the initial flexural rigidity values. The torsional rigidity at the working load level was approximately 0.4 of the initial flexural rigidity before cracking.

2. For the unsymmetrical loading case, the vertical deflection of the loaded web was approximately twice that of the unloaded web. The lateral and longitudinal displacements of the webs in the horizontal plane varied from about 5 per cent to 8 per cent of the respective midspan vertical deflections. The present tendency to use smaller wall thicknesses in concrete box section structures results in increasing these displacements, therefore torsional and distortional deformations should be considered in the analysis and design of this type of structure.

3. The resulting longitudinal stress distributions across the width of the top and the bottom slabs of the box section were not uniform for both the symmetrical and the unsymmetrical loading cases. The differences between the maximum and the minimum stresses in these cases were approximately 30 per cent and 70 per cent for the symmetrical and unsymmetrical loading cases, respectively. The simple beam theory is obviously not capable in predicting these distributions.

4. For the symmetrical loading case, the shear lag effect in the box section caused an increase of 30 per cent in the stresses at the web-flange junction above those at the cantilever tips or between the webs; these stresses were approximately 40 per cent higher than those calculated from the simple beam theory.

5. For the unsymmetrical loading case, the longitudinal stresses calculated from the measured strains were approximately twice those predicted from the simple beam theory. This is due to the effect of warping restraint for this loading case, and the cracking of the section; also, the simple beam theory does not account for the torsional and distortional longitudinal warping stresses. These torsional and distortional longitudinal warping stresses can be calculated using the Kollbrunner and Hajdin method and the beam-on-elastic foundation method, respectively. These can then be added to the stress values calculated from the simple beam theory assuming a cracked section to obtain the total stresses. The designer should therefore be cautious about the increase in the longitudinal stresses on account of the reasons stated above.

6. The values of the transverse stresses for the symmetrical loading case varied from approximately 20 per cent to 40 per cent of the longitudinal stresses at the same location. For the unsymmetrical loading case, these transverse stresses were approximately of the same order as the longitudinal stresses at the same location. Significant transverse tensile stresses occurred over the unloaded web and caused a serious longitudinal crack to form parallel to the longitudinal axis of the bridge. The experimental transverse stresses as calculated from the measured strain values were higher than those predicted from the available methods. Therefore more research is needed to develop suitable methods to predict these stresses. Again, suitable care should be exercised in designing and detailing the transverse reinforcement at the web-flange junction.

7. All cracks which occurred in the cantilever slabs were mainly flexural cracks. Therefore the contribution of the cantilever slabs in the torsional stiffness of the box girder can be neglected.

8. A general non-linear finite element analysis of a reinforced concrete structure to account for cracking, and material non-linearities can be very expensive and time consuming. Therefore it was not used to study the sensitivity of structural response to the various parameters. Instead, a quasi-nonlinear finite element analysis was used in the present study for which the stiffness of

the box girder bridge was modified in stages by incorporating information about the cracking patterns and crack widths from the experimental data. This quasi-nonlinear analysis was used to conduct a parametric study to investigate the effect of the propagation and widening of the cracks in the analysis by modifying the stiffness of the element perpendicular to the crack and the shearing force transferred across the cracks depending on the observed crack widths.

9. A non-zero concrete modulus value perpendicular to the cracks has a significant influence on bridge behaviour as compared with a zero value for this modulus. However, at the ultimate load stage, the computed stresses are insensitive to this value.

10. A reduction in the shearing force transferred across the cracks with widening of the cracks does not have a significant influence on stress distribution in the bridge except at the ultimate load level.

Suggested Areas for Further Research

The following are some suggested topics for further research in the area of box girder bridges.

1. The present design methods for designing box girder bridges are generally based on an elastic analysis, although the behaviour of concrete is not elastic even at the early stages of loading.

Obviously, these methods do not predict the structural response through all the loading stages, therefore more research is needed in this area to provide a consistent design philosophy based on actual behaviour.

2. The ACI Code (318-77) suggests that the total quantity of longitudinal and transverse reinforcement required should be the sum of that required for bending and torsion separately. This method over-estimates the true resisting capacity of the structure. Therefore more work is needed to develop a rational theory for designing reinforced concrete elements subjected to combined torsion, bending and shear. Also, such work should include study of the behaviour of hoop steel, longitudinal steel and the concrete under such combined stresses through the length of the bridge.

3. Existing shear lag theory must be extended to include the case of singly symmetric box sections with wide cantilevers. Also, the effect of the width of the cantilever on the behaviour and analysis of distortional warping stresses is not completely understood; more work is needed in this area.

4. In the torsional and distortional analyses of box girder bridges, all known methods divide the eccentric load as follows: 1/2 for longitudinal symmetrical bending, 1/4 for torsion and 1/4 for distortion. Such load division should be derived on the basis

of the flexural, torsional and shear stiffnesses of the uncracked and the cracked box section subject to combined bending, torsion and shear. Experimental and analytical studies on a reinforced concrete box girder bridge model can be helpful in determining these stiffnesses. This information would also be useful in the area of limit analysis of such structures.

5. With the current tendency to reduce the dimensions of the concrete elements by using the ultimate strength design method, the short and long time deflections have become a problem. This phenomenon of long time deflection and its effects in box girder bridges are still not completely understood, therefore more work is needed in this area.

6. The theoretical development necessary for limit state design would probably result from an extension of nonlinear finite element analysis to predict cracking and ultimate load behaviour of box beams under combined bending, shear and torsion. This can be valuable in understanding the behaviour of box section structures at the serviceability and collapse limit states and in developing suitable tools for the limit states design of box section structures.

REFERENCES

1. Bieger, K.W., "Vorberechnung zweistegiger Plattenbalken",(Preliminary analysis of double T beams), Beton- und Stahlbetonbau. Vol.57, No. 8, August 1962, pp. 188-195.

2. Bretthauer, G. and Kappei, H., "Zur Querverteilung bei unsymmetrisch geraden und gekrummten zweistegiger Plattenbalkenbricken", (Transverse distribution in asymmetric straight and curved double T beam bridges), Beton- und Stahlbetonbau, Vol. 58, No. 12, December 1963, pp. 288-295.

3. Ghali, A., "Design of simply-supported skew concrete girder bridges", Paper presented at the American Concrete Institute Annual Convention, Chicago, 1969.

4. Homberg, H. and Trenks, K., "Drehsteife Kreuzwerke", (Torsionally stiff grids), Springer-Verlag, Berlin, 1962.

5. American Association of State Highway Officials, AASHTO. "Standard Specifications for Highway Bridges". Ninth Edition, Washington D.C., 1965.

6. Massonnet, C. and Gandolfi, A., "Sur certains cas exceptionnels dans la théorie des ponts à poutres multiples", (Some exceptional cases in the theory of multigirder bridges), International Association for Bridge and Structural Engineering (Zurich), Vol. 27, 1967, pp. 73-94.

7. Scordelis, A.C., "Analysis of simply supported box girder bridges", Structural Engineering and Structural Mechanics Report No. SESM 66-17, University of California, Berkeley, October 1966.

8. Chu, K.H. and Longinow, A., "Torsion in sections with open and closed parts", Proceedings of the American Society of Civil Engineers, Vol. 93, No. ST6, December 1967, pp. 213-227.

9. Kollbrunner, C.F. and Basler, K., "Torsionskonstanten und Schubspannungen bei St. Venantscher Torsion", (Torsion constants and shear stresses in St. Venant torsion), Mitteilungen der Technischen Kommission der Schweizer Stahlbau-Vereinigung, No. 23, July 1962 and No. 27, October 1963.

10. Heilig, R., "Beitrag zur Theorie der Kastentrager beliebiger Querschnittsform", (Contribution to the theory of box girders of arbitrary cross-sectional shape), Der Stahlbau, Vol. 30, No. 11, November 1961, pp. 333-349. English translation (unpublished) available from C & CA Library.

11. Blaise, M.P., "La torsion des prismes multicellulaires à parois minces", (Torsion of multi-cellular prisms with thin walls), Annals des Ponts et Chaussees, Vol. 122, No. 5, September-October 1952, pp. 601-611.

12. Benscoter, S.U.,"A theory of torsion bending for multicell beams", Journal of Applied Mechanics, Vol. 21, No. 1, March 1954, pp. 25-34.

13. Dziewolski, R., "Coefficient de répartition transversale dans les ponts", (Transverse distribution factors for bridges), Construction Metallique, No. 2, June 1965, pp. 18-32.

14. Valentin, G., "Zum Einfluss der Querkräfte auf die Formänderungen dunnwandiger, mehrzelliger Stäbe", (The influence of shear forces on the deformations of thin-walled multicell members), Der Bauingenieur, Vol. 42, No. 6, June 1967, pp. 218-221.

15. Cziesielski, E., "Ermittlung des Schubwiderstandes F_y^Q symmetrischer I- und Hohlkastenquerschmitte sowie symmetrischer und unsymmetrischer Winkelquerschnitte", (Determination of the shear resistance, F_y^Q of symmetrical I sections and box sections and of symmetrical and asymmetrical angle sections), Die Bautechnik, Vol. 42, No. 7, July 1965, pp. 232-237.

16. Panc, V., "Theorie der dünnwandigen auf elastischer Unterlage gebetteten Stäbe", (Theory of thin-walled beams on elastic foundations), Acta Technica Academiae Scientiarum Hungaricae, Vol. 53, No. 314, 1966, pp. 389-405.

17. Von Karman, T. and Christensen, N.B., "Methods of analysis for torsion with variable twist", Journal of the Aeronautical Sciences, Vol. 11, No. 2, April 1944, pp. 110-124.

18. Benscoter, S.U., "Secondary stresses in thin-walled beams with closed cross-sections", NACA Technical Note 2529, National Advisory Committee for Aeronautics, Washington D.C., October 1951.

19. Rudiger, D., "Wölbkrafttorsion dünnwandiger Hohlquerschnitte", (Warping torsion of thin-walled hollow cross-sections), Ingenieur-Archiv, Vol. 33, No. 5, 1964, pp. 346-350.

20. Grasse, W., "Wölbkrafttorsion dünnwandiger prismatischer Stäbe beliebigen Querschnitts", (Warping torsion of prismatic thin-walled bars of arbitrary cross-section), Ingenieur-Archiv, Vol. 34, No. 5, 1965, pp. 330-338.

21. Dabrowski, R., "Torsion bending of thin-walled members with non-deformable closed cross-section", School of Engineering, Columbia University, New York, September 1963.

22. Heilig, R., "Verbundbrücken unter Torsionsbelastung", (Composite bridges under torsional loading), Der Stahlbau, Vol. 23, No. 2, February 1954, pp. 25-33.

23. Leonhardt, F. and Walther, R., "Torsions- und Schubversuche an vorgespannten Hohlkastentragern 1963-64", (Torsion and shear tests on prestressed box girders, 1963-64), Beton- und Monierbau Aktien-Gesell-Schaft 1889-1964, Beton- und Monierbau AG, Stuttgart, 1965. Translation made by C.V. Amerongen, (Library Translation Cj. 130), Cement and Concrete Association, London, 1968, pp. 41.

24. Knittel, G., "Zur Berechnung des dünnwandigen Kastentragers mit gieichbieibendem symmetrischen Querschnitt", (The analysis of thin-walled box girders of constant symmetrical cross-section), Beton und Stahlbetonbau, Vol. 60, No. 9, September 1965, pp. 205-211.

25. Gibson, J.E. and Gardner, N.J., "Investigation of multi-folded plate structures", Proceedings of the Institution of Civil Engineers, Vol. 31, No. 1, May 1965, pp. 57-69.

26. Johnston, S.B. and Mattock, A.H., "Lateral distribution of load in composite box girder bridges", Highway Research Record, No. 167, 1967, pp. 25-31.

27. Schardt, R., "Eine Erweiterung der technischen Biegelehre für die Berechnung biegesteifer prismatischer Faltwerke", (Extension of engineers' bending theory to the analysis of flexurally stiff prismatic folded-plate structures), Der Stahlbau, Vol. 35, No. 6, June 1966, pp. 161-171.

28. Meyer, C. and Scordelis, A.C., "Computer program for prismatic folded plates with plate and beam elements", Structural Engineering and Structural Mechanics Report No. SESM 70-3, University of California, Berkeley, February 1970.

29. Goldberg, J.E. and Leve, H.L., "Theory of prismatic folded plate structures", International Association for Bridge and Structural Engineering, Zurich, Vol. 17, 1957, pp. 59-86.

30. Aass, A., "Matrix progression method", Report No. CE 1963, Department of Civil Engineering, University of Southampton, Southampton, England, 1963.

31. Tottenham, H., "A new method for the structural analysis of thin-walled spatial structures", Parts 1-4, Department of Civil Engineering, University of Southampton, Southampton, England, 1958.

32. Maisel, B.I., "Review of literature related to the analysis and design of thin-walled beams", Technical Report No. 42, Concrete and Cement Association, London, July 1970.

33. Wittfoht, H., "Considerations on the cross-sectional design of prestressed concrete bridges with reference to bridges built in 1960", Beton- und Stahlbetonbau, Vol. 57, No. 6, June 1962, pp. 129-141. Translated from the German by C.V. Amerongen, Library Translation No. Cj. 124, Cement and Concrete Association, London, 1966, pp. 24.

34. American Concrete Institute, "Preliminary design and proportioning of reinforced concrete bridge structures", ACI Journal, Vol.70, No. 5, May 1973, pp. 328-337.

35. Heilig, R., "Der Verbunträger mit beliebiger offener Profilform", (The composite girder with arbitrary open cross-section), Der Stahlbau, Vol. 21, No. 10, October 1952, pp. 186-189.

36. Vlasov, V.Z., "Theory of prestressed thin-walled beams in plates and shells", Paper presented at the International Congress of Builders, Budapest, 1955. Foreign Literature Study No. 323, Portland Cement Association, Skokie, Illinois, 1965, 19 pp.

37. Bingham, T.G. and Lee, D.J., "The Mancunian Way elevated road structure", Proceedings of the Institution of Civil Engineers, Vol. 42, No. 1, April 1969, pp. 459-492.

38. Huntley, H.D., "Western Avenue extension", The Structural Engineer, London, Vol. 47, No. 3, March 1969, pp. 85-97.

39. Maisel, B.E., Rowe, R.E. and Swann, R.A., "Concrete box girder bridges", The Structural Engineer, London, Vol. 51, No. 10, October 1973, pp. 363-386.

40. Rowe, R.E. and Best, B.C., "The use of model analysis and testing in bridge design", Seventh IABSE Congress, Preliminary Publication, International Association for Bridge and Structural Engineering, Zurich, 1964, pp. 115-121.

41. Scordelis, A.C., "Analysis of continuous box girder bridges", Structural Engineering and Structural Mechanics Report No. SESM 67-25, University of California, Berkeley, November 1967.

42. Cordoba, R.A., "Behaviour of open web precast bridge girder - Experimental Study", M. Eng. Thesis, Department of Civil Engineering and Applied Mechanics, McGill University, Montreal, August 1974.

43. Tschanz, T., "Behaviour of open web precast bridge girders - Analytical Study", M. Eng. Thesis, Department of Civil Engineering and Applied Mechanics, McGill University, Montreal, August 1974.

44. Soliman, M.I. and Mirza, M.S., "Analysis and design of reinforced concrete box girder bridges", Structural Concrete Series No. 76-1, Department of Civil Engineering and Applied Mechanics, McGill University, Montreal, February 1976.

45. Tabba, M.M., "Free vibrations of curved box girder bridges", M. Eng. Thesis, Department of Civil Engineering and Applied Mechanics, McGill University, Montreal, July 1972.

46. Little, G. and Rowe, R.E., "Load distribution in multi-webbed bridge structures from tests on plastic models", Magazine of Concrete Research, Vol. 7, No. 21, November 1955, pp. 133-142.

47. Nasser, K.W.,"Design procedure for lateral load distribution in multi-beam bridges", Journal of the Prestressed Concrete Institute, Vol. 10, No. 4, August 1965, pp. 54-68.

48. Flessner, H., "Computation of bending strength of reinforced concrete beams", Paper presented at the International Symposium on the Use of Electronic Digital Computers in Structural Engineering, University of Newcastle upon Tyne, June 1966.

49. Tinawi, R.A., "Behaviour of orthotropic bridge decks", Ph.D. Thesis, Department of Civil Engineering and Applied Mechanics, McGill University, Montreal, May 1972.

50. Fam, A.R., "Static and free vibration analysis of curved box bridges", Ph.D. Thesis, Department of Civil Engineering and Applied Mechanics, McGill University, Montreal, March 1973.

51. Swamy, N., "Prestressed concrete hollow beams under combined bending and torsion", Journal of the Prestressed Concrete Institute, Vol. 10, No. 2, April 1965, pp. 48-61.

52. Somerville, G., Roll, F. and Caldwell, J.A.D., "Tests on a one-twelfth scale model of the Mancunian Way", Technical Report TRA 394, Cement and Concrete Association, London, December 1965, 46 pp.

53. Aktas, Z. and Vanhorn, D.A., "Bibliography on load distribution in beam-slab highway bridges", Report No. 349.1, Fritz Engineering Laboratory, Lehigh University, Bethlehem, Pennsylvania, September 1968.

54. Lin, C.S. and Vanhorn, D.A., "The effect of midspan diaphragms on load distribution in a prestressed concrete box-beam bridge", Report No. 315.6, Fritz Engineering Laboratory, Lehigh University, Bethlehem, Pennsylvania, June 1968.

55. Scordelis, A.C., "Analytical and experimental studies of multi-cell concrete box girder bridges", Bulletin of the International Association for Shell and Spatial Structures, Madrid, No. 58, August 1975.

56. William, K.H. and Scordelis, A.C.,"Computer program for cellular structures of arbitrary plan geometry", Structural Engineering and Structural Mechanics Report No. UC SESM 70-10, University of California, Berkeley, September, 1970.

57. Bouwkamp, J.G., Scordelis, A.C. and Wasti, S.T., "Structural behavior of a two-span reinforced concrete box girder bridge model", Volume I, Structural Engineering and Structural Mechanics Report No. UC SESM 71-5, University of California, Berkeley, April 1971.

58. Scordelis, A.C., Bouwkamp, J.G. and Wasti, S.T., "Structural behavior of a two-span reinforced concrete box girder bridge model", Volume II, Structural Engineering and Structural Mechanics Report No. UC SESM 71-16, University of California, Berkeley, October 1971.

59. Godden, W.G. and Aslam, M., "Model studies of skew box girder bridges", Structural Engineering and Structural Mechanics Report No. UC SESM 71-26, University of California, Berkeley, December 1971.

60. Comartin, C.D. and Scordelis, A.C., "Analysis and design of skew box girder bridges", Structural Engineering and Structural Mechanics Report No. UC SESM 72-14, University of California, Berkeley, December 1972.

61. Scordelis, A.C., Bouwkamp, J.G. and Larsen, P.K., "Structural behavior of a curved two-span reinforced concrete box girder bridge model", Volume I, Structural Engineering and Structural Mechanics Report No. UC SESM 74-5, University of California, Berkeley, September 1974.

62. Scordelis, A.C., Bouwkamp, J.G. and Larsen, P.K., "Structural behavior of a curved two-span reinforced concrete box girder bridge model", Volume II, Structural Engineering and Structural Mechanics Report No. UC SESM 74-6, University of California, Berkeley, September 1974.

63. Scordelis, A.C., Bouwkamp, J.G. and Larsen, P.K., "Structural behavior of a curved two-span reinforced concrete box girder bridge model", Volume III, Structural Engineering and Structural Mechanics Report No. UC SESM 74-7, University of California, Berkeley, September 1974.

64. Klaus, J.B., Wilson, E.L. and Peterson, F.E., "SAP IV - A structural analysis program for static and dynamic response of linear systems", Earthquake Engineering Research Center, Report No. EERC 73-11, University of California, Berkeley, April 1974.

65. Task Committee on Folded Plate Construction, "Phase 1 report on folded plate construction", Proceedings of the American Society of Civil Engineers, Vol. 89, No. ST6, December 1963, pp. 365-406.

66. American Association of State Highway Officials, AASHTO, "Standard Specifications for Highway Bridges". Eleventh Edition, Washington D.C., 1973.

67. Swann, R.A., "The construction and testing of a one-sixteenth-scale model for the prestressed concrete super-structure of Section 5, Western Avenue Extension", Technical Report TRA 441, Cement and Concrete Association, London, July 1970.

68. Swann, R.A., "A feature survey of concrete box spine-beam bridges", Technical Report No. 42.469, Cement and Concrete Association, London, June 1972.

69. Redwood, R.G. and Gurevich, S., "An analysis for multicell skew box bridges", Proceedings of Conference on the Finite Element Method in Civil Engineering, McGill University, Montreal, June 1972.

70. Meyer, C. and Scordelis, A.C., "Analysis of curved folded plate structures", Structural Engineering and Structural Mechanics Report No. UC SESM 70-8, University of California, Berkeley, June 1970.

71. Kabir, A.F. and Scordelis, A.C., "Computer program for curved bridges on flexible bents", Structural Engineering and Structural Mechanics Report No. UC SESM 74-10, University of California, Berkeley, September 1974.

72. Van Zyl, S., "Analysis of curved segmentally erected prestressed concrete box girder bridges", Structural Engineering and Structural Mechanics Report No. UC SESM 78-2, University of California, Berkeley, January 1978.

73. Mirza, M.S. (Editor), "Structural Concrete Models (Materials, Instrumentation, Correlation): A-State-of-the-Art Report". McGill University, Montreal, October 1972.

74. American Concrete Institute Commitee ACI-318, "Building Code Requirements for Reinforced Concrete (ACI 318-77)", American Concrete Institute, Detroit, 1977.

75. Canadian Standards Association/National Building Code Joint Committee on Reinforced Concrete Design, "Code for the Design of Concrete Structures for Building, CSA Standard A 23-3 - M 77". Canadian Standards Association, Rexdale, Canada, 1977.

76. Mirza, M.S., "Bond in reinforced concrete models", Proceedings of the Institute of Structural Engineers/Building Research Establishment Seminar on Reinforced and Prestressed Micro-Concrete Models, Garston, England, May 1978.

77. Mirza, M.S. and McCutcheon, J.O., "Direct models of prestressed concrete beams in bending and shear", Proceedings of the Institute of Structural Engineers/Building Research Establishment Seminar on Reinforced and Prestressed Micro-Concrete Models, Garston, England, May 1978.

78. Mitchell, D. and Collins, M.P., "The behaviour of structural concrete beams in pure torsion", Publication 74-06, Department of Civil Engineering, University of Toronto, Toronto, March 1974.

79. Mirza, M.S., White, R.N. and Roll, F., "Materials for structural models", Preprints of the Symposium on Models of Concrete Structures, American Concrete Institute Committee 444, Dallas, March 1972.

80. Syamal, P.K., "Direct models in combined stress investigations", M. Eng. Thesis, Department of Civil Engineering and Applied Mechanics, McGill University, Montreal, July 1969.

81. Hsu, C.T., "Investigation of bond in reinforced concrete models", M. Eng. Thesis, Department of Civil Engineering and Applied Mechanics, McGill University, Montreal, April 1969.

82. Pang, C.L., "Reliability of models in the analysis of prestressed concrete beams in flexure", M. Eng. Thesis, Department of Civil Engineering and Applied Mechanics, McGill University, Montreal, April 1965.

83. Mirza, M.S., Labonté, L.R.S. and McCutcheon, J.O., "Size effect in model concrete mix", Structural Concrete Series No. 72-7, Department of Civil Engineering and Applied Mechanics, McGill University, Montreal, April 1972.

84. Mirza, M.S., "An investigation of combined stresses in reinforced concrete beams", Ph.D. Thesis, Department of Civil Engineering and Applied Mechanics, McGill University, Montreal, March 1967.

85. Rockey, K.C., Bannister, J.L. and Evans, H.R., Development in bridge design and construction , Crosby Lockwood, London, 1971.

86. Kollbrunner, C.F. and Hajdin, N., "Wolbkrafttorsion dunnwandiger Stabe mit geschlossenem Profil", (Warping torsion of thin-walled beams of closed section), Mitteilungen der Technischen, Kommission, Schweizer Stahlbau-Vereinigung, Zurich, Heft 32, 1966.

87. Maisel, B.I. and Roll, F., "Methods of analysis and design of concrete box beams with side cantilevers", Technical Report No. 42.494, Cement and Concrete Association, London, November 1974.

88. Branson, D.E., Deformation of Concrete Structures McGraw-Hill Inc., New York, New York, 1977.

89. American Concrete Institute, ACI Committee 443 Report, "Analysis and design of reinforced concrete bridge structures", American Concrete Institute, Detroit, 1977.

90. Houde, J. and Mirza, M.S., "A finite element analysis of shear strength of reinforced concrete beams", Shear in Reinforced Concrete, Vol. I, ACI Special Publication SP-42, American Concrete Institute, Detroit, 1974, pp. 103-128.

91. Fenwick, R.C., "The shear strength of reinforced concrete beams", Ph.D. Thesis, University of Canterbury, Christchurch, New Zealand, 1966.

92. Taylor, H.P.J., "Investigation of the dowel shear forces carried by the tensile steel in reinforced concrete beams", Report No. TRA 431, Cement and Concrete Association, London, November 1969.

93. Mitchell, D., "The behaviour of structural concrete beams in pure torsion", Ph.D. Thesis, Department of Civil Engineering, University of Toronto, Toronto, 1974.

94. State of California, Department of Public Works, Division of Highway, Bridge Department, Manual of Bridge Design Practice, 3rd edition, 1972.

95. Zienkiewic, O.C., The Finite Element Method in Engineering Science McGraw-Hill Inc., New York, New York, 1971.

96. McCutcheon, J.O., Mirza, M.S. and Mufti, A., (Ed.), "Proceedings of the McGill-CSCE-EIC Specialty in Civil Engineering on the Finite Element Method", McGill University, Montreal, 1972.

97. Ngo, D. and Scordelis, A.C., "Finite element analysis of reinforced concrete beams", ACI Journal, Vol. 64, No. 3, March 1967, pp. 152-163.

98. Berg, S., "Nonlinear finite element analysis of reinforced concrete plates", Division of Structural Mechanics, The Norwegian Institute of Technology, Trondheim, Norway, February 1973.

99. Soliman, M.I., Mirza, M.S. and Thomas, G.R., "Finite element analysis of a reinforced concrete box girder bridge", Finite Element Methods in Engineering, Proceedings of the International Conference on Finite Element Methods in Engineering, The University of New South Wales, Australia, July 1979.

100. Agrawal, A.B., "Nonlinear analysis of reinforced concrete planar structures subjected to monotonic, reversed cyclic and dynamic loads", Ph.D. Thesis, Department of Mechanical Engineering, The University of New Brunswick, Fredricton, New Brunswick, March 1977.

101. Clough, R.W. and Felippa, C.A., "A refined quadrilateral element for analysis of plate bending", 2nd Conference on Matrix Methods in Structural Mechanics, Wright-Patterson Air Force Base, Ohio, October 1968.

102. Soliman, M.I., Mirza, M.S. and Thomas, G.R.,"Behaviour and analysis of reinforced concrete box girder bridges", Paper presented at the Research Session of the Fall Convention of the American Concrete Institute, Houston, Texas, November 1978.

103. Richmond, B., "Twisting of thin-walled box girders", Proceedings of the Institution of Civil Engineers, Vol. 33, No. 4, April 1966, pp. 659-675.

104. Kupfer, H., "Box beam with elastically stiffened cross-section under line and point loads", Stahlbetonbau: Berichte aus Forschung und Praxis. Ed. Knittel, G. and Kupfer, H. W. Ernst u. Sohn, Berlin, 1969. pp. 251-263.

105. Steinle, A., "Torsion and cross-sectional distortion of a single-cell box beam", Beton- und Stahlbetonbau, Berlin, September 1970.

106. Elfgren, L., "Reinforced concrete beams loaded in combined torsion, bending and shear: A study of the ultimate load-carrying capacity", Publication 73:3, Division of Concrete Structures, Chalmers University of Technology, Sweden, 1972.

107. Wagner, H., "Ebene Blechwandtrager mit Sehr Dunnem Stegblech", Zeitschrift fur Flugtechnik und Motorluftschiffahrt, Vol. 20, Nos. 8 to 12, 1929.

APPENDIX A

APPENDIX A

AVAILABLE METHODS FOR ANALYSIS OF A BOX GIRDER BRIDGE

A summary of the available methods is listed in Table A.1. The types of structural actions considered in each method are detailed in this table [39,85,86]. A brief summary of these methods is presented in this Appendix for completeness. The computer program developed for these methods (input data, output data and listing of the program) is also given.

A.1 The Conventional Simple Beam Theory and St. Venant Torsion

Using the engineering theory of bending, which assumes plane cross-sections to remain plane, the following expression is obtained for the normal stresses in longitudinal bending of a thin-walled beam with a symmetrical section:

$$f_{\ell} = \frac{M_x y}{I_x} + \frac{M_y x}{I_y} \qquad \text{(A.1)}$$

where f_{ℓ} = normal longitudinal stress in longitudinal bending

x, y = co-ordinates of a point on the centre-line of the walls of the cross-section

M_x, M_y = bending moments about the x- and y-axes

I_x, I_y = second moments of area of the entire concrete cross-section about the centroidal x- and y-axes.

	Type of structural action considered						
Analytical method	Longitudinal bending	St. Venant torsion	Distortion (Transverse bending)	Torsional warping	Distortional warping	Shear lag	Local effects
Simple beam theory	x	x					
Knittel			x				
Equivalent beam			x		x		
Kupfer			x		x		
Kolbrunner and Hajdin				x			
Heilig							
Beam on elastic foundation analogy			x				
Reissner						x	

Table A.1 Available methods for analysis of box girder bridges.

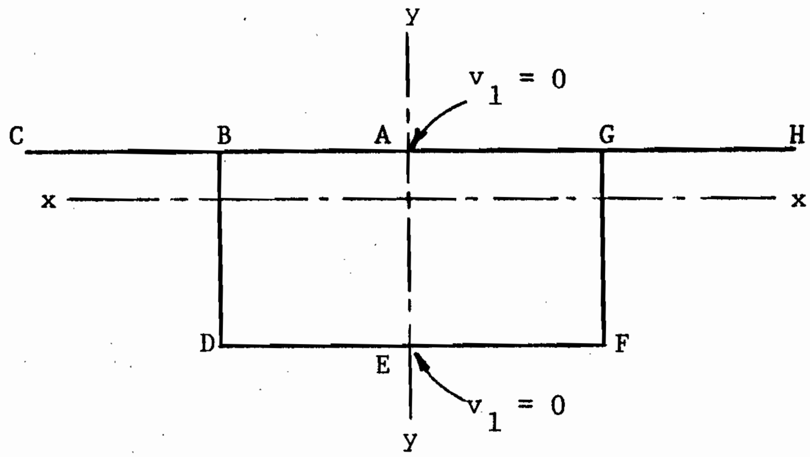

Fig. A.1 Zero Shear Stress v_1 on Axis of Symmetry for Vertical Loading

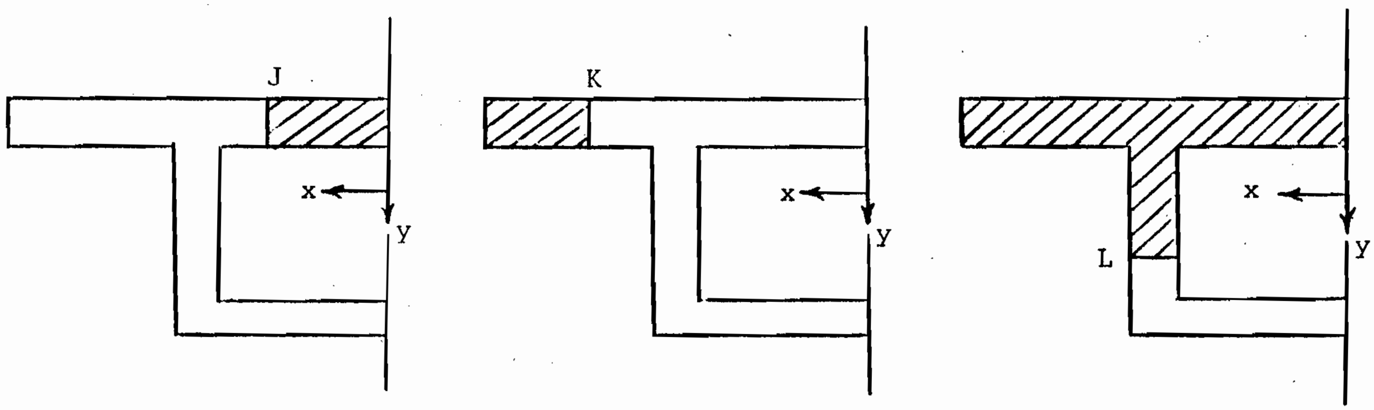

Fig. A.2 Evaluation of (Ay) the First Moment of Area of the Partial Half Cross-section About the Centroidal x-Axis

Because of symmetry of the cross-section, the longitudinal shear stress is zero at the vertical axis, hence the complementary shear stress v_1 in the plane of cross-section is also zero at $x = 0$ as shown in Fig. A.1. Since the boundary conditions for open sections are now satisfied, i.e., zero longitudinal shear stress at the ends of the cross-section (A, C and E), half of the section (ABCDE) in Fig. A.1 can be analysed as an open section. Kollbrunner and Basler [9] developed an equation which is applicable in this case:

$$(v_\ell \cdot h) = \frac{V_y (Ay)}{I_x} \qquad \text{(A.2)}$$

where $(v_\ell \cdot h)$ = shear flow in longitudinal bending

v_ℓ = shear stress in longitudinal bending

V_y = shear force parallel to the y-axis

Ay = first moment of area of the partial half cross-section about the centroidal x-axis (see Fig. A.2 (Ay) at j, k or L is the first moment of the shaded area about the x-axis).

The St. Venant torsional shear stress in thin-walled beams of open-closed section is given by [9]:

$$(v_{stv} h) = \frac{T_{stv}}{2A_{enc}} \qquad \text{(A.3)}$$

where $(v_{svt}h)$ = shear flow in a thin-walled section in St. Venant torsion

v_{svt} = shear stress in St. Venant torsion at the center-line of the wall

h = wall thickness of closed portion of the cross-section

T_{svt} = torsional moment at the cross-section in St. Venant torsion

A_{enc} = area enclosed by the centreline of the wall of the closed portion of the cross-section

$= bd$.

A.2 Analysis of Simple Bending, Torsion and Distortion by Knittel's Method [24]

A.2.1 Loading

Knittel's method is formulated in terms of line loads along the webs of the box beam. The representation of practical loading cases by equivalent sinusoidally distributed loadings is discussed in the following section.

A.2.2 Fourier Series Representation of Practical Loadings

Concentrated and uniformly distributed loads may each be represented by a sum of sinusoidal load distributions, as shown in Fig. A.3. The applied concentrated load is equivalent to a distributed

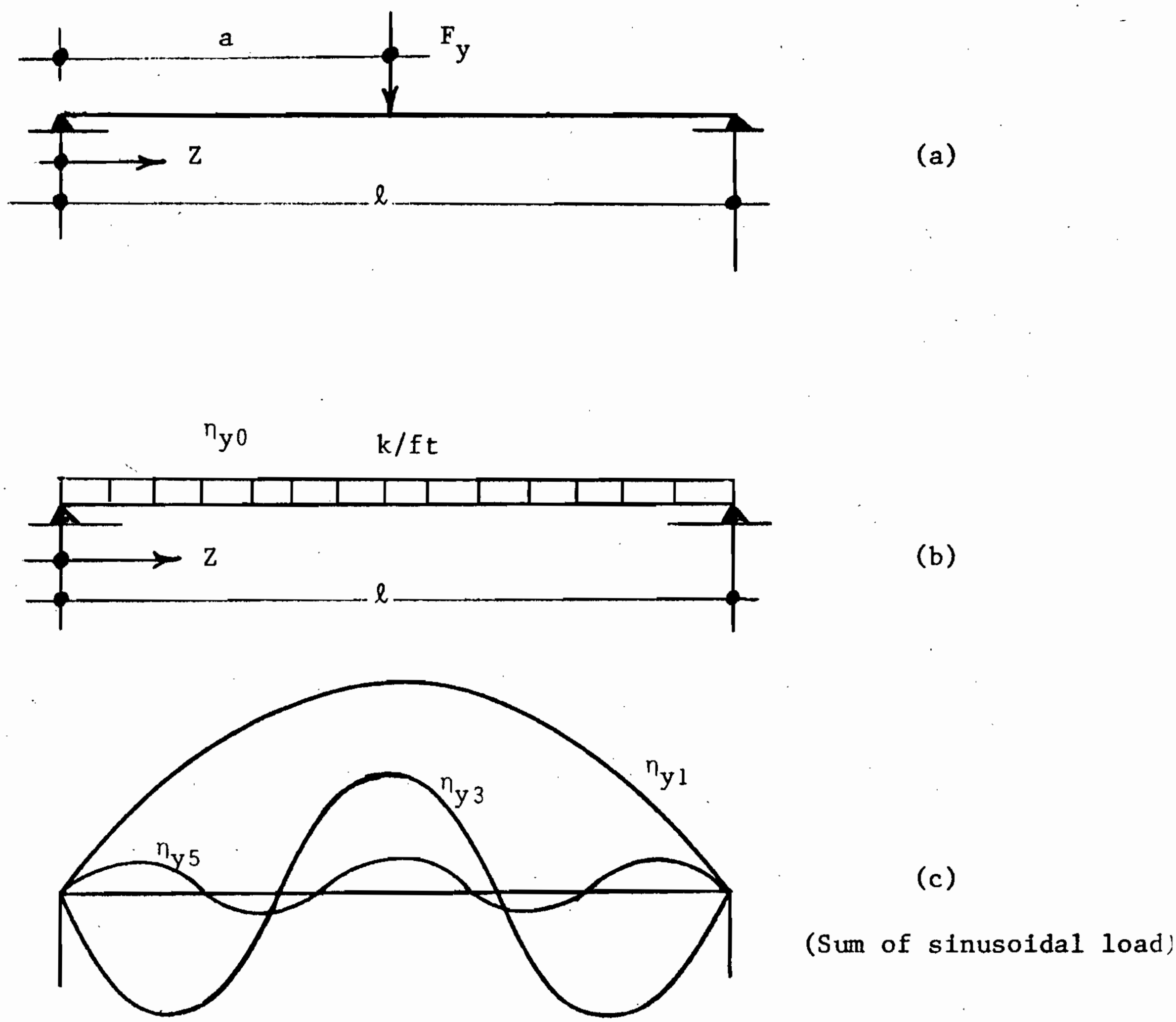

Fig. A.3 Fourier Series Representation of Practical Loadings load of intensity $\eta_{n,pt\ell}$ given by

$$\eta_{y,pt\ell} = \sum_{n=1}^{\infty} \bar{\eta}_{y,n} \operatorname{Sin} \frac{n\pi z}{\ell} \tag{A.4}$$

and $$\bar{\eta}_{y,n} = \frac{2F_y}{\ell} \operatorname{Sin} \frac{n\pi a}{\ell} \tag{A.5}$$

where ℓ is the span of the bridge.

Using only the first term of the Fourier series

$$\bar{\eta}_y = \frac{2F_y}{\ell} \operatorname{Sin} \frac{\pi a}{\ell} \tag{A.6}$$

and $$\eta_{y,pt\ell} = \bar{\eta}_y \operatorname{Sin} \frac{\pi z}{\ell} \tag{A.7}$$

For the uniformly distributed load shown in Fig. A.3, considering only the first term of the Fourier series

$$\bar{\eta}_y = \frac{4\eta_{y_o}}{\pi} \tag{A.8}$$

and $$\eta_{y,ud} = \Sigma\, \bar{\eta}_y \operatorname{Sin} \frac{\pi z}{\ell} \tag{A.9}$$

where the additional subscripts $pt\ell$ and ud stand for point load and uniform load, respectively.

A.2.3 Resolution of Loading

A given line loading is replaced by a statically equivalent combination of symmetric and antisymmetric line loadings at the webs. The resolution for a line load η_y at a web is shown in Fig. A.4.

A concentrated load on the structure is resolved using symmetric and antisymmetric point loading at the webs,which in turn are replaced by the Fourier components of the equivalent line loading, as indicated in Fig. A.4.

A.2.4 Summary of Analysis by Knittel's Method

1. For symmetric loads, analyse the structure using the engineering bending theory (Eqs. A.1 and A.2). Include consideration of transverse and normal forces as discussed below.

2. For antisymmetric loads, analyse the following two effects separately:

   a) pure (St. Venant) torsion,giving rise to shear stresses in the cross-section (Eq. A.3),

   b) distortion, giving rise to transverse bending on the flanges and webs and transverse normal forces.

Knittel's method neglects the effects due to loads not acting at the webs (i.e., transverse bending under symmetric loading) as shown in Fig. A.4(a). However, for the case of an antisymmetric loading, the transverse bending action is approximated by statically equivalent loads at the webs as shown in Fig. A.5(a).

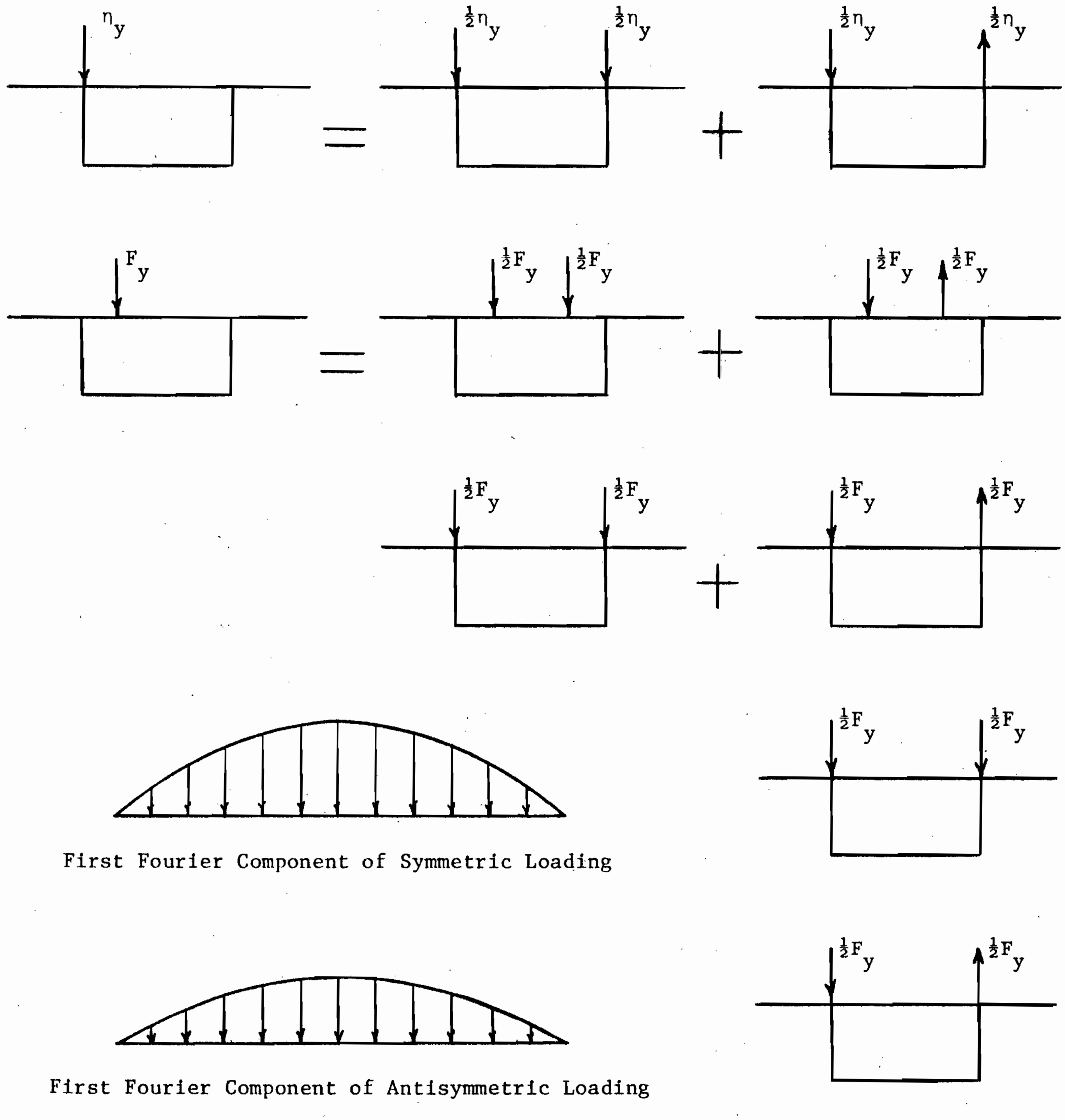

Fig. A.4 Resolution of Loading

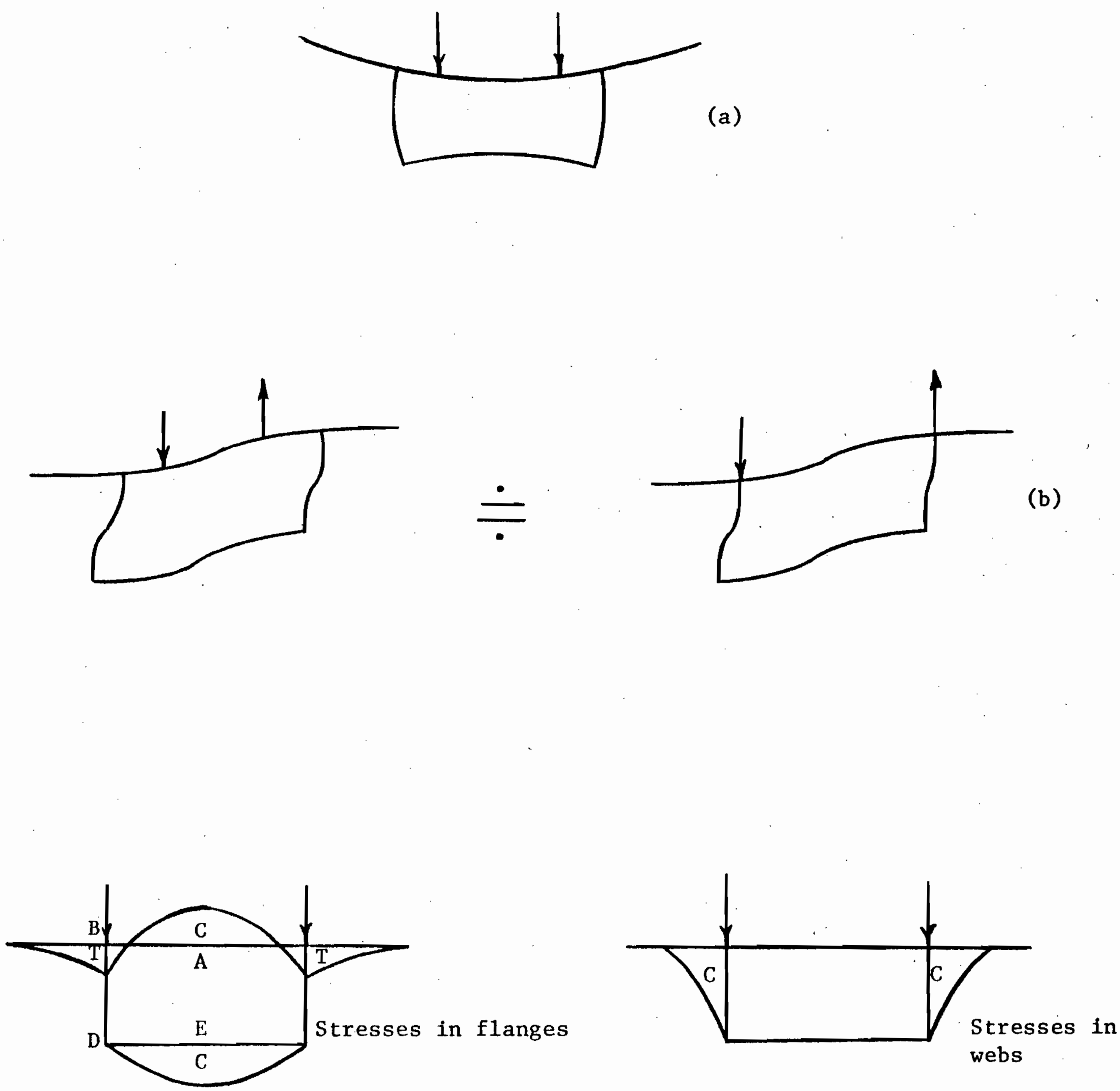

Fig. A.5 Distribution of Transverse Normal Stresses f_{trn} at Cross-section Under Symmetric Loading

(C: compression, T: tension)

(1) Symmetric Loading Case

Putting η_y equal to the intensity at section z (Fig. A.3), it follows from the Fourier Series representation of loading on each web in the symmetric load case and the simple beam theory that

$$M_x = -2 \int_o^z \int_o^z \eta_y (z)\, dz\, dz \tag{A.10}$$

and

$$V_y = -2 \int_o^z \eta_y (z) dz + (V_y)_{z=o} \tag{A.11}$$

where

$$(V_y)_{z=o} = 2 \int_o^{\ell/2} \eta_y (z) dz \tag{A.12}$$

Normal stresses f_ℓ and shear stresses v_ℓ can now be obtained from Eqs. A.1 and A.2.

Knittel [24] presented the following expressions for obtaining the maximum ordinates for the transverse normal forces under symmetric downward loading as shown in Fig. A.5. The transverse stresses f_{trn} are found by dividing the force per unit length by the thickness of the flange or web.

At point A (upper flange at axis of symmetry)

Transverse (horizontal) compressive force per unit length of the beam

$$= \frac{\eta_{y(z)}}{4I_x} (A_{top}\, b - 4\, A_{cant}\, b_{cant})\, d_{cg} \tag{A.13}$$

where $A_{top} = b\ h_{top}$

$A_{cant} = b_{cant}\ h_{top}$

d_{cg} = depth of the centroid of the cross-section below the centreline of the top slab

b = breadth between centreline of webs (Fig. A.7)

d = depth between centrelines of top and bottom slabs (Fig. A.7)

b_{cant} = breadth of the cantilever slab (Fig. A.7)

h_{top} = thickness of top slap (Fig. A.7)

h_{bot} = thickness of lower slab (Fig. A.7)

h_{web} = thickness of web (Fig. A.7)

<u>At point B</u> (upper flange at web)

Transverse (horizontal) tensile force per unit length of the beam

$$= \frac{\eta_{y(z)}}{I_x} A_{cant}\ b_{cant}\ d_{cg} \tag{A.14}$$

<u>At point B</u> (top of web)

Transverse (vertical) compressive force per unit length of the beam

$$= \eta_y(z) \tag{A.15}$$

At point E (lower flange at axis of symmetry)

Transverse horizontal tensile force per unit length of the beam

$$= \frac{\eta_y(z)}{4I_x} A_{bot}\, b(d-d_{cg}) \qquad \text{(A.16)}$$

where $A_{bot} = b\, h_{bot}$

(2) Antisymmetric Loading Case

(a) Pure (St. Venant) torsion

The torsional moment T_{svt} is calculated using the Fourier representation of antisymmetric loading and hence the torsional shear stresses v_{stv} can be obtained using Eq. A.3.

(b) Distortion

It is assumed that the transverse bending action of the closed frame takes place independently of the adjacent portions of the structure, i.e., no distortional warping stresses are set up. However, a distributed differential resistive shear flow $\frac{d}{dz}(v_{svt}h)$ is assumed to be applied to the frame by the adjacent portions of the structure, as shown in Fig. A.4.

$$\text{Differential resistive shear flow} = \frac{d}{dz}(v_{svt}h) = \frac{\eta_y(z)}{2d} \qquad \text{(A.17)}$$

The differential resistive shear forces acting on each flange or web (Fig. A.6) are given by the following:

$$V_1 = \frac{\eta_y(z)}{2d} \cdot 1 \cdot b \quad \text{in the top flange/unit length of structure} \tag{A.18}$$

$$V_3 = \frac{\eta_y(z)}{2d} \cdot 1 \cdot b \quad \text{in the bottom flange/unit length of structure} \tag{A.19}$$

$$V_2 = \frac{\eta_y(z)}{2d} \cdot 1 \cdot d \quad \text{in the web unit length of structure .} \tag{A.20}$$

A moment distribution analysis is performed for the closed frame under the action of the antisymmetric loading $\eta_y(z)$ and the forces V_1, V_2, and V_3. This gives the transverse bending moments and the transverse normal forces.

A.3 Analysis of Distortion and Distortional Warping by the Equivalent Beam Method [103]

Loading

As in the Knittel method, the applied loading is resolved into statically equivalent distributed loading along the webs as shown in Fig. A.4. Only the antisymmetric load case is considered in the equivalent beam method, and the action under symmetric load, i.e., bending without torsion, is treated separately using the simple beam theory.

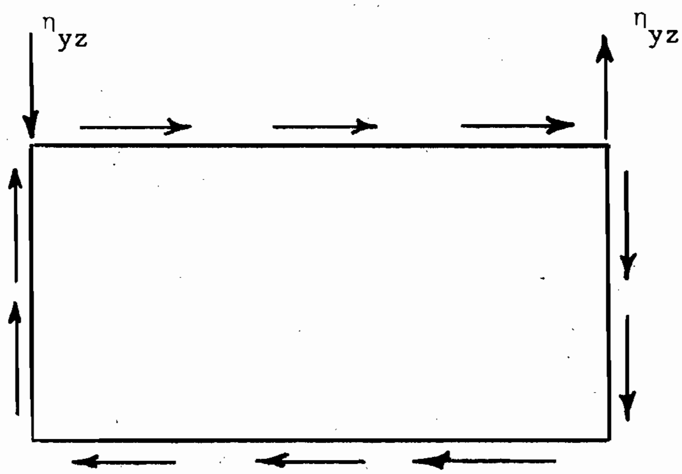

Differential resistive shear flow $\frac{d}{dz}(v_{svt} \cdot 1)$

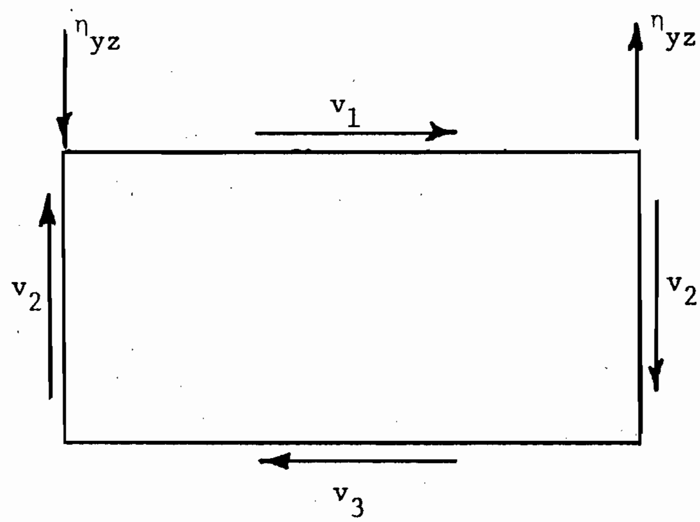

Differential resistive shear force

Fig. A.6 Force Systems in Distortion Under Antisymmetric Loading

A.3.1 Summary Analysis Procedure

A.3.1.1 Pure (St. Venant) Torsion

Using the Fourier representation of antisymmetric loading as in the Knittel method, the torsional moment T_{svt} is calculated. The torsional shear stresses v_{svt} can then be obtained using Eq. A.3

A.3.1.2 Distortion and Distortional Warping

It is assumed that rigid diaphragms at the supports prevent distortion but do not provide any warping restraint. The flanges of a single-span, simply supported box beam are replaced by equivalent flanges as shown in Fig. A.7. Note that this is not applicable to the symmetric load case. The two equivalent beams thus formed are considered to be latticed in the planes of the flanges, and their section properties are obtained using the following expressions:

$$A_{top\ eff} = \frac{2\bar{I}_{top}}{b^2} = \text{area of top flange of one equivalent beam}$$

$$A_{bot\ eff} = \frac{2\bar{I}_{bot}}{b^2} = \text{area of bottom flange of one equivalent beam}$$

$$A_{web\ eff} = dh_{web} = \text{area of web of one equivalent beam}$$

$$= \text{area of one web of actual beam}$$

where

$$\bar{I}_{top} = \frac{h_{top}(b + 2b_{cant})^3}{12} \tag{A.21}$$

= second moment of the cross-sectional area of the top flange about its vertical axis of symmetry

$$\bar{I}_{bot} = \frac{h_{bot} b^3}{12} \tag{A.22}$$

= second moment of the cross-sectional area of the bottom flange about its vertical axis of symmetry.

The depth d of one equivalent beam, measured between the centroids of $A_{top\ eff}$, $A_{bot\ eff}$ is equal to the depth d measured between the centreline of the top and bottom flanges.

If an equivalent beam is subjected to a sinusoidal loading such that $\eta_y = 1$ at midspan, then

$$\eta_y(z) = \text{Sin}\ \frac{\pi z}{\ell}$$

Then using the simple beam theory, the vertical deflection is given by

$$a_y = \int\int\int \frac{\eta_y(z)}{EI_{eff}}\ dz\ dz\ dz\ dz$$

Thus,
$$a_y = \frac{1}{EI_{eff}}\ \frac{\ell^4}{\pi^4}\ \text{Sin}\ \frac{\pi z}{\ell}$$

where I_{eff} is the second moment of area of the equivalent beam about its horizontal centroidal axis.

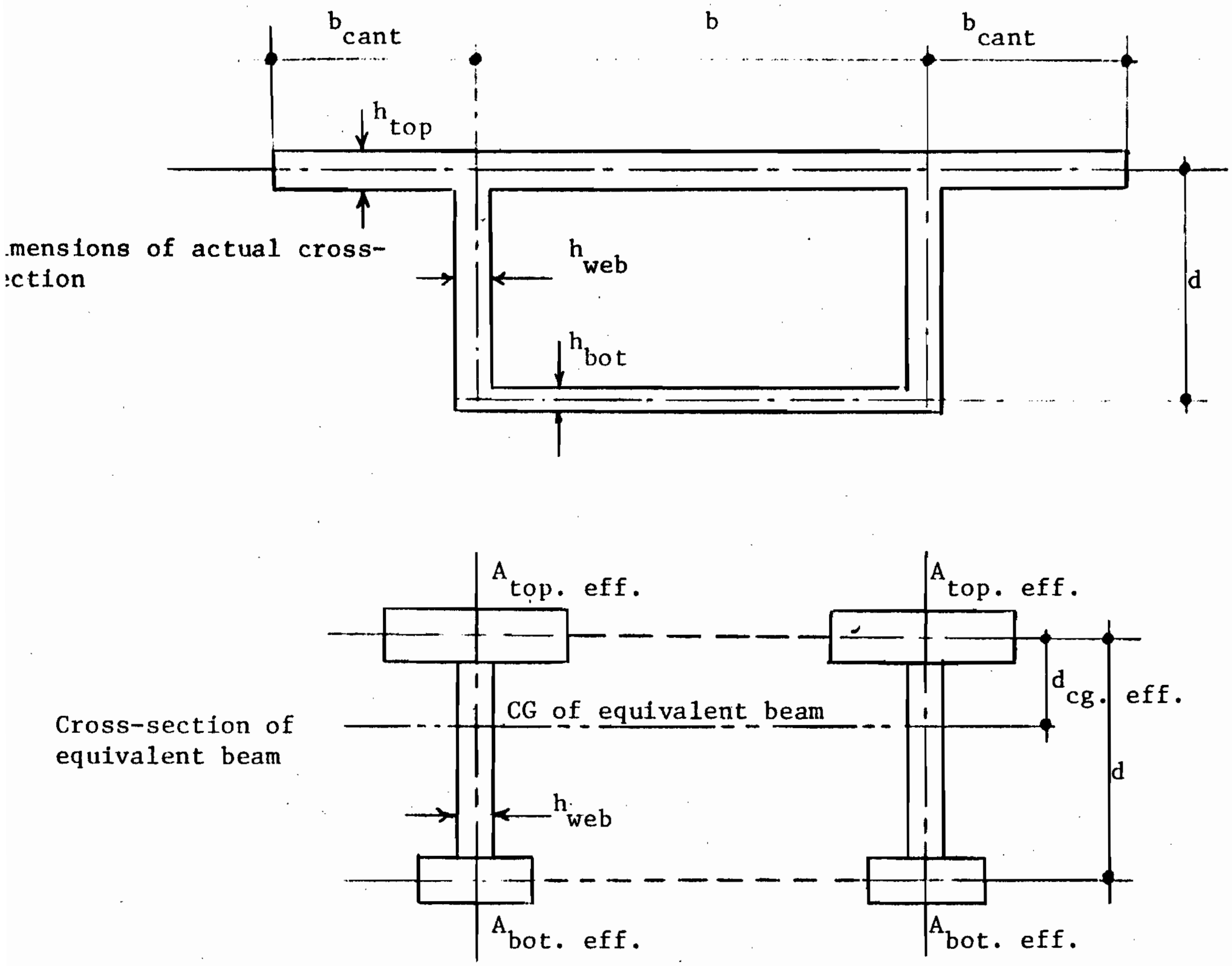

Fig. A.7 Cross-section of Actual and Equivalent Beams

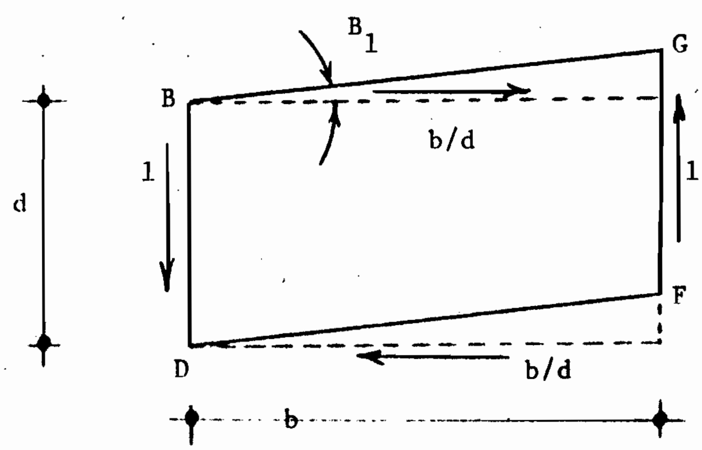

Fig. A.8 Diaphragms Shear Flexibility B_1

At midspan ($z = \frac{\ell}{2}$), the deflection under a unit sinusoidal load is

$$k_1 = \frac{1}{EI_{eff}} \frac{\ell^4}{\pi^4} \tag{A.23}$$

The resistance of a box beam to torsional loading may be visualized as arising partly from pure (St. Venant) torsion (no distortion), and partly from the differential bending of the equivalent beams, which is associated with the distortion of the cross-section of the box beam. The proportion of the applied torsional moment resisted by the box section in pure torsion, k_2 , is given by:

$$k_2 = \frac{1}{\frac{b\beta_1}{8k_1} + 1} \tag{A.24}$$

where β_1 is the diaphragm shear flexibility, which is the value of shear strain due to a unit shear force applied to the vertical faces of the diaphragm. The diaphragm shear flexibility coefficient, β_1 , is defined in Fig. A.8.

Thus the distributed load on each equivalent beam = $(\eta_y - 2\eta_{y,dmd})$ where

η_y = the intensity of the antisymmetric distributed loading on each web of the box beam

$\eta_{y,dmd}$ = the intensity of the distributed loading applied to each web by the diaphragm medium.

The resistance to distortion provided by the transverse bending strength of the wall is also termed the "diaphragm medium".

Richmond [103] developed the following expression for $\eta_{y,dmd}$

$$\eta_{y,dmd} = \frac{k_2}{2}\eta_y = \frac{\eta_y}{2\left(\frac{b\beta_1}{8k_1} + 1\right)} \qquad \text{(A.25)}$$

Hence $$\left(\eta_y - 2\eta_{y,dmd}\right) = \eta_y\left[\frac{1}{\frac{8k_1}{b\beta_1} + k}\right] \qquad \text{(A.26)}$$

Thus the load carried by differential bending is $(\eta_y - 2\eta_{y,dmd})$ along the span on each web, and the load carried by torsional shear flow is $(\eta_{y,dmd}/d)$ around the perimeter of cross-section. If k_2 equals zero, the entire load is resisted by differential bending and if k_2 equals unity, the entire load is resisted in pure torsion.

A.3.2 Stress Analysis

The bending flexibility coefficient, k_1, for an equivalent beam can be calculated for a given cross-section geometry and span. However, to evaluate the value of the diaphragm shear flexibility, β_1, a moment distribution analysis must be performed on a unit length of the closed frame. Then, knowing the value of k_2, the St. Venant or the pure torsional moment T_{svt} and the resulting shear stresses v_{svt}

can be calculated. Also, since η_y and $\eta_{y,dmd}$ are known, the transverse bending stress, f_{trb}, and the transverse normal stress, f_{trn}, in the closed frame can now be determined along with the value of the distortional warping stress, f_{dwr}, in the equivalent beam.

A.3.3 Warping Moment due to Cross-section Distortion

The longitudinal distortional warping stresses, f_{dwr}, at the top and the bottom of each web are obtained using the following expression for the distortional warping moment, M_{dwr}, on one web of the equivalent beam

$$M_{dwr} = (\eta_y - 2\eta_{y,dmd}) \frac{\ell^2}{\pi^2} \tag{A.27}$$

A.4 Analysis of Distortion and Distortional Warping by Kupfer's Method [104]

A.4.1 Loading

The vertical loading is assumed to be applied over a web, and is resolved into three systems as shown in Fig. A.9. These systems generate the following structural actions in the box beam: (a) longitudinal bending, (b) torsion and (c) distortion. Kupfer recommended that the first two be treated using Knittel's method and St. Venant's torsion

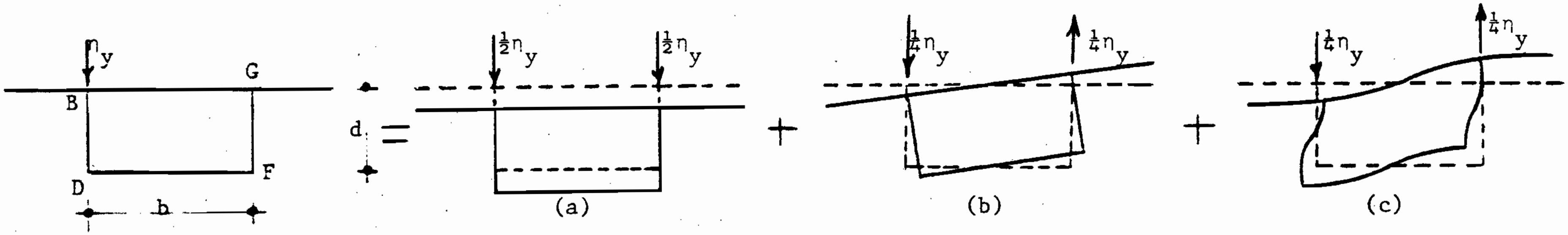

Fig. A.9 Resolution of Loading

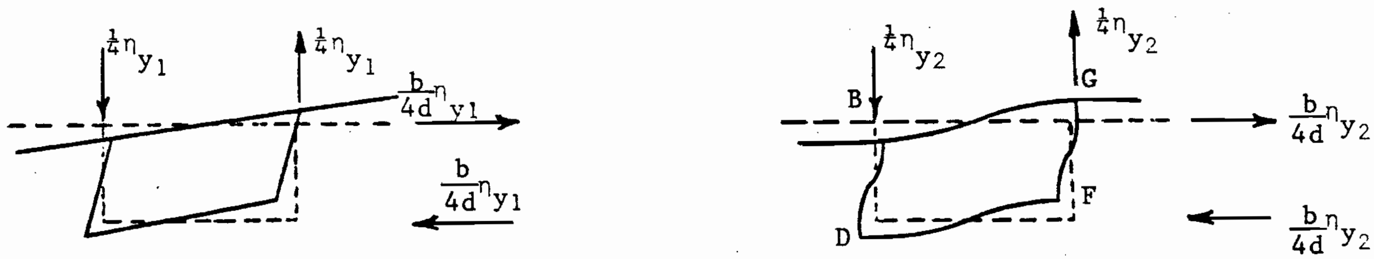

a) System (1) (Hinged folded plate)

b) System (2) (Rigid jointed closed frame)

Fig.A.10 Subdivision of Distortional System theory, respectively, and he developed an analysis dealing mainly with distortion and distortional warping. The method is formulated in terms of a distributed loading using a Fourier Series representation.

A.4.2 Summary of Analysis Procedure

In analysing the box beam for distortion (Fig. A.9c), the applied load is divided between two mutually independent and deformationally compatible structural systems 1 and 2, as shown in Fig. A.7. In system 1, the box beam is treated as a hinged folded plate structure subjected to a sinusoidal load in the plane of each wall. Here only longitudinal structural action of the walls is considered, with each wall behaving as a longitudinal beam bending in its own plane. The influence of shear deformation is neglected. System 2 consists of a rigid jointed closed-frame structure as shown in Fig. A.10(b) which is also subjected to a sinusoidal load in the plane of each wall. In this case, only the transverse structural action is considered, and each wall develops transverse bending stresses.

The distribution of the distortional load system in Fig. A.9(c) between systems 1 and 2 of Fig. A.10 is determined by ensuring the compatibility of deflections at the corners of all cross-sections.

A.4.3 Analysis of Structure Under a Distortional Load System

Kupfer developed the following expressions to determine the components of distortional load η_{y_1} and η_{y_2} acting on systems 1 and 2, respectively:

$$\eta_{y_1} = \eta_y \frac{k_3}{1 + k_3} \quad \text{(A.28)}$$

and

$$\eta_{y_2} = \eta_y \frac{1}{1 + k_3} \quad \text{(A.29)}$$

where

$$k_3 = \frac{\pi^4}{48} \left(\frac{bd^2}{h_{web}\ell^2}\right) k_4 k_5 \quad \text{(A.30)}$$

$$= \frac{\eta_{y_1}}{\eta_{y_2}}$$

$$= \frac{\text{distortional load taken by system 1}}{\text{distortional load taken by system 2}}$$

$$k_4 = \frac{3 + 2(k_6 + k_7) + k_6 k_7}{6 + k_6 + k_7} \quad \text{(A.31)}$$

$$k_5 = \frac{3 + 2(k_8 + k_9) + k_8 k_9}{6 + k_8 + k_9} \quad \text{(A.32)}$$

$$k_6 = \frac{bh_{top}}{dh_{web}} \left[\frac{b + 2b_{cant}}{b}\right]^3 \quad \text{(A.33)}$$

$$k_7 = \frac{bh_{bot}}{dh_{web}} \quad \text{(A.34)}$$

$$k_8 = \frac{bh^3_{web}}{dh^3_{top}} \quad \text{(A.35)}$$

$$k_9 = \frac{bh^3_{web}}{dh^3_{bot}} \quad \text{(A.36)}$$

To evaluate the longitudinal stresses due to the distortional load system, the actual box beam is replaced by two equivalent beams similar to those illustrated in Fig. A. 7, but with the value of I_{eff} equal to half of the second moment of area of one equivalent beam, since the loading on each beam is now $\left(\frac{\eta_y}{4}\right)$. For system 1, the equivalent beams are taken as simply supported over the actual span ℓ and subjected to a sinusoidally distributed vertical load $\left(\frac{\eta_{y_1}}{4}\right)$ which can be calculated using Eq. A.37

$$\frac{\eta_{y_1}(z)}{4} = \frac{\eta_{y_1}(z)}{4} \quad \frac{k_3}{1 + k_3} \tag{A.37}$$

For system 2, the transverse bending strength of the upper and the lower slabs of the box beam provides a continuous elastic support for the equivalent beams, which must therefore be analysed as beams on an elastic foundation. The vertical loading can be taken either as the sinusoidal Fourier representation $\left(\frac{\eta_{y_2}}{4}\right)$ or as the actual loading resolved into system 2. This loading can be used for evaluating the longitudinal (distortional warping) stresses and the transverse bending stresses in system 2. The foundation modulus, k_{10}, for the equivalent beam on elastic foundation is given by

$$k_{10} = \frac{4Eh^3_{web}}{b^2 d\ k_5} \tag{A.38}$$

A.4.3.1 Longitudinal Stresses in System 1

The longitudinal stress at the junction of the centreline of the upper slab and the web is given by

$$|f_{dwr,1}| = \frac{1}{4} \eta_{y_1} \frac{\ell}{2} \frac{\ell^2}{\pi^2} \frac{d_{cg}}{\frac{1}{2} I_{eff}} \qquad (A.39)$$

The longitudinal stress at the junction of the centreline of the lower slab and the web is given by

$$|f_{dwr,1}| = \frac{1}{4} \eta_{y_1} \frac{\ell}{2} \frac{\ell^2}{\pi^2} \frac{d - d_{cg}}{\frac{1}{2} I_{eff}} \qquad (A.40)$$

A.4.3.2 Longitudinal Stresses in System 2

Under a uniformly distributed loading of intensity $\frac{\eta_{y_o}}{4}$, a simply supported beam (span ℓ) on an elastic foundation with a modulus k_{10}, develops a midspan bending moment given by

$$M_1 = \frac{\eta_{y_o}}{4k^2_{11}} \frac{\sinh \frac{k_{11}\ell}{2} \sin \frac{k_{11}\ell}{2}}{\cosh k_{11}\ell + \cos k_{11}\ell} \qquad (A.41)$$

where $$k_{11} = \sqrt[4]{\frac{k_{10}}{4E\left(\frac{1}{2} I_{eff}\right)}} \qquad (A.42)$$

When subjected to a concentrated load, $\frac{F_y}{4}$, at midspan the beam develops a midspan bending momemtn M_2 given by

$$M_2 = \frac{F_y}{16\ k_{11}} \frac{\sinh k_{11}\ell + \sin k_{11}\ell}{\cosh k_{11}\ell + \cos k_{11}\ell} \qquad \text{(A.43)}$$

Kupfer [104] argued that in an infinitely long beam on an elastic foundation, subjected to a single concentrated load within the span, the bending moment M_2 will have become negligible at a distance ℓ_{ch} (characteristic length) from the concentrated load, given by

$$\ell_{ch} = \frac{1}{k_{11}} \qquad \text{(A.44)}$$

Therefore, it follows that under the action of a concentrated load, the distortional warping effects in system 2 are confined within a length $(2\ell_{ch})$ of the equivalent beam, treated as an infinitely long beam, provided the concentrated load is at a minimum distance of ℓ_{ch} from the end of the beam. Kupfer used the following approximate expression to calculate M_2

$$M_2 = \frac{F_y\ \ell_{ch}}{16} \qquad \text{(A.45)}$$

The same expression results from letting ℓ tend to infinity in Eq. A.43. The distortional warping stresses due to a concentrated load $\left(\frac{F_y}{4}\right)$ can be calculated as follows:

The distortional warping stress at the junction of the centreline of the upper slab and the web is given by

$$\left| f_{dwr,2} \right| = M_2 \frac{d_{cg}}{\frac{1}{2} I_{eff}} \tag{A.46}$$

The distortional warping stress at the junction of the centreline of the lower slab and the web is given by

$$\left| f_{dwr,2} \right| = M_2 \frac{(d - d_{cg})}{\frac{1}{2} I_{eff}} \tag{A.47}$$

A.4.4 Transverse Bending Stresses

The transverse bending moments at the corners of the closed frame for a unit length of the actual structure are first evaluated. In system 1, there are no transverse bending moments, as the folded plate structure is hinged, and the loads act at the web-plate junction.

In system 2, the transverse bending moments under a distributed loading are given by (see Fig. A.10)

$$M_M = M_G = \pm \frac{\eta_{y_2} b}{8} \frac{3 + k_9}{6 + k_8 + k_9} \tag{A.48}$$

$$M_D = M_F = \pm \frac{\eta_{y_2} b}{8} \frac{3 + k_8}{6 + k_8 + k_9} \tag{A.49}$$

Under a concentrated midspan load, the transverse bending moments are given by

$$M_B = M_G = \pm \frac{F_y b}{16\, \ell_{ch}} \frac{3 + k_8}{6 + k_8 + k_9} \qquad \text{(A.50)}$$

$$M_D = M_F = \pm \frac{F_y b}{16\, \ell_{ch}} \frac{3 + k_8}{6 + k_8 + k_9} \qquad \text{(A.51)}$$

The transverse bending moments for the system resisting pure torsion (Fig. A.9b) are given by

$$M_B = M_G = \pm \frac{\eta_y b}{8} k_{12} \frac{3 + k_9}{6 + k_8 + k_9} \qquad \text{(A.52)}$$

$$M_D \quad M_F = \pm \frac{\eta_y b}{8} k_{12} \frac{3 + k_8}{6 + k_8 + k_9} \qquad \text{(A.53)}$$

where $$k_{12} = \frac{E}{G} \frac{\pi^2}{48} \frac{d^2}{\ell^2} k_4 \left(\frac{bh_{web}}{dh_{top}} + \frac{bh_{web}}{dh_{bot}} - 2 \right) \frac{1}{1 + k_3} \qquad \text{(A.54)}$$

The transverse bending stress f_{trb} at B is given by

$$f_{trb} = \pm \frac{GM_B}{h^2_{top}} \qquad \text{(A.55)}$$

where E and G are Young's and shear modulus of elasticity.

A.5 Analysis of Torsional Warping by the Method of Kollbrunner, Hajdin and Heilig [86]

A.5.1 Loading

The analysis considers only the torsional component of the actual loading and not its Fourier representation.

A.5.2 Bimoment B_{twr}, Sectional Coordinate W_{twr} and Torsional Warping Second Moment of Area C_{twr}

The bimoment is the force system associated with warping. A quantitative definition of the torsional warping bimoment B_{twr} is

$$B_{twr} = \int_A f_{twr} \, W_{twr} \, dA \qquad (A.56)$$

where A = total area of cross-section including the side cantilevers

f_{twr} = torsional warping stress

W_{twr} = sectional coordinate in torsional warping (referrrd to the shear centre)

The sectional coordinate W_{twr} is defined as

$$W_{twr} = \int_o^{s_{per}} \left(\bar{a} - \frac{C_{svt}}{2A_{enc} h} \right) ds_{per} \qquad (A.57)$$

where C_{svt} = torsional constant of cross-section

$$= \frac{4A_{enc}}{\oint \frac{ds_{per}}{h}}$$

$$\oint \frac{ds_{per}}{h} = \frac{b}{h_{top}} + \frac{b}{h_{bot}} + \frac{2d}{h_{web}}$$

A_{enc} = area enclosed by centreline of wall of closed portion of the cross-section

s_{per} = peripheral coordinate along centreline of wall (Fig. A.11)

h = wall thickness

where $\bar{a}$ is the perpendicular distance from the shear centre to the tangent to the wall centreline at the point considered, s_{per} is the peripheral coordinate along the centreline of the wall (Fig. A.11). Note that the term $(C_{svt}/2A_{enc}h)$ is included in the integrand only for integration around the wall of the closed portion of the cross-section. It is not included for integration along the side cantilevers. The torsional warping second moment of area of the cross-section, C_{twr}, is defined as

$$C_{twr} = \int_A W_{twr}^2 \, dA \qquad (A.58)$$

The following expression gives the torsional warping stress, f_{twr}:

$$f_{twr} = \frac{B_{twr} W_{twr}}{C_{twr}} \qquad (A.59)$$

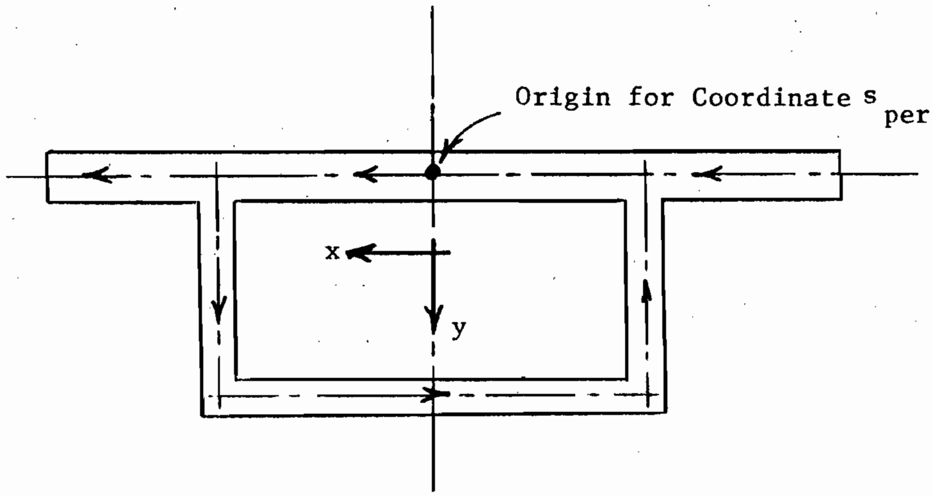

Fig.A.11 Peripheral Coordinate s_{per} Showing Origin and Positive Direction

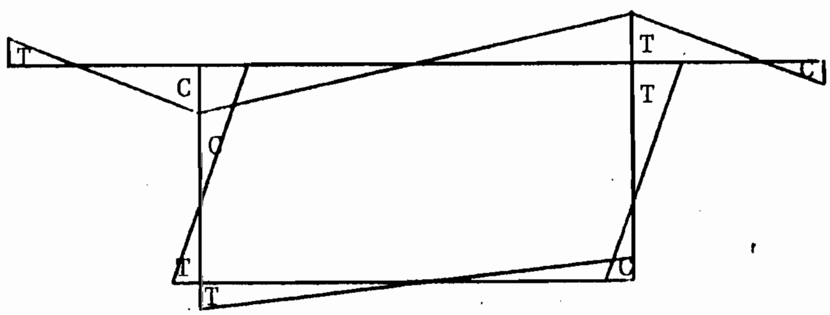

Fig.A.12 Torsional Warping Stress Distribution at Cross-section

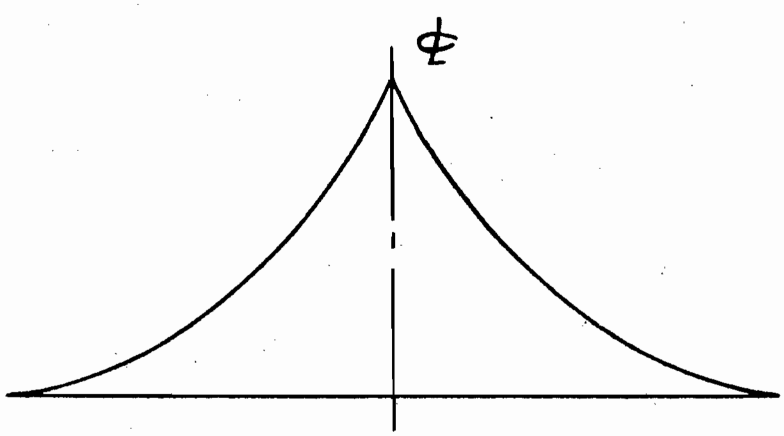

Fig.A.13 Torsional Warping Stress Distribution Along Beam

The form of this expression is the same as Equation A.1, since M_x, M_y and B_{twr} are all stress-resultants at the section z; x,y and W_{twr} are coordinates of the point considered on the cross-section; and I_x, I_y and C_{twr} are geometrical properties of the entire cross-section. Under an eccentric loading, the longitudinal stresses f_ℓ calculated using Eq.A.1 and f_{twr} evaluated using Eq. A.59 are added algebraically. Figure A.12 shows the variation of f_{twr} around the perimeter of cross-section, and Fig. A.13 shows its distribution along the beam.

A.5.3 Torsional Warping Shear Stresses

Torsional warping shear stress v_{twr} at any point is given by

$$v_{twr} = T_{twr} \frac{\dfrac{dW_{twr}}{ds_{per}}}{(C_{cen} - C_{svt})} \qquad \text{(A.60)}$$

where $\dfrac{dW_{twr}}{ds_{per}} = \bar{a} - \dfrac{C_{svt}}{2A_{enc}h}$ for a single-cell cross-section (A.61)

C_{cen} = central torsional moment of inertia of the cross-section

$$= \int_A \bar{a}^2 \, dA \qquad \text{(A.62)}$$

A.6 Analysis of Distortion and Distortional Warping by the Analogy of Beam on Elastic Foundation [105]

A.6.1 Loading

The analysis considers only the distortional system. The distortional component of the actual loading is used in this analysis, and not a Fourier representation of the loading.

A.6.2 Basic Analysis Procedure

A mathematical analogy exists between the distortional behaviour of a rectangular single-cell section box beam and the flexural behaviour of a beam on elastic foundation. The physical basis for the analogy stems from the fact that the transverse bending strength of the upper and lower slabs of a box beam provides a continuous elastic support for the webs which therefore behave like beams on elastic foundation.

A.6.3 Bimoment, B_{dwr}, Warping Coordinate W_{dwr}, Distortional Warping Second Moment of Area, C_{dwr}, and Frame Stiffness, EI_{fra}

The beam-on-elastic-foundation analogy shows that the bimoment, B_{dwr}, is analogous to the bending moment in a beam on an elastic foundation. Also, the angle of distortion of the cross-section of the box beam is analogous to the deflection of the beam on an elastic foundation.

Diaphragms in the box beam, which prevent distortion but not warping, correspond to unyielding simple supports, while an end support condition, where warping is prevented, is analogous to a built-in end support for the beam on elastic foundation. A diaphragm which provides elastic restraint to distortion is analogous to an elastically yielding support. Distribution of the distortional warping coordinate, W_{dwr}, is shown in Fig. A.14. W_{dwr} varies linearly along the wall centreline and the coefficients shown in Fig. A.14 are given by

$$k_{25} = \frac{3 + k_6}{3 + k_7} \tag{A.63}$$

where
$$k_6 = \frac{bh_{top}}{dh_{web}} \left(\frac{b + 2b_{cant}}{b}\right)^3 \tag{A.64}$$

and
$$k_7 = \frac{bh_{bot}}{dh_{web}} \tag{A.65}$$

The distortional warping second moment of area of the cross-section, C_{dwr}, is given by

$$C_{dwr} = \frac{b^2 d^3 h_{web}}{48} k_4 \tag{A.66}$$

where
$$k_4 = \frac{3 + 2(k_6 + k_7) + k_6 k_7}{6 + k_6 + k_7} \tag{A.67}$$

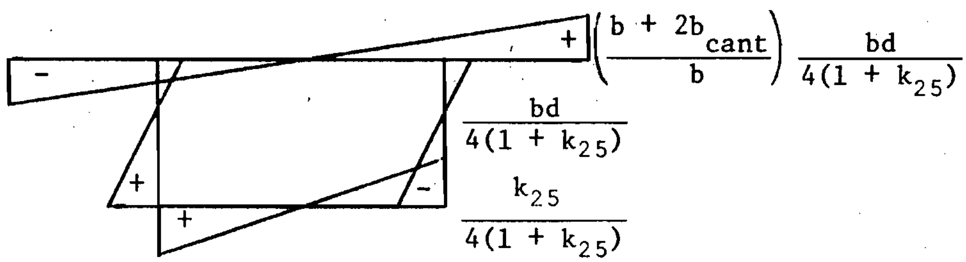

Fig.A.14 Distortional Warping Coordinate W_{dwr}

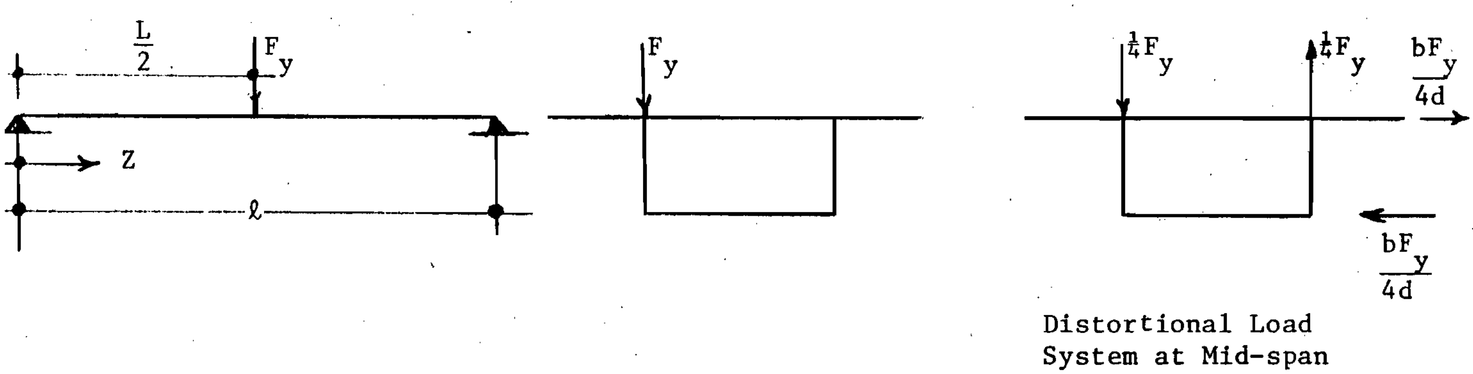

Fig.A.15 Concentrated Distortional Load System
Applied to Beam at Mid-span

The frame stiffness, EI_{fra}, is obtained from

$$I_{fra} = \frac{24\ I_{web}}{k_{26} d} \tag{A.68}$$

where
$$k_{26} = 1 + \frac{2\frac{b}{d} + 3\frac{I_{top} + I_{bot}}{I_{web}}}{\frac{I_{top} + I_{bot}}{I_{web}} + 6\frac{d}{b}\frac{I_{top} I_{bot}}{I^2_{web}}} \tag{A.69}$$

$$I_{top} = \frac{h^3_{top}}{12(1-\nu^2)} \tag{A.70}$$

$$I_{bot} = \frac{h^3_{bot}}{12(1-\nu^2)} \tag{A.71}$$

$$I_{web} = \frac{h^3_{web}}{12(1-\nu^2)} \tag{A.72}$$

Here ν = Poisson's ratio.

Under a concentrated load, F_y, at midspan over one web, resolved as shown in Fig. A.15, the stresses are given by the following:

A.6.3.1 Distortional Warping Stresses

The distortional warping stress, f_{dwr}, is given by

$$f_{dwr} = \frac{B_{dwr}\ W_{dwr}}{C_{dwr}} \tag{A.73}$$

W_{dwr} is obtained from Fig. A.14

where $$B_{dwr}(z) = B_{dwr,o}(z) - \frac{F_y b\ell}{2\pi^2} \sum_{n=1}^{\infty} \frac{\sin\frac{n\pi}{2}\sin\frac{n\pi z}{\ell}}{n^2\left[1 + n^4\left(\frac{\pi^4 C_{dwr}}{I_{fra}\ell^4}\right)\right]} \quad \text{(A.74)}$$

$$B_{dwr,o}(z) = \frac{F_y b}{8} z \quad \text{for} \quad o \le z \le \frac{\ell}{2}$$

$$B_{dwr,o}(z) = \frac{F_y b}{8} (\ell-2) \quad \text{for} \quad \frac{\ell}{2} \le z \le \ell$$

The distortional warping coordinate, W_{dwr}, is calculated using Fig. A.15 and Equations A.63, A.64 and A.65. The value of B_{dwr} at midspan for the load case in Fig. A.15 is given by

$$B_{dwr} = \frac{F_y b}{16k_{27}} \frac{\sinh k_{27}\ell + \sin k_{27}\ell}{\cosh k_{27}\ell + \sin k_{27}\ell} \quad \text{(A.75)}$$

where $$k_{27} = \sqrt[4]{\frac{I_{fra}}{4C_{dwr}}} \quad \text{(A.76)}$$

Also, note that Eq. A.73 is the same as Eq. A.1. Under eccentric loading, the longitudinal stresses, f_ℓ (calculated using Eq. A.1), f_{twr} (from Eq. A. 59) and f_{dwr} (from Eq. A.73) are added algebraically to obtain the final longitudinal stresses. Figure A.16 shows the variation of f_{dwr} around the perimeter of the cross-section and Fig. A.17 shows its distribution along the length of the beam.

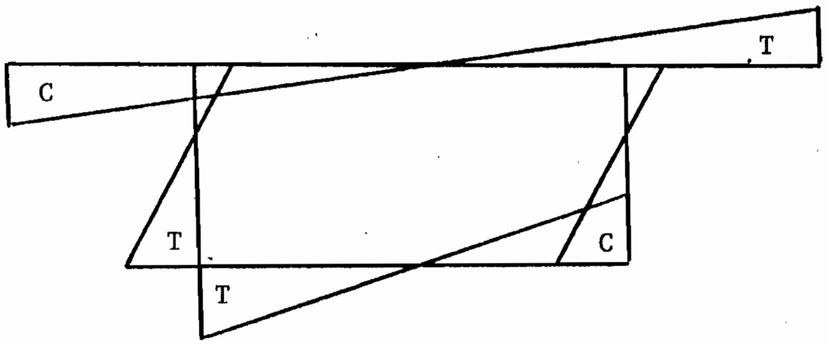

Fig.A.16 Distortional Warping Stress Distribution
at Cross-section

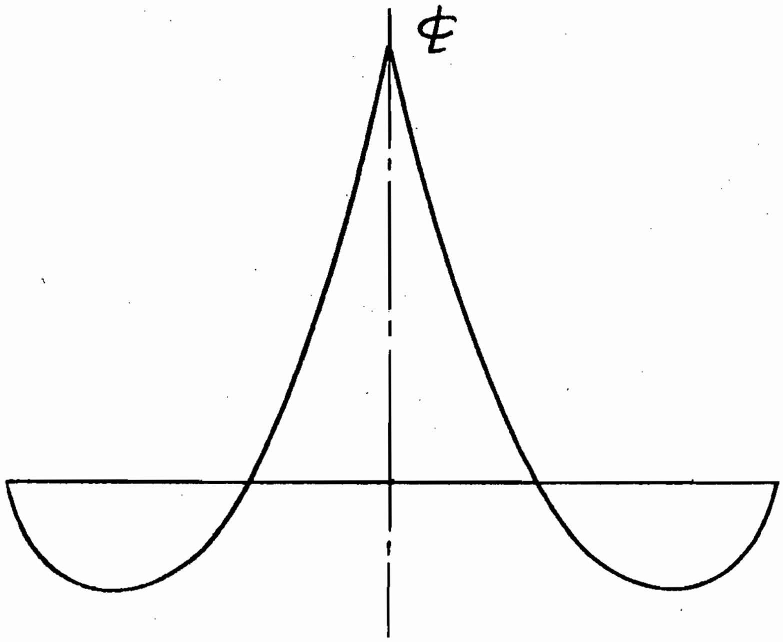

Fig.A.17 Distortional Warping Stress Distribution
Along Beam

A.6.3.2 Distortional Warping Shear Stresses

The distortional warping shear stress, v_{dwr}, at any point on the cross-section is given by

$$v_{dwr} = \frac{-\frac{d}{dz} B_{dwr}}{h\, C_{dwr}} k_{28} \frac{bd}{4(1 + k_{25})} \tag{A.77}$$

where, for the load case considered:

$$\frac{d}{dz} B_{dwr}(z) = \frac{d}{dz} B_{dwr,o}(z) - \frac{F_y b}{2\pi} \sum_{n=1}^{\infty} \frac{\sin\frac{n\pi}{2} \cos\frac{n\pi z}{\ell}}{n\left[1 + n^4\left(\frac{\pi^4 C_{dwr}}{I_{fra}\ell^4}\right)\right]} \tag{A.78}$$

where $\frac{d}{dz} B_{dwr,o}(z) = \frac{F_y b}{8}$ for $o \le z \le \frac{\ell}{2}$

$\frac{d}{dz} B_{dwr,o}(z) = \frac{-F_y b}{8}$ for $\frac{\ell}{2} \le z \le \ell$

The values of k_{28} at the various points on the cross-section can be obtained from Reference [105].

A.6.3.3 Transverse Bending Stresses

The transverse bending stress, f_{trb}, at any point is given by:

$$f_{trb} = \frac{6M_{trb}}{h^2} \tag{A.79}$$

where M_{trb} = transverse bending moment due to the distortional load system

f_{trb} = transverse bending stress at the wall face.

Using the beam-on-electric foundation analogy for the load case under consideration, one obtains the following two equations:

At the top of the web:

$$M_{trb,B} = \frac{EI_{fra}\, \beta_{trb}}{2(1 + k_{30})} \qquad (A.80)$$

At the bottom of the web:

$$M_{trb,o} = \frac{-k_{30}EI_{fra}\, \beta_{trb}}{2(1 + k_{30})} \qquad (A.81)$$

where

$$k_{30} = \frac{3 + \frac{b}{d}\frac{I_{web}}{I_{top}}}{3 + \frac{b}{d}\frac{I_{web}}{I_{bot}}} \qquad (A.82)$$

$$\beta_{trb}(z) = \beta_{trb,o}(z) - \frac{F_y b \ell^3}{2\pi^4 E\, C_{dwr}} \sum_{n=1}^{\infty} \frac{\sin\frac{n\pi}{2}\sin\frac{n\pi z}{\ell}}{n^4\left[1 + n^4\left(\frac{\pi^4\, C_{dwr}}{I_{fra}\ell^4}\right)\right]} \qquad (A.83)$$

$$\beta_{trb,o}(z) = \frac{F_y b}{24E\, C_{dwr}}\left[\frac{\ell}{2}\, z\left(\frac{3\ell}{4} - \frac{z^2}{\ell}\right)\right] \qquad \text{for} \quad o \le z \le \frac{\ell}{2}$$

$$\beta_{trb,o}(z) = \frac{F_y b}{24E\, C_{dwr}} \left[\frac{\ell}{2} \; z\left(\frac{3\ell}{4} - \frac{z^2}{\ell}\right) + \left(z - \frac{\ell}{3}\right)^3 \right] \text{ for } \frac{\ell}{2} \leq z \leq \ell$$

The value of β_{trb} at midspan for the load case in Fig. A.8 is given by

$$\beta_{trb} = \frac{F_y b\, k_{27}}{8E\, I_{fra}} \; \frac{\sinh k_{27}\ell - \sin k_{27}\ell}{\cosh k_{27}\ell - \cos k_{27}\ell} \qquad \text{(A.84)}$$

The distortional angle, β_{trb}, is a measure of the distortion of the cross-section due to the distortional load system.

A.7 Analysis of Shear Lag [87]

The distribution of the longitudinal bending stress taking into consideration the effect of shear lag is shown in Figs.A.18 and A.19. The distribution is parabolic across the width of the top and bottom slabs, and linear along the webs, as shown.

The stresses at the top and bottom of the web can be calculated using the following equations.

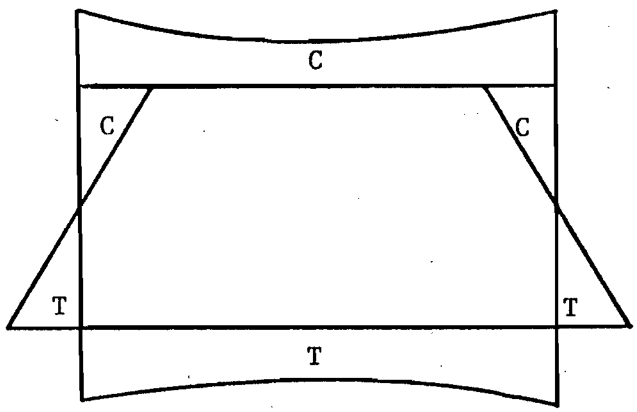

Fig.A.18 Shear Lag Effects

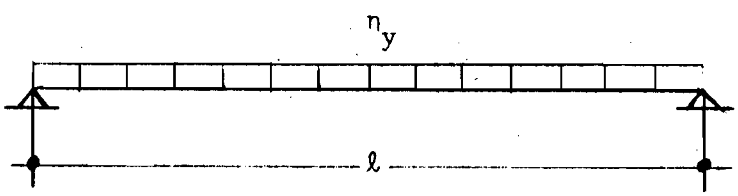

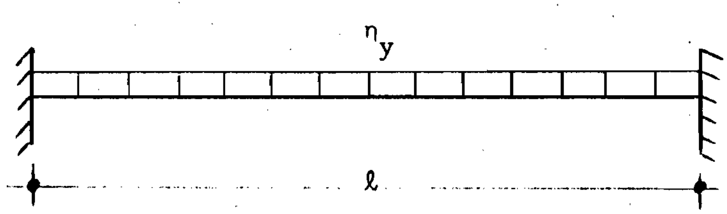

Fig.A.19 Load Cases for Shear Lag Analysis

A.7.1 CASE 1. No Warping Restraint and No Bending Restraint at Supports

A.7.1.1 Uniformly Distributed Vertical Loading η_y Over Entire Span

At midspan

$$f_{vlg} = \pm \frac{\eta_y \ell^2}{8 I_x} \cdot \frac{d}{2} \left[1 + \frac{4(k_{33} - 1)}{k_{34}\ell} \left(\tanh \frac{k_{34}\ell}{2} - \frac{2}{k_{34}\ell} + \frac{2}{k_{34}\ell \cosh \frac{k_{34}\ell}{2}} \right) \right] \qquad \text{(A.85)}$$

where f_{vlg} = longitudinal bending stress at the top and the bottom of the web, considering shear lag effect

η_y = intensity of vertical distributed loading

$$k_{33} = \frac{1}{1 - \frac{5}{12} \frac{bd^2 h_{top}}{I_x}}$$

$$k_{34} = \frac{2}{b} \sqrt{\frac{5k_{33}\, G}{2E}}$$

G = shear modulus of elasticity.

A.7.2 CASE 2. Full Warping Restraint and Bending Restraint at Supports

A.7.2.1 Uniformly Distributed Vertical Loading η_y Over Entire Span

At supports

$$f_{vlg} = \pm \frac{\eta_y \ell^2}{2I_x} \cdot \frac{d}{2} \frac{1}{6} + \frac{k_{33} - 1}{k_{34}\ell} \frac{1}{\tanh \frac{k_{34}\ell}{2}} - \frac{2}{k_{34}\ell} \qquad \text{(A.86)}$$

At midspan

$$f_{vlg} = \pm \frac{\eta_y \ell^2}{2I_x} \cdot \frac{d}{2} \left[\frac{1}{12} + \frac{k_{33} - 1}{k_{34}\ell} \left(\frac{2}{k_{34}\ell} - \frac{1}{\sinh \frac{k_{34}\ell}{2}} \right) \right] \tag{A.87}$$

In Equations A.85, A.86 and A.87, the second term in the square bracket gives the increase in longitudinal bending stress at the web due to shear lag.

A.8 Computer Program for the Analysis of Box Girder Bridges

The listing of the computer program developed for the available methods for the analysis of box girder bridges summarized in Sections A.1 through A.7 is given below, along with the requirement for the input data.

The program calculates the stresses in the top slab over both webs and at the tips of the cantilever slabs, and in the lower slab beneath the webs.

The program has the following features:

1) The complete longitudinal and transverse stresses within the box section at different locations through the bridge span are calculated.

2) The program can handle a box section with and without side cantilever.

3) The program can handle both simply-supported and fixed-ended conditions for any bridge span.

The analysis consists of the following operations:

1) Input bridge data

2) Calculation of the longidutinal bending and St. Venant torsional shear stresses

3) Calculation of the distortion transverse bending stresses using the Knittel Method

4) Calculation of the distortional transverse bending stresses and the distortional longitudinal warping stresses using the equivalent beam theory

5) Calculation of the distortional transverse bending stresses and the distortional longitudinal warping stresses using the Kupfer Method

6) Calculation of the longitudinal torsional warping stresses using the Kollbrunner and Hajdin Method

7) Calculation of the distortional transverse bending stresses and the longitudinal distortion warping stresses using the beam-on-elastic foundation method.

Restrictions

Units must be consistent throughout the program. The program handles only box sections with constant wall thickness.

List of Symbols

B	width of the box section between the webs
BCAN	width of the cantilever slab
HT	thickness of the top slab
HB	thickness of the lower slab
HW	thickness of the web
D	depth of the cross-section (distance between the centrelines of the top and bottom flanges)
L	bridge span
P	load
G	shear modulus of concrete
E	elastic modulus of concrete
WDL	self weight of bridge per unit length
BC	boundary condition: 1 fixed end 0 simply supported

Input Data

First Card

READ B, BCAN, HT, HB, HW, O

FORMAT 6 F10.5

Second Card

READ L, P, G, E

FORMAT 4 E15.5

Third Card

READ WDL, BC

FORMAT F10.5, I5

Output Data

(See the listing of the Computer Program)

```
$WATFIV SOLIMAN,PAGES=400,TIME=60
C
C
C
C      METHOD OF ANALYSIS AND DESIGN OF BOX GIRDER BRIDGES
C
C
C
      REAL IX,IY,L,MDWR,IEFF,   K1,K2,K9,K8,K7,K6,K5,K4,K3,K10,K11,K12
     $,K13,K14,K15,K16,K17,K19,K18,LL,K20,K21,K66,K77,K25,K44,K26,
     $K27,K30,K29,NY1,NY2,ITOP,IBOT,IWEB,LCH,MTRBT,MTRBB,IFRA
      READ(5,10)B,BCAN,HT,HB,HW,D
   10 FORMAT(6F10.5)
      READ(5,15)L,P,G,E
   15 FORMAT(4F15.5)
      READ(5,19) WDL,KS
   19 FORMAT(F10.5,I5)
C
C
C
C     ************************************************************************
C      ANALYSIS OF SIMPLE BENDING AND ST VENANT TORION
C     ************************************************************************
C
C
C
      PI=3.1415
      BMX=P*L/8.0
      T=P*B/2.
      V=P/4.0
      XCG=(B*HB*D+2.*HW*D*D/2.)/((B+2.*BCAN)*HT+B*HB+2.*HW*D)
      IX=(((B+2.*BCAN)*(HT**3.))/12.)+(B+2.*BCAN)*HT*(XCG**2.)+((B*(HB**
     $3.))/12.)+B*HB*((D-XCG)**2.)+2.*((HW*(D**3)/12.)+(HW*D*((D/2.)-XCG
     $)**2))
      IY=(HT*((B+2.*BCAN)**3)/12.)+(HB*(B**3)/12.)+2.*(D*HW*((B*.5)**2)
     $+D*(HW**3)/12.0)
      AYC=BCAN*HT*XCG
      AYB=.5*B*HB*(D-XCG)
      AYF=.5*B*HT*XCG
      AYM=(B+BCAN)*HT*XCG+HW*((XCG-HT*.5)**2.0)/2.0
      VLC=(V*AYC)/(IX*HT)
      VLF=(V*AYF)/(IX*HT)
      VLB=(V*AYB)/(IX*HB)
      VLM=(V*AYM)/(IX*HW)
      AENC=B*D
      VSVT=T/(2.*AENC*HT)
      VSVB=T/(2.*AENC*HB)
      VSVW=T/(2.*AENC*HW)
      WRITE(6,16)XCG,IX,IY
   16 FORMAT(3F20.10)
      MDLC=WDL*(L**2)/24.0
      MDLS=WDL*(L**2)/12.0
      FDLTC=MDLC*(XCG+0.5*HT)/IX
      FDLBC=MDLC*(D-XCG+0.5*HB)/IX
      FDLTS=MDLS*(XCG+0.5*HT)/IX
      FDLBS=MDLS*(D-XCG+0.5*HB)/IX
      FLTC=BMX*(XCG+0.5*HT)/IX
      FLBC=BMX*(D-XCG+0.5*HB)/IX
      FLTS=BMX*(XCG+0.5*HT)/IX
      FLBS=BMX*(D-XCG+0.5*HB)/IX
      WRITE(6,17)
   17 FORMAT('1',//,10X,'STRESSES DUE TO DEAD LOAD')
```

```
      WRITE(6,18)FDLTC,FDLBC,FDLTS,FDLBS
   18 FORMAT(/,4F20.10)
      WRITE(6,20)
   20 FORMAT('1',//,10X,'ANALYSIS OF  SIMPLE BINDING AND ST VENANT TORTIO
     $N')
      WRITE(6,25)
   25 FORMAT(//,8X,'FLT',11X,'FLB',12X,'VLC',11X,'VLF',10X,'VLB',10X,'VL
     $M',10X,'VSVT',10X,'VSVB',10X,'VSVW')
      WRITE(6,30)FLTC,FLBC,FLTS,FLBS,VLC,VLF,VLB,VLM,VSVT,VSVB,VSVW
   30 FORMAT(/,11F10.5)
C
C
C
C
C     ***************************************************************
C     ANALYSIS OF SIMPLE BENDING & TORION AND DISTORION BY KNITTEL
C     ***************************************************************
C
C
C
C     TRANSVERSE NORMAL STRESSES PER UNIT LENGTH (SYMMETRIC LOADING)
C
      DO 1000 I=1,2
      XX=I-1
      Z=(L*XX)/2.0
      X=L/2.0
      QX=(2.*P/L)*SIN(PI*X/L)*SIN(PI*Z/L)*0.5
      ATOP=B*HT
      ACAN=BCAN*HT
      ABOT=B*HB
      CT=QX*(ATOP*B-4.*ACAN*BCAN)*XCG/(4.*IX)
      TT=QX*ACAN*BCAN*XCG/IX
      TB=QX*ABOT*B*(D-XCG)/(4.*IX)
      CW=QX
      WRITE(6,40)
   40 FORMAT('1',//,10X,'SIMPLE BENDING,TORTION AND DISTORION BY KINIYTE
     $L METHOD')
      WRITE(6,45)
   45 FORMAT(//,10X,'SYMMETRIC LOADING')
      WRITE(6,49)
   49 FORMAT(//,12X,'CT',15X,'TT',17X,'TB',16X,'CW')
      WRITE(6,50)CT,TT,TB,CW
   50 FORMAT(/,4F20.10)
C
C     ANALYSIS FOR UNTISYMMETRIC LOADING
C
      V5T=QX*B/(2.*D)
      V6B=QX*B/(2.*D)
      V7W=QX*B/(2.*D)
      WRITE(6,55)
   55 FORMAT(////,10X,'UNTISYMMETRIC LOAD')
      WRITE(6,59)
   59 FORMAT(//,12X,'V5T',15X,'V6B',17X,'V7W')
      WRITE(6,60)V5T,V6B,V7W
   60 FORMAT(/,3F20.10)
C
C     A MOMENT DISTRUBUTION ANALYSIS IS BERFORMED TO CALCULAT INTERNAL
C     FORSES FOR THE CLOSED FRAME
C
C
```

```
C
C     ******************************************************************
C     ANALYSIS OF DISTORTION AND DISTORIONAL WARPING BY THE EQUIVELANT
C     BEAM METHOD
C     ******************************************************************
C
      ITOP=(HT*((B+2.*BCAN)**3))/12.
      IBOT=(HB*(B**3))/12.
      ATE=(2.*ITOP)/(B**2)
      ABE=(2.*IBOT)/(B**2)
      AWE=D*HW
      DCGE=(D*ABE+(D/2.)*AWE)/(ATE+ABE+AWE)
      IEFF=ATE*(DCGE**2)+ABE*((D-DCGE)**2)+(HW*(D**3))/12.+AWE*(((D/2.)-
     $DCGE)**2)
      K1=((1./(E*IEFF))*(L**4)/(PI**4))*SIN(PI*Z/L)*0.25
C
C
C     K1: BENDING FLEXIBILITY OF ONE EQUIVELANT BEAM
C     K2:THE PROPORTION OF APPLIED TORTIONAL MOMENT TAKEN IN PURE TRTION
C     B1:THE DIAPHRAGM SHEAR FLEXIBILITY (MOMENT DISTRUBUTION)
C     QXS:LOAD CARRED BY TORTIONAL SHEAR FLOW AROUND THE PERIMETER
C     QXX; LOAD CARRED BY DIFFERENTIOL BENDING
C
C
      B1=0.021
      K2=0.9
      QXX=QX*(1.0/(((8.0*K1)/(B*B1))+1.0))
      QXS=QX/(2.*((B*B1)/(8.*K1)+1.))
      MDWR=QXX*((L**2)/(PI**2))
      FDWT=MDWR*DCGE/IEFF
      FDWB=MDWR*(D-DCGE)/IEFF
C
C
C     THE STRESSES AT THE END OF CANTELEVER IS OBTAIND BY INTERPOLAION
C
C
C     VERTICAL DIFLECTION DUE TO SYMMETRIC LOADING 'DLS'
C
C
      DLS=(2.*(L**4))/(E*IX*(PI**4))*QX
C
C     VERTICAL DIFLECTION DUE TO TORSIONAL LOAD 'DTU'
C
C     TZ: TOTAL INTERNAL TORSIONAL MOMENT AT SECTION 'Z'
      TZ=T/2.
      SPEE=(1./G)*((B/HT)+(B/HB)+(2.*D)/HW)
      TSVT=TZ*K2
      DTHE=((TSVT*SPEE)/(4.0*(AENC**2)))*L/2.0
      DTV=DTHE*B/2.0
C
C     VERTICAL DIFLECTION DUE TO DISTORTIONAL  'DDIS'
C
      DDIS=QXX*((L**4)/(E*IEFF*(PI**4)))
      WRITE(6,65)
   65 FORMAT('1',///,10X,'ANALYSIS OF DIS.AND DIS.WARPING BY EQUIVELANT
     *BEAM THEORY')
      WRITE(6,61)K2
   61 FORMAT(/,F20.10)
      WRITE(6,62)
   62 FORMAT(//,6X,'FDWT',15X,'FDWB',20X,'DLS',18X,'DTV',18X,'DDIS')
```

```
      WRITE(6,70)FDWT,FDWB,DLS,DTV,DDIS
   70 FORMAT(/,5F20.10)
C
C
C
C     *****************************************************************
C     DISTORION & DISTORIONAL WARPING BY KUPFERS METHOD
C     *****************************************************************
C
C
      K9=(B*(HW**3))/(D*(HB**3))
      K8=(B*(HW**3))/(D*(HT**3))
      K7=(B*HB)/(D*HW)
      K6=((B*HT)/(D*HW))*(((B+2.*BCAN)/B)**3)
      K5=(3.+2.*(K8+K9)+K8*K9)/(6.+K8+K9)
      K4=(3.+2.*(K6+K7)+K6*K7)/(6.+K6+K7)
C
C
C     K3:PERCINTAGE OF LOAD BETWEEN SYSTEM 1 & 2
C     NY1:LOAD TAKEN BY SYSTEM 1
C     NY2: LOAD TAKEN BY SYSTEM 2
C     FDWT1,FDWB1 ARE THE LONGITUDINAL STRESSSES IN SYSTEM 1
C     FDWT2,FDWB2 ARE TYE LONGITUDINAL STESSES IN SYSTEM 2
C
C
      K3=K4*K5*((PI**4)/48.)*(((B*(D**2))/(HW*(L**2)))**2)
      NY1=2.*QX*K3/(1.+K3)
      NY2=2.*QX*1.0/(1.0+K3)
      K10=(4.*E*(HW**3))/(D*K5*(B**2))
      FDWB1=(0.25*NY1*(L**2)*(D-DCGE))/(0.5*IEFF*(PI**2))*0.5
      FDWT1=(0.25*NY1*(L**2)*DCGE)/(IEFF*0.5*(PI**2))*0.5
      K66=((B*HT)/(D*HW))*(((B+2.*BCAN)/B)**3)
      K77=(B*HB)/(D*HW)
      K44=(3.+2.*(K66+K77)+K66*K77)/(6.+K66+K77)
      CDWR=((B**2)*(D**3)*HW*K44)/48.0
      ITOP=(HT**3)/11.5
      IBOT=(HB**3)/11.5
      IWEB=(HW**3)/11.5
      K26=1.0+(((2.0*B/D)+(3.0*((ITOP+IBOT)/IWEB)))/(((ITOP+IBOT)/IWEB)
     $+(6.0*D/B)*(ITOP*IBOT)/(IWEB**2)))
       IFRA=(   24.0*IWEB)/(K26*D)
      K27=(IFRA/(4.0*CDWR))**0.25
      M2=(-TEXT/(8.0*K27))*(1.0/(SINH(K27*L)+SIN(K27*L)))*((SIN(K27*(Z-
     $L/2.0))*(SINH(K27*(Z-L/2.0))+SINH(K27*((3.0*L/2.0)-Z))))+(SINH(K27
     $*(Z-L/2.0)))*(SIN(K27*(Z-L/2.0))+SIN(K27*((3.0*L/2.0)-Z)))-COS(K27
     $*(Z-L/2.0))*COSH(K27*((3.0*L/2.0)-Z))+COSH(K27*(Z-L/2.0))*COS(K27*
     $((3.0*L/2.0)-Z)))
      LCH=1.0/K11
      FDWT2=(M2*DCGE)/(0.5*IEFF)
      FDWB2=M2*(D-DCGE)/(0.5*IEFF)
C
C     TRANSVERSE BENDING STRESSES DUE DISTORTION
C
      BMTD=(P*B/(16.0*LCH))*((3.0+K9)/(6.0+K8+K9))
      BMBD=(P*B/(16.0*LCH))*((3.0+K8)/(6.0+K8+K9))
      FDTS=(6.*BMTD)/(HT**2)
      FDTW=(6.*BMTD)/(HW**2)
      FDBS=(6.*BMBD)/(HB**2)
      FDBW=(6.*BMBD)/(HW**2)
C
```

```
C     TRANSEVERSE BENDING STRESSES DUE TORTION
C
      K12=(E*K4*(PI**2))/(G*48.0*(L**2))*(D**2/(1.+K3))*((B*HW/(D*HT))
     $+(B*HW/(D*HB))-2.0)
      BMTT=(QX*B*K12/8.)*((3.+K9)/(6.+K8+K9))*2.0
      BMTB=(QX*B*K12/8.)*((3.+K8)/(6.+K8+K9))*2.0
      FTTS=(6.*BMTT)/(HT**2)
      FTTW=(6.*BMTT)/(HW**2)
      FTBS=(6.*BMTB)/(HB**2)
      FTBW=(6.*BMTB)/(HW**2)
      WRITE(6,75)
   75 FORMAT('1',///,10X,'DISTORION&DISTORIONAL WARPING BY KUPFERS METHO
     $D')
      WRITE(6,79)
   79 FORMAT(//,9X,'FDWT1',14X,'FDWB1',12X,'FDWT2',16X,'FDWB2')
      WRITE(6,80)FDWT1,FDWB1,FDWT2,FDWB2
   80 FORMAT(/,4E20.10)
      WRITE(6,82)
   82 FORMAT(////,9X,'FDTS',14X,'FDTW',14X,'FDBS',14X,'FDBW')
      WRITE(6,85)FDTS,FDTW,FDBS,FDBW
   85 FORMAT(/,4E20.10)
      WRITE(6,86)
   86 FORMAT(////,9X,'FTTS',14X,'FTTW',14X,'FTBS',14X,'FTBW')
      WRITE(6,85)FTTS,FTTW,FTBS,FTBW
C
C
C
C     ******************************************************************
C     ANALYSIS OF TORTIONAL BY THE METHOD OF KOLLBRUNER
C     ******************************************************************
C
C
      K13=0.25*B*HB*HW*(0.333*B*HB+3.0*D*HW)
      K14=B*D*HT*(0.166*(HB**2)-(0.25*(HW**2)))
      K15=0.5*HT*HB*HW*(0.166*(B**2)+(D**2))
      K16=BCAN*HT*HB*HW*(BCAN+B)
      K17=B*HW*(HT+HB)+2.0*HT*HB*D
C
C
C
C     DSHC: DEPTH OF SHEAR CENTER FROM TOP C-L
C     CSVT: TORTIONAL MOMENT OF INERTIA
C     CCEN: CENTRAL TORTIONAL MOMENT OF INERTIA
C     CTWR:TORTIONAL WARPING MOMENT OF INERTIA
C     BTWR:BIMOMENT OF TORTIONAL WARPING
C     TSVT: TORTIONAL MOMENT OT CROSS SECTION IN ST VENANT TORTION
C     TTWR:TORTIONAL MOMENT AT CROSS SECTION IN TORTOINAL WARPING
C
C
C
      DSHC=(((K13+K14+K15+K16)/K17)*D*(B**2))/IY
      CSVT=(4.*(AENC**2))/((B/HT)+(B/HB)+(2.*D/HW))
      ABT=DSHC
      ABW=B/2.
      ABB=D-DSHC
      LL=CSVT/(2.*AENC)
      WTWT=(ABT-LL/HT)*B/2.0
      WTWC=WTWT+ABT*BCAN
      WTWB=WTWT+(ABW-(LL/HW))*D
      CTWR=2.*(BCAN**2)*(HT/3.)*(WTWC**2+WTWT**2-WTWC*WTWT)+2.*(D**2)
```

```
     $*(HW/3.0)*(WTWT**2+WTWB**2-WTWT*WTWB)+(HT/3.)*(B**2)*(1.*(WTWT**2)
     $)+(HB/3.)*(B**2.)*(1.*(WTWB**2))
      CCEN=(HT*(B+2.*BCAN)*(ABT**2))+(2.*D*HW*((B/2.)**2))+(B*HB*((D-ABT
     $)**2))
      K19=CCEN/(CCEN-CSVT)
      CTWRD=K19*CTWR
      K18=SQRT((G*CSVT)/(E*CTWRD))
      TEXT=P*B/2.0
      A2=L-Z
      K20 =((K18*K19*A2-SINH(K18*A2))*(1.0-COSH(K18*L))-(1.0-COSH(K18*A2
     $))*(K18*K19*L-SINH(K18*L)))/(K18*K19*(2.0-2.0*COSH(K18*L)+K18*K19*
     $L*SINH(K18*L)))
      K21=((1.0-COSH(K18*L))*(1.0-COSH(K18*A2))+SINH(K18*L)*(K18*K19*A2-
     $SINH(K18*A2)))/(2.0-2.0*COSH(K18*L)+K18*K19*L*SINH(K18*L))
      BTWR=TEXT*(K20*COSH(K18*Z)+(K21/(K18*K19))*SINH(K18*Z))
      TSVT=TEXT*(-K20*K19*SINH(K18*Z)+K21*(1.0-(1.0/K19)*COSH(K18*Z)))
      TTWR=TEXT*(K20*K18*SINH(K18*Z)+(K21/K19 )*COSH(K18*Z))
      ANGL=(TEXT/(G*CSVT))*(K20*(1.0-COSH(K18*Z))+K21*(Z-(1.0/(K18*K19))
     $*SINH(K18*Z)))
C
C     FTWR:TORTIONAL WARPING STRESSES
C
      FTWRT=BTWR*WTWT/CTWR
      FTWRC=BTWR*WTWC/CTWR
      FTWRB=BTWR*WTWB/CTWR
C
C     VTWR;TORTIONAL WARPING SHEAR STRESSES
C
      BB=TTWR/(CCEN-CSVT)
      VTWRT=BB*WTWT/(B/2.)
      VTWRC=BB*(WTWC-WTWT)/BCAN
      VTWRW=BB*(WTWB-WTWT)/D
      VTWRB=BB*(-WTWB/(B/2.0))
C
C     VSVT: ST VENANT SHEAR STRESSES
C
      VSVTT=TSVT/(2.*AENC*HT)
      VSVTW=TSVT/(2.*AENC*HW)
      VSVTB=TSVT/(2.*AENC*HB)
      DIF=ANGL*P/2.0
      WRITE(6,90)
   90 FORMAT('1',///,10X,'ANALISIS OF TORTIONAL WARPING BY KOLLBRANNER
     $METHOD')
      TOTAL=TTWR+TSVT
      WRITE(6,89)TTWR,TSVT,TOTAL,TEXT
   89 FORMAT(4F20.10)
      WRITE(6,91)
   91 FORMAT(//,6X,'CSVT',14X,'CCEN',12X,'CTWR')
      WRITE(6,95)CSVT,CCEN,CTWR
   95 FORMAT(/ ,3F20.10)
      WRITE(6,100)
  100 FORMAT(//,10X,'TORTIONAL WARPING STRESSSES')
      WRITE(6,101)
  101 FORMAT(//,6X,'FTWRT',14X,'FTWRC',12X,'FTWRB')
      WRITE(6,95)FTWRT,FTWRC,FTWRB
      WRITE(6,105)
  105 FORMAT(//,10X,'TORTIONAL WARPING SHEAR STRESSSES')
      WRITE(6,106)
  106 FORMAT(//,3X,'VTWRT',12X,'VTWRC',11X,'VTWRW',12X,'VTWRB')
      WRITE(6,110)VTWRT,VTWRC,VTWRW,VTWRB
```

```
 110 FORMAT(/ ,4E20.10)
     WRITE(6,115)
 115 FORMAT(//,10X,' ST VENANT SHEAR STRESSES')
     WRITE(6,116)
 116 FORMAT(//,9X,'VSVTT',12X,'VSVTW',11X,'VSVB')
     WRITE(6,95)VSVTT,VSVTW,VSVB
     WRITE(6,120)
 120 FORMAT(///,20X,'  DEFLECTION')
     WRITE(6,125)DIF
 125 FORMAT(/,6X,F20.10)
C
C
C
C     ****************************************************************
C     DISTORTIONA&DISTORTIONAL WARPING BY BEAM ON ELASTIC FOUNDATION
C     ****************************************************************
C
C
      K66=((B*HT)/(D*HW))*(((B+2.*BCAN)/B)**3)
      K77=(B*HB)/(D*HW)
      K25=(3.0+K66)/(3.0+K77)
      WDWFC=((B+2.0*BCAN)/B)*B*D/(4.0*(1.0+K25))
      WDWFW=B*D/(4.*(1.0+K25))
      WDWFB=(K25*B*D)/(4.0*(1.0+K25))
C
C     CDWR:DISTORIONAL WARPING MOMENT OF INRTIA
C     FDWR: DISTORTIONAL WARPING STRESSES
C     EIFRA: FRAME STIFFNESS
C
      K44=(3.+2.*(K66+K77)+K66*K77)/(6.+K66+K77)
      CDWR=((B**2)*(D**3)*HW*K44)/48.0
      ITOP=(HT**3)/11.5
      IBOT=(HB**3)/11.5
      IWEB=(HW**3)/11.5
      K26=1.0+(((2.0*B/D)+(3.0)*((ITOP+IBOT)/IWEB)))/(((ITOP+IBOT)/IWEB)
     $+(6.0*D/B)*(ITOP*IBOT)/(IWEB**2)))
       IFRA=(   24.0*IWEB)/(K26*D)
      K27=(IFRA/(4.0*CDWR))**0.25
      BDWR=(-TEXT/(8.*K27))*(1.0/(SINH(K27*L)+SIN(K27*L)))*((SIN(K27*(Z-
     $L/2.0))*(SINH(K27*(Z-L/2.0))+SINH(K27*((3.0*L/2.0)-Z))))+(SINH(K27
     $*(Z-L/2.0)))*(SIN(K27*(Z-L/2.0))+SIN(K27*((3.0*L/2.0)-Z)))-COS(K27
     $*(Z-L/2.0))*COSH(K27*((3.0*L/2.0)-Z))+COSH(K27*(Z-L/2.0))*COS(K27*
     $((3.0*L/2.0)-Z)))
      FDWRC=BDWR*WDWFC/CDWR
      FDWRW=BDWR*WDWFW/CDWR
      FDWRB=BDWR*WDWFB/CDWR
C
C     FTRB: TRANSEVERSE BENDING STRESSES
C
      K30=(3.0+(B*IWEB)/(D*ITOP))/(3.0+(B*IWEB)/(D*IBOT))
      BTRB=((TEXT*K27)/(4.0*E*IFRA*(SINH(K27*L)+SIN(K27*L))))*(SIN(K27*(
     $Z-L/2.0))*SINH(K27*((3.0*L/2.0)-Z))-SINH(K27*(Z-L/2.0))*SIN(K27*((
     $3.0*L/2.0)-Z))-COS(K27*(Z-L/2.0))*(COSH(K27*(Z-L/2.0))-COSH(K27*(3
     $.0*L/2.0)-Z))-COSH(K27*(Z-L/2.0))*(COS(K27*(Z-L/2.0))-COS(K27*(3.0
     $*L/2.0)-Z)))
      MTRBT=E*IFRA*BTRB/(2.*(1.0+K30))
      MTRBB=-K30*E*IFRA*BTRB/(2.0*(1.0+K30))
      FTRBT=6.0*MTRBT/(HT**2)
      FTRBB=6.0*MTRBB/(HB**2)
      FTRBWT=6.0*MTRBT/(HW**2)
```

```
      FTRBWR=6.0*MTRBB/(HW**2)
      WRITE(6,130)
  130 FORMAT('1',//,10X,'DISTORTIONAL AND DISTORTIONAL WARPING BY BEAM
     $ON ELASTIC FOUNDATIONMETHOD')
      WRITE(6,135)
  135 FORMAT(//,10X,'DISTORTONAL WARPING STRESSES')
      WRITE(6,136)
  136 FORMAT(//,5X,'FDWRC',12X,'FDWRW',12X,'FDWRB')
      WRITE(6,140)FDWRC,FDWRW,FDWRB
  140 FORMAT(/,3E20.10)
      WRITE(6,145)
  145 FORMAT(////,10X,'TRANSEVERSE BENDING STRESSES')
      WRITE(6,146)
  146 FORMAT(//,5X,'FTRBT',12X,'FTRBB',12X,'FTRBWT',12X,'FTRWR')
      WRITE(6,150)FTRBT,FTRBB,FTRBWT,FTRBWR
  150 FORMAT(/,4E20.10)
C
C     VDWR: DISTORTIONAL WARPINH SHEAR STRESSES
C
      K29=(B+2.0*BCAN)/B
      AWEB=D*HW
      Q1=(K29*(ATOP+2.0*ACAN)/4.0)+((5.0-4.*K25)*AWEB/12.0)
     $-(K25*ABOT/12.0)
      Q2=(((K29**2)-1.0)*(ATOP+2.*ACAN)/(4.*K29))+((5.0-4.*K25)*
     $AWEB/12.0)-(K25*ABOT/12.0)
      Q3=((K29**2)-1.0)*(ATOP+2.0*ACAN)/(4.0*K29)
      Q4=(K29-1.0)*(3.0*K29+1.0)*(ATOP+2.0*ACAN)/(16.0*K29)
      Q5=Q2-Q3
      Q6=((1.0-5.0*K25)*AWEB      /24.0)-(K25*ABOT/12.0)
      Q7=(-(1.0-2.0*K25)*AWEB/12.0)-(K25*ABOT/12.0)
      Q8=Q7
      Q9=(K25*ABOT/4.0)-((1.0-2.0*K25)*AWEB/12.0)-(K25*ABOT/12.0)
      DBDWR=(-0.25*TEXT/(SINH(K27*L)+SIN(K27*L)))*(COSH(K27*(Z-0.5*L))
     $*(SIN(K27*(Z-0.5*L))+SIN(K27*(1.5*L-Z)))+COS(K27*(Z-L*0.5))
     $*(SINH(K27*(Z-0.5*L))+SINH(K27*(1.5*L-Z))))
      VV=-DBDWR*B*D/(CDWR*4.0*(1.0+K25))
      V1=VV*DBDWR*Q1/HT
      V2=VV*DBDWR*Q2/HT
      V3=VV*DBDWR*Q3/HT
      V4=VV*DBDWR*Q4/HT
      V5=VV*DBDWR*Q5/HW
      V6=VV*DBDWR*Q6/HW
      V7=VV*DBDWR*Q7/HW
      V8=VV*DBDWR*Q8/HB
      V9=VV*DBDWR*Q9/HB
      WRITE(6,155)
  155 FORMAT(////,10X,' DISTORTIONAL WARPING SHEAR STRESSES')
      WRITE(6,156)
  156 FORMAT(//,5X,'V1',10X,'V2',10X,'V3',10X,'V4',10X,'V5',10X,'V6',10X
     $,'V7',10X,'V8',10X,'V9')
      WRITE(6,160)V1,V2,V3,V4,V5,V6,V7,V8,V9
  160 FORMAT(/,9E13.6)
 1000 CONTINUE
      STOP
      END
```

APPENDIX B

APPENDIX B

ANALYSIS FOR PURE TORSION

B.1 General

Combined torsion, bending and shear is a frequent loading combination encountered in many structures and perhaps it is the most complex loading combination to analyse. Current design procedure is based on the individual analysis and design procedure for each type of loading. The torsional stiffness of the section is generally determined using Bredt's formula for elastic analysis of the uncracked section. Once the section cracks, this method cannot be used because the section is no longer a homogeneous continuum. Test results show that the torsional stiffness of a concrete member is influenced by cracking and interaction with other types of loadings [78,106]. The ultimate capacity of the structure after cracking in this case is a function of the strengths of the reinforcement and the concrete and also of the ratio between width and depth of the section and the ratio between the cross-sectional areas of the longitudinal and the transverse reinforcements. In 1929 Wagner developed a tensile stress field theory to study the post-buckling resistance of thin walled metal beams. However, in discussing Wagner's work, Elfgren [106] suggested that a better name for the model used by Wagner would be "the compressive field theory" or the more commonly used name the "truss analogy". Mitchell [93] used a similar compression field theory to analyse reinforced concrete beams subjected to pure torsion. The longitudinal and transverse reinforcements are considered as tension members of the truss while the concrete regions between cracks are regarded as compression struts. It is assumed that all compressive stresses are concentrated within the diagonals between the cracks.

B.2 Computer Program

The computer program developed for the diagonal compression field theory was adopted from Reference [93]. For completeness, the input data and output data, and the listing of the program are given below. The program analyses the complete behaviour of structural concrete sections subjected to pure torsion and has the following features:

1) The complete torque-twist relationship, hoop stresses and strains, longitudinal stresses and strains, concrete surface strain and the inclination of the diagonal strut.

2) A wide variety of cross-sectional shapes can be handled (e.g., circular, triangular, rectangular and T-shaped sections).

3) The program handles both reinforced and prestressed concrete beams.

4) Different shapes of stress-strain curves can be used for both steel and concrete.

Restrictions

Units must be consistent throughout the program.

Only St. Venant torsional response is predicted.

List of Symbols

BMNO beam number

NJ total number of joints

SOURCE name of investigator

JUNTR	number of joints
X(I)	X- coordinate
Y(I)	Y- coordinate
XH(I)	hoop X- coordinate
YH(I)	hoop Y- coordinate
T	least wall thickness in the cross-section
AC	cross-sectional area of concrete
FPC	strength of concrete
EO	strain of concrete when $f_c = f'_c$
BETA	inclination of concrete struts (in degrees)
AH	area of one hoop leg
S	hoop spacing
ES(1)	modulus of elasticity of hoop steel
FY(1)	yield strength of hoop steel
FULT(1)	ultimate strength of hoop steel
AL	area of longitudinal steel
ES(2)	modulus of elasticity of longitudinal steel
FY(2)	yield strength of longitudinal steel
FULT(2)	ultimate strength of longitudinal steel
AP	area of prestressing steel
FPI	initial stress in prestressing steel
ES(3)	modulus of elasticity of prestressing steel
FY(3)	yield strength of prestressing steel
FULT(3)	ultimate strength of prestressing steel

Input Data

1) Read	BMNO, NJ, SOURCE	
Format	AS, I2, 6A4	
2) Read	(For each joint) One card for each X and Y outside coordinate	
Format	2F10.0	
3) Read	(For each joint) One card for each XH and YH loop centreline coordinate	
Format	2F10.0	
4) Read	T, AC, FPC, EO, BETA	
Format	5F10.0	
5) Read	AH, S, ES(1), FY(1), FULT(1)	
Format	5F10.0	
6) Read	AL, ES(2), FY(2), FULT(2)	
Format	4F10.0	
7) Read	AP, FPI, ES(3), FY(3), FULT(3)	
Format	5F10.0	

Computer Program Listing

```
C
C       PROGRAM NAME - DIAGONAL COMPRESSION FIELD ANALYSIS
C       PURPOSE - TO ANALYSE THE COMPLETE BEHAVIOUR OF STRUCTURAL
C       CONCRETE BEAMS IN PURE TORSION
C
C       VARIABLE LIST
C
C       AO   AREA ENCLOSED BY SHEAR FLOW
C       AC   CROSS SECTIONAL AREA OF CONCRETE
C       AH   CROSS SECTIONAL AREA OF ONE HOOP LEG
C       AL   TOTAL AREA OF SYMMETRICALLY PLACED LONG REINFORCING
C       AP   TOTAL AREA OF SYMMETRICALLY PLACED PRESTRESSING
C       A  DEPTH OF EQUIVALENT RECTANGULAR STRESS DISTRIBUTION
C       BMNO  BEAM NUMBER
C       EC,ES   MODULUS OF ELASTICITY OF CONCRETE AND STEEL
C       FPC  COMPRESSIVE STRENGTH OF CONCRETE
C       FH,FL,FP   STRESS IN HOOPS, LONG STEEL , AND PRESTRESSING STEEL
C       FY   YIELD STRESS
C       FPI   INITIAL STRESS IN PRESTRESSING STEEL
C       NJ   NUMBER OF SIDES OF CROSS SECTION
C       HOOP CENTERLINE PERIMETER
C       PO   PERIMETER OF SHEAR FLOW PATH
C       Q   SHEAR FLOW
C       S   HOOP SPACING
C       T   LEAST WALL THICKNESS OF CROSS SECTION
C       TD   THICKNESS OF COMPRESSION DIAGONALS
C       TSSC  TYPE OF STRESS STRAIN CUVE
C       X,Y   COORDINATES OF CROSS SECTION
C       XH,YH   HOOP CENTERLINE COORDINATES
C       ALPHA,ANGLE   ANGLE OF DIAGONAL COMPRESSION
C       K1,K2   RECTANGULAR STRESS BLOCK FACTORS
C       BETA  ANGLE OF CONCRETE STRAIN TARGETS
C       E0   STRAIN IN CONCRETE CORRESPONDING TOCOMPRESSIVE STRENGTH
C       ED   CONCRETE DIAG STRAIN AT POSITION OF RESULTANT SHEAR FLOW
C       EDS   CONCRETE DIAGONAL SURFACE STRAIN (COMP POS)
C       EH,EL,EP   STRAINS IN HOOPS , LONG STEEL , AND PRESTRESSING
C        (TENSION POS)
C       DEP   STRAIN DIFFERENCE
C       PSI   TWIST PER UNIT LENGTH
C
        DIMENSION ES(3),FY(3),FULT(3),TITSL(2),SOURCE(6)
        DIMENSION X(30),Y(30),XH(30),YH(30),XP(30),YP(30)
        INTEGER TSSC(3)
        INTEGER BMNO,END
        REAL K1K2,K2,K1
        COMMON /CALCAA/ EL,EP,EH,FL,FP,FH,AL,AP,AH,
       1                 A,AO,PO,EDS,K1K2,K1,K2,FPC,DEP,S,FH,IUNTW
        COMMON /CFFS/ TSSC,ES,FY,FULT
        DATA END/5HEND  /
                                 $
IO38I SIZE WRN.
        IUNTR=5
        IUNTW=6
        IP=5
```

```
      MM=30
      EP=0.
      WRITE(IUNTW,699)
C
C     INPUT BEAM DATA
C
  100 READ(IUNTR,501)BMNO,NJ,SOURCE
      IF(BMNO.EQ.END)GOTO999
      DATA X/30*0.,/,Y/30*0./,XH/30*0./,YH/30*0./
      IF(NJ-1)101,102,103
  101 READ(IUNTR,502)X(1)
      READ(IUNTR,502)XH(1)
      Y(1)=0.
      YH(1)=0.
      GOTO104
  102 READ(IUNTR,502)X(3),Y(3)
      READ(IUNTR,502)XH(3),YH(3)
      Y(2)=Y(3)
      X(4)=X(3)
      YH(2)=YH(3)
      XH(4)=XH(3)
      NJ=4
      GOTO104
  103 READ(IUNTR,502)(X(I),Y(I),I=1,NJ)
      READ(IUNTR,502)(XH(I),YH(I),I=1,NJ)
  104 READ(IUNTR,503)T,AC,FPC,E0,BETA
      READ(IUNTR,504)AH,S,ES(1),FY(1),FULT(1)
      READ(IUNTR,505)AL,ES(2),FY(2),FULT(2)
      READ(IUNTR,504)AP,FPI,ES(3),FY(3),FULT(3)
  106 WRITE(IUNTW,601)BMNO,SOURCE,NJ,(I,X(I),Y(I),I,XH(I),YH(I),I=1,NJ)
      WRITE(IUNTW,602)T,AC,FPC,E0,BETA
      WRITE(IUNTW,603)AH,S,ES(1),FY(1),FULT(1),AL,ES(2),FY(2),FULT(2)
     1,AP,FPI,ES(3),FY(3),FULT(3)
      BETA=BETA/57.2958
      EPI=FPI/ES(3)
      DO 112 I=1,3
      IF(FULT(I).EQ.0.)GOTO111
      TSSC(I)=2
      GOTO112
  111 TSSC(I)=1
  112 CONTINUE
C
C     CALCULATION OF INITIAL CONDITIONS
C
  120 EC=2.*FPC/E0
      ACPAL=AC+AL*(ES(2)/EC)
      ELI=-(AP*FPI)/(ACPAL*EC)
C
C     CALCULATE STRAIN DIFFERENCE
C
      DEP=EPI-ELI
      DEDS=(1.75*E0)/33.
      CALL SHAPE(XH,YH,MM,NJ,AA,PH)
      NOPG=2
```

```
      DO 399 ISPAL=1,2
      DATA TITSL/2H   ,2HUN/
      WRITE(IUNTW,701)TITSL(ISPAL),BMNO,SOURCE,BMNC,NCPG
      WRITE(IUNTW,700)
      IERR=0
C
C     INITIALIZE A VALUE OF EDS
C
      EDS=1.75*E0
      FL=FY(2)
      FH=FY(1)
      FP=FY(3)
      P0=0.9*PH
      DO 299 I=1,32
C
C     CALCULATE STRESS BLOCK FACTORS
      K1K2=FK1K2(EDS,E0)
C
      K2=FK2(EDS,E0)
      K1=K1K2/K2
C
C     ESTIMATE A
C
      A=(AL*FL+AP*FP)/(K1*FPC*P0)+(AH*FH)/(K1*FPC*S)
      A=AMIN1(A,AA/PH)
      CALL CALCA(XH,YH,XF,YF,MM,NJ,IERR)
      IF(IERR.EQ.1.AND.ISPAL.EQ.1)GOTO397
  211 IF(IERR.EQ.1)GOTO399
C
C     CALCULATE TORQUE AND TWIST
C
      Q=SQRT(((AL*FL+AP*FP)/P0)*(AH*FH/S))
      TORQUE=2.*A0*Q
      PSI=(EDS/2.)*(K1K2*FPC/Q)
      TD=A/K2
      ED=EDS*(1.-K2/2.)
      TANAA=(ED+EL)/(ED+EH*(PH/P0))
      TANA=SQRT(TANAA)
      ALPHA=ATAN(TANA)
      EBETA=(EDS/2.)*(1.+COS(2.*(BETA-ALPHA)))
      ANGLE=ALPHA*57.2958
C
C     OUTPUT RESULTS
C
      WRITE(IUNTW,702)TORQUE,PSI,FH,EH,FL,EL,FP,EP,EDS,ANGLE,TD,A0,P0,EB
     1ETA
      IF((I/IP)*IP.EQ.I)WRITE(IUNTW,703)
C
C     CHOOSE A NEW VALUE OF EDS
C
  299 EDS=EDS-DEDS
C     OUTPUT INITIAL CONDITIONS
      FL=ELI
      FL=ELI*ES(2)
```

```
      EP=FPI/ES(3)
      FF=FPI
      FBETA=(EDS/2.)*(1.+COS(2.*(BETA-ALPHA)))
      WRITE(IUNTW,704)FL,EL,FP,EP,EDS,FBETA
  397 DO 398 I=1,NJ
      XH(I)=X(I)
  398 YH(I)=Y(I)
  399 NOPG=NOPG+1
      GOTO100
  900 WRITE(IUNTW,999)
      STOP
  999 FORMAT(1H1)
C
C ***INPUT FORMAT
C
  505 FORMAT(F10.0,-3PF10.0,0P2F10.0)
  504 FORMAT(2F10.0,-3PF10.0,0P2F10.0)
  503 FORMAT(3F10.0,3PF10.0,0PF10.0)
  502 FORMAT(2F10.0)
  501 FORMAT(A5,I2,6A4)
C
C ***OUTPUT FORMAT
C
  601 FORMAT(1H0/18X,11HBEAM NO. - ,A5,10H SOURCE - ,6A4/
     118X,7H=======,10X,6H======//
     15X,16HSECTION GEOMETRY/
     15X,16H======= ========//
     15X,16HNO. OF JOINTS = ,I2//
     15X,19HOUTSIDE COORDINATES,7X,27HHOOP CENTRELINE COORDINATES/
     15X,19H------- -----------,7X,27H---- ---------- -----------/
     15X,5HJOINT,4X,1HX,6X,1HY,13X,5HJOINT,3X,2HXH,5X,2HYH/(
     17X,I2,2X,F6.2,1X,F6.2,13X,I2,2X,F6.2,1X,F6.2))
  602 FORMAT(1H0/5X,20HCONCRETE INFORMATION/
     15X,20H======== ===========//
     15X,66HLEAST WALL     AREA     CONCRETE        PEAK        CONC STRAIN
     *TARGET/
     15X,64HTHICKNESS(T)  (AC)  STRENGTH(FPC)  STRAIN(E0)  INCLINATION(B
     1ETA)/
     16X,F6.3,6X,F7.2,2X,F7.3,7X,F9.5,9X,F4.1///)
  603 FORMAT(1H ,4X,25HREINFORCEMENT INFORMATION/
     15X,25H============= ===========//
     15X,10HHOOP STEEL/
     15X,10H---- -----/
     18X,2HAH,4X,1HS,7X,3HESH,6X,12HFYH     FULTH/
     15X,F6.3,1X,F5.2,1X,-3PF7.2,1X,0PF8.2,1X,F8.2//
     15X,18HLONGITUDINAL STEEL/
     15X,18H------------ -----/
     19X,2HAL,6X,3HESL,6X,12HFYL     FULTL/
     15X,F7.3,1X,-3PF7.2,1X,0PF8.2,1X,F8.2//
     15X,18HPRESTRESSING STEEL/
     15X,18H------------ -----/
     19X,2HAP,6X,3HFPI,4X,3HESP,5X,12HFYP     FULTP/
     15X,F7.3,F8.2,-3PF7.2,0PF8.2,F8.2)
  699 FORMAT(1H1/21X,30(1H*)/
```

```
      *21X,30H*     STRUCTURAL CONCRETE      */
      121X,30H*    BEAM IN PURE TORSION      */
      121X,30H* COMPRESSION FIELD ANALYSIS */
      121X,30H*VERSION 2.0          JAN 1974*/ 21X,30(1H*))
  700 FORMAT(1H0,106H TORQUE   TWIST      HOOP STEEL       LONG.STEEL     PRE
      1S. STEEL  MAX CONC  ALPHA    TD        A0      P)    EBETA /18X,3(15H
      1STRESS STRAIN  ),6HSTRAIN//)
  701 FORMAT(1H1/3X,A2,27HSPALLED SECTION FOR - BEAM ,A5,3H - ,6A4,35X,
      1A5,1H-,I2)
  702 FORMAT(1H ,F6.0,3PF8.2,3(0PF7.1,3PF8.2),F8.2,0PF7.1,F8.2,F9.0,F7.1
      1,3PF7.2)
  703 FORMAT(1H )
  704 FORMAT(1H ,4X,2H0.,4X,4H0.00,4X,3H0.0,4X,4H0.00,2(0PF7.1,3PF8.2),
      13PF8.2,4X,3H0.0,4X,4H0.00,7X,2H0.,4X,3H0.0,3PF7.2)
      END

FECT*  NOTERM,ID,EBCDIC,SOURCE,NOLIST,NODECK,LOAD,NOMAP,NOTEST
FECT*  NAME = MAIN    , LINECNT =       56
 SOURCE STATEMENTS =      116,PROGRAM SIZE =      5400
01 DIAGNOSTICS GENERATED, HIGHEST SEVERITY CODE IS 4
```

```
      SUBROUTINE CALCA(X,Y,XP,YP,MM,NJ,IERR)
C
C ABSTRACT - ITERATION TO FIND A , STEEL STRAINS AND STRESSES
C
      DIMENSION X(MM),Y(MM),XP(MM),YP(MM)
      REAL K1K2,K2,K1
      COMMON /CALCAA/ EL,EP,EH,FL,FP,FH,AL,AP,AH,
     1A,A0,P0,EDS,K1K2,K1,K2,FPC,DEF,S,PH,IUNTW
      DATA ITA,ITE,ATCL,ETCL /150,100,.01,.05/
C
C     ITERATE ON A
C
      DO 400 I=1,ITA
C
C     CALCULATE A0,P0
C
      CALL COORD(X,Y,XP,YP,MM,NJ,A/2.)
      CALL SHAPE(XP,YP,MM,NJ,A0,P0)
C
C     ITERATE ON STEEL STRAINS
C     ITERATE ON STEEL STRAINS - LONGITUDINAL
C
      DO 200 K=1,ITE
      SUM=FL+FP
      EL=(EDS/2.)*(K1K2*FPC*A0)/(AL*FL+AP*FP)-EDS*(1.-K2/2.)
      EP=DEP+EL
      FLTEST=FFS(2,EL)
      FPTEST=FFS(3,EP)
      SUMT=FLTEST+FPTEST
      IF(ABS(SUMT-SUM).LE.ETCL)GOTO210
      FL=.5*(FL+FLTEST)
  200 FP=.5*(FP+FPTEST)
      GOTO900
  210 FL=FLTEST
      FP=FPTEST
C
C     ITERATE ON STEEL STRAINS - HOOP
C
      DO 300 K=1,ITE
      EH=(EDS/2.)*(K1K2*FPC*A0*S)/(AH*FH*PH)-EDS*(1.-K2/2.)
      FHTEST=FFS(1,EH)
      IF(ABS(FHTEST-FH).LE.ETCL)GOTO310
  300 FH=.5*(FH+FHTEST)
      GOTO0900
  310 FH=FHTEST
C
C     RETURN TO A CALCULATIONS
C
      ATEST=(AL*FL+AP*FP)/(K1*FPC*P0)+(AH*FH)/(K1*FPC*S)
      IF(ABS(ATEST-A).LE.ATCL)GOTO410
  400 A=ATEST
      GOTO901
  410 A=ATEST
      RETURN
```

```
C       ERROR ON ITERATIONS
  900 WRITE(IUNTW,950)ITE
      GOTO902
  901 WRITE(IUNTW,951)ITA
  902 IERR=1
      RETURN
  950 FORMAT(1H0,24HNO OF ITERATIONS EXCEEDS I5,11H FOR STRESS/1H1)
  951 FORMAT(1H0,24HNO OF ITERATIONS EXCEEDS I5, 6H FOR A/1H1)
      END


      FUNCTION FFS(K,E)
C
C ABSTRACT - THIS FUNCTION CALCULATES THE STRESS FOR A GIVEN STEEL
C       STRAIN USING EITHER A CONTINUOUS OR BILINEAR FUNCTION
C
      DIMENSION ES(3),FY(3),FULT(3),TSSC(3)
      INTEGER TSSC
      COMMON /CFFS/ TSSC,ES,FY,FULT
      REAL N
C
      IF(TSSC(K).EQ.01)GOTO100
C       CONTINUOUS STRESS STRAIN CURVE
C       INVERSE RAMBERG-OSGOOD POLYNOMIAL
      X=FULT(K)/FY(K)
      N=0.30103/ALOG10(X)
      FFS=ES(K)*E*((1.+(ES(K)*E/FULT(K))**N)**(-1./N))
      RETURN
C       BI-LINEAR STRESS STRAIN CURVE
  100 FFS=ES(K)*E
      IF(FFS.GT.FY(K))FFS=FY(K)
C     BI-LINEAR CURVE IN COMPRESSION
      FYC=-.99*FY(K)
      IF(FFS.LT.FYC)FFS=FYC
      RETURN
      END


      FUNCTION FK1K2(EC,E0)
C
C ABSTRACT - THIS FUNCTION CALCULATES K1K2 (EQUIVALENT STRESS BLOCK
C       MULTIPLIERS) FOR A PARABOLIC STRESS STRAIN CURVE
C
      X=EC/E0
      FK1K2=X*(1.-X/3.)
      RETURN
      END


      FUNCTION FK2(EC,E0)
C
C ABSTRACT - SEE FUNCTION FK1K2
C
      X=EC/E0
      FK2=(4.-X)/(2.*(3.-X))
      RETURN
      END
```

```
RELEASE 2.0                  COORD                  DATE = 78111            17/17/44
      SUBROUTINE COORD(X,Y,XP,YP,MM,NJ,T)
C
C ABSTRACT - CALCULATES INTERIOR COORDINATES GIVEN T
C
      DIMENSION X(MM),Y(MM),XP(MM),YP(MM)
      SIDE(DX,DY)=SQRT(DX*DX+DY*DY)
      IF(NJ.EQ.3)GOTO101
      X(NJ+1)=X(1)
      Y(NJ+1)=Y(1)
      X(NJ+2)=X(2)
      Y(NJ+2)=Y(2)
      M=NJ+1
      DO 100 I=2,M
      DX=X(I)-X(I-1)
      DY=Y(I)-Y(I-1)
      A=SIDE(DX,DY)
      DX=X(I+1)-X(I-1)
      DY=Y(I+1)-Y(I-1)
      B=SIDE(DX,DY)
      DX=X(I+1)-X(I)
      DY=Y(I+1)-Y(I)
      C=SIDE(DX,DY)
      S=0.5*(A+B+C)
      XT=T*SQRT((S-A)*(S-C)/(S*(S-B)))/C
      XP(I)=X(I)+XT*DX+T*DY/C
  100 YP(I)=Y(I)+XT*DY-T*DX/C
      XP(1)=XP(NJ+1)
      YP(1)=YP(NJ+1)
      RETURN
  101 XP(1)=X(1)-2.*T
      RETURN
      END

 FECT*  NOTERM,ID,EBCDIC,SOURCE,NOLIST,NODECK,LOAD,NOMAP,NOTEST
 FECT*  NAME = COORD    , LINECNT =        56
   SOURCE STATEMENTS =         29,PROGRAM SIZE =       1278
 NO DIAGNOSTICS GENERATED
```

```
RELEASE 2.0                SHAPE                 DATE = 78111               17/17/44
        SUBROUTINE SHAPE (X,Y,MM,NJ,A,P)
  C ABSTACT - THIS SUBROUTINE CALCULATES AREA AND PERIMETER
  C       OF AN NJ SIDED POLYGON
  C
        DIMENSION X(MM),Y(MM)
        IF(NJ.EQ.0)GOTO200
        P=0.
        A=0.
        X(NJ+1)=X(1)
        Y(NJ+1)=Y(1)
        DO 100 I=1,NJ
        DX=X(I+1)-X(I)
        DY=Y(I+1)-Y(I)
        P=P+SQRT(DX*DX+DY*DY)
    100 A=A+DX*(Y(I)+0.5*DY)
        RETURN
    200 PI=3.141593
        P=PI*X(1)
        A=P*X(1)/4.
        RETURN
        STOP
  $
 I002I LABEL
        END

 FECT*  NOTERM,ID,EBCDIC,SOURCE,NOLIST,NODECK,LOAD,NOMAP,NOTEST
 FECT*  NAME = SHAPE    , LINECNT =          56
   SOURCE STATEMENTS =         19,PROGRAM SIZE =        782
 01 DIAGNOSTICS GENERATED, HIGHEST SEVERITY CODE IS 0

 02 DIAGNOSTICS THIS STEP
```

B.3 Analysis for Combined Torsion, Bending and Shear

Space Truss Analogy

The extension of the truss analogy to include combined bending and shear in addition to torsional loads has been conducted by Elfgren [106]. The basic formulation and details of this method can be found in the Reference. This method can be used to analyse a box section structure to determine its ultimate load-carrying capacity under combined torsion, bending and shear. Table B.1 compares the calculated ultimate loads of the box section under the cases of pure torsion, combined torsion and bending, and combined torsion, bending and shear for the two cases of tension and compression failure modes at both the midspan and the support sections.

The experimental data showed that failure at both the midspan and the support sections was characterized by yielding of the reinforcing steel on the tension side of the section (tension mode).

The experimental ultimate load was higher than that predicted from pure torsion consideration, and approximately equal to that obtained from combined bending and torsion considerations. The following is a summary of the equations used in Reference [106] for calculating the strength of a reinforced concrete box section structure under combined torsional and bending moments and shearing force. The symbols used in these equations are described in Figure B.1.

Table B.1

Calculated Ultimated Load Values (Compression Field Theory for Pure Torsion and Combined Torsion, Shear and Bending

Support Section

Case \ Ultimate load due to (kips)	M_T	M	V
Pure Torsion (M_T)	64.25		
Tension Mode(M_T+M)	128.3	88.38	
Tension Mode(M_T+M+V)	128.3	88.38	46.06

Midspan Section

Case \ Ultimate load due to (kips)	M_T	M	V
Pure Torsion (M_T)	52.85		
Tension Mode (M_T+M)	87.34	59.7	
Tension Mode (M_T+M+V)	87.34	59.7	46.06

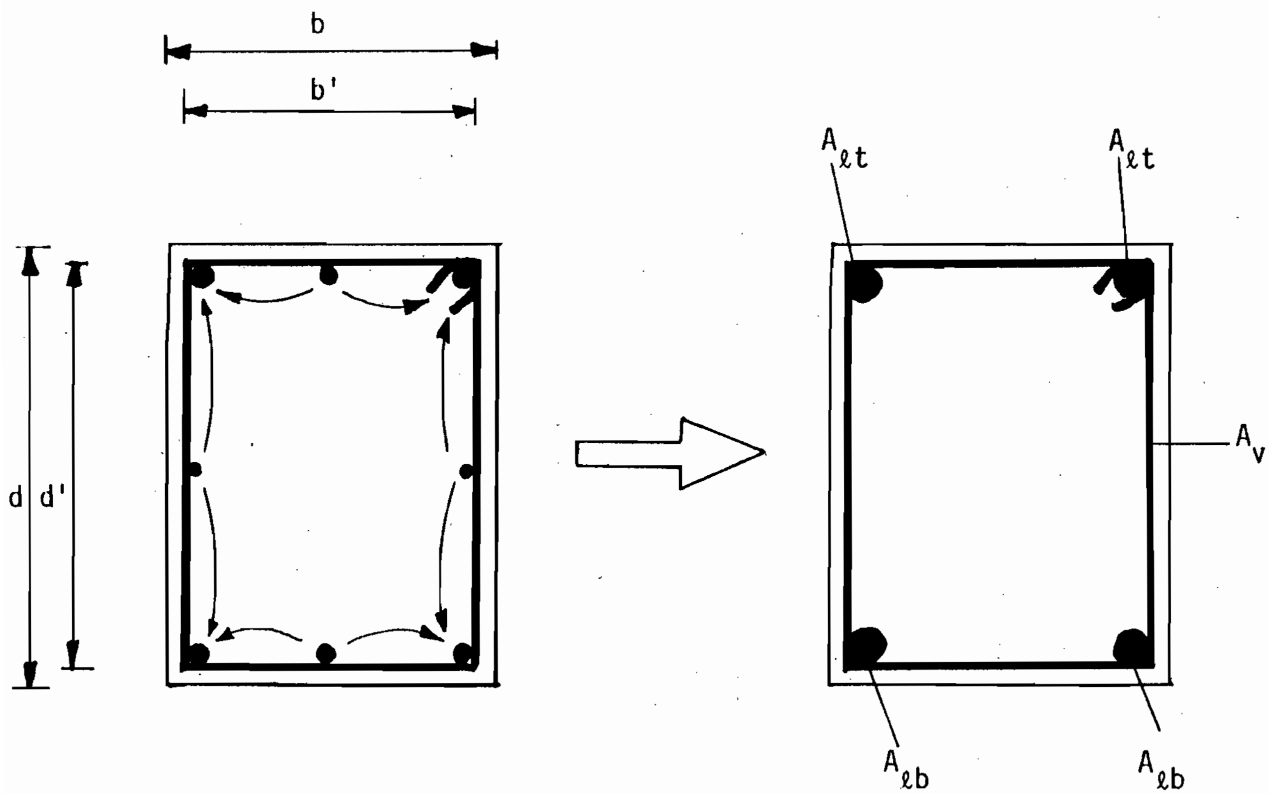

S	Stirrup Spacing
$f_{y\ell t}$	Yield Strength of longitudinal top reinforcement
$f_{y\ell b}$	Yield Strength of longitudinal bottom reinforcement
f_v	Yield Strength of the web reinforcement

FIG. B.1 IDEALIZATION OF THE STEEL REINFORCEMENT

B.3.1 Pure Torsion (M_T)

The ultimate torsional capacity of a concrete section under pure torsion M_T is given by the following equation:

$$M_{To} = 2\ b'\ d'\ \frac{A_v\ f_{yw}}{S} \sqrt{\frac{2\ A_\ell\ f_{y\ell}}{b' + d'} \cdot \frac{S}{A_w\ f_{yv}}} \qquad (B.1)$$

A condition for the validity of this equation is that the section is under-reinforced for torsion. Both the longitudinal and transverse reinforcements reach their yield stresses before failure and therefore the compressive strength of the concrete is not a primary factor in the load-carrying capacity.

B.3.2 Combined Torsion and Bending (M_T + M)

B.3.2.1 Tension Failure Mode

In this failure mode the compressive zone is formed on the top of the section while yielding of the reinforcement starts at the bottom on account of bending. The calculated ultimate torsional and bending moments capacities of the concrete box section under combined torsion and bending are given by the following equations:

$$M_o^t = 2\ A_{\ell b}\ f_{y\ell b}\ d' \qquad (B.2)$$

$$M_{To}^t = 2\ b'\ d'\ \frac{A_v\ f_{yv}}{S} \sqrt{\frac{2\ A_{\ell b}\ f_{y\ell b}}{b' + d'}\ \frac{S}{A_v\ f_{yv}}} \qquad (B.3)$$

where M_o^t is the pure ultimate flexural capacity of the section for tension failure mode (without any torsion present) and M_{To}^t is the pure ultimate torsional strength of the section for tension failure mode (without any flexure present).

In a non-dimensional form the interaction between torsion M_T and bending moment M can be expressed as follows:

$$\frac{M}{M_o^t} + \left(\frac{M_T}{M_{To}^t}\right)^2 = 1 \tag{B.4}$$

B.3.2.2 <u>Compression Failure Mode</u>

This failure mode is characterized by yielding of the top reinforcement and a compression zone formed at the bottom of the section.

The ultimate torsional and bending moments capacities of the concrete box section under combined torsion and bending are given by the following equations:

$$M_o^c = -2\, A_{\ell t}\, f_{y\ell t}\, d' \tag{B.5}$$

$$M_{To}^c = 2\, b'\, d'\, \frac{A_v\, f_{yv}}{s} \sqrt{\frac{2\, A_{\ell t}\, f_{y\ell t}}{b' + d'} \cdot \frac{s}{A_v\, f_{yv}}} \tag{B.6}$$

where M_o^c is the pure ultimate flexural capacity of the section for compression failure mode (without any torsion present) and M_{To}^c is the pure ultimate torsional strength of the section for compression failure mode (without any flexure present).

In a non-dimensional form, the relationship between twisting moment M_T and bending moment M under combined loading is similar to that equation given for the tension failure mode as follows:

$$\frac{M}{M_o^c} + \left(\frac{M_T}{M_{To}^c} \right)^2 = 1 \qquad (B.7)$$

There is another mode of failure called the shear failure mode which is characterized by the formation of the compression zone on one of the vertical sides of the section and the yielding of the reinforcement on the other side. However, since this mode of failure was not encountered in the present study, it will not be discussed.

B.3.3 Combined Torsion, Bending and Shear (M_T + M + V)

B.3.3.1 Tension Failure Mode

This failure is characterized by the compression zone in the top of the section and yielding of the reinforcement in the bottom. However, the effect of shear causes different inclinations of the compression struts on the remaining three sides of the beam due to different shear flows occurring on these faces. The ultimate torsional and bending moments and shearing force capacities (M_{To}^t, M_o^t and V_o^t) of the concrete box section under this loading combination are given by the following equations:

$$M_{To}^{t} = 2\ A_{\ell b}\ f_{y\ell b}\ d' \tag{B.8}$$

$$M_{To}^{t} = 2\ b'\ d'\ \frac{A_v\ f_{yv}}{S} \sqrt{\frac{2\ A_{\ell b}\ f_{y\ell b}}{b' + d'} \quad \frac{S}{A_v\ f_{yv}}} \tag{B.9}$$

$$V_{o}^{t} = 2\ d'\ \frac{A_v\ f_{yv}}{S} \sqrt{\frac{2\ A_{\ell b}\ f_{y\ell b}}{d'} \quad \frac{S}{A_v\ f_{yv}}} \tag{B.10}$$

where M_o^t and M_{To}^t have been defined before and V_o^t is the pure ultimate shear strength of the section.

In a non-dimensional form, the relationship between torsional and bending moments and shearing force is as follows:

$$\frac{M}{M_o^t} + \left(\frac{M_T}{M_{To}^t}\right)^2 + \left(\frac{V}{V_o^t}\right)^2 = 1 \tag{B.11}$$

B.3.3.2 <u>Compression Failure Mode</u>

Again, this case is characterized by the compression zone in the bottom of the section while yielding of the reinforcement starts at the top. The ultimate torsional and bending moments and shearing force capacities (M_{To}^t, M_o^t and V_o^t) of a concrete box section under this loading combination are given by the following equations:

$$M_o = 2\, A_{\ell t}\, f_{y\ell t}\, d' \tag{B.12}$$

$$M_{To}^c = 2\, b'\, d'\, \frac{A_v\, f_{yv}}{s} \sqrt{\frac{2\, A_{\ell t}\, f_{y\ell t}}{b' + d'} \cdot \frac{s}{A_v\, f_{yv}}} \tag{B.13}$$

$$V_o^c = 2\, d'\, \frac{A_v\, f_{yv}}{s} \sqrt{\frac{2\, A_{\ell t}\, f_{y\ell t}}{d'} \cdot \frac{s}{A_v\, f_{yv}}} \tag{B.14}$$

where M_o^c and M_{To}^c have been defined before and V_o^c is the pure ultimate shear strength of the section.

The non-dimensional interaction equation for the ultimate strength of the section under combined torsion, bending and shear is a as follows:

$$\frac{M}{M_o^c} + \left(\frac{M_T}{M_{To}^c}\right)^2 + \left(\frac{V}{V_o^c}\right)^2 = 1 \tag{B.15}$$

APPENDIX C

STEEL AND CONCRETE STRESS VARIATION ACROSS THE TOP AND BOTTOM SLAB WIDTHS

(EXPERIMENTAL DATA)

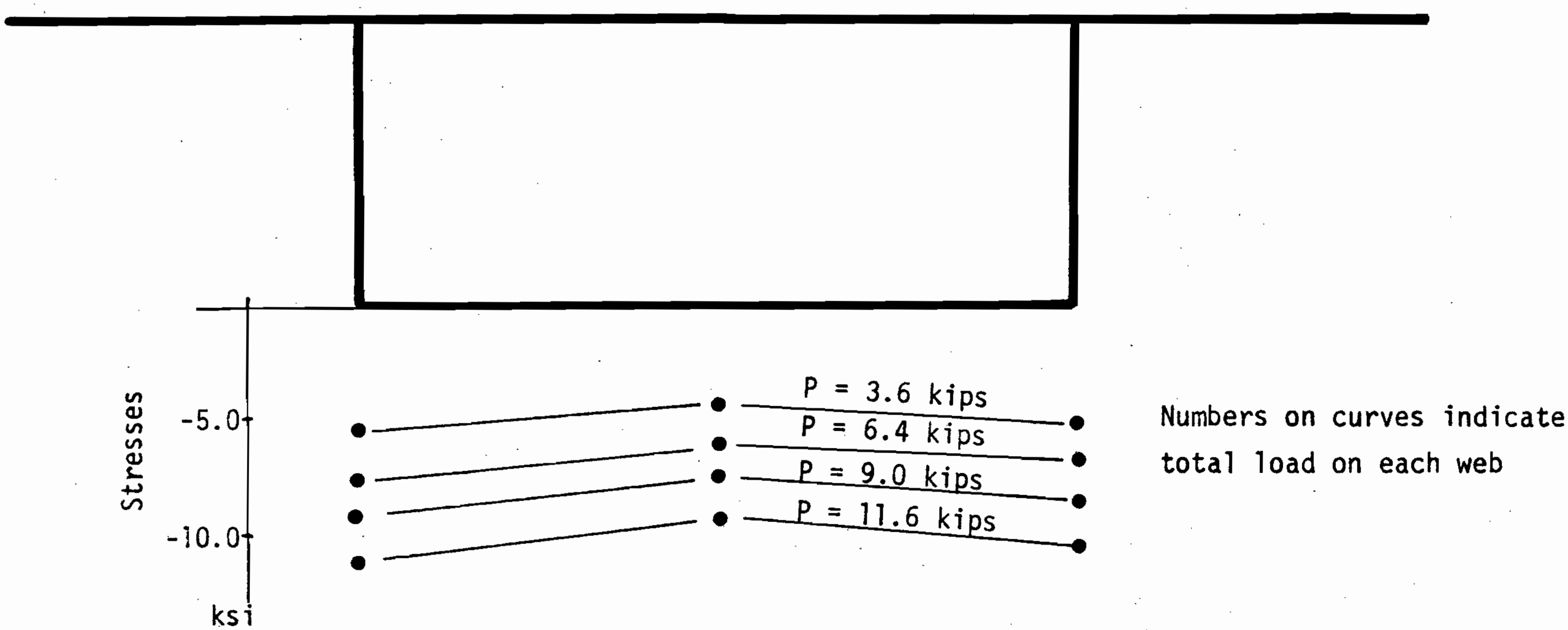

FIG. C.1 LONGITUDINAL STEEL STRESS VARIATION ACROSS THE LOWER SLAB WIDTH (AT SUPPORT SECTION)
(SYMMETRICAL LOADING CASE)

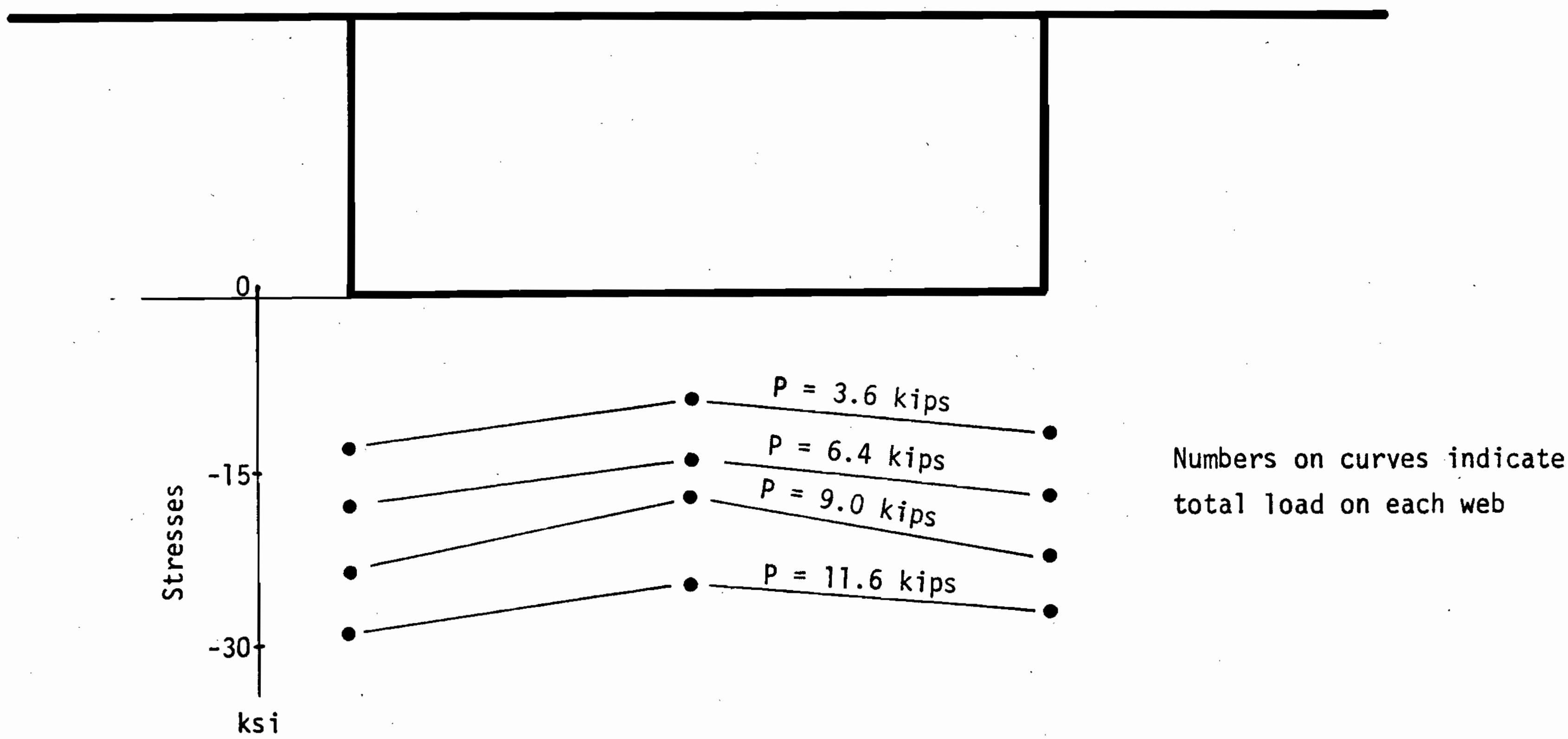

FIG. C.2 LONGITUDINAL STEEL STRESS VARIATION ACROSS THE LOWER SLAB WIDTH (AT MIDSPAN SECTION)
(SYMMETRICAL LOADING CASE)

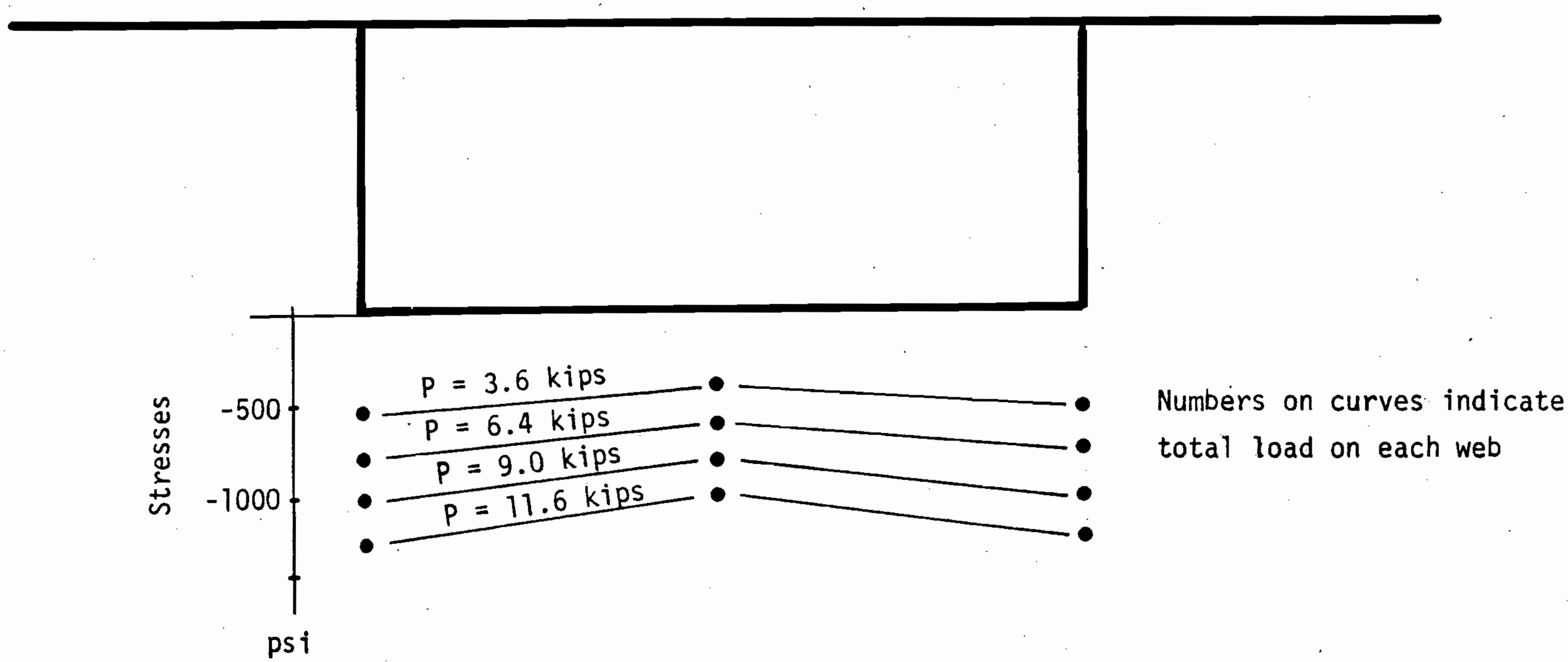

FIG. C.3 LONGITUDINAL CONCRETE STRESS VARIATION ACROSS THE LOWER SLAB WIDTH (AT SUPPORT SECTION)
(SYMMETRICAL LOADING CASE)

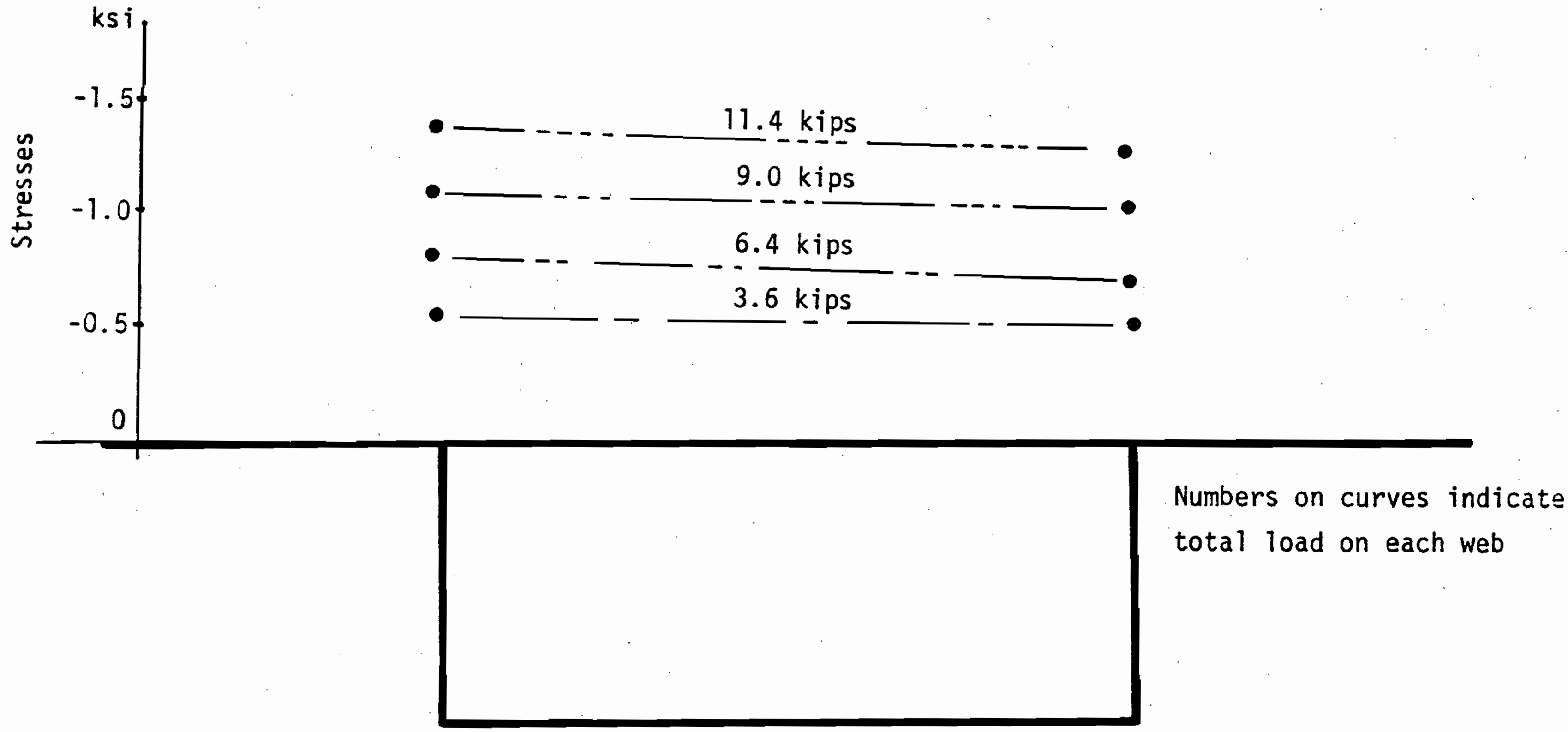

FIG. C.4 TRANSVERSE STEEL STRESS VARIATION ACROSS THE TOP SLAB WIDTH (SECTION AT 12" FROM SUPPORT)
(SYMMETRICAL LOADING CASE)

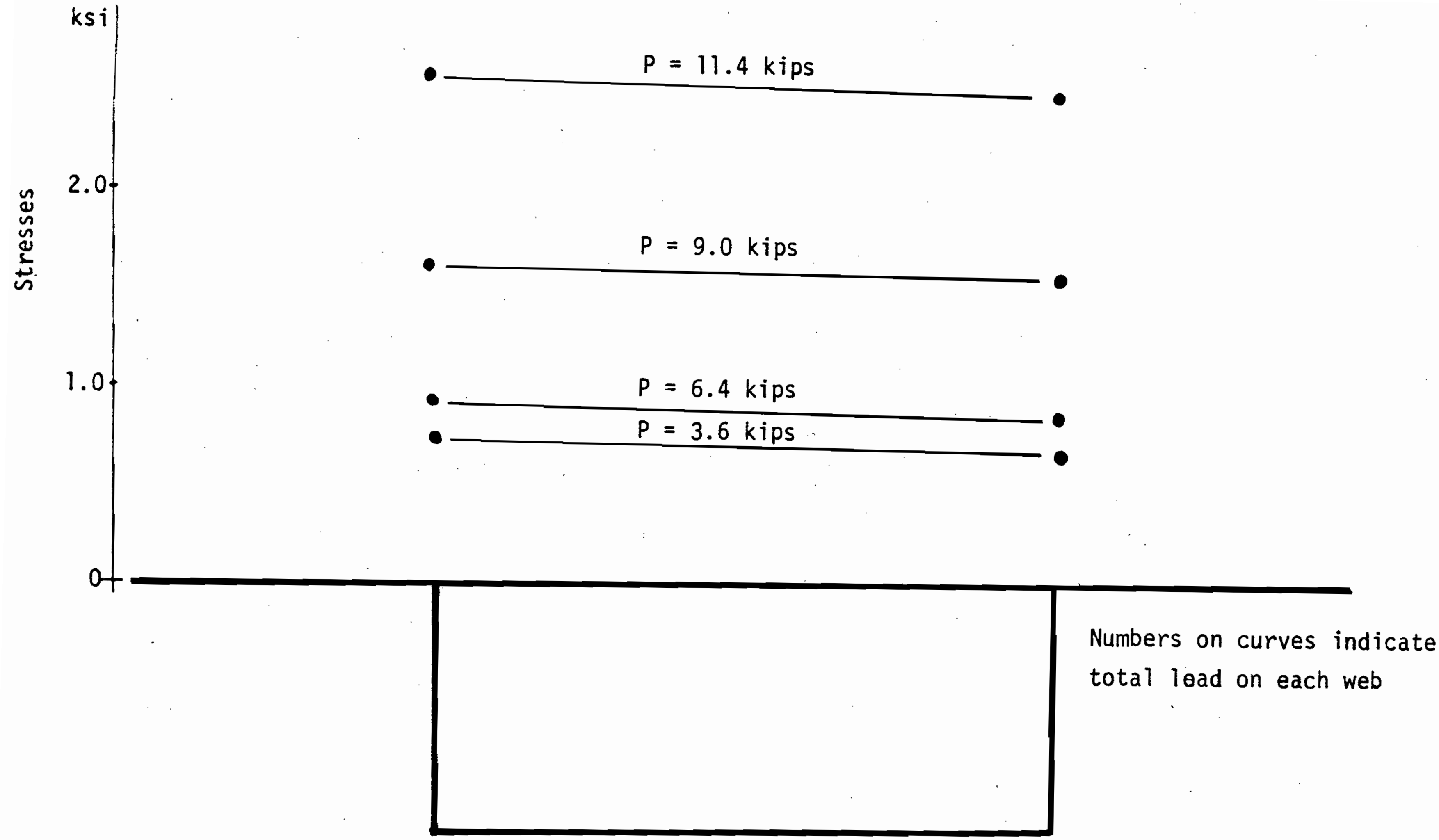

FIG. C.5 TRANSVERSE STEEL STRESS VARIATION ACROSS THE TOP SLAB WIDTH (AT MIDSPAN SECTION)
(SYMMETRICAL LOADING CASE)

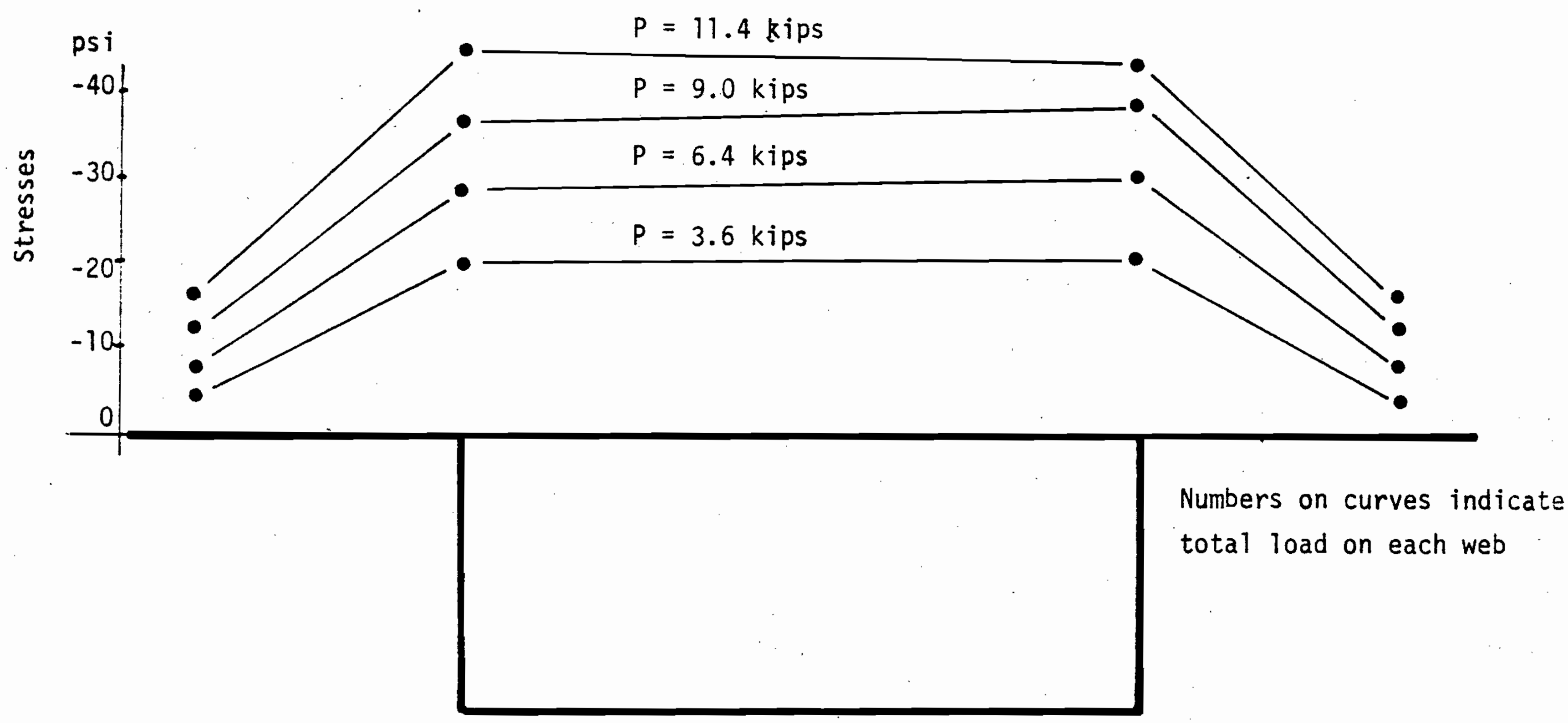

FIG. C.6 TRANSVERSE CONCRETE STRESS VARIATION ACROSS THE TOP SLAB WIDTH (AT SUPPORT SECTION)
(SYMMETRICAL LOADING CASE)

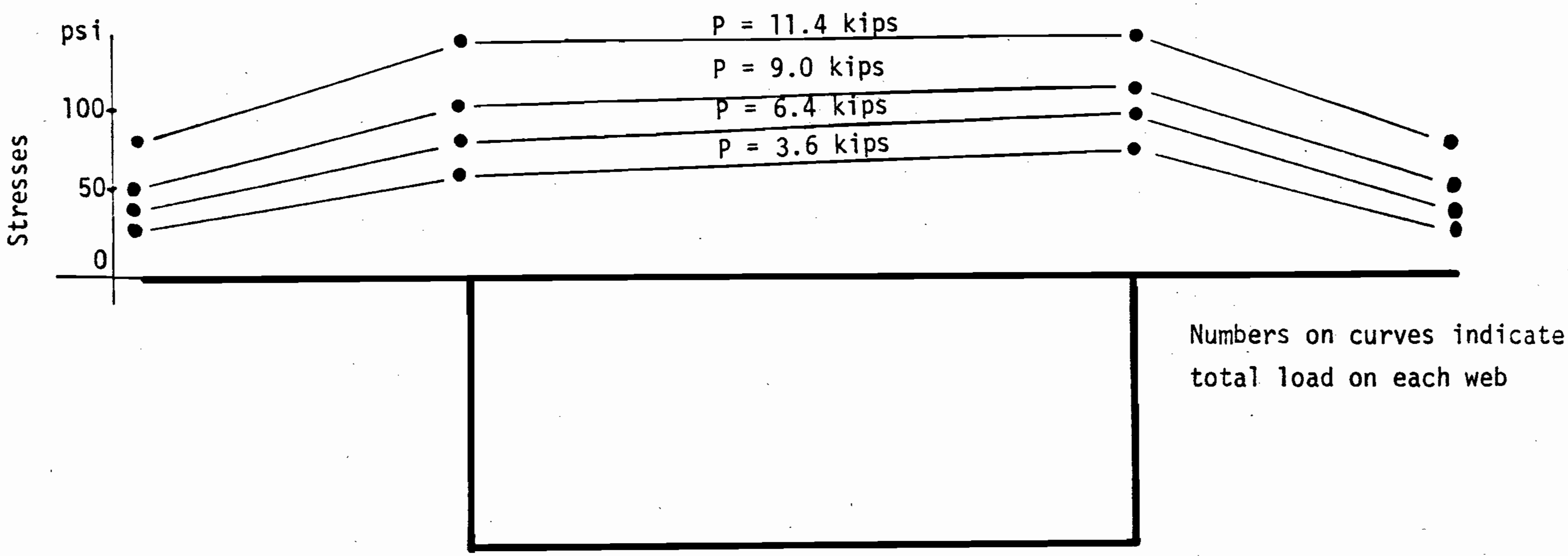

FIG. C.7 TRANSVERSE CONCRETE STRESS VARIATION ACROSS THE TOP SLAB WIDTH (AT MIDSPAN SECTION)
(SYMMETRICAL LOADING CASE)

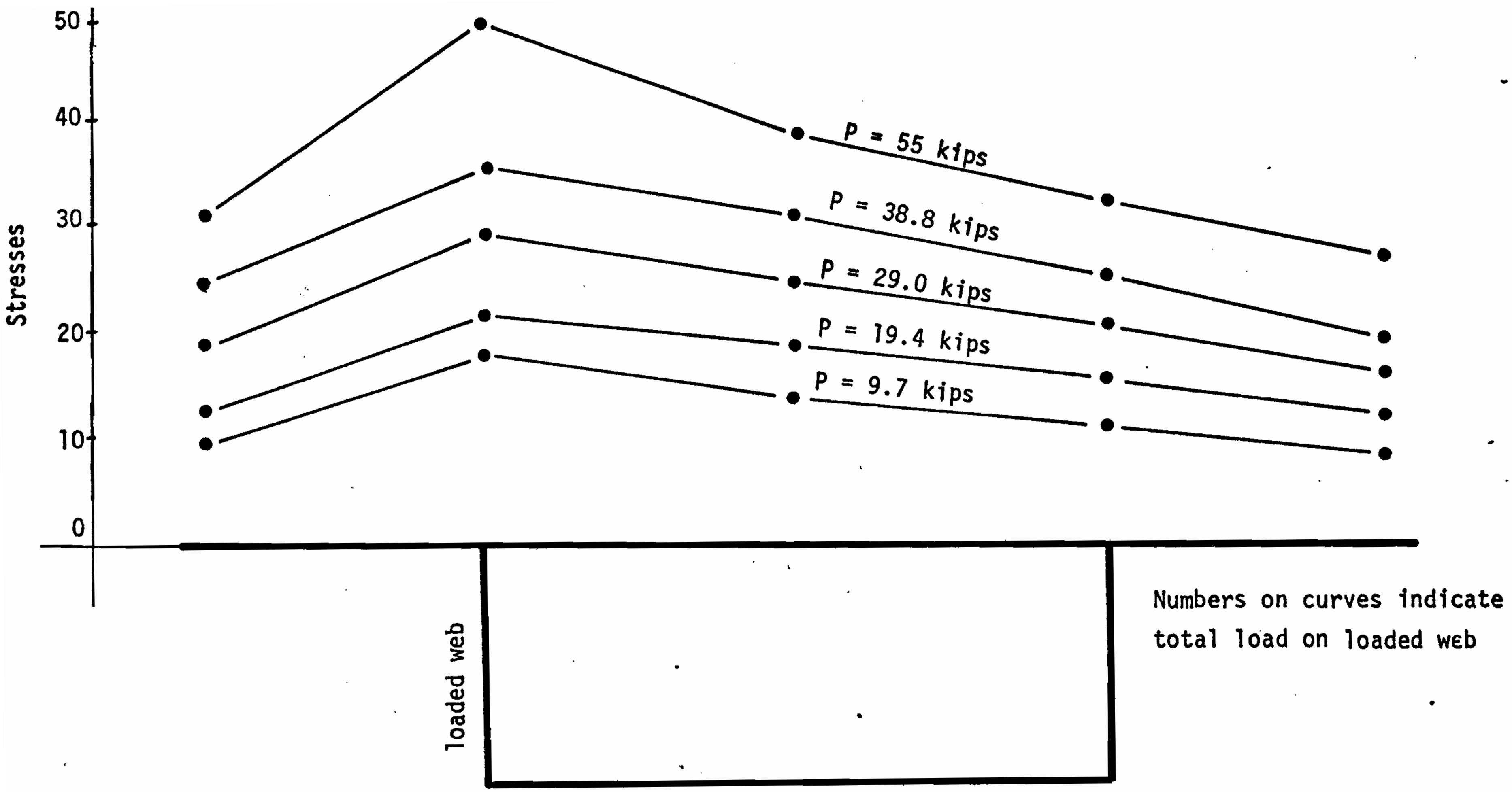

FIG. C.8 LONGITUDINAL STEEL STRESS VARIATION ACROSS THE TOP SLAB WIDTH (SECTION AT 4" FROM SUPPORT)
(UNSYMMETRICAL LOADING CASE)

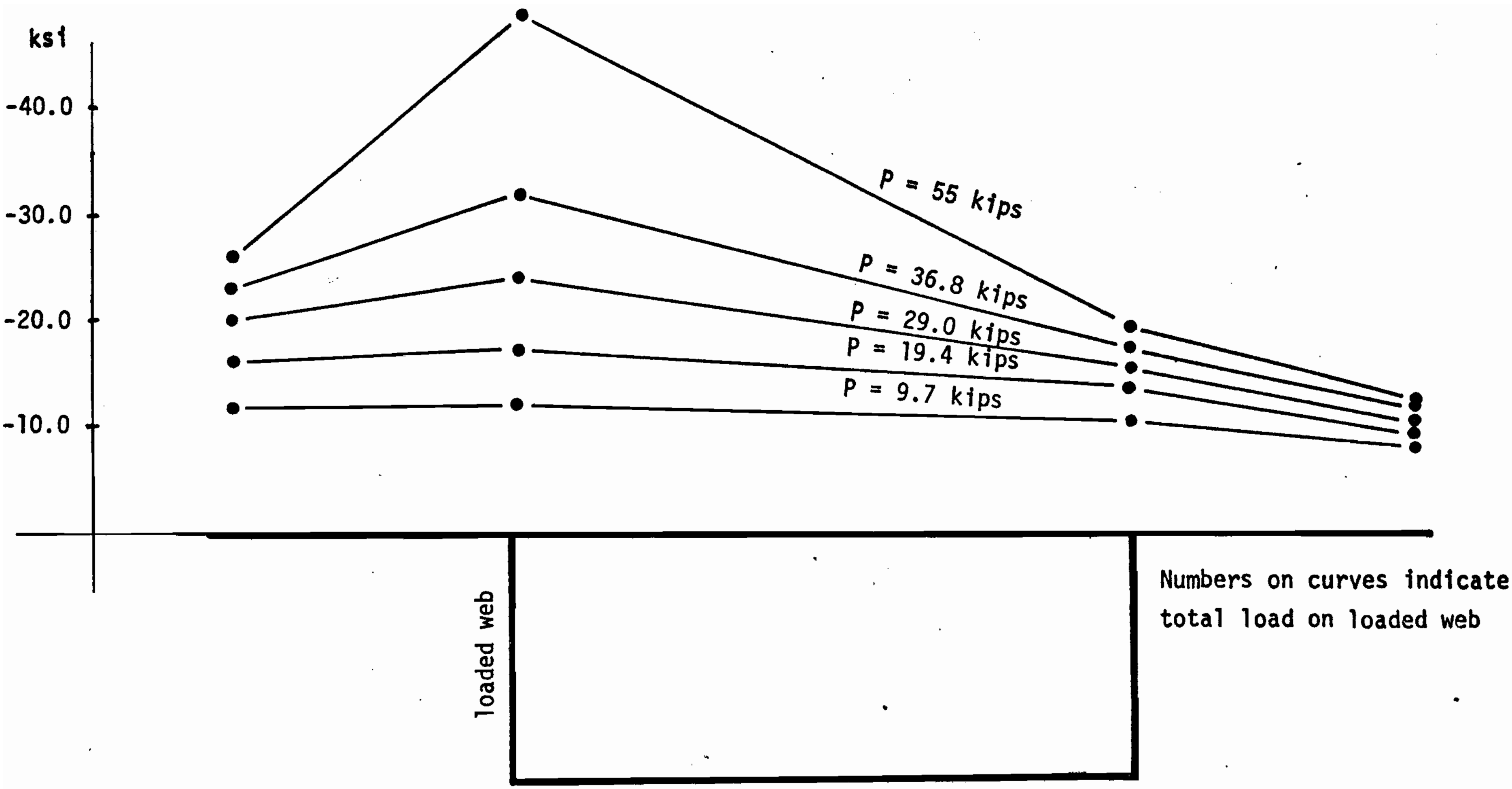

FIG. C.9 LONGITUDINAL STEEL STRESS VARIATION ACROSS THE TOP SLAB WIDTH (AT MIDSPAN SECTION)
(UNSYMMETRICAL LOADING CASE)

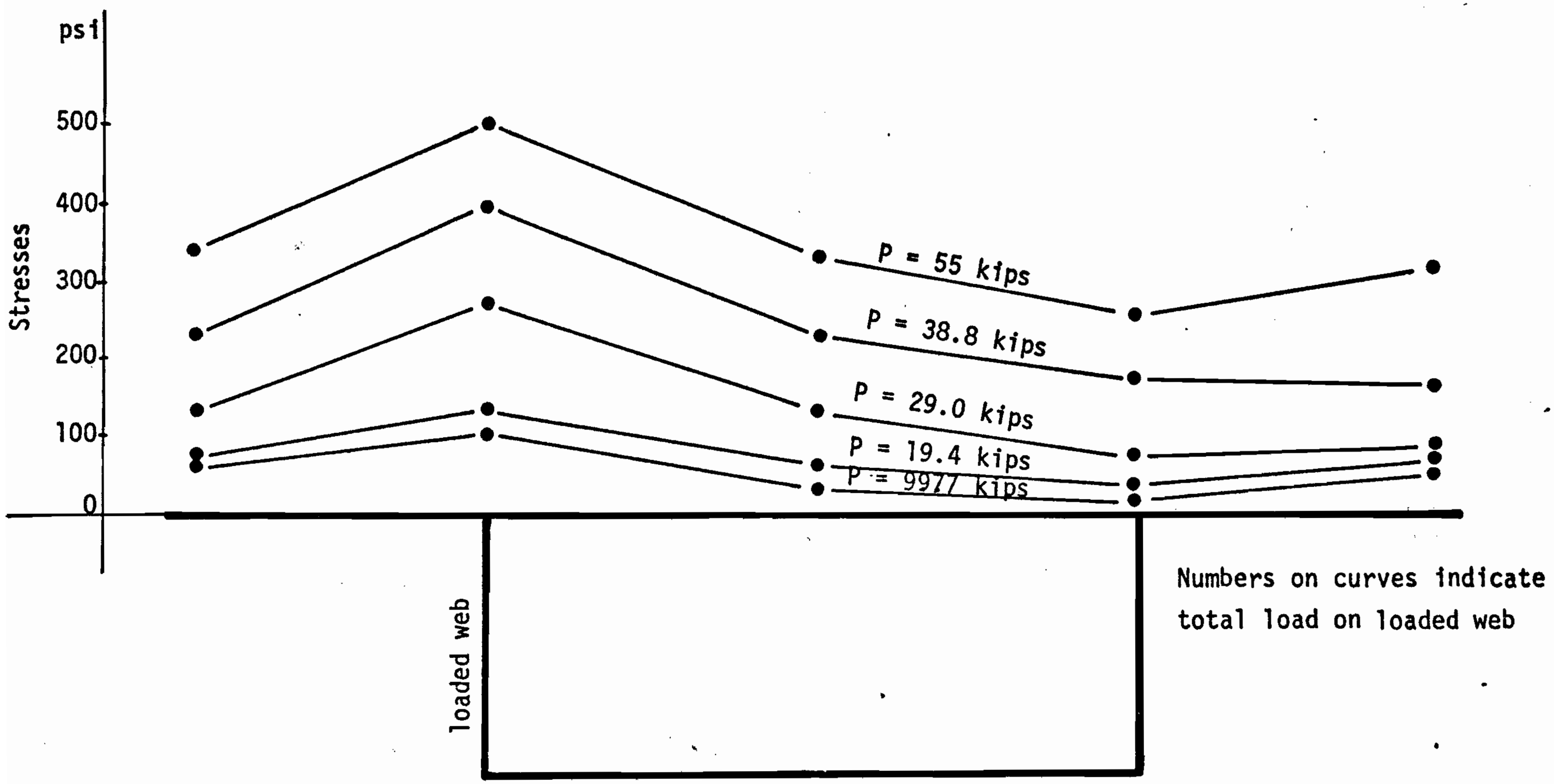

FIG. C.10 LONGITUDINAL CONCRETE STRESS VARIATION ACROSS THE TOP SLAB WIDTH (SECTION AT 19" FROM SUPPORT)
(UNSYMMETRICAL LOADING CASE)

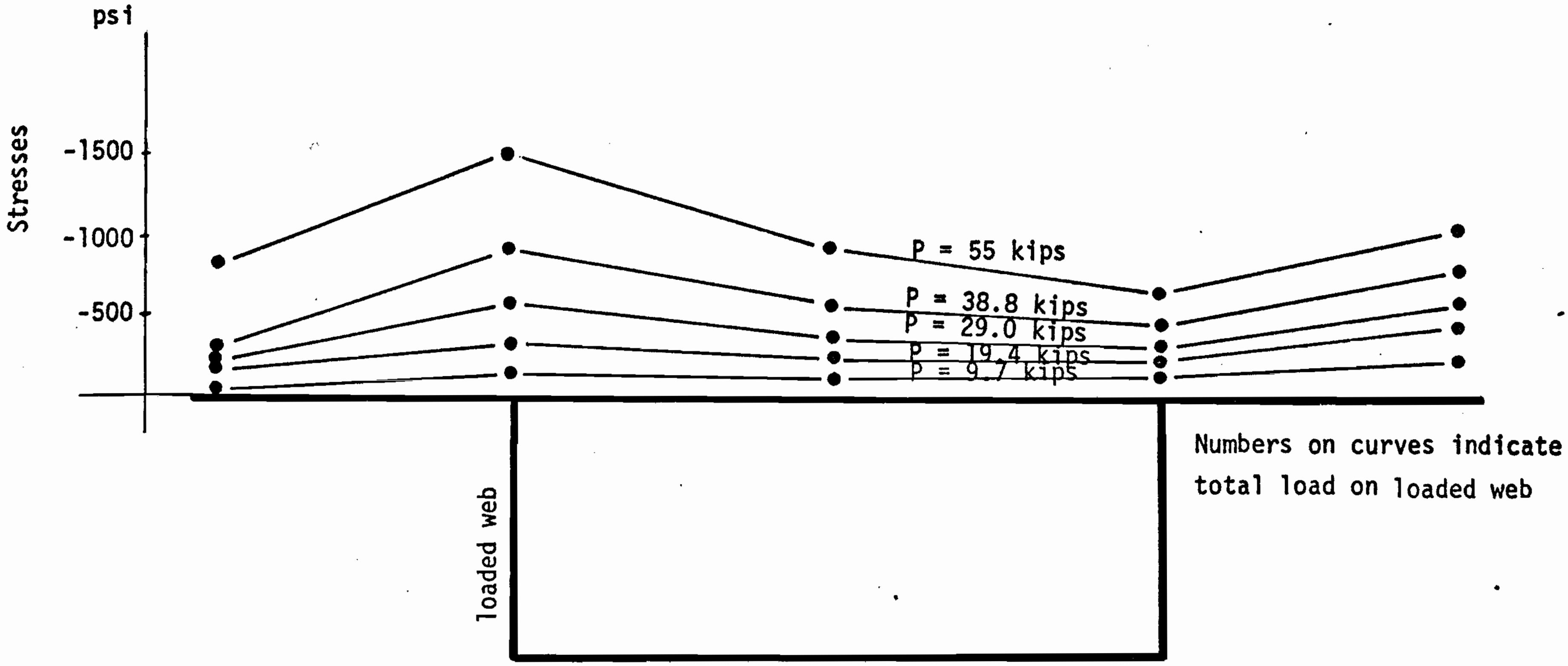

FIG. C.11 LONGITUDINAL CONCRETE STRESS VARIATION ACROSS THE TOP SLAB WIDTH (AT MIDSPAN SECTION)
(UNSYMMETRICAL LOADING CASE)

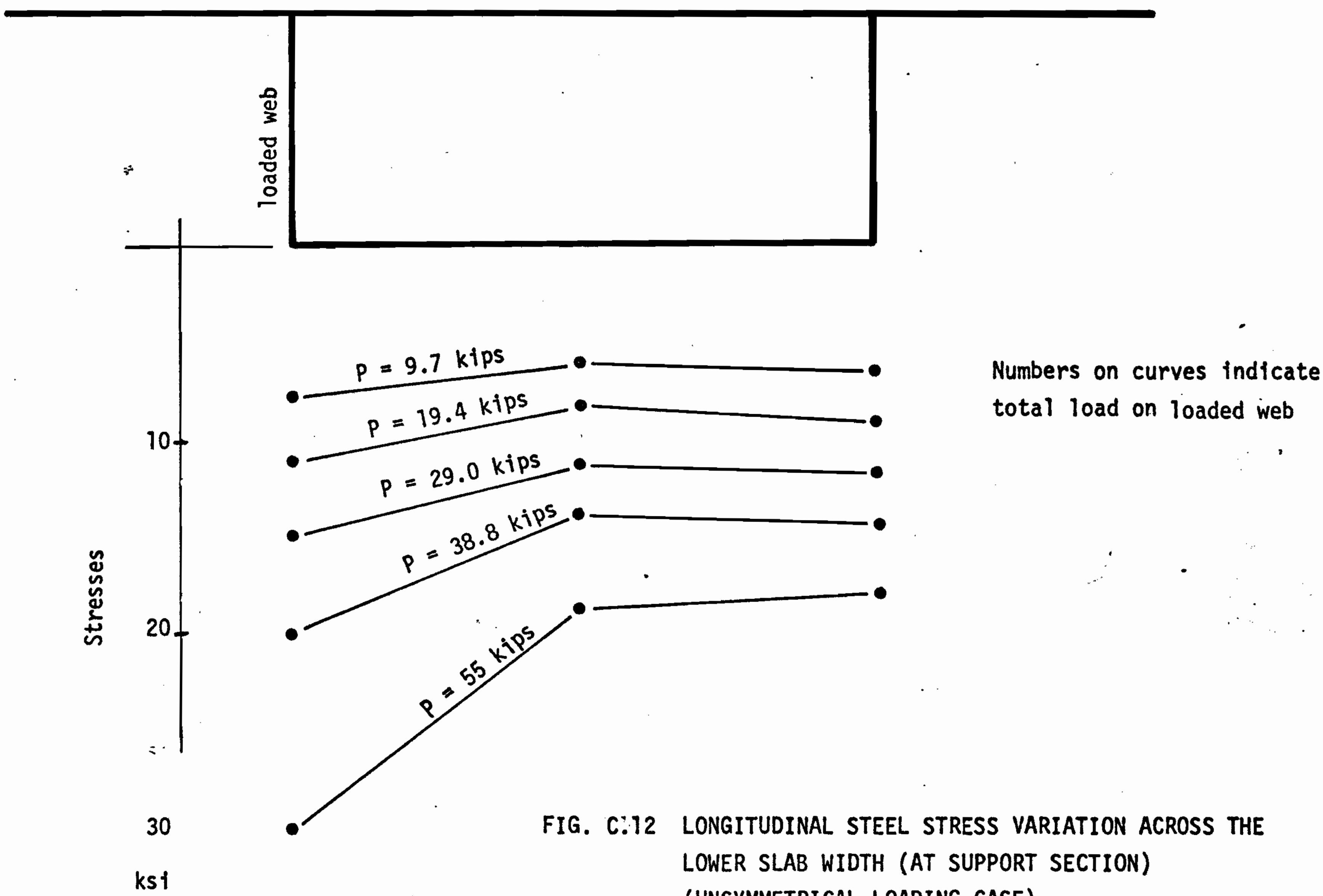

FIG. C.12 LONGITUDINAL STEEL STRESS VARIATION ACROSS THE LOWER SLAB WIDTH (AT SUPPORT SECTION) (UNSYMMETRICAL LOADING CASE)

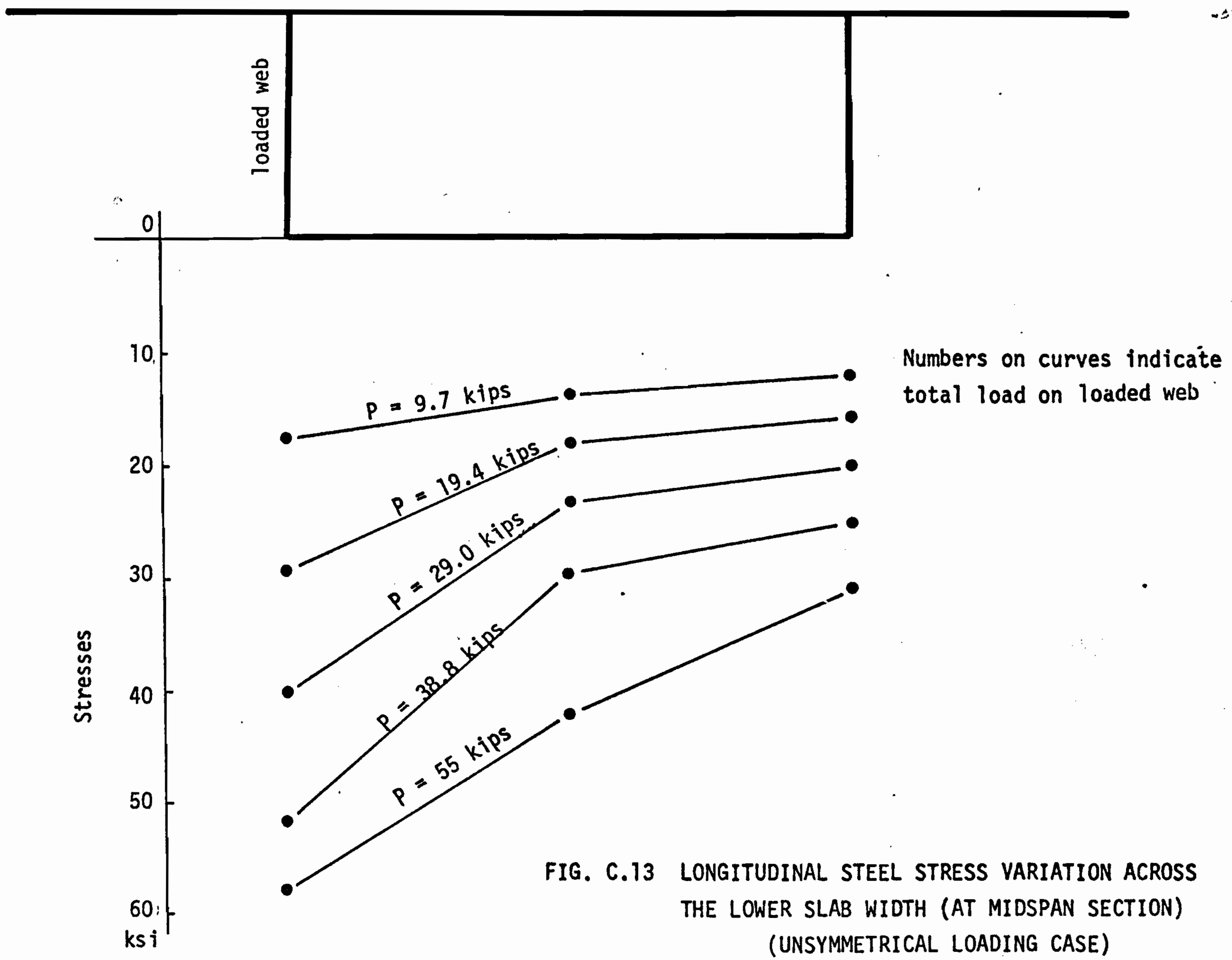

FIG. C.13 LONGITUDINAL STEEL STRESS VARIATION ACROSS THE LOWER SLAB WIDTH (AT MIDSPAN SECTION) (UNSYMMETRICAL LOADING CASE)

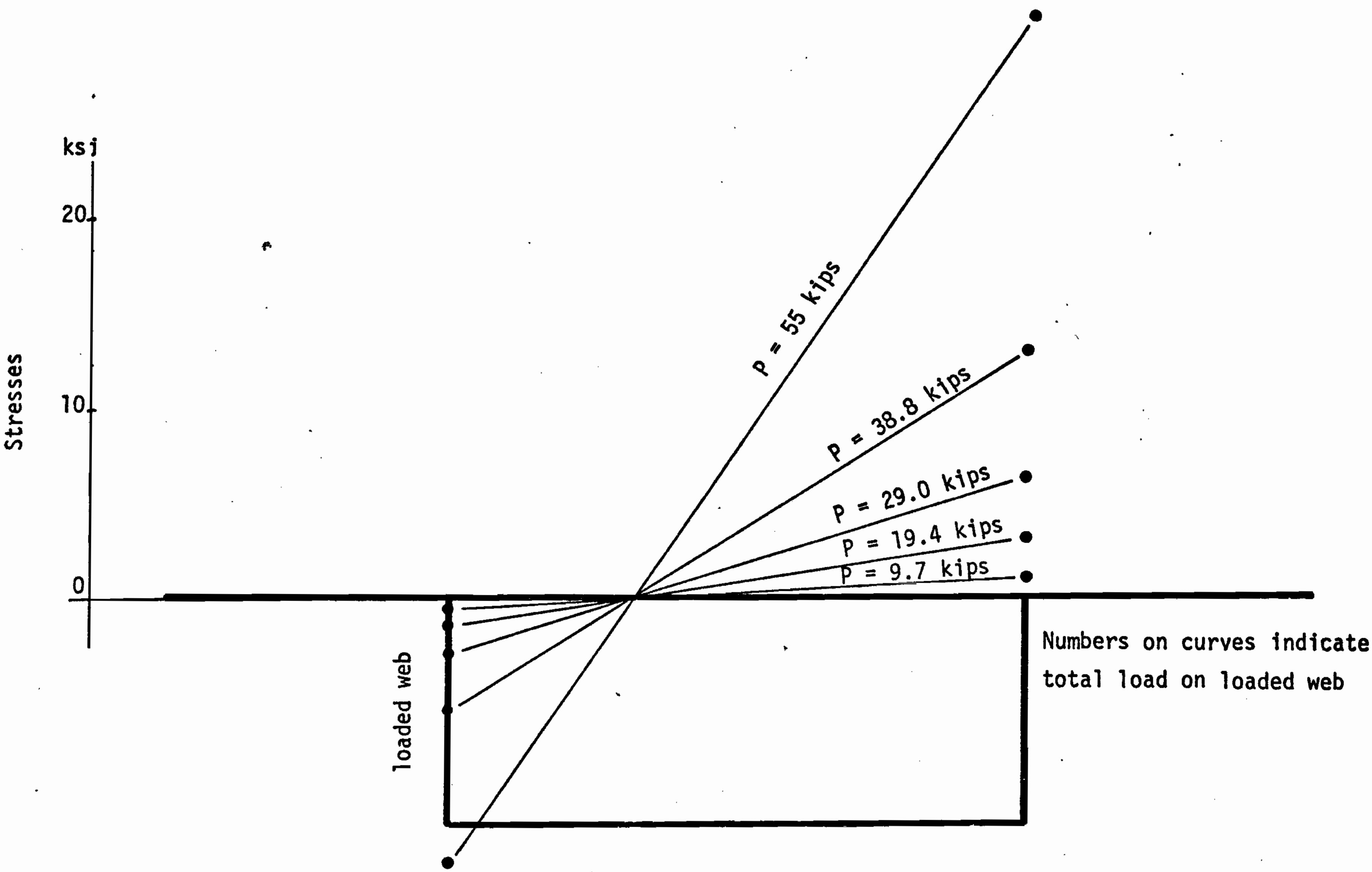

FIG. C.14 TRANSVERSE STEEL STRESS VARIATION ACROSS THE TOP SLAB WIDTH (SECTION AT 78" FROM SUPPORT)
(UNSYMMETRICAL LOADING CASE)

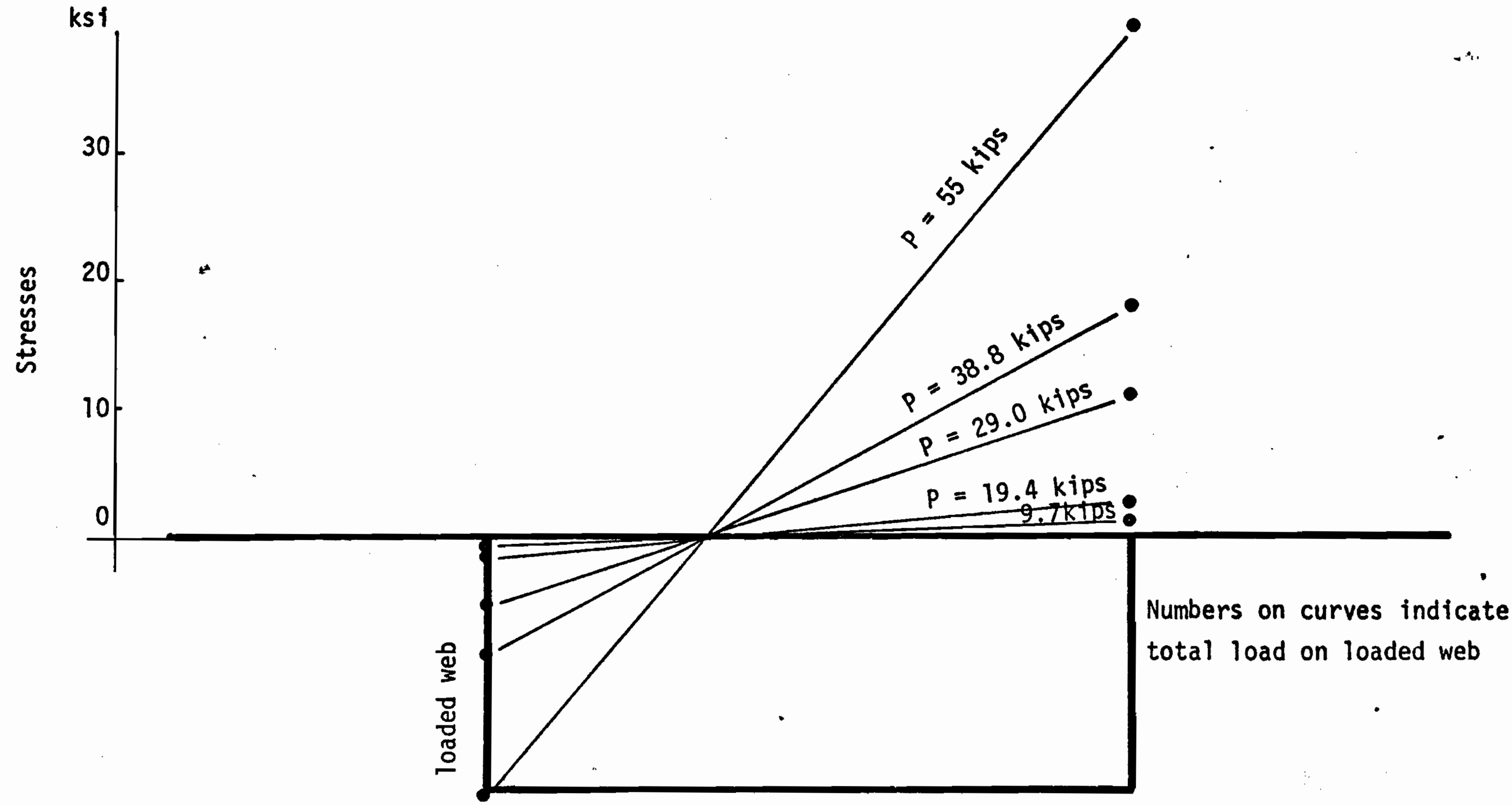

FIG. C.15 TRANSVERSE STEEL STRESS VARIATION ACROSS THE TOP SLAB WIDTH (SECTION AT 96" FROM SUPPORT)
(UNSYMMETRICAL LOADING CASE)

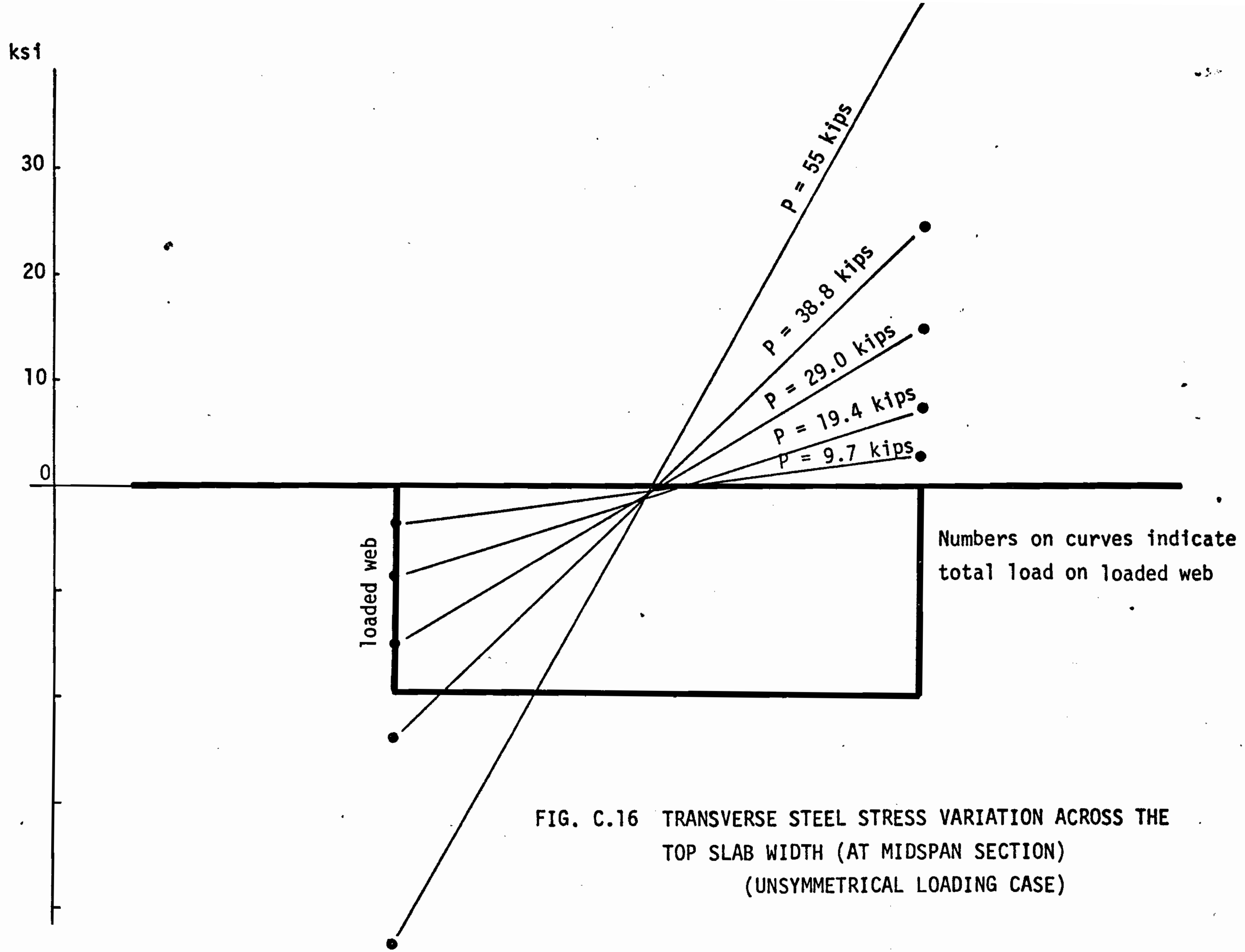

FIG. C.16 TRANSVERSE STEEL STRESS VARIATION ACROSS THE TOP SLAB WIDTH (AT MIDSPAN SECTION) (UNSYMMETRICAL LOADING CASE)

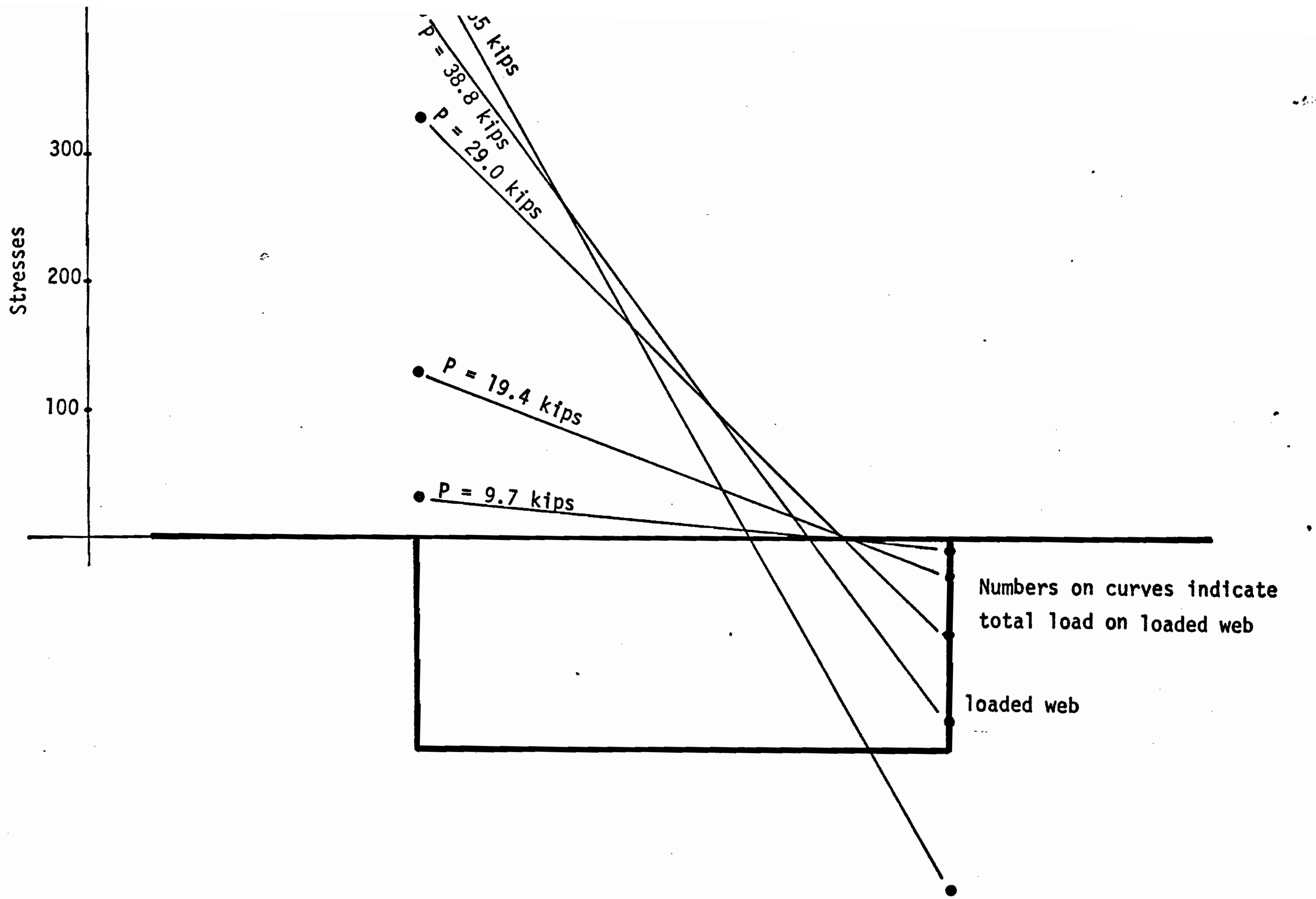

FIG. C.17 TRANSVERSE CONCRETE STRESS VARIATION ACROSS THE TOP SLAB WIDTH (AT MIDSPAN SECTION)
(UNSYMMETRICAL LOADING CASE)

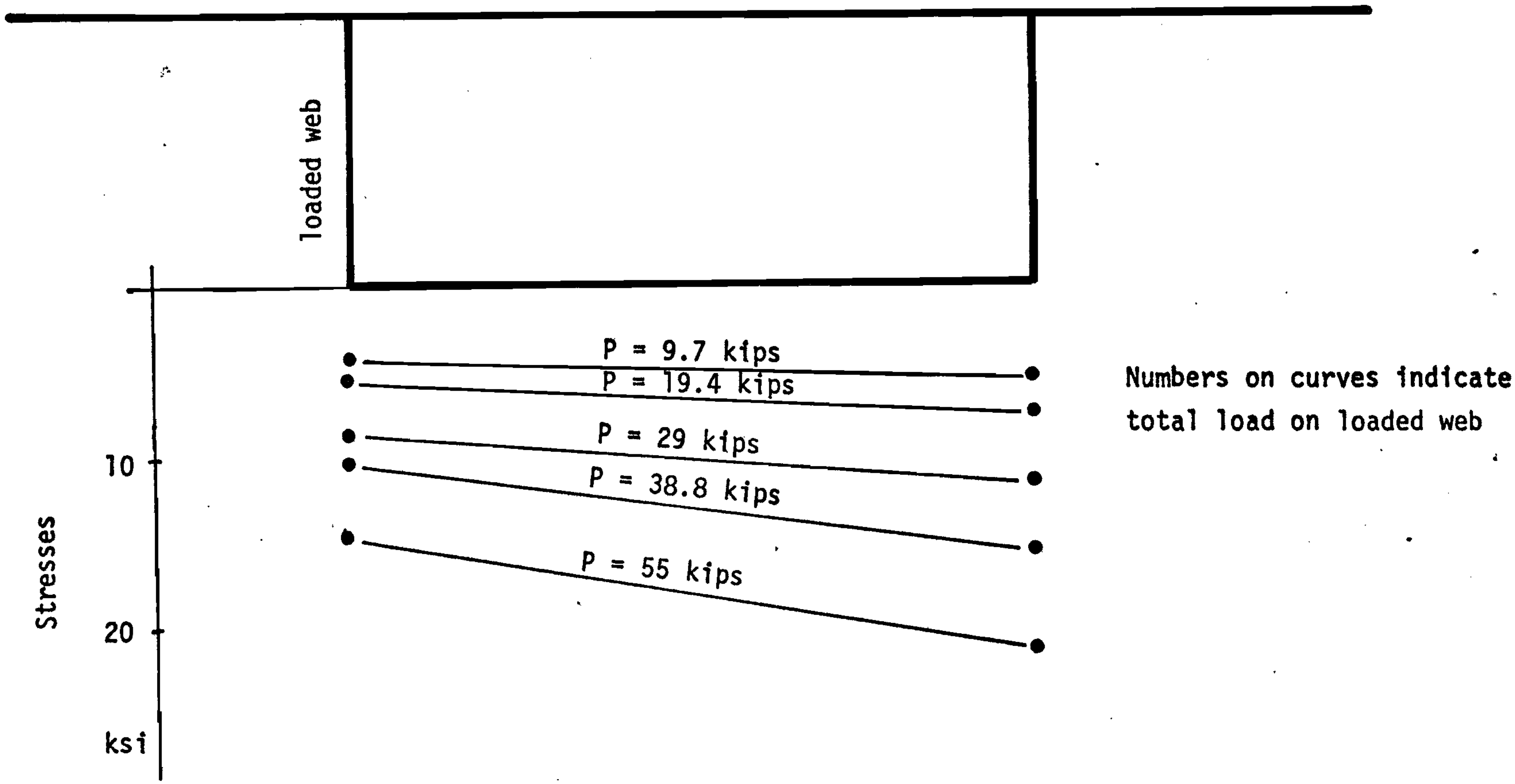

FIG. C.18 TRANSVERSE STEEL STRESS VARIATION ACROSS THE LOWER SLAB WIDTH (SECTION AT 33" FROM MIDSPAN) (UNSYMMETRICAL LOADING CASE)

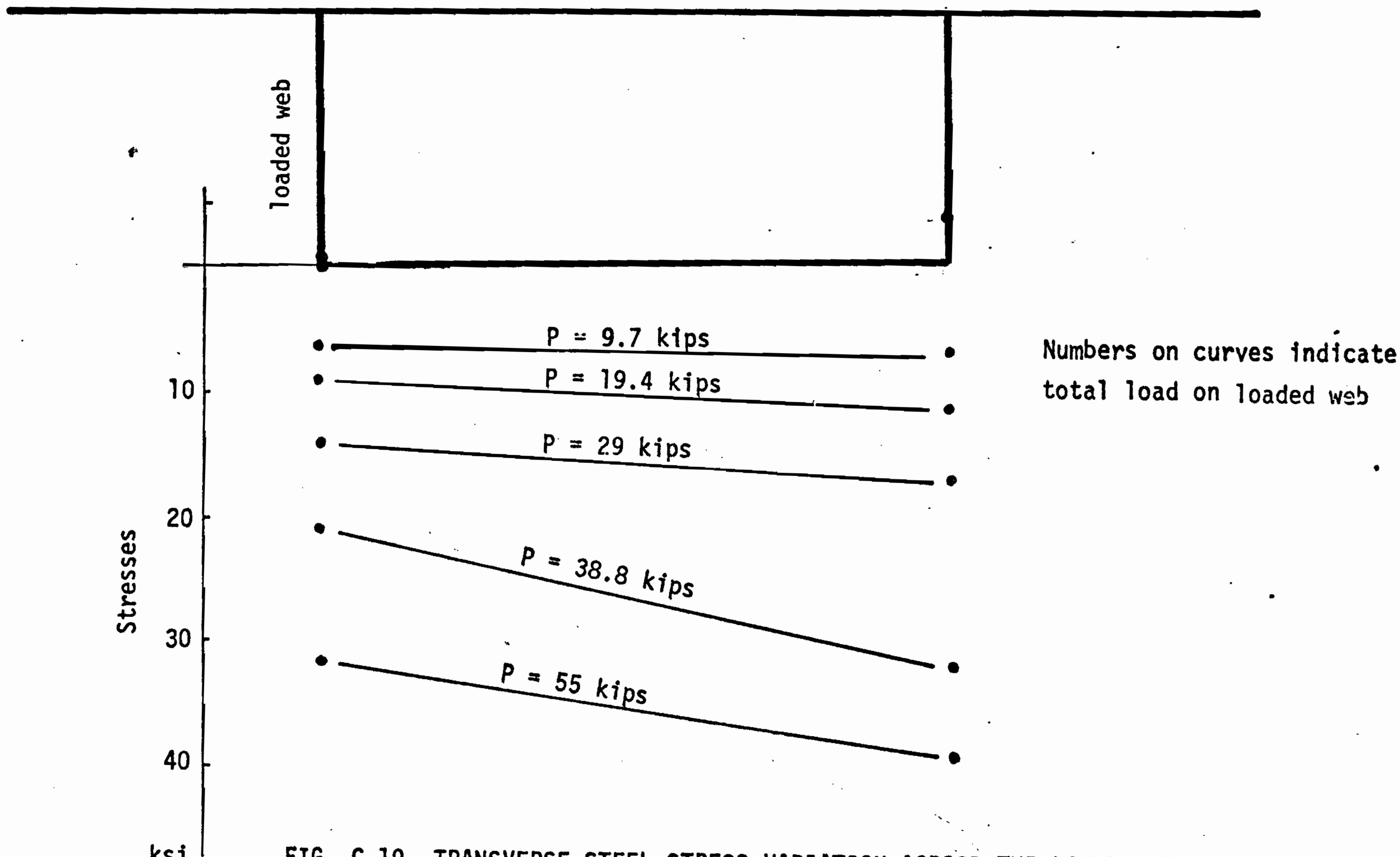

FIG. C.19 TRANSVERSE STEEL STRESS VARIATION ACROSS THE LOWER SLAB WIDTH
(AT MIDSPAN SECTION) (UNSYMMETRICAL LOADING CASE)